National Library
of Canada

Acquisitions and
Bibliographic Services Branch

395 Wellington Street
Ottawa, Ontario
K1A 0N4

Bibliothèque nationale
du Canada

Direction des acquisitions et
des services bibliographiques

395, rue Wellington
Ottawa (Ontario)
K1A 0N4

Your file Votre référence

Our file Notre référence

NOTICE

The quality of this microform is heavily dependent upon the quality of the original thesis submitted for microfilming. Every effort has been made to ensure the highest quality of reproduction possible.

If pages are missing, contact the university which granted the degree.

Some pages may have indistinct print especially if the original pages were typed with a poor typewriter ribbon or if the university sent us an inferior photocopy.

Reproduction in full or in part of this microform is governed by the Canadian Copyright Act, R.S.C. 1970, c. C-30, and subsequent amendments.

AVIS

La qualité de cette microforme dépend grandement de la qualité de la thèse soumise au microfilmage. Nous avons tout fait pour assurer une qualité supérieure de reproduction.

S'il manque des pages, veuillez communiquer avec l'université qui a conféré le grade.

La qualité d'impression de certaines pages peut laisser à désirer, surtout si les pages originales ont été dactylographiées à l'aide d'un ruban usé ou si l'université nous a fait parvenir une photocopie de qualité inférieure.

La reproduction, même partielle, de cette microforme est soumise à la Loi canadienne sur le droit d'auteur, SRC 1970, c. C-30, et ses amendements subséquents.

Canada

UNIVERSITY OF ALBERTA

MODELLING TURBULENT FLAME GROWTH IN A CUBICAL CHAMBER

BY

DAVID SING-KHING TING ©

A thesis submitted to the Faculty of Graduate Studies and Research
in partial fulfilment of the requirements
for the degree of Doctor of Philosophy.

DEPARTMENT OF MECHANICAL ENGINEERING

Edmonton, Alberta
Spring, 1995

National Library
of Canada

Acquisitions and
Bibliographic Services Branch

395 Wellington Street
Ottawa, Ontario
K1A 0N4

Bibliothèque nationale
du Canada

Direction des acquisitions et
des services bibliographiques

395, rue Wellington
Ottawa (Ontario)
K1A 0N4

Your file Votre référence

Our file Notre référence

The author has granted an irrevocable non-exclusive licence allowing the National Library of Canada to reproduce, loan, distribute or sell copies of his/her thesis by any means and in any form or format, making this thesis available to interested persons.

L'auteur a accordé une licence irrévocable et non exclusive permettant à la Bibliothèque nationale du Canada de reproduire, prêter, distribuer ou vendre des copies de sa thèse de quelque manière et sous quelque forme que ce soit pour mettre des exemplaires de cette thèse à la disposition des personnes intéressées.

The author retains ownership of the copyright in his/her thesis. Neither the thesis nor substantial extracts from it may be printed or otherwise reproduced without his/her permission.

L'auteur conserve la propriété du droit d'auteur qui protège sa thèse. Ni la thèse ni des extraits substantiels de celle-ci ne doivent être imprimés ou autrement reproduits sans son autorisation.

ISBN 0-612-10809-0

Canada

UNIVERSITY OF ALBERTA

RELEASE FORM

NAME OF AUTHOR:	DAVID SING-KHING TING
TITLE OF THESIS:	MODELLING TURBULENT FLAME GROWTH IN A CUBICAL CHAMBER
DEGREE:	DOCTOR OF PHILOSOPHY
YEAR THIS DEGREE GRANTED:	1995

Permission is hereby granted to the University of Alberta Library to reproduce single copies of this thesis and to lend or sell such copies for private, scholarly or scientific research purposes only.

The author reserves all other publication and other rights in association with the copyright in the thesis, and except as hereinbefore provided neither the thesis nor any substantial portion thereof may be printed or otherwise reproduced in any material form whatever without the author's prior written permission.

7707-37 Avenue
Edmonton, Alberta
CANADA T6K 1T9

Date: Dec 9th /94

UNIVERSITY OF ALBERTA

FACULTY OF GRADUATE STUDIES AND RESEARCH

The undersigned certify that they have read, and recommend to the Faculty of Graduate Studies and Research for acceptance, a thesis entitled MODELLING TURBULENT FLAME GROWTH IN A CUBICAL CHAMBER submitted by DAVID SING-KHING TING in partial fulfilment of the requirements for the degree of DOCTOR OF PHILOSOPHY.

Dr. M.D. Checkel
(Supervisor)

Dr. L.W. Kostiuk

Dr. P.R. Smy

Dr. J.D. Dale

Dr. O.L. Gulder

Date: 2 December, 1994

TO

the enduring dreamers

Some scientists are born gifted, others build their successes on extreme perseverance and excessive effort.

MODELLING TURBULENT FLAME GROWTH IN A CUBICAL CHAMBER

ABSTRACT

Pressure trace and high speed schlieren video analyses were employed to investigate the effects of turbulence on spark-ignited flame growth in a closed vessel. Premixed methane-air mixtures of equivalence ratios between 1.0 and 0.6 were ignited at 300 K and 1 atm. Schlieren flame growth images were recorded at 2000 frames per second while the combustion chamber pressure was concurrently recorded. Pre-ignition turbulence was generated by pulling a perforated plate across the chamber. The ignition-time turbulence intensity was up to 2 m/s with integral scale of 1, 2, 4 or 8 mm. In the analysis, the turbulence parameters during flame propagation were adjusted for the effects of decay, compression and rapid distortion.

The schlieren video laminar flame growths agreed well with those calculated from the pressure traces. After the ignition phase, the laminar burning velocity remains quasi-steady until it is quenched by the chamber walls. The schlieren turbulent flame growths were somewhat faster than those deduced from the pressure traces, roughly by the amount of unburnt mixture embraced by the two-dimensional turbulent flame contour. Over the ranges of turbulence parameters studied, the turbulent burning velocity can be modelled by: $S_t/S_l - 1 = C_L u'/S_l$; where S_t is the turbulent burning velocity, S_l is the laminar burning velocity and u' is the root-mean-square turbulence intensity. The linear coefficient, C_L, designates the effectiveness of turbulence enhancement on the turbulent burning velocity. This linear coefficient increased continuously as the flame grew from ignition spark up to 55 mm radius limited by the size of the chamber. The linear coefficient decreased with the increase in the integral scale. In consequence, $C_L = C_D r/\sqrt{\Lambda} + C_I$; where C_D and C_I are constants, r is the flame radius and Λ is the integral scale. Alternatively, the turbulent burning velocity-turbulence intensity relation can be expressed as $S_t/S_l - 1 = C_D (r/\sqrt{\Lambda}) u'/S_l + C_I$.

A semi-empirical, multi-zone thermodynamics equilibrium flame growth model has been proposed. The model simulations are in sound qualitative agreement and fair quantitative agreement with the experiments.

ACKNOWLEDGEMENTS

The author is indebted to the following individuals for contributing their expertise in making this thesis successful:

Dr. W.T. Ashurst, for his studious guidance and valuable comments.

Dr. M.D. Checkel, for his diligent supervision.

Dr. J.D. Dale, for his productive inputs.

Dr. O.L. Gulder, for his willingness to be the external examiner and his beneficial comments.

Mr. R. Haley, for taking the high speed video and his generous supply of papers.

Dr. B. Johansson, for his helpful discussion and his generous supply of papers.

Dr. L.W. Kostiuk, for his unfailing assistance and constructive remarks.

Dr. P.R. Smy, for his worthwhile suggestions.

Mr. I. Buttar, Mr. B. Cielin, Mr. B. Faulkner, Mr. J. Foy, Mrs. T. Hilva, Mr. A. Muir, Mr. T. Nord and Mr. W. Pittman for their prompt assistance in solving various technical problems.

The generous supplies of papers and/or rewarding inputs by the following experts are gratefully acknowledged:

Dr. I.G. Assovskii, Prof. D. Bradley, Dr. T. Chikahisa, Prof. R. Evans, Prof. G.M. Faeth, Prof. Y. Hamamoto, Prof. P.H. Hill, Prof. S. Ishizuka, Prof. H. Kido, Mr. B. Leisenheimer, Dr. A. Maxson, Dr. D.L. Reuss, Dr. W. Roberts, Dr. P.D. Ronney, Dr. Y. Sakai, Dr. P. Witze, Prof. A. Yoshida and the reviewers of our papers.

The author is most grateful to the all-round support from his wife, Naomi, and his family.

The Mechanical Engineering Department, NSERC and the author's family are recognized for their financial support.

The author appreciates the companionship and support from the mechanical engineering graduate students of the years 1989 to 1994. Special thanks to Dr. L. Cremers, for translating a French paper, and Mr. C. Johnston, for easing the image digitization process.

The author is most grateful to the heavenly father for answering the prayers.

TABLE OF CONTENTS

CHAPTER PAGE

1. INTRODUCTION 1

1.1 Root of study 1

1.2 Objectives 3

1.3 Scope of study 3

1.4 Outline of thesis 5

2. BACKGROUND STUDIES 6

2.1 History of premixed turbulent flame study 6

2.1.1 Engine turbulence 7

2.2 Premixed laminar flame propagation 7

2.3 Premixed turbulent flame propagation 10

2.4 Wrinkled laminar flame versus distributed reaction zone 12

2.5 Modelling premixed turbulent flame 14

2.5.1 Turbulent burning velocity-turbulence intensity relation 17

2.6 Progressive turbulence enhancement 19

2.7 The effects of turbulent length scale 21

2.7.1 Tumble versus swirl flows in engines 24

2.8 Grid turbulence in a constant volume chamber 25

2.8.1 Normal decay 25

2.8.2 Rapid distortion 26

2.9 Concluding remarks 29

3. THE NUMERICAL FLAME GROWTH MODEL 46

3.1 Numerical algorithm 46

3.1.1 Quiescent combustion 46

3.1.2 Turbulent combustion 48

3.2 Semi-empirical parameters 49

3.3 Sensitivity analysis 50

4. EXPERIMENTAL DETAILS 54

4.1 Experiment and analysis 54

5. LAMINAR FLAME GROWTH RESULTS AND DISCUSSION 59

5.1 Experimental results 59

5.1.1 Comparison between schlieren video and pressure trace analysis 59

5.1.2 The effects of mixture stoichiometry on laminar flame growth 61

5.1.3 The effects of pressure on laminar flame growth 62

5.1.4 Laminar burning velocity as a function of flame radius 64

5.2 Comparing numerical simulations with experiments 65

5.2.1 Constant burning velocity laminar flame propagation 65

5.2.2 Laminar flame growth in a closed chamber 66

5.3 Summary of laminar flame growth in a chamber 66

6. TURBULENT FLAME GROWTH RESULTS AND DISCUSSION 81

6.1 Comparing schlieren images with pressure trace analysis 81

6.2 Turbulent flame growth versus laminar flame growth 83

6.3 Progressive wrinkling of a turbulent flame 85

6.4 Turbulent burning velocity-turbulence intensity relation 86

6.5 Turbulent burning velocity-mean strain rate relation 94

6.6 Eddy structure model 97

6.7 Overall combustion rate 99

6.8 Numerical flame growth model calculations 99

6.9 Summary of developing turbulent flame in a combustion chamber 102

7. CONCLUSIONS AND RECOMMENDATIONS 153

7.1 Summary and Conclusions 153

7.1.1 Laminar flame growth in a closed chamber 153

7.1.2 Turbulent flame growth in a closed chamber 154

7.2 Recommendations 157

7.2.1 Improvements in the experimental apparatus and analysis 157

7.2.2 Wider ranges of experimental parameters 158

REFERENCES 160

APPENDICES: 176

A. Idealized turbulent flows of single-size vortex tubes 176

B. Multi-zone thermodynamic equilibrium flame growth model 178

C. Pressure transducer calibration 194

D. Gas mixing using choked flow method 197

E. Gas analysis using MTI gas chromatograph 205

F. High speed schlieren video 208

G. Data collecting and analysis 210

H. Premixed laminar methane-air flame results 256

I. Premixed turbulent methane-air flame results 274

LIST OF TABLES

TABLE PAGE

2.1 Coefficients of turbulence correlation equations. 26

3.1 Comparison of methane-air adiabatic flame temperatures predicted by the present model with those calculated by STANJAN [Re87]. 48

3.2 Sensitivity analysis on 0.9 equivalence ratio, laminar methane-air flame ignited at 300 K and 1 atm. 51

3.3 Sensitivity analysis on 0.9 equivalence ratio, turbulent methane-air flame with initial turbulence intensity of 1 m/s and integral of 4 mm. 53

5.1 Pressure exponent of laminar burning velocity. 63

6.1 Summary of linear coefficient results. 91

6.2 Summary of least-squares fit results. 94

LIST OF FIGURES

FIGURE PAGE

2.1 One-dimensional, planar laminar flame growth. 30

2.2 One-dimensional, spherical laminar flame growth in open atmosphere. 31

2.3 One-dimensional, spherical laminar flame growth in a confined chamber. 32

2.4 One-dimensional, planar turbulent flame growth. 33

2.5 One-dimensional, spherical turbulent flame growth. 34

2.6 Wrinkled laminar flame. 35

2.7 Distributed reaction zone. 36

2.8 The eddy structure model. 37

2.9 The linear relation between u' and S_t. 38

2.10 Fully saturated wrinkled laminar flame fronts by small-core and large-core vortices. 39

2.11 Partially saturated wrinkled laminar flame fronts by small-core and large-core vortices.
Equal turbulence intensity and kinetic energy. 40

2.12 Normal turbulence decay behind a 60% solid, perforated plate. 41

2.13 The ideal vortex tube. 42

2.14 Compressing the ideal vortex tube. 43

2.15 Vortex tube distortion by a spherically advancing flame. 44

2.16 The rapid distortion effects on flame front turbulence. 45

4.1 The 125 mm cubical combustion chamber. 56

4.2 The 60% solid, perforated plate with 20 mm diameter holes. 57

4.3 A schematic of the experimental apparatus. 58

5.1 Typical laminar flame growth schlieren images.
Ø=0.7, 0.9; $P_{init}=1$ atm; $T_{init}=300$ K; $\Delta t=5.0$ ms for Ø=0.7 and 2.5 ms for Ø=0.9. 68

5.2 Comparison of laminar flame growth measured from schlieren images and the pressure trace.
Ø=0.7, 0.9; $P_{init}=1$ atm; $T_{init}=300$ K. 69

5.3 Comparison of laminar flame growth rate and laminar burning velocity calculated from schlieren images and the pressure trace.
Ø=0.9; P_{init}=1 atm; T_{init}=300 K. 70

5.4 The effects of mixture stoichiometry on laminar flame growth.
Ø=1.0, 0.9, 0.8, 0.7, 0.6; P_{init}=1 atm; T_{init}=300 K; Δt=2.5 ms for Ø=1.0, 0.9, 0.8; Δt=5.0 ms for Ø=0.7 and 10.0 ms for Ø=0.6. 71

5.5 The effects of mixture stoichiometry on combustion chamber pressure rise.
Ø=1.0, 0.9, 0.8, 0.7, 0.6; P_{init}=1 atm; T_{init}=300 K. 72

5.6 Laminar burning velocity as a function of equivalence ratio compared with others.
T_o=300 K, P_o=1 atm; Solid horizontal lines are the error bars due to uncertainty in mixture stoichiometry. 73

5.7 The effects of pressure on 0.9 equivalence ratio laminar flame growth.
P_{init}=0.5, 1.0, 2.0 atm; T_{init}=300 K; Δt=2.5 ms. 74

5.8 The effects of pressure on 0.7 equivalence ratio laminar flame growth.
P_{init}=0.5, 1.0, 2.0 atm; T_{init}=300 K; Δt=5 ms. 75

5.9 The effects of pressure on laminar burning velocity.
Ø=0.9, 0.7; P_{init}=0.5, 1.0, 1.5, 2.0 atm; T_{init}=300 K. 76

5.10 Typical laminar burning velocities as functions of flame radius.
Ø=1.0, 0.9, 0.8, 0.7, 0.6; P_{init}=1.0 atm; T_{init}=300 K. 77

5.11 Stretch rates for the outwardly propagating spherical flames.
Ø=1.0, 0.9, 0.8, 0.7, 0.6; P_{init}=1.0 atm; T_{init}=300 K. 78

5.12 Comparing experimental pressure traces with numerical calculations assuming constant laminar burning velocities.
Ø=1.0, 0.9, 0.8, 0.7, 0.6; P_{init}=1.0 atm; T_{init}=300 K. 79

5.13 Comparing experimental pressure traces with numerical calculations using quasi-steady laminar burning velocities.
Ø=1.0, 0.9, 0.8, 0.7, 0.6 with Pexp=-0.26, -0.26, -0.35, -0.43, -0.43 respectively and Texp=2; P_{init}=1.0 atm; T_{init}=300 K. 80

6.1 Typical turbulent and laminar flame schlieren images.

$\O=0.9$; $P_{init}=1$ atm; $T_{init}=300$ K. 104

6.2a Typical 0.9 equivalence ratio turbulent and laminar flame growths from schlieren images compared with pressure trace analysis.
$\Lambda \approx 8$ mm; $P_{init}=1$ atm; $T_{init}=300$ K. 105

6.2b Typical 0.9 equivalence ratio turbulent and laminar flame growths from schlieren images compared with pressure trace analysis.
$\Lambda \approx 4$ mm; $P_{init}=1$ atm; $T_{init}=300$ K. 106

6.2c Typical 0.9 equivalence ratio turbulent and laminar flame growths from schlieren images compared with pressure trace analysis.
$\Lambda \approx 2$ mm; $P_{init}=1$ atm; $T_{init}=300$ K. 107

6.2d Typical 0.9 equivalence ratio turbulent and laminar flame growths from schlieren images compared with pressure trace analysis.
$\Lambda \approx 1$ mm; $P_{init}=1$ atm; $T_{init}=300$ K. 108

6.3a Typical 0.7 equivalence ratio turbulent and laminar flame growths from schlieren images compared with pressure trace analysis.
$\Lambda \approx 8$ mm; $P_{init}=1$ atm; $T_{init}=300$ K. 109

6.3b Typical 0.7 equivalence ratio turbulent and laminar flame growths from schlieren images compared with pressure trace analysis.
$\Lambda \approx 4$ mm; $P_{init}=1$ atm; $T_{init}=300$ K. 110

6.3c Typical 0.7 equivalence ratio turbulent and laminar flame growths from schlieren images compared with pressure trace analysis.
$\Lambda \approx 2$ mm; $P_{init}=1$ atm; $T_{init}=300$ K. 111

6.3d Typical 0.7 equivalence ratio turbulent and laminar flame growth from schlieren images compared with pressure trace analysis.
$\Lambda \approx 1$ mm; $P_{init}=1$ atm; $T_{init}=300$ K. 112

6.4 Effects of turbulence level on typical 0.9 equivalence ratio flame growth rate as a function of flame size.
$\O=0.9$; $\Lambda=4$ mm; $u'_{ign}=0$, 1.0, 1.5 m/s; $P_{init}=1$ atm; $T_{init}=300$ K. 113

6.5 Effects of turbulence level on typical 0.7 equivalence ratio flame growth rate as a function of flame size.
$\O=0.7$; $\Lambda=4$ mm; $u'_{ign}=0$, 1.0, 1.5 m/s; $P_{init}=1$ atm; $T_{init}=300$ K. 114

6.6 Effects of turbulence intensity on typical 0.9 equivalence ratio burning velocity as a function of flame size.
$\O=0.9$; $\Lambda=4$ mm; $u'_{ign}=0$, 1.0, 1.5 m/s; $P_{init}=1$ atm; $T_{init}=300$ K. 115

6.7 Effects of turbulence intensity on typical 0.7 equivalence ratio burning velocity as a function of flame size.
$\O=0.7$; $\Lambda=4$ mm; $u'_{ign}=0$, 1.0, 1.5 m/s; $P_{init}=1$ atm; $T_{init}=300$ K. 116

6.8 Progressive turbulence enhancement illustrated by schlieren flame growth images.
$\O=0.9$; $\Lambda\approx8$ mm; $P_{init}=1$ atm; $T_{init}=300$ K. 117

6.9 The square of flame perimeter ratio as functions of flame radius and turbulence intensity.
$\O=0.9$; $\Lambda\approx8$ mm; $P_{init}=1$ atm; $T_{init}=300$ K. 118

6.10 Normalized turbulent burning velocities as functions of normalized turbulence intensities, $S_t/S_l - 1 = C_L u'/S_l$, for typical 23 mm radius, 0.9 equivalence ratio turbulent flames.
$\O=0.9$; $\Lambda\approx2$, 4, 8 mm; $P_{init}=1$ atm; $T_{init}=300$ K. 119

6.11 Typical plots of $S_t/S_l - 1$ against u'/S_l as the flame grows.
$\O=0.9$; $\Lambda\approx4$ mm; $r=23$, 46, 55 mm; $P_{init}=1$ atm; $T_{init}=300$ K. 120

6.12a Plots of normalized turbulent burning velocity, S_t/S_l-1, against normalized turbulence intensity, u'/S_l, for typical 23 mm radius, fine scale, turbulent flames.
$\O=0.7$, 0.9; $\Lambda\approx1$ mm; $P_{init}=1$ atm; $T_{init}=300$ K. 121

6.12b Plots of normalized turbulent burning velocity, S_t/S_l-1, against normalized turbulence intensity, u'/S_l, for typical 23 mm radius, small scale, turbulent flames.
$\O=0.7$, 0.9; $\Lambda\approx2$ mm; $P_{init}=1$ atm; $T_{init}=300$ K. 122

6.12c Plots of normalized turbulent burning velocity, S_t/S_l-1, against normalized turbulence intensity, u'/S_l, for typical 23 mm radius, medium scale, turbulent flames.
$\O=0.7$, 0.9; $\Lambda\approx4$ mm; $P_{init}=1$ atm; $T_{init}=300$ K. 123

6.12d Plots of normalized turbulent burning velocity, S_t/S_l-1, against normalized

turbulence intensity, u'/S_l, for typical 23 mm radius, large scale, turbulent flames.
$\phi=0.7, 0.9$; $\Lambda\approx 8$ mm; $P_{init}=1$ atm; $T_{init}=300$ K. 124

6.13a Plots of normalized turbulent burning velocity, S_t/S_l-1, against normalized turbulence intensity, u'/S_l, for typical 55 mm radius, fine scale, turbulent flames.
$\phi=0.7, 0.9$; $\Lambda\approx 1$ mm; $P_{init}=1$ atm; $T_{init}=300$ K. 125

6.13b Plots of normalized turbulent burning velocity, S_t/S_l-1, against normalized turbulence intensity, u'/S_l, for typical 55 mm radius, small scale, turbulent flames.
$\phi=0.7, 0.9$; $\Lambda\approx 2$ mm; $P_{init}=1$ atm; $T_{init}=300$ K. 126

6.13c Plots of normalized turbulent burning velocity, S_t/S_l-1, against normalized turbulence intensity, u'/S_l, for typical 55 mm radius, medium scale, turbulent flames.
$\phi=0.7, 0.9$; $\Lambda\approx 4$ mm; $P_{init}=1$ atm; $T_{init}=300$ K. 127

6.13d Plots of normalized turbulent burning velocity, S_t/S_l-1, against normalized turbulence intensity, u'/S_l, for typical 55 mm radius, large scale, turbulent flames.
$\phi=0.7, 0.9$; $\Lambda\approx 8$ mm; $P_{init}=1$ atm; $T_{init}=300$ K. 128

6.14 Linear coefficient as a function of flame radius and the square-root of integral scale. 129

6.15a Normalized turbulent burning velocity, S_t/S_l-1, as a function of $(r/\sqrt{\Lambda})(u'/S_l)$. The turbulence intensity, u', is based on normal turbulence decay. 130

6.15b Normalized turbulent burning velocity, S_t/S_l-1, as a function of $(r/\sqrt{\Lambda})(u'/S_l)$. The turbulence intensity, u', is based on normal turbulence decay and compression. 131

6.15c Normalized turbulent burning velocity, S_t/S_l-1, as a function of $(r/\sqrt{\Lambda})(u'/S_l)$. The turbulence intensity, u', is based on normal turbulence decay, compression and rapid distortion. 132

6.16a Normalized turbulent burning velocity, S_t/S_l-1, as a function of the rate of strain. $\Lambda \approx 8$ mm; Ø=0.7, 0.9; $r=19$ mm (schlieren images), 27 mm (schlieren images), 55 mm (pressure traces). 133

6.16b Normalized turbulent burning velocity, S_t/S_l-1, as a function of the rate of strain. $\Lambda \approx 4$ mm; Ø=0.7, 0.9; $r=19$ mm (schlieren images), 27 mm (schlieren images), 55 mm (pressure traces). 134

6.16c Normalized turbulent burning velocity, S_t/S_l-1, as a function of the rate of strain. $\Lambda \approx 2$ mm; Ø=0.7, 0.9; $r=19$ mm (schlieren images), 27 mm (schlieren images), 55 mm (pressure traces). 135

6.17a Normalized turbulent burning velocity, S_t/S_l-1, as a function of the rate of strain. $\Lambda \approx 2$, 4, 8 mm; Ø=0.9; $r=55$ mm (pressure traces). 136

6.17b Normalized turbulent burning velocity, S_t/S_l-1, as a function of the rate of strain. $\Lambda \approx 2$, 4, 8 mm; Ø=0.7; $r=55$ mm (pressure traces). 137

6.18 Normalized turbulent burning velocity, S_t/S_l-1, as a function of Karlovitz stretch factor. $\Lambda \approx 2$, 4, 8 mm; Ø=0.7, 0.9; $r=55$ mm (pressure traces). 138

6.19a The normalized turbulent burning velocity, S_t/S_l-1, as a function of Karlovitz stretch factor and flame size. $\Lambda \approx 2$, 4, 8 mm; Ø=0.9; $r=19$ mm (schlieren images), 55 mm (pressure traces). 139

6.19b The normalized turbulent burning velocity, S_t/S_l-1, as a function of Karlovitz stretch factor and flame size. $\Lambda \approx 2$, 4, 8 mm; Ø=0.7; $r=19$ mm (schlieren images), 55 mm (pressure traces). 140

6.20a Comparing eddy structure model predictions with experiments. Ø=0.9; $\Lambda \approx 2$, 4, 8 mm; $r=19$ mm (schlieren images), 55 mm (pressure traces). 141

6.20b Comparing eddy structure model predictions with experiments. Ø=0.7; $\Lambda \approx 2$, 4, 8 mm; $r=19$ mm (schlieren images), 55 mm (pressure traces). 142

6.21 Comparing turbulent flame pressure rise simulations with experiments. Ø=0.7; $\Lambda \approx 8$ mm; $u'_{ign}=0$, 1.0, 2.0 m/s; $P_{init}=1$ atm; $T_{init}=300$ K. 143

6.22 Numerical simulations of u' effects on combustion chamber pressure rise. Ø=0.7; $\Lambda \approx 4$ mm; $u'_{ign}=0$, 0.5, 1.0, 1.5, 2.0 m/s; $P_{init}=1$ atm;

$T_{init}=300$ K. 144

6.23 Numerical simulations of u' effects on burning velocity as a function of flame radius.
$\varnothing=0.7$; $\Lambda\approx4$ mm; $u'_{ign}=0$, 0.5, 1.0, 1.5, 2.0 m/s; $P_{init}=1$ atm; $T_{init}=300$ K. 145

6.24 Numerical simulations of fixed u' effects on combustion chamber pressure rise.
$\varnothing=0.7$; $\Lambda\approx4$ mm; u' fixed at 0, 0.5, 1.0, 1.5, 2.0 m/s; $P_{init}=1$ atm; $T_{init}=300$ K. 146

6.25 Numerical simulations of fixed u' effects on burning velocity as a function of flame radius.
$\varnothing=0.7$; $\Lambda\approx4$ mm; u' fixed at 0, 0.5, 1.0, 1.5, 2.0 m/s; $P_{init}=1$ atm; $T_{init}=300$ K. 147

6.26 Numerical simulations of integral scale effects on combustion chamber pressure rise.
$\varnothing=0.7$; $\Lambda\approx2$, 4, 8 mm; $u'_{ign}=1.0$ m/s; $P_{init}=1$ atm; $T_{init}=300$ K. 148

6.27 Numerical simulations of integral scale effects on burning velocity as a function of flame radius.
$\varnothing=0.7$; $\Lambda\approx2$, 4, 8 mm; $u'_{ign}=1.0$ m/s; $P_{init}=1$ atm; $T_{init}=300$ K. 149

6.28 Numerical simulations of integral scale effects with fixed u' on combustion chamber pressure rise.
$\varnothing=0.7$; $\Lambda\approx2$, 4, 8 mm; u' fixed at 1.0 m/s; $P_{init}=1$ atm; $T_{init}=300$ K. 150

6.29 Numerical simulations of integral scale effects with fixed u' on burning velocity as a function of flame radius.
$\varnothing=0.7$; $\Lambda\approx2$, 4, 8 mm; u' fixed at 1.0 m/s; $P_{init}=1$ atm; $T_{init}=300$ K. 151

6.30 Numerical simulations of spark size effects on combustion chamber pressure rise.
$\varnothing=0.7$; $\Lambda\approx4$ mm; $u'_{ign}=1.0$ m/s; $r_{spark}\approx2$, 4, 6 mm; $P_{init}=1$ atm; $T_{init}=300$ K. 152

NOMENCLATURE

A	flame front surface area
A_m	surface area of a smooth-surfaced spherical flame
$c, c_1, \ldots$	constants or coefficients
$C, C_1, \ldots$	constants or coefficients
C_D	dependence coefficient, displaying how strongly C_L depends on $r/\sqrt{\Lambda}$
C_I	initial coefficient, the spark-induced turbulence enhancement on burning velocity.
C_L	linear coefficient, showing the effectiveness of turbulence enhancement on the turbulent burning velocity
C_p	specific heat capacity at constant pressure
d	diffusivity of the deficient reactant
D	plate hole diameter
Da	Damkohler's number, turbulent residence time/chemical residence time, $(\Lambda/u')/(\delta_l/S_l)$
EGR	exhaust gas recirculation
k	stretch rate
K	Karlovitz stretch factor, turbulent strain rate/laminar strain rate, $(u'/\lambda)/(S_l/\delta_l)$
L, L_o, L_1	length
Le	Lewis number, thermal diffusivity/deficient reactant diffusivity, $\alpha/(\rho C_p d)$
m	mass
m_u	mass of the unburned mixture element to be burned
M	mass
N	newton
P	pressure
P_e	pressure after combustion at thermodynamic equilibrium
P_i	pressure before combustion
P_{init}	initial unburned mixture pressure
P_o	reference pressure, 1 atm
Pexp	pressure exponent, designating the pressure effects

Q	heat transfer
r	flame radius
r_o, r_1	radius
r_c	core radius of a vortex
r_m	mean flame radius
r_{spark}	spark radius
r_u	radial thickness of the unburnt element to be burned
r_{um}	mean radial thickness of the unburnt element to be burned
rms	root-mean-square
R	radius
R_o	a specific size radius
R^2	coefficient of determination
Re	Reynolds number
Re_η	Reynolds number based on Kolmogorov scale, $u'\eta/\nu$
Re_Λ	Reynolds number based on integral scale, $u'\Lambda/\nu$
R_l	laminar flame growth rate
R_t	turbulent flame growth rate
$S_{b,w}$	burnt gas velocity relative to the combustion wave in the direction normal to the wave
S_l	laminar burning velocity
S_{lo}	laminar burning velocity at 1 atm and 300 K
S_t	turbulent burning velocity
$S_{u,w}$	unburnt gas velocity relative to the combustion wave in the direction normal to the wave
t	time
T	temperature
T_o	reference temperature, 300 K
T_{ad}	adiabatic flame temperature
T_{init}	initial unburned mixture temperature
Texp	temperature exponent, designating the temperature effects on burning velocity

u'	root-mean-square turbulence intensity
u'_{ign}	ignition-time root-mean-square turbulence intensity
U	perforated plate velocity
U_p	internal energy of the products
U_r	internal energy of the reactants
V_e	element volume after combustion at thermodynamic equilibrium
V_i	element volume before combustion
W_{comp}	work of compression
x	distance from a reference location
x_m	mean distance from a reference location
x_{um}	mean distance of the unburnt mixture from a reference location
X	distance downstream of the perforated plate
α	thermal diffusivity
Δ	delta, a small interval
δ_l	laminar flame front thickness
ϵ	turbulence dissipation rate
Ø	equivalence ratio of the mixture
Γ	circulation
γ	specific heat ratio
η	Kolmogorov scale
η_{th}	thermal efficiency or indicated fuel conversion efficiency
Λ	integral length scale
λ	Taylor microscale
ν	kinematic viscosity
π	pi, 3.1415927
ρ	density
ρ_b	density of the burnt mixture
ρ_u	density of the unburnt mixture
ω, ω_o, ω_1	vorticity

UNIT

atm	pressure in atmospheres (1 atm = 101.325 kPa)
K	degree Kelvin
kPa	kilo-Pascals or 10^3 N/m^2
m	metre
mJ	10^{-3} Joule
mm	10^{-3} metre
ms	10^{-3} second
s	second
V	Volt
μF	10^{-6} Faraday

CHAPTER 1
INTRODUCTION

This thesis studies how turbulence affects the propagation of a spark-ignited, premixed, methane-air flame in a combustion chamber. The effects due to root-mean-square (rms) turbulence intensity, turbulent length scale and flame radius on the growing flame are investigated. The experimental results evolve to a semi-empirical turbulent flame growth model. This model can predict the separate effects of rms turbulence intensity, turbulent length scale and spark size on the combustion process over a wide range of turbulence conditions.

1.1: ROOT OF STUDY

Part of the practical incentive behind this fundamental study is to enhance slow burning flame propagation. The slow burning mixtures can be either fuel lean or exhaust diluted (exhaust gas recirculation, EGR). For an ideal Otto cycle [He88, VS78][1], the thermal efficiency or the indicated fuel conversion efficiency,

$$\eta_{th} = 1 - \frac{1}{(\text{compression ratio})^{(\gamma - 1)}} \qquad 1.1$$

where γ is the specific heat ratio. The equation illustrates that the thermal efficiency can be increased by increasing the compression ratio and/or the specific heat ratio. Both fuel lean and EGR mixtures lead to higher specific heat ratio and hence, higher thermal efficiency [He88]. Many studies [CN59, CM56, CC49, Ke47, Sp21, Gi20, Ke20] have confirmed that raising the compression ratio is a feasible practice to increase the engine efficiency. Increasing the compression ratio in an engine increases the tendency towards knocking [HT94, CN59, Ke47, WL21, Ke20]. Therefore, in order to allow the use of higher compression ratios, the mixture octane number needs to be improved. Fuel lean and EGR mixtures improve the mixture chemical octane quality, and hence, these mixtures permit the use of higher compression ratios [RS94, RC93, CL28].

---

[1] Symbols in brackets, [], designate references which are presented after Chapter 7.

In short, fuel lean or EGR mixtures can improve engine efficiency [Jo94, Ev92, DN90, HS87]. The excess oxygen in fuel lean mixtures can oxidize carbon monoxide and unburnt hydrocarbons [Ev92]. This can result in more complete combustion and lower emissions. Very lean or high EGR mixture lowers the combustion temperature and hence reduces NO_x emissions [He88]. In other words, in addition to improving engine efficiency and fuel economy [MI85], lean or EGR combustion in spark-ignition engine is also means of lowering emissions [Jo94, Op93, Ev92, DN90].

Fuel lean and high EGR mixtures burn more slowly than stoichiometric mixtures. These slower burning mixtures can lead to poor combustion phasing in which combustion can not be completed around top-dead-centre. Slower burning can also result in larger heat losses. Both poor combustion phasing and increased heat losses can lead to a loss of engine power. In short, while fuel lean and EGR mixtures can be used for reducing combustion emissions and increasing thermal efficiency, enhancement in combustion rate is required in order to reduce the negative effects of slow burning.

Turbulence has been known to enhance burning rate for many decades. In general, researchers [BC94, Al92, EN92, Je92, HI90, LN90, LL88, AB87, AA84, AB83, NT83, LK76, BL75, Ka52, Da40, BT37, Ma34, Ho21, WL21, MH20, Wh19, Cl13, ML83] agree qualitatively that the burning rate increases with increasing rms turbulence intensity. However, there is a lack of quantitative agreement on turbulence intensity effect on the burning rate. There are also disagreements about the turbulent length scale effects. Moreover, experimental results obtained from combustion engines are difficult to interpret. The moving piston along with the uniqueness of the individual engine usually complicate the data reduction and analysis process. It is the scope of this thesis to resolve some of these discrepancies. The centre of this study is the progressive turbulence enhancement on the burning rate of a flame as it grows. In other words, this study focuses on understanding the turbulence enhancement of flame growth rate and burning rate of a premixed, expanding flame.

1.2: OBJECTIVES

The main objective here is to understand the various turbulence effects on a premixed flame ball as it grows in a combustion chamber. Whether turbulence enhancement is beneficial or not, understanding the interaction between the turbulence and the flame can allow engineers and scientists to control and model the system. The study separates the rms turbulence intensity effect on the expanding flame from the turbulent length scale effect. Most importantly, the flame size effect on the turbulence-burning rate relation is examined.

The experimental part of the study was conducted in a 125 mm cubical combustion chamber. Premixed methane-air mixtures were ignited at 300 K and 1 atm. In the turbulent flame growth studies, the ignition time rms turbulence intensity was up to 2 m/s with integral scale of 1, 2, 4 or 8 mm.

With the experimentally determined relations between burning rate, turbulence intensity, turbulent length scale and flame size, a semi-empirical, multi-zone thermodynamic equilibrium, flame growth model is proposed. With this flame growth model, it is possible to simulate noise-free combustion processes (such as smooth pressure traces without noise interference) given the initial conditions. The numerical simulations are used to analyze the sensitivity of various parameters on the combustion rates. The semi-empirical model can predict the independent effects of turbulence intensity, integral scale and spark size on the combustion rates.

1.3: SCOPE OF STUDY

Previous studies such as [Mo90, Mc88, CT83, Ch81] provide the foundation of this study. The accumulated knowledge from these previous studies along with the more recent studies such as [CT92, CT92a, Ti92, CT93, TC93, AC93, TC94, TC94a, TC94b, TC94c, TC94d, AC94] evolves to the present thesis.

The only fuel considered in this study is methane. Methane is the main component of natural gas. Natural gas is a promising alternative fuel because of its availability, ease of integration into the mainstream market, and its potential economic and environmental benefits [BL93, UB93]. Natural gas can allow a remarkable reduction of pollutant emissions, a decrease in CO_2 production, and an improvement in thermal efficiency [UB93]. In addition, the strength and vigorous requirements of compressed natural gas systems on automobiles coupled with the physical and combustion characteristics of methane make natural gas a safe automotive fuel [Ka83]. Natural gas has the advantages over gasoline because of its wide flammability [CK92] and its much higher octane number [FO85, UB93]. Methane is less suspectable to mixture stoichiometry error than propane due to its larger volume fraction for the same stoichiometric mixture.

From stoichiometric to 70% stoichiometric methane-air flames, the Lewis number stays close to unity. Lewis number is the ratio of thermal diffusivity over deficient reactant diffusivity, that is,

$$Le = \frac{\alpha}{\rho \, C_p \, d} \qquad 1.2$$

where α is the thermal conductivity, ρ is the density, C_p is the specific heat capacity at constant pressure and d is the diffusivity of the deficient reactant. Stoichiometric and 72% stoichiometric methane-air mixtures have Lewis number of 1.01 and 0.97 respectively [AA84, AB84]. The near unity Lewis number, lean methane-air mixtures simplify the problem as the Lewis number effect can be omitted. Lean methane-air mixtures also have near-zero Markstein numbers. Markstein length is a measure of the response of a flame to stretch [page 22 of Ma64, Cl85]. A dimensionless Markstein number can be defined as the Markstein length divided by the local characteristic flame thickness. A flame with zero Markstein number is not affected by stretch. The Markstein numbers for 0.9 and 0.7 equivalence ratio[2] flames are 1.8 and -0.2 respectively [TI93]. These values are used to illustrate that most of the methane-air flames considered in this study are relatively insensitive to stretch. The actual flame response to stretch and the validity of these Markstein numbers are outside the scope of this thesis.

---

[2] Equivalence ratio, Ø = 9.52 Fuel-Air ratio by volume, since the ideal stoichiometric methane-air combustion reaction is $CH_4 + 2\,(O_2 + 3.76\,N_2) \rightarrow CO_2 + 2\,H_2O + 7.52\,N_2$.

The combustion chamber used in this study has several advantages over many other combustion chambers. The current chamber generates clean and controllable decaying grid turbulence. It allows the variation of turbulence intensity and turbulent length scale independently over wide ranges. The expanding, roughly spherical flame closely resembles idealized engine combustion.

1.4: OUTLINE OF THESIS

This research is an extension of previous studies by Ting [Ti92], Modien [Mo90], McDonell [Mc88], and Checkel and Thomas [CT83, Ch81]. The combustion chamber used in this study was the same as that used by Ting, Modien and McDonell [Ti92, Mo90, Mc88]. With improvements in experimental apparatus and improved analysis, this study aimed at uncovering the transient relation between turbulence and burning rate as the flame grows.

The next chapter reviews the background studies in this area. It examines some of the theories about laminar and turbulent flame growth in a combustion chamber. The decaying turbulence in the combustion chamber and the effects due to an expanding flame are also discussed. Chapter 3 details the semi-empirical flame growth model. Chapter 4 presents the experimental details. It covers the data collecting and analysing procedure. Laminar flame growth results are summarized and discussed in Chapter 5. Chapter 6 summarizes the turbulent flame growth results. Conclusions are drawn in Chapter 7 along with various recommendations for further research in this area.

CHAPTER 2

BACKGROUND STUDIES

This chapter goes through the theory and literature of premixed turbulent flame growth. It defines some important terms used throughout this thesis. Some of the definitions may not agree universally with the definitions in the literature. However, all definitions used here are self consistent in this thesis. The evolution of decaying combustion chamber turbulence under the influence of a propagating flame is also addressed.

2.1: HISTORY OF PREMIXED TURBULENT FLAME STUDY

Our ancestors must had been very amazed by fire when it was first passed down to the earth by the Prometheus [Wi92], if the legend was true. Human beings have since taken this very complicated piece of science for granted. Their knowledge about fire was limited by their experience. Even in antiquity, they learned the trick of blowing and fanning the fire to enhance its burning rate. It was centuries from there before Lavoisier [La17] discovered the role of oxygen in combustion in the eighteenth century. Blowing introduces extra air and hence, oxygen, to the flame. The additional oxygen offered by blowing enables a faster oxidation process to take place and hence a faster burning rate. It was not until the late nineteenth century that combustion scientists started to understand the other reason behind the enhanced burning rate with blowing or fanning. The phenomenon is called turbulence enhancement.

Mallard and Le Chatelier [ML83] were the first persons who recorded the effects of turbulence on flame propagation. According to them [ML83], turbulence enhancement in combustion was first noted by Schloesing and de Mondesir in 1864 [WL21]. The discovery was then forgotten until Clerk and Hopkinson's investigations in 1912 [WL21]. Many scientists and engineers have since struggled with the turbulent flame problem. Other than Schloesing, de Mondesir, Mallard, La Chatelier [ML83], Clerk and Hopkinson [WL21], Wheeler [Wh19], Mason and Ricardo are also among the pioneers in turbulent combustion research [Ho21]. Damkohler [Da40] came in late among the pioneers in turbulent flame research. However, he is still recognized as the most important contributor in premixed turbulent study by many researchers today.

2.1.1: ENGINE TURBULENCE

Ever since the invention of the first internal combustion engine, turbulence had been playing its crucial role in engine combustion. Gas engines would had been impracticable had the rates of explosion been the same in actual engine cylinders as in closed-vessel experiments [Cl13]. Indeed, Clerk and Hopkinson were the first engine researchers who uncovered the important role of turbulence in engine combustion [Cl13, Cl21]. Separately, they discovered that the rate of combustion increases as a consequence of the eddying motion of the combustion gas. In other words, they found that an increase in piston speed increases the in-cylinder eddying motion and hence, increases the combustion rate significantly. Other than increasing the engine speed engine turbulence can also be increased via valve design [SC93, HN92], chamber design [HN92, LB82, Ma75] and piston design [Ev92, ET90]. While the fundamental physics behind turbulent combustion is yet to be completely uncovered, many engine designers [CS88, CM56, HF50] have accomplished numerous successes in optimizing particular engines. Most of these earlier successes in fast-burn, efficient engines were based on trail and error along with limited knowledge about turbulent combustion. More systematic, idealized studies (such as this study) are needed to better understand the effects of turbulence on engine combustion.

2.2: PREMIXED LAMINAR FLAME PROPAGATION

Figure 2.1 shows a tube with the quiescent combustible gas mixture ignited at the closed end. A combustion wave spreads through the gas towards the open end. In the idealized situation, the combustion wave propagates as a one dimensional, planar wave at a constant speed relative to the tube. The flame growth rate, R_l, is simply the rate of flame front propagation with respect to the tube. Specifically,

$$R_l = \frac{dx}{dt} \qquad 2.1$$

where dx/dt is the rate of change of flame front or combustion wave location with respect to the tube. Mass burning rate is the mass consumption rate of the unburnt mixture by the flame. The mass burning rate is equal to the rate at which the flame wave overtakes the unburnt mixture, that is,

$$\frac{dm_u}{dt} = \rho_u S_{u,w} A \qquad 2.2$$

where ρ_u is the unburnt gas density, $S_{u,w}$ is the unburnt gas velocity relative to the combustion wave in the direction normal to the wave and A is the flame front surface area. For the one dimensional, planar flame illustrated in Figure 2.1, the flame front surface area is a constant which is equal to the cross-sectional area of the tube. Laminar burning velocity is the velocity of the combustion wave relative to the unburned gas ahead of the wave in the direction normal to the wave surface. In other words, laminar burning velocity, S_l, is equal to $S_{u,w}$. This laminar burning velocity is also called flame velocity, normal combustion velocity or laminar flame speed [LV67, Gl87, Wi85]. This laminar burning velocity can be calculated as the mass burning rate per unit unburnt gas density per unit flame front area according to Equation 2.2. Alternatively, laminar burning velocity is the rate of unburnt mixture thickness consumed by the flame or dx_u/dt as shown in the figure.

For a spark-ignited, radially expanding spherical flame in an open atmosphere as shown in Figure 2.2, the flame growth rate and laminar burning velocity are similar to those of the planar case when the flame is large. The flame growth rate is the rate at which the flame front propagates away from the ignition point or the centre of the spherical flame. As shown in the figure, the flame growth rate,

$$R_l = \frac{dr}{dt} \qquad 2.3$$

where dr/dt is the rate of increase in flame radius. The laminar burning velocity is the rate at which the thickness of the unburnt mixture is consumed. The expression for the laminar burning velocity is

$$S_l = \frac{dr_u}{dt} \tag{2.4}$$

where dr_u/dt is the consumption rate of the concentric shell thickness of the unburnt mixture. For a spherically expanding flame of zero flame front thickness, the laminar burning velocity can also be calculated from

$$S_l = \frac{1}{\rho_u A}\frac{dm_u}{dt} \tag{2.5}$$

since the area on the unburned side, A, is equal to the area on the burned side. It should be noted that for a finite thickness flame front, the value for the laminar burning velocity, S_l, depends on the flame front area, A. However, there is an effective flame sheet location for flame area calculations in a strained flame [CB94, Ko94, SK94]. The laminar burning velocity calculated at this effective flame sheet location is equal to the one-dimensional, planar laminar burning velocity. In other words, the equivalent flame sheet location can characterize the flame in both physical space and progress variable space [CB94].

In a closed chamber, the confinement limits the free movement of the unburnt mixture ahead of the flame front. The expanding spherical flame shown in Figure 2.3 causes the combustion chamber pressure to rise. The laminar burning velocity is the concentric shell thickness of the unburnt mixture divided by the time taken to consumed it. The concentric shell thickness of the unburnt mixture is calculated as the volume of the unburnt mixture divided by the mean flame surface area. The mean flame surface area is the surface area of the sphere of the geometric mean flame radius. The geometric mean flame radius is the root-mean-square of the compressed initial flame radius and the final flame front radius as illustrated in Figure 2.3.

Closed vessel combustion causes the chamber pressure to rise. Higher pressure tends to lower the burning velocity of hydrocarbon-air flames. In other words, pressure has a negative effect on methane-air flame propagation. One of the indirect effects caused by the pressure rise in compressing both burnt and unburnt mixtures is the increase in the corresponding temperatures. The rise in unburnt mixture temperature tends to increase the burning velocity. It is a common practise to express the pressure and temperature effects in the power form [MK80, RG80]. Specifically,

$$S_l = S_{lo} \left(\frac{P}{P_o}\right)^{Pexp} \left(\frac{T}{T_o}\right)^{Texp} \qquad 2.6$$

where S_{lo} is the reference laminar burning velocity at the reference pressure, P_o, of 1 atm and the reference temperature, T_o, of 300 K, and Pexp and Texp are the pressure and temperature exponents respectively.

Other than the pressure and temperature effects, the laminar flame can also be affected by non-unity Lewis number, non-zero Markstein number, curvature, stretch, instabilities and the shape of the combustion chamber. As mentioned in section 1.3, only near-unity Lewis number and near-zero Markstein number cases are considered. With relatively thin flame front thickness of the order of 0.5 mm [GM92], the effect due to curvature is only significant when the flame radius is of the same order. The smallest mean flame radius considered in this thesis is about 15 mm. At this 15 mm flame radius, the mean flame radius is more than an order of magnitude larger than the flame thickness and hence, the curvature is small. The stretch effect is small for the near-zero Markstein number flames considered in this study. The various effects on the laminar flame are discussed again in Chapter 5 along with the experimental laminar flame results.

2.3: PREMIXED TURBULENT FLAME PROPAGATION

Under the influence of a moderate level of turbulence, the planar flame front or combustion wave can be wrinkled and distorted as shown in Figure 2.4. The rate of flame front propagation can be altered significantly due to changes in flame front surface area and flame front geometry along with possible modifications in the local burning velocity. The turbulent flame growth rate is the rate at which the mean flame front propagates relative to the tube. The "mean" flame front is an arbitrary smoothed planar flame front of zero thickness which embraces the burnt fraction to the left of it as shown in Figure 2.4. In other words, the turbulent flame growth rate as defined here is really the flame travel rate. Therefore, this flame growth rate also applies to turbulent flames in the distributed reaction zone. Specifically, the flame growth rate,

$$R_t = \frac{dx_m}{dt} \tag{2.7}$$

where dx_m/dt is the rate of mean flame front displacement with respect to the tube. The turbulent burning velocity is defined as the volumetric rate of consumption of the unburnt mixture per unit cross-sectional area of the tube. Figure 2.4 expresses the turbulent burning velocity as

$$S_t = \frac{dx_{um}}{dt} \tag{2.8}$$

where dx_{um}/dt is the mean consumption rate of the thickness of the unburned mixture assuming a smooth-surfaced, one-dimensional, planar flame front. This turbulent burning velocity can be calculated from the mass burning rate as:

$$S_t = \frac{1}{\rho_u A} \frac{dm_u}{dt} \tag{2.9}$$

With the unburnt gas density, ρ_u, and the tube cross-sectional area, A, the same as the laminar values, the turbulent burning velocity is different from its laminar partner due to the different mass burning rates. The modification in the mass burning rate in the presence of turbulence includes alteration in flame surface area and variation of local laminar burning velocity due turbulence interactions. These features are further investigated in section 2.4.

For a spark-ignited, spherically growing flame, the presence of turbulence can wrinkle and distort the flame front in a similar way as that of Figure 2.4. The flame growth rate is calculated as the propagation rate of the mean flame front in the radial direction. Figure 2.5 illustrates that the wrinkled and distorted flame is treated as a smooth-surfaced sphere with volume equal to that of the burnt volume. According to the figure, the flame growth rate can be expressed as

$$R_t = \frac{dr_m}{dt} \tag{2.10}$$

where dr_m/dt is the growth rate of the mean flame radius of a smooth-surfaced sphere of volume equal to the burnt mixture. The turbulent burning velocity is the rate of consumption of the average thickness of the unburnt mixture over the smooth-surfaced sphere of burnt volume. Specifically, the turbulent burning velocity,

$$S_t = \frac{dr_{um}}{dt} \qquad 2.11$$

where dr_{um}/dt is the rate of consumption of the concentric shell thickness of the unburnt mixture spread over the smooth-surfaced sphere of the burnt volume. Over a time step, Δt, the mean unburnt gas thickness consumed by the smooth-surfaced spherical flame, Δr_{um}, is generally larger than the actual unburnt gas thickness consumed over the wrinkled turbulent flame front surface. The actual unburnt gas thickness as shown in the figure would be equal to the laminar value if there is no change in the local laminar burning velocity. For a spherically expanding turbulent flame, the turbulent burning velocity can be calculated from the mass burning rate as

$$S_t = \frac{1}{\rho_u A_m} \frac{dm_u}{dt} \qquad 2.12$$

where A_m is the surface area of the smooth-surfaced spherical flame of the burned mixture. In other words, the flame is treated as a sphere of zero flame front thickness which embraces the burned volume.

2.4: WRINKLED LAMINAR FLAME VERSUS DISTRIBUTED REACTION ZONE

Damkohler's turbulent premixed combustion study in 1940 [Da40] has significant impact on today's work in this area. Damkohler proposed the concept that eddies larger than the flame front thickness wrinkle the flame front while smaller eddies increase the transport rate within the reaction zone. Therefore, a flame subjected to a large-scale turbulent flow would be wrinkled. The combustion rate would increase mostly due to increase in flame front surface area. On the other hand, a flame subjected to very small-scale turbulence would burn faster because of increased transport rate within the reaction zone.

The concept of "wrinkled laminar flame" in which the relatively thin flame front is wrinkled by larger turbulence eddies has since been a popular research subject [Sh43, SG52, AB83, As87, BC91, CD91, Al92]. This wrinkled laminar flame is schematically shown in Figure 2.6. The reaction chemistry is fast compared with the turbulent mixing.

The Damkohler number, Da, is the ratio of the characteristic turbulence time scale to the characteristic chemical time scale. Damkohler number can be [YN93, YN92, YN92a, BC91, Yo90, AW85] expressed as

$$Da = \frac{\Lambda / u'}{\delta_l / S_l} \qquad 2.13$$

where Λ is the integral length scale, u' is the rms turbulence intensity and δ_l is the laminar flame front thickness. The Damkohler number is much larger than unity in the wrinkled laminar flame regime. Therefore, turbulence acts primarily by increasing the flame surface area and hence the mass burning rate, without changing the reaction rate significantly. Many researchers [CB88, CB89, Br90, BC91, CD91, Pe92] have lowered the upper limit (lower Da) for wrinkled laminar flame to allow changes in the reaction rate and hence, the local laminar burning velocity due to straining and stretching. With the changes in local laminar burning velocity accounted for, turbulent flames of continuous flame surfaces can be classified under the "laminar flamelet" regime provided the characteristic turbulent length scale is larger than the flame front thickness. It is generally accepted that an adequate criterion for laminar flamelet is when the Kolmogorov scale, η, is larger than the laminar flame front thickness, δ_l [Ba79, Wi85, Gu90]. In other words, the classic Klimov-Williams criteria for the wrinkled laminar flame is $\delta_l < \eta$ or $Re_\eta > u'/S_l$ (the turbulent Reynolds number based on η, $Re_\eta = u'\eta/\nu$, where ν is the kinematic viscosity) [Wi76]. Note that the Reynolds number used in the Klimov-Williams criteria is based on η. Therefore, Re based on other length scales can not be used directly as for fixed S_l and u', wrinkled laminar flame occurs at large, not small Re_Λ [KF92, Wi76].

The other extreme from the wrinkled laminar flame is the "distributed reaction zone" in which the notion of a flame front is not well defined. The eddies bring unburnt mixture into the reaction zone and increase the transport processes as shown in Figure 2.7. The turbulent mixing is rapid compared with the reaction chemistry in this small Damkohler number, Da << 1, regime. Hence, the reaction rate can be altered profoundly by the eddies. This high intensity, small scale turbulent flame is also described as an "eddy entrainment-combustion in depth flame" [Ba79, Ba79a, Ba79b].

Typical recent studies of distributed reaction zone combustion can be found in [YN93, YN92, TK90]. It is worth noting that there are other researchers who believe that this "distributed reaction zone" does not actually exist.

In between the two extreme turbulent combustion regimes is a transition regime called "corrugated flamelet" regime [Cl94, HD92, Gu90] or multiple sheet regime [AW85]. Clavin [Cl94] identifies the transition from wrinkled laminar flame to corrugated flamelet as the point where rms turbulence intensity reaches the laminar burning velocity. However, the precise nature of the transition from wrinkled laminar flame to distributed reaction zone is still debatable [Yo90, AW85].

Several researchers [BC91, Yo90, KH87, ZB87, AW85] found that conditions in practical equipment such as internal combustion engines cover the wrinkled laminar regime and the transition regime, but not the distributed reaction regime. Most of the engine combustion likely occurs in the laminar flamelet regime in which the flame front is continuous [AW85].

2.5: MODELLING PREMIXED TURBULENT FLAME

Williams has been categorizing different approaches of turbulent combustion modelling for many years [Wi93]. While new approaches are still emerging, different methods have advantages in different regimes of turbulent combustion [Wi93]. Some discussion about recent turbulent premixed flame propagation models can be found in [Ya93, Gu90]. In general, turbulent burning velocity is commonly correlated with the turbulent straining rate, the flame surface fractal dimension, the turbulence structures and the turbulence intensity.

The laminar strain rate is also called the chemical strain rate [AB88]. For a laminar flame, the strain rate is simply the flame (velocity) gradient, S_l/δ_l [AB84]. Correlating the turbulent burning velocity with the mean strain rate has been well-accepted for many decades [AB81, AA84, Th86, AB87, AB88, AB89, BL92, Br92, CT94]. In isotropic and isothermal turbulence, the turbulent strain rate can be expressed as u'/λ [BL92, AB75], where λ is the Taylor microscale. According to [As94], u'/λ is a reasonable estimate for the mean strain rate. For isotropic turbulence, the turbulence dissipation is given by, $\epsilon = C\, u'^3/\Lambda$, where C is a constant of the order of unity [TL72]. Based on the centre-line properties in pipe flow, Abdel-Gayed et al [AB81] recommended $C = 0.37$ which leads to

$$\frac{\lambda^2}{\Lambda} = C_1 \frac{\nu}{u'} \tag{2.14}$$

where C_1 is about 40.4 for $Re_\Lambda > 60$ [AB81]. Kido et al [KH91, KW83] obtained a slightly different expression based on turbulence properties measured in their constant-volume combustion chamber. Specifically, their expression is

$$\frac{\lambda}{\Lambda} = \frac{\sqrt{15}}{C_2^{0.4}\, Re_\Lambda^{0.2}} \tag{2.15}$$

where C_2 is a constant of about 11. The major draw back in correlating the turbulent burning velocity with the mean strain rate is that the mean strain rate can not be measured directly. The turbulent burning velocity-mean straining rate correlation is further examined in Chapter 6.

The other commonly used parameter in strain rate studies is the Karlovitz flame stretch factor. Karlovitz flame stretch factor is the turbulent strain rate divided by the laminar strain rate. It is usually defined as

$$K = \frac{u' / \Lambda}{S_l / \delta_l} \quad \text{OR} \quad \frac{u' / \lambda}{S_l / \delta_l} \tag{2.16}$$

[BG94, BL92, AB89, AB88, AB87, AB84, AA84]. Note that this Karlovitz number is the inverse of the Damkohler number defined earlier.

Gouldin introduced fractal analysis into combustion research in 1987 [Go87]. He used Mandelbrot's results [Ma75a] to express flamelet surface area for $u' >> S_l$ (Mandelbrot suggested that constant property surfaces in homogeneous, isotropic turbulence exhibit fractal characteristics.). Since then, many researchers have been using fractals to characterize the premixed turbulent flame [GH88, MT88, NS90, SL90, HD92, YA92, YA93a, DE94]. However, the popularity of fractal analysis is decreasing due to its various limitations. The first limitation is that a slight change in the inner and/or outer cutoff can lead to enormous errors [MF88]. Even the more recent studies produce significantly different values for the inner and outer cutoffs from one study to the other.

In general, the fractal dimension increases with increasing u'/S_l [KF92, NS90]. The rms turbulence intensity, u', is usually easier to measure than the fractal dimensions.

Due to the importance of the laminar flamelet regime in practical combustion systems, many researchers [As87, Th86, Br90, BC91, CD91, Al92, VH92, As93, DV93, AC94, As94, As95] have developed models for this type of turbulent flame. For an ideal wrinkled laminar flame, the sole change of mass burning rate from its laminar value is caused by the increase in flame front surface area. Under low to moderate levels of turbulence, u'/S_l < 10, this is believed to be roughly the case. However, it is difficult to justify this statement experimentally because of the difficulties in measuring the flame surface area accurately [As93]. Most flame tomography studies are limited to large scale, low intensity turbulent flame [KF92, KW92].

Vortex dynamics has been used to model, simulate and study the turbulent flame for many years [As78, AB83, As87, AM89, RD91, RF91, WD92, As93, RD93, RT93, LS93, As94a, As95]. With the advancement in numerical computation power, the vortical structures in a turbulent flow field can be simulated from Navier-Stokes equations [SJ90, SJ91, JW93, VM94]. These intense vortical structures can be used to estimate the turbulent flamelet propagation [As93, As94, As94a]. A simplified eddy structure model [As93] is described here.

The basic idea behind Ashurst's eddy structure model [As93, AC94, As94a] is to estimate the flame surface area increase due to the interaction of the vortex tubes. This turbulent flamelet model assumes that the modifications of the local laminar burning velocity due to stretch, curvature and strain rate effects are small. The excess flame surface area due to turbulence enhancement is related to the size of the tube, the number of tubes per unit area and the rotational speed of the tube relative to the flame consumption rate, u'/S_l. The intense vortical tubes are not space filling [SJ90, JW93, VM94] under moderate turbulence levels. Due to the non-space-filling behaviour of the vortex tubes, the instantaneous flame can travel in two different pathways. Figure 2.8 shows that between the eddies, there is no vortex interference. Therefore, the flame consumes the unburned mixture at its laminar burning velocity between eddies. Within an eddy, as shown in Figure 2.8, the flame burns at a velocity equal to the sum of u' and

S_l. On average, the turbulent burning velocity is equal to the distance between two consecutive eddies divided by the sum of the two different time scales of burning. Going through the derivation in [AC94], the correlation equation can be expressed as

$$\frac{S_t}{S_l} = \frac{1 + \frac{u'}{S_l}}{C_3 + C_4 \frac{u'}{S_l}} \qquad 2.17$$

where C_3 is of the order of unity and $C_4 < C_3$. Note that when $u' >> S_l$, S_t approaches S_l/C_4. In other words, the parts of the flame travelling between the intense vortical tubes are limiting the continuous turbulent burning velocity increase with increasing turbulence intensity. This limiting effect can cause the plot of S_t/S_l versus u' to level off at high u'. Chapter 6 discusses this correlation equation along with the experimentally determined constants, C_3 and C_4.

2.5.1: TURBULENT BURNING VELOCITY-TURBULENCE INTENSITY RELATION

The turbulent burning velocity is correlated with rms turbulent intensity and integral length scale in this study. These parameters are used because they can be measured directly and relatively accurately. The basic experimentally determined results are used to check the validity of various turbulent flame models in Chapter 6.

For moderate levels of turbulence, most researchers [Sc34, LK76, AB81, AB83, KW83, AA84, AB84, AB86, BG86, AB87, AB88, HT88, AB89, Gu90, LN90, WH90, HI91, KH91, AI92, Je92, KF92, KK92, BC94, BG94, DE94] agree qualitatively that the turbulent burning velocity increases with increasing turbulence intensity. Many researchers believe that turbulent burning velocity levels off and decreases slightly before the flame is quenched completely at high turbulence levels. While the exact locations of partial quenching and total quenching are still uncertain, some current studies [LN90, BC94] showed that turbulent burning velocity continues to increase linearly with turbulence intensity up to more than ten times the laminar burning velocity. The roughly proportional relation between turbulent burning velocity and turbulence intensity can be explained with the help of Figure 2.9. Figure 2.9 shows a one-dimensional, pianar flame front approaching a two-dimensional vortex at a laminar burning velocity of S_l. The two-dimensional vortex is rotating at a rotational speed of u' at the core radius, r_{core}. For $u' << S_l$, the flame consumes the vortex before it has any significant effect on the flame front. With increasing u' relative to S_l, the vortex wrinkles the flame front progressively more severely. For $u' >> S_l$, the vortex can bring in unburnt volume into the flame.

The variation of turbulent burning velocity with rms turbulence intensity can be expressed as $S_t = S_t(S_l + u')$. Assuming a linear relation between turbulent burning velocity and turbulence intensity for low to moderate turbulence levels, the expression can be rewritten as

$$S_t = S_l + C_L u' \qquad 2.18$$

where the linear coefficient, C_L, illustrates the effectiveness of turbulence enhancement on the turbulent burning velocity. The linear coefficient, C_L, may be a function of flame size, turbulent length scale, flame front thickness, time elapsed, turbulence intensity and laminar burning velocity. These effects are examined in Chapter 6. Normalizing the equation with the laminar burning velocity results in

$$\frac{S_t}{S_l} - 1 = C_L \frac{u'}{S_l} \qquad 2.19$$

At higher turbulence levels, C_L could decrease with further increase in u' due to local flame quenching.

It is worth mentioning that turbulent flames can alternatively be characterized using Da and Re [KH94, KH93, YN93, YN92a, Yo90, Br90, AW85]. In fact the Re-Da, η/δ_l-u'/S_l and Λ/δ_l-u'/S_l planes are equivalent and it is possible to transform one plane into the other according to [KH94, KH93]. It is claimed in [KH94] that comparison of models on these planes is more effective and more thorough than the conventional S_t/S_l-u'/S_l plane. Nevertheless, Re, Da and η can not be measured directly and δ_l is not measured in this study. Therefore, the conventional S_t/S_l-u'/S_l plane is used extensively while the other planes can be used when comparing the current results with other models.

2.6: PROGRESSIVE TURBULENCE ENHANCEMENT

It is a common practise to assume that a premixed flame propagates quasi-steadily in a frozen or steady-state turbulent flow. The term, "quasi-steady", is used in the sense that the turbulence-flame interactions are in equilibrium. Under this equilibrium condition the turbulent flame is called fully developed turbulent flame. A fully developed turbulent flame propagates at a steady rate in a constant turbulent flow field, similar to a laminar flame in a quiescent mixture. If the turbulence parameters along with the temperature and pressure are held constant, a fully developed turbulent flame burns at a constant turbulent burning velocity. In other words, the turbulent burning velocity / turbulence intensity ratio remains constant for a fully developed turbulent flame. Some numerical simulations [FL93] illustrate the existence of one-dimensional, steadily propagating, premixed turbulent flame. However, there is no experimental evidence of a steadily propagating or fully developed turbulent flame.

In 1952, Scurlock and Grover [SG52] studied the propagation of an initially flat flame into isotropic turbulence with scales larger than the laminar flame front thickness. They deduced from their study that turbulence takes time to become fully active in interacting with the flame. They commented that in most practical instances, turbulent flame elements do not reach the asymptote or the fully developed stage during the short existence of the flame elements.

Right after ignition, the length and time scales for the developing turbulent flame are less than those associated with the turbulence [Sh43, De65, AB83, AA84, AB84, AB86, AB87, SL90, CV91, Br92, CV92, HM92, BS94]. Therefore, the initial small flame kernel is not exposed to the full turbulent spectrum. With the passage of time or as the flame grows, the full spectrum of turbulence frequencies increasingly affects the turbulent burning velocity. According to this classical explanation alone, the turbulent flame becomes fully developed when it is somewhat larger than the turbulent length scale or after a short time period. This classical assumption has been well-accepted and used widely despite the lack of justification. In short, many researchers (including [NH80, AB85, Ka85, ZB87, RF90, RF90a, TG90, BH94, MB94]) are aware of the unsteady effects during a spark-ignited, premixed turbulent flame's first period of propagation. However, most of these researchers assume the existence of fully developed turbulent flames after a short period of time or after the flames reach a certain size [HM92, HB88, ZB87], or a certain relative size [CV92, CV91].

The first concrete experimental evidence showing the development of spark-ignited, premixed turbulent flame phase is that of Palm-Leis and Strehlow [PS69]. They experimented with spark ignited, freely expanding spherical, premixed propane- and methane-air flames downstream of a perforated plate in open atmosphere. Even up to 8.4 cm in radius, turbulent flames continued to accelerate, showing no sign of approaching the "fully developed turbulent flame" stage. The integral scale used in their experiment ranged from 1.4 to 7.6 mm. Therefore, the largest flame radius/integral scale ratio considered is more than fifty.

Other than the evidence in [PS69], many engine studies [LK76, GM80, AW85, Ka85, Ba89, BK94] showed the same developing turbulent flame phase in research and automotive engines. Due to the complexity involved in an engine, the turbulent flame tends to accelerate and then sort of level off. The levelling off is usually assumed to be the evolution of the turbulent flame into the fully developed phase. However, the turbulent flame in an engine is usually partially in contact with the chamber walls at the levelling off stage. The levelling off in turbulent burning velocity is more likely due to heat losses and flame area losses than the maturing of a fully developed turbulent flame. Moreover, engine turbulence is highly transient. Hence, it is important to correlate the instantaneous turbulent burning velocity with the instantaneous turbulence level.

Careful examination of many engine turbulent flame growth studies [LK76, GM80, GH84, AW85, KH87] along with recent experimental evidence from [TG90, KF92, KW92] shows that the turbulent flame continues to developed over the range of flame sizes studied. These observations and the experimental results given in Chapter 6 agree qualitatively with those of [PS69]. It is slowly becoming clear that engine-size turbulent flames never become fully developed [TG90]. On the contrary, turbulent flames in engines are usually at their early stages of turbulent flame development.

It is worth mentioning that turbulent flame development also occurs in a burner or jet type flame. The turbulent flame can become progressively more distorted downstream of the burner. The flame surface area, the flame brush thickness and the fractal dimension have been found to progressively increase with distance from the flame holder [WK91]. The rate of development increases with increasing u'/S_l.

Does the spherically expanding turbulent flame initiated from a point source ever become fully developed? Some researchers [Br92, CT94] believe it does. According to Batchelor [Ba52], a passive material surface in a homogeneous isotropic flow field will grow exponentially with time. A flame surface is a reacting surface which consumes the un-reacted mixture ahead of the flame front. This consumption or Huygens effect counteracts against the flame surface area creation process by the flow field turbulence. The upper limit or the fully developed turbulent flame is reached when the excess flame surface area creation process is balanced by the Huygens effect [CT94].

On the other hand, some researchers [AC94] tend to think that a spherically expanding turbulent flame may eventually reach such a huge size that it may detonate. Very large-scale "laminar" explosions have lead to much more vigorous (more than ten times the laminar burning velocity) explosions compared to those laboratory- or engine-size explosions [Li75, LW77]. These expanding flames in [Li75, LW77] become rough with cells as they grow. Whether a turbulent flame of similar size will lead to the same conclusion is yet to be found. However, since methane-air flames do not detonate [Li75, LW77], they are likely to become fully developed eventually. The size at which these fully developed turbulent flames occur is beyond the scope of this thesis.

2.7: THE EFFECTS OF TURBULENT LENGTH SCALE

One of the most controversial issues in turbulent combustion research is the effect of turbulent length scale on the combustion rate. Even among the more current studies, there is still a lack of qualitative agreement, not to mention quantitative agreement. The qualitative turbulent length scale effect appears to vary with changing experimental and numerical conditions.

Studies such as [KH93, LL93, LN90] found that large-scale turbulence is more effective in enhancing the burning rate. It should be noted that some of these studies do not maintain the turbulence intensity or the turbulence energy fixed while varying the length scale.

On the contrary, studies such as [Br92, HI90, AB83, CT83, KW83] found that small-scale turbulence is more effective in augmenting the burning rate. Many researchers [BH94, Jo94, CV92] agree that increasing the energy content of the small-scale flow structures can speed up the flame development process. This trend can be explained based on the reasoning in the classical developing turbulent flame model. According to the classical logic behind the turbulent flame development, eddies which are smaller than the flame kernel become effective in wrinkling the flame while the larger eddies are only convecting the flame around. Larger eddies become effective in wrinkling the flame later in the flame development process as the flame grows larger than these eddies. Hence, a small-scale turbulent flow accelerates the flame sooner and faster compared with a large-scale turbulent flow, for the same turbulence intensity. The other reasons behind the more effective and more favourable small-scale turbulence are addressed following the discussion about zero-turbulent length scale effect.

Some studies [LK76, BL75] found that under certain turbulence conditions the turbulent length scale has little or no effect on the turbulent burning velocity-turbulence intensity relation. According to [BL75], there are two counter-acting mechanisms in turbulence enhancement. Flame front wrinkling increases with increasing scale. This argument is used in [BL75] to explain the increase in wrinkled flame burning rate due to an increase in turbulent length scale. On the other hand, eddy entrainment decreases with increasing turbulent length scale. Therefore, according to [BL75], an increase in scale decreases the burning rate in the distributed reaction zone. It is shown in the next paragraph that in the wrinkled flame regime larger length scales do not necessarily increase the flame front wrinkling. While small eddies do increase the interface area in a thick reaction zone, it is not certain that the interface area is a predominant parameter in the distributed reaction zone.

The core of this study is about spark-ignited flame propagation. Physical arguments have shown that smaller eddies become effective in corrugating the flame front more rapidly and earlier in the development stage. The flame behaviour at any instant is likely influenced by both the current and previous environments [RF90, GM80]. Consequently, the more wrinkled flame will continue to remain more wrinkled in a turbulent flow of small eddies compared with the less wrinkled flame in a turbulent flow of larger eddies.

Moreover, for the same turbulent intensity or turbulent kinetic energy, there are many more smaller eddies in a small-scale turbulent flow than the number of eddies in a large-scale turbulent flow. Consider a two-dimensional turbulent flow in which all the eddies are of the same size. These eddies can be considered as vortex tubes of the same core radius and of unit length behaving like rotating solid rods. Figure 2.10 shows the ideal "fully saturated wrinkled laminar flame fronts" in small-scale and large-scale turbulent flows. The total flame front areas per unit width in both small-scale and large-scale turbulent flows are equal to $16\pi R_o$ per unit depth. In other words, if turbulent eddies are space filling tubes as shown in Figure 2.10, the change in eddy size does not affect the wrinkled flame front area. It should be noted that the local curvature and rate of strain effects are larger for the smaller eddy case.

Figure 2.11 shows the unsaturated wrinkled laminar flame fronts in small-scale and large-scale turbulent flows. The total flame front surface area in the unit width shown for the case with eddies of core radius of R_o is equal to $(16+8\pi)R_o$ per unit depth. The excess area created is $(8\pi-16)R_o$, since the corresponding laminar flame front area is $32R_o$. Doubling the core radius while keeping the turbulent kinetic energy and the turbulent intensity constant results in four times fewer eddies in the flow. The detailed calculations which lead to this result is given in Appendix A. As a result of the four times reduction in the number of eddies, the total wrinkled laminar flame front area per unit width for the large-scale turbulent flow case shown is only $(24+4\pi)R_o$ per unit depth. In other words, doubling the vortex core radius leads to a 11% reduction in the flame surface area. Most importantly, the excess area created by the larger eddies is only, $(4\pi-8)R_o$, which half of that created by the smaller eddies. In other words, doubling the core radius of the eddies lead to a 50% reduction in the excess area created.

In short, for the ideal conditions considered, smaller scale turbulence is more effective in wrinkling the flame front and creating extra flame surface area than larger scale turbulent for the same turbulence intensity. Obviously there are many other factors which can change along with changes in the vortex core size. The following points are worth noting:

1) A turbulent flow always consists of eddies of different sizes.
2) Smaller eddies decay faster than larger eddies.
3) Smaller eddies lead to higher curvature and higher rate of strain.
4) The vortical structures in a three-dimensional turbulent flow are different from the ideal two-dimensional case considered.

It is worth mentioning that decreasing the size of the eddies has the tendency to reduce the cyclic variations in an engine [Hi88, HK89]. The reason behind this trend is that the initial flame kernel is convected around by the larger eddies while wrinkled by the smaller eddies. It is mostly the convection of larger eddies that leads to cycle-to-cycle variations in flame growth rate, flame kernel location and the amount of heat loss to the spark electrodes. In a homogeneously charged engine, these variations in the flame kernel caused by the flow are likely responsible for the cycle-to-cycle variation of combustion [HW82, AB83a, KH87, ZB87, Le92, Jo93, BH94, Jo94]. It is also found [Ma75, HW82, LB82, Ka85, SC93] that cyclic variations can be lowered when the early combustion rate is augmented. In short, other than more effective enhancement in the burning rate, smaller-scale turbulence also has the tendency to reduce cyclic variations.

2.7.1: TUMBLE VERSUS SWIRL FLOWS IN ENGINES

Swirl and tumble are commonly used in enhancing engine combustion [Dy79, Ba89, DN90, ET90, AE91, BC91a, HD91, Ev92, HK92, GE93, KK93, LA93]. Swirl is a form of large-scale turbulence while tumble generates smaller scale turbulence. In general, for the same turbulence level, tumble flow leads to faster burning rate than swirl flow. For the same level of turbulence intensity in an engine, uniform small-scale turbulent mixture burned fastest, and tumble mixture burned faster than swirl mixture [WH90]. This same trend is also found in [LA93], in which a tumble flow engine shows slightly faster kernel growth rate and decidedly faster 0-90% burn rate than do swirl and quiescent engines. Another example of more effective combustion rate enhancement by tumble compared with swirl is [BC91a]. These studies [WH90, BC91a, LA93] confirmed that the small-scale turbulence, generated by tumble flow, is more effective in augmenting the burning rate than the large-scale turbulence, swirl.

However, there are other studies which seem to disagree that tumble is more effective in enhancing the burning rate than swirl. The confusion is mostly due to the fact that tumble also leads to faster turbulence decay than swirl. The larger scale turbulence along with continuous turbulence generation by the velocity gradient in a swirl flow result in a much slower turbulence decay rate compared with a tumble flow of the same initial turbulence level. These reasons explain why the tumble case in [BC91a] has the largest improvement at the early part of the cycle. The same arguments hold for the fact that the swirl case in [BC91a] has the best improvement at the middle of the burning process.

In general, the engine combustion studies indicate that smaller scale turbulence is more effective at speeding combustion than larger scale turbulence at the same intensity. However, larger turbulence decays more slowly and may become more effective at later stages of combustion.

2.8: GRID TURBULENCE IN A CONSTANT VOLUME CHAMBER

In this study, a perforated plate is used to generate the pre-ignition turbulence level in the combustion chamber as described in section 4.1. The characteristics of the turbulence after the plate passage are discussed here. The modifications in the turbulence level due to the propagating flame are also investigated.

2.8.1: NORMAL DECAY

After the plate passage across the chamber, the turbulence in the chamber decays in a similar fashion to grid turbulence in a wind tunnel [Ch86, Mc88]. The justification for applying wind tunnel measurements for combustion chamber turbulence can be found in [Ch86, Mc88].

A power law equation is used to describe the turbulence decay. Specifically,

$$\frac{u'}{U} = c_5 \left(\frac{X}{D}\right)^{c_6} \qquad 2.20$$

where U is the perforated plate velocity, X is the distance downstream of the plate and D is the plate hole diameter. The change of integral scale is expressed as:

$$\frac{\Lambda}{D} = c_7 \left(\frac{X}{D}\right)^{c_8} \qquad 2.21$$

The coefficients c_5, c_6, c_7 and c_8 of these correlation equations are fitted over different ranges to accurately predict turbulence in the combustion chamber. These coefficients are tabulated in Table 2.1. Figure 2.12 shows a typical turbulence decay profile behind a perforated plate according to the normal decay model.

Table 2.1: Coefficients of turbulence correlation equations.

region	c_5	c_6	c_7	c_8
$5<X/D<10$	10.96	-1.812		
$X/D<14.3$			0.38	0
$10<X/D<20$	2.627	-1.191		
$14.3<X/D$			0.1	0.5
$20<X/D$	0.773	-0.783		

2.8.2: RAPID DISTORTION

Turbulence which undergoes a rapid compression may decay more slowly than would be the case for unaffected turbulence. This section examines the effects of compression and distortion on flame front turbulence.

Consider the vortex tube as shown in Figure 2.13, the two-dimensional circulation of the vortex is

$$\Gamma = \pi\, r_{core}^2\, \omega \qquad 2.22$$

where ω is the vorticity. Conservation of angular momentum and conservation of mass result in the conservation of circulation. With the circulation as an invariant the vorticity is inversely proportional to the square of r_{core}, that is,

$$\omega = \frac{\text{constant}}{r_{\text{core}}^{2}} \qquad 2.23$$

The mass of the vortex tube is

$$m = \rho \ \pi \ r_{\text{core}}^{2} \ L \qquad 2.24$$

where L is the length of the tube. If the density remains constant, stretching the vortex tube will lead to a reduction in the core radius and hence, an increase in vorticity. In other words, conservation of angular momentum in a inviscid flow leads to the inverse proportionality of the square of the core radius and the vorticity.

Figure 2.14 shows that compression can lead to reductions of both vortex tube length and vortex core radius. Conservation of circulation according to Equation 2.22 results in Equation 2.23 which shows that the vorticity is inversely proportional to the square of the vortex tube core radius. Therefore, compression which reduces the vortex core radius also results in an increase in vorticity.

In combustion chamber experiments, the unburned mixture turbulence level can be altered significantly by the expanding flame ball. The curved, advancing flame front as shown in Figure 2.15 causes stretching of the vorticity in the unburnt mixture just ahead of the flame front [CB92]. In the ideal situation as shown in the figure, the two components parallel to the flame surface are stretched while the normal component is squashed. While stretching the two parallel components leads to an increase in turbulence intensity, the squashing of the normal component reduces the turbulence intensity in the normal direction. This geometric distortion is most intense immediately ahead of the flame front. Therefore, it can enhance the flame front turbulence significantly just as the flame arrives. However, it has little effect on the overall turbulence decay rate in the unburned mixture away from the flame front.

Similarly, the spherically expanding flame in a closed vessel compresses the unburned mixture. The vortex tubes in the unburned mixture can be compressed as shown in Figure 2.14. Therefore, compression due to flame expansion increases the turbulence intensity in the unburned mixture. The smaller, compressed vortical structures can also lead to an increase in the turbulence decay rate.

Figure 2.16 shows the effects of straining and compression on the flame front turbulence according to rapid distortion theory [CB92]. The detailed assumptions of the rapid distortion model are given in [CB92]. The equations used for the present closed vessel combustion can be found in [Ti92]. The typical case shown in the figure is a 0.7 equivalence ratio methane-air flame. The integral scale is about 4 mm. Richer flame and/or larger scale turbulence can lead to a larger rapid distortion effect. On the other hand, leaner flame and/or smaller scale turbulence can result in larger turbulence decay over the combustion period. Curve 1 shows the on-going power law decay curve. Immediately after ignition, the turbulence ahead of the flame front is enhanced by geometric distortion as shown by Curve 2. The enhancement due to geometric distortion decreases to zero as the flame approaches the walls. The compression enhancement as shown by Curve 3 increases as the combustion chamber pressure rise increases. The combined effect due to normal decay, geometric straining and compression is shown by Curve 4.

There are controversies about the application of rapid distortion in engine-type combustion. At present, there is still a lack of quantitative experimental evidence to justify the theory. Studies by Reuss et al [RA89, RA89a, RB90] showed smaller turbulence enhancement than that predicted by the rapid distortion theory. The disagreements can be due to a number of factors. It is difficult to measure the turbulence just ahead of the flame front accurately. Chew and Britter also mentioned that their rapid distortion theory can be improved to include only the scales which are affected by the flame. In other words, when the flame kernel is small only the smaller eddies of the order of the kernel size are strained by the expanding flame. The other complication is that the turbulent flame front is wrinkled and corrugated. The corrugated expanding flame can interact with the vortical structures differently compared to a smooth flame.

Ashurst's model [As94] predicts that the vortex tubes tend to align with the flame surface. Vortex tubes initially at random angles with the flame surface will end up parallel to the flame surface. The end of the tube closer to the flame will be pushed away from the flame surface more severely than the portion further away from the flame surface. This is likely the reason why the flame front curvature is mostly cylindrical

[BC91, As93, RT93]. If this vortex tube alignment model holds over the combustion process, the geometric straining would be larger than that predicted by rapid distortion theory. Therefore, it seems that while the normal decay is the lower limit for modelling the unburned mixture turbulence, the upper limit might exceed the rapid distortion model predictions slightly. Hence, the question of the true accuracy of turbulence modelling is still debatable. However, the effects of distortion simply amplify the decaying turbulence by a fairly consistent amount over the range of turbulence and flame growth parameters measured in this study. Experimental results in Chapter 6 justify that the turbulence enhancement only changes the experimentally determined constants, but not the conclusions.

2.9: CONCLUDING REMARKS

A review of research in premixed turbulent flame propagation is given in this chapter. The focus is on spark-ignited, turbulent flames growing from spark kernels under engine-like conditions. This thesis aims at unveiling the controversy about fully developed turbulent flames in engine combustion. The effects of turbulent length scale in engine-like combustion are also clarified. Premixed turbulent flame results are discussed in Chapter 6. Progressive turbulence enhancement as the flame grows, developing turbulent flame in engine-like combustion and more effective small-scale turbulence are further examined in Chapter 6.

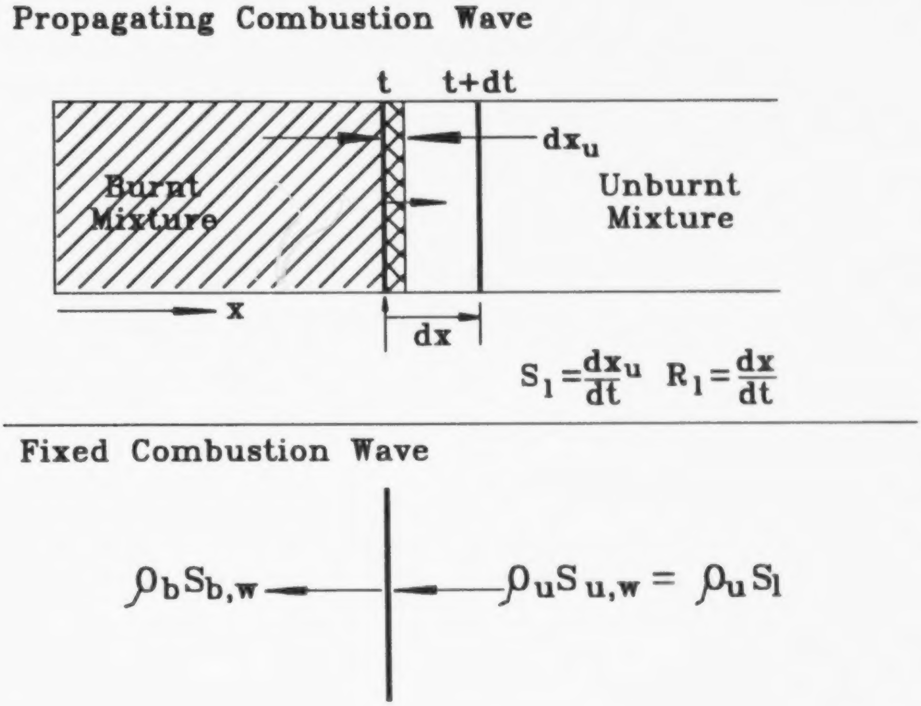
Propagating Combustion Wave
t
t+dt
dx_u
Burnt Mixture
Unburnt Mixture
x
dx
$S_l = \frac{dx_u}{dt}$
$R_l = \frac{dx}{dt}$
Fixed Combustion Wave
$\rho_b S_{b,w}$
$\rho_u S_{u,w} = \rho_u S_l$

Figure 2.1: One-dimensional, planar laminar flame growth.

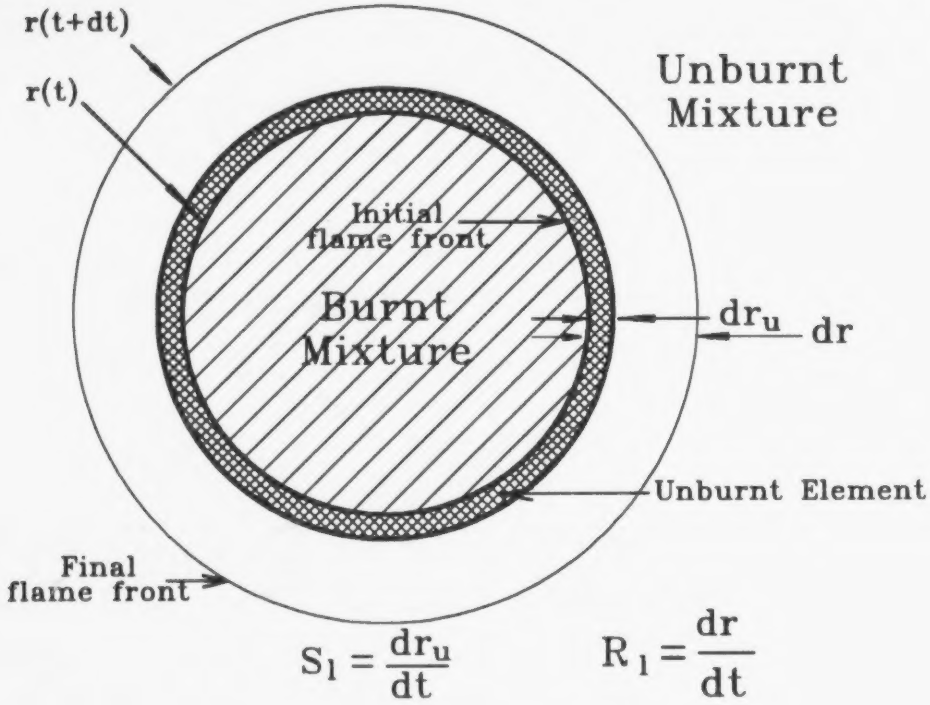
r(t+dt)
r(t)
Unburnt Mixture
Initial flame front
Burnt Mixture
dr_u
dr
Unburnt Element
Final flame front
$S_l = \frac{dr_u}{dt}$
$R_l = \frac{dr}{dt}$

Figure 2.2: One-dimensional, spherical laminar flame growth in open atmosphere.

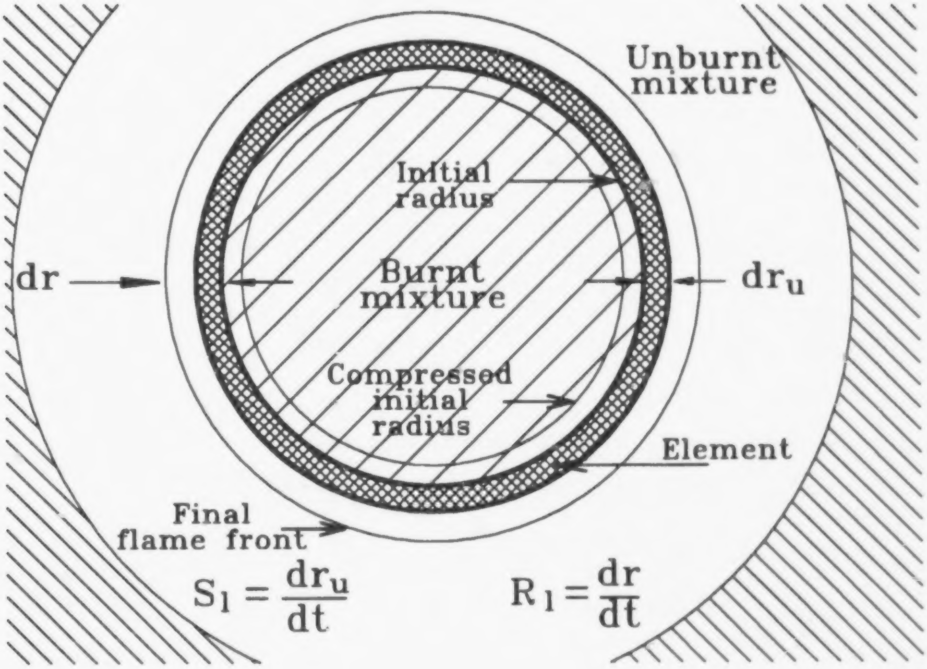
Unburnt mixture
Initial radius
dr
Burnt mixture
dr_u
Compressed initial radius
Element
Final flame front
$S_l = \frac{dr_u}{dt}$
$R_l = \frac{dr}{dt}$

Figure 2.3: One-dimensional, spherical laminar flame growth in a confined chamber.

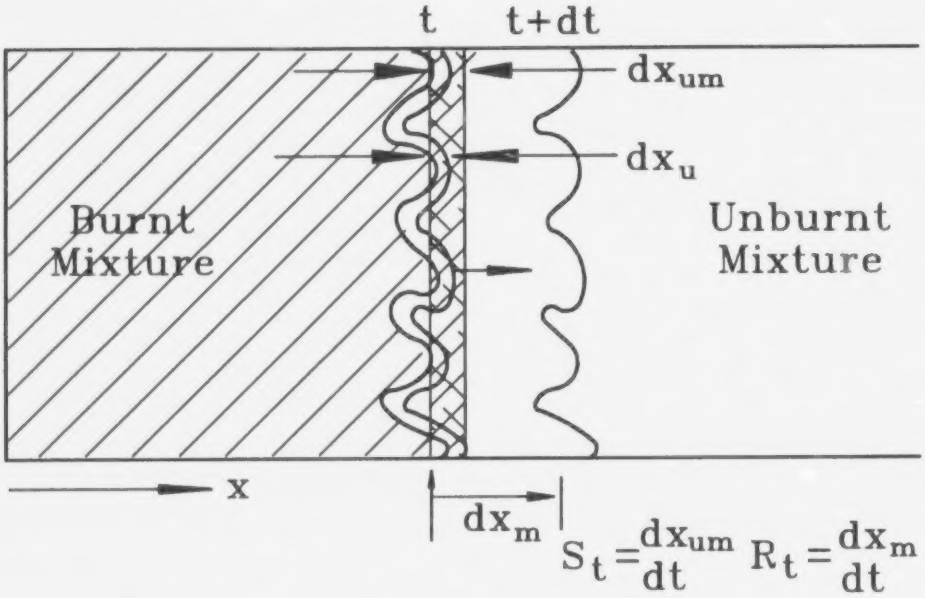
t
t+dt
dx_{um}
dx_u
Burnt Mixture
Unburnt Mixture
x
dx_m
$S_t = \frac{dx_{um}}{dt}$
$R_t = \frac{dx_m}{dt}$

Figure 2.4: One-dimensional, planar turbulent flame growth.

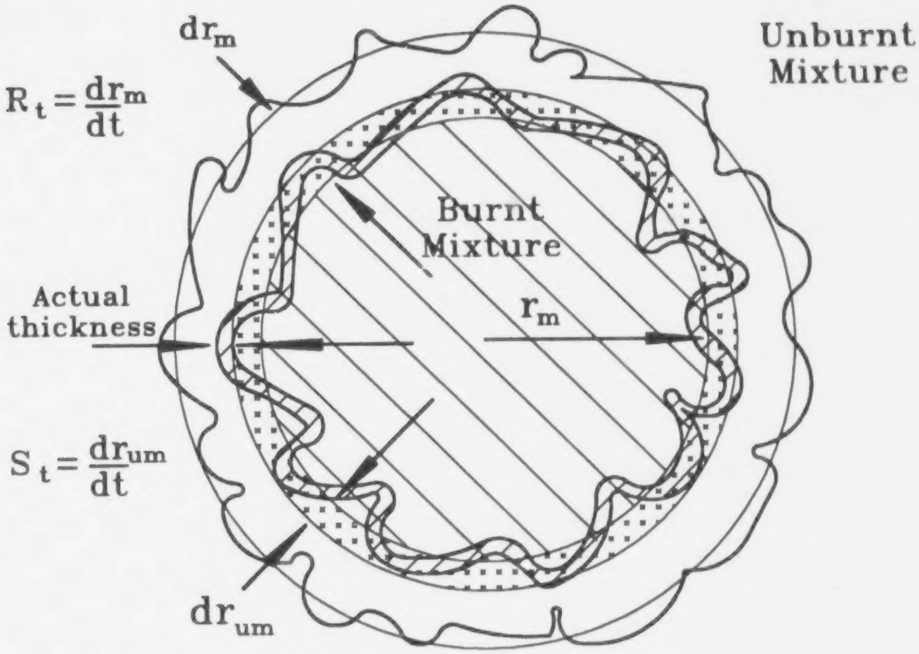
dr_m
$R_t = \frac{dr_m}{dt}$
Unburnt Mixture
Burnt Mixture
Actual thickness
r_m
$S_t = \frac{dr_{um}}{dt}$
dr_um

Figure 2.5: One-dimensional, spherical turbulent flame growth.

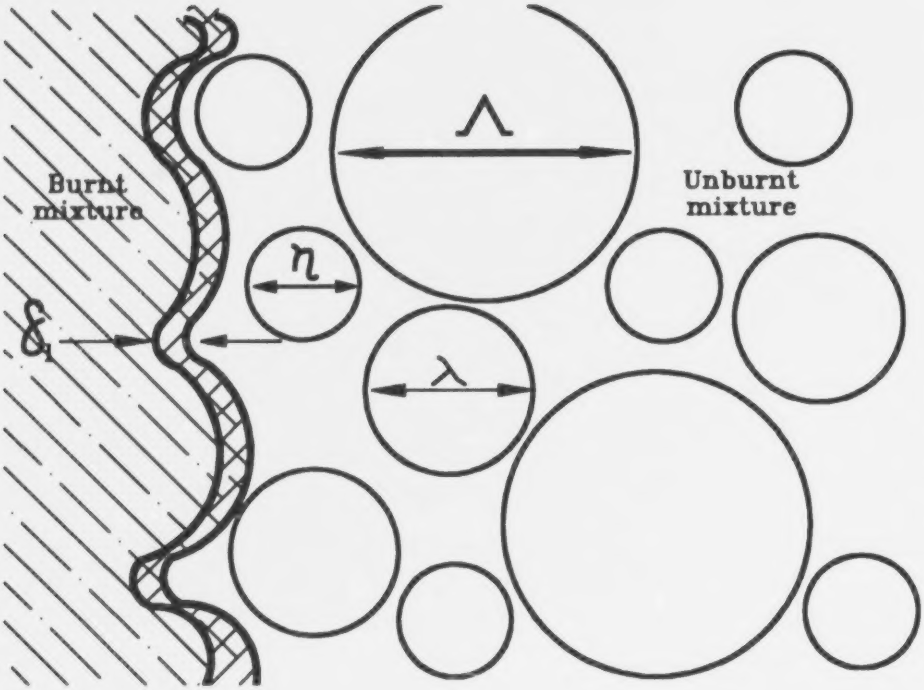
Burnt mixture
Unburnt mixture
Λ
η
λ
δ_l

Figure 2.6: Wrinkled laminar flame.

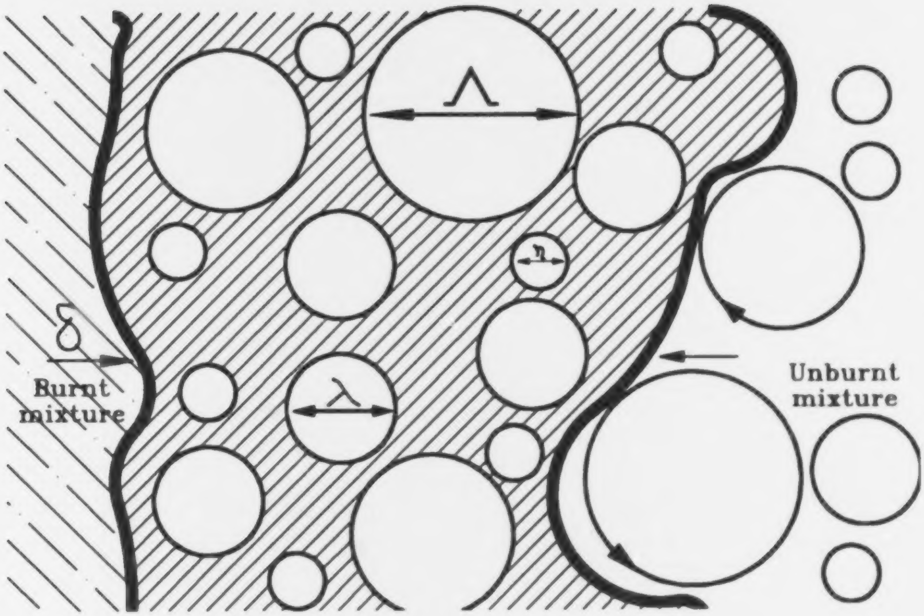
Λ
η
δ
λ
Burnt mixture
Unburnt mixture

Figure 2.7: Distributed reaction zone.

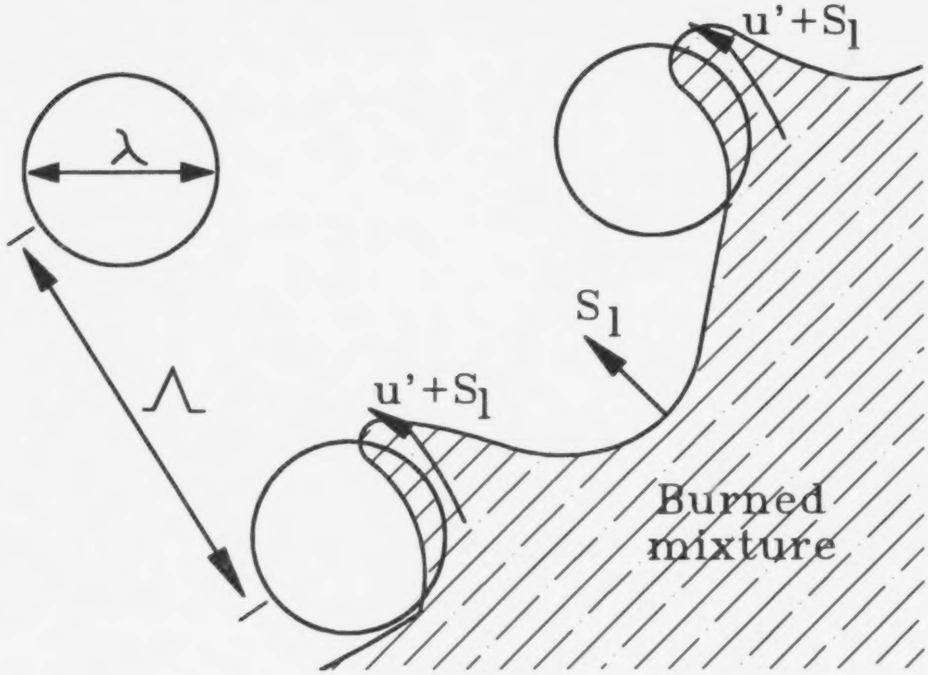
λ
Λ
u'+S_l
S_l
u'+S_l
Burned
mixture

Figure 2.8: The eddy structure model.

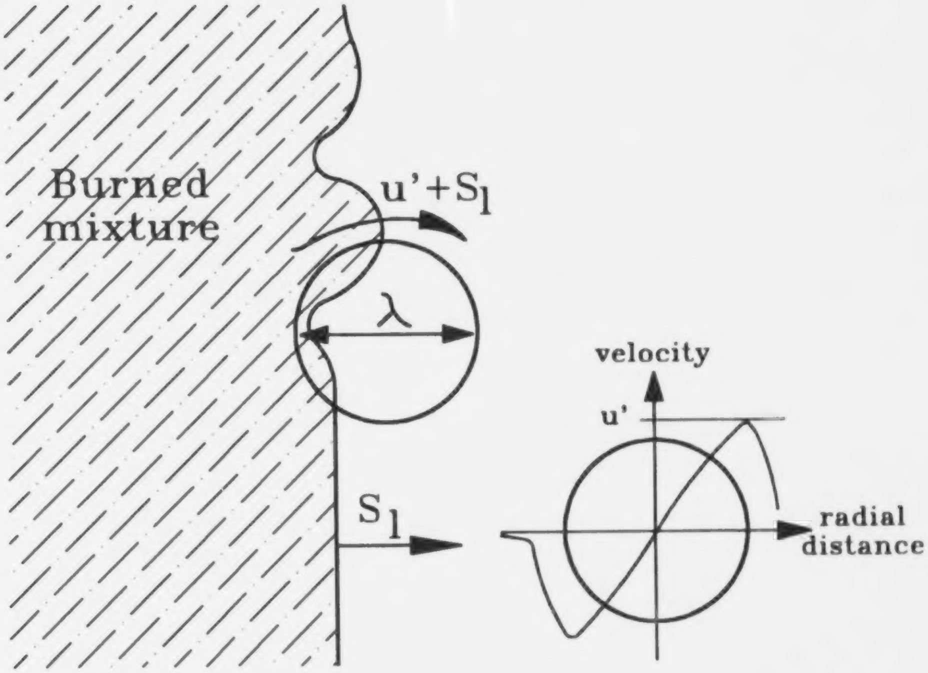
Burned mixture
u'+S_l
λ
S_l
velocity
u'
radial distance

Figure 2.9: The linear relation between u' and S_t.

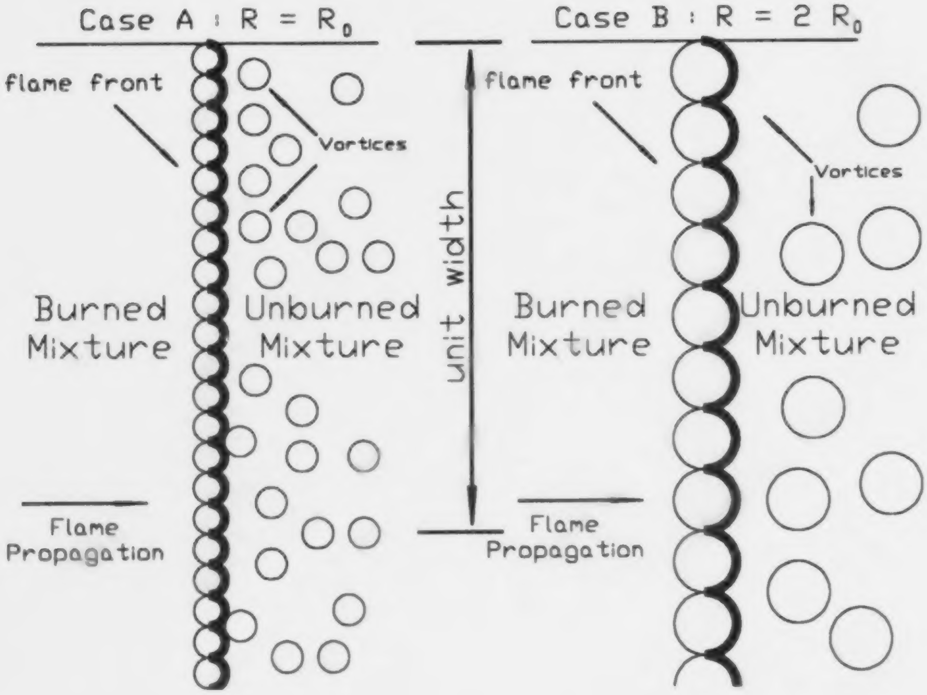
Case A : R = R_0
Case B : R = 2 R_0
flame front
Vortices
Burned Mixture
Unburned Mixture
Flame Propagation
unit width
flame front
Vortices
Burned Mixture
Unburned Mixture
Flame Propagation

Figure 2.10: Fully saturated wrinkled laminar flame fronts by small-core and large-core vortices.

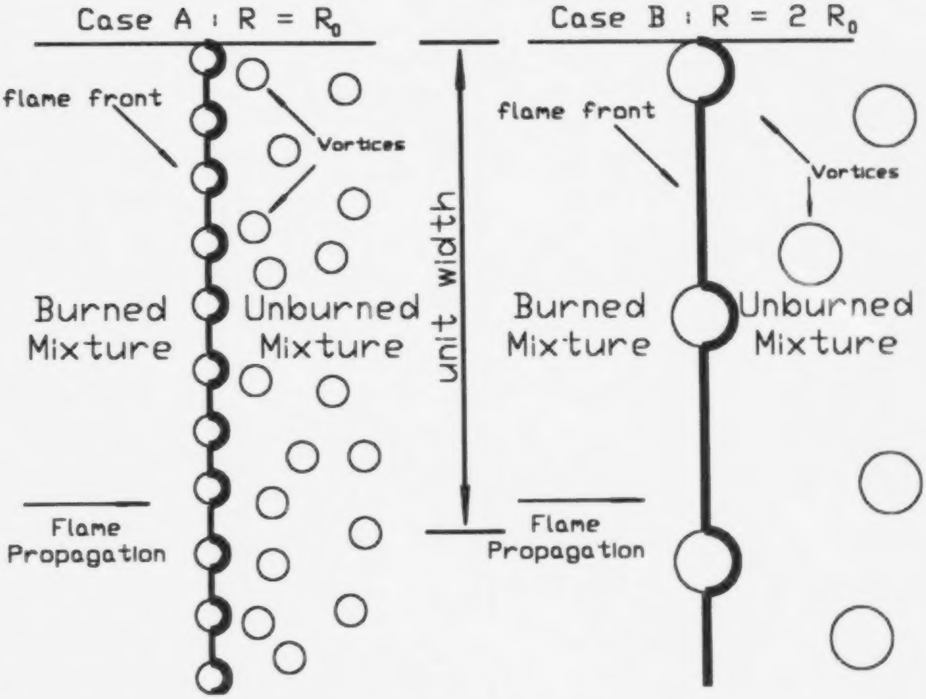
Case A : R = R_0
Case B : R = 2 R_0
flame front
Vortices
Burned Mixture
Unburned Mixture
unit width
Flame Propagation
flame front
Vortices
Burned Mixture
Unburned Mixture
Flame Propagation

Figure 2.11: Partially saturated wrinkled laminar flame fronts by small-core and large-core vortices.
Equal turbulence intensity and kinetic energy.

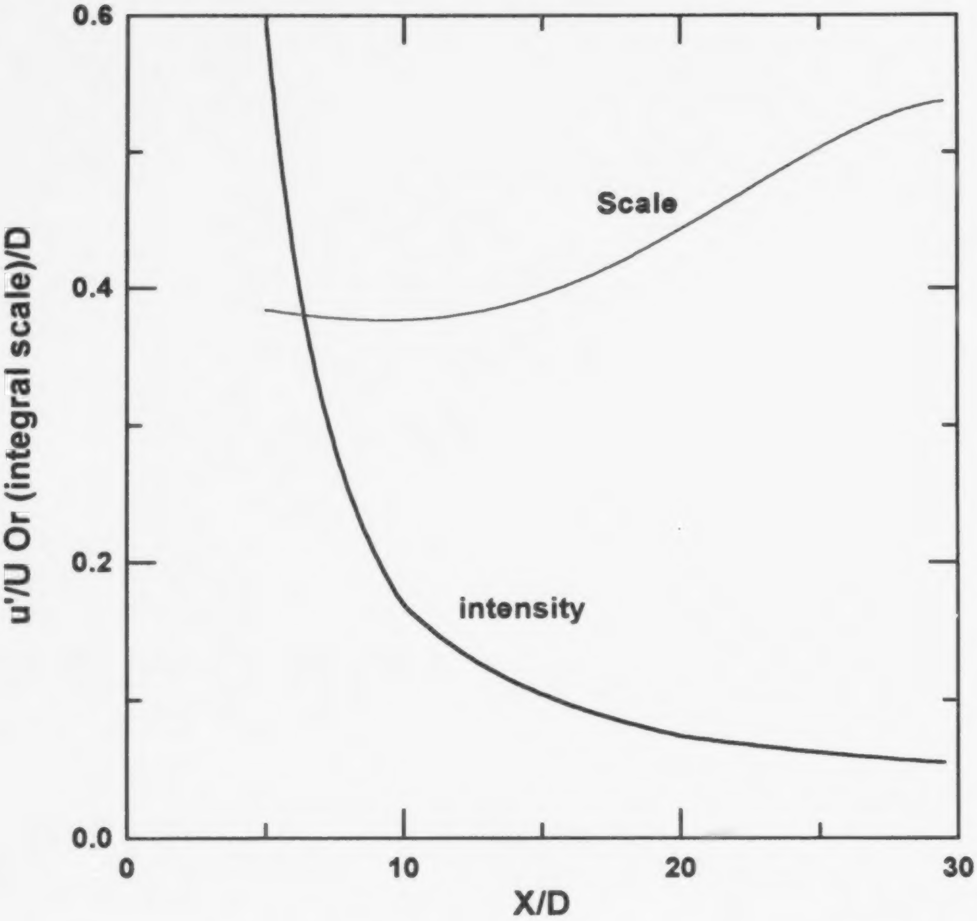

Figure 2.12: Normal turbulence decay behind a 60% solid, perforated plate.

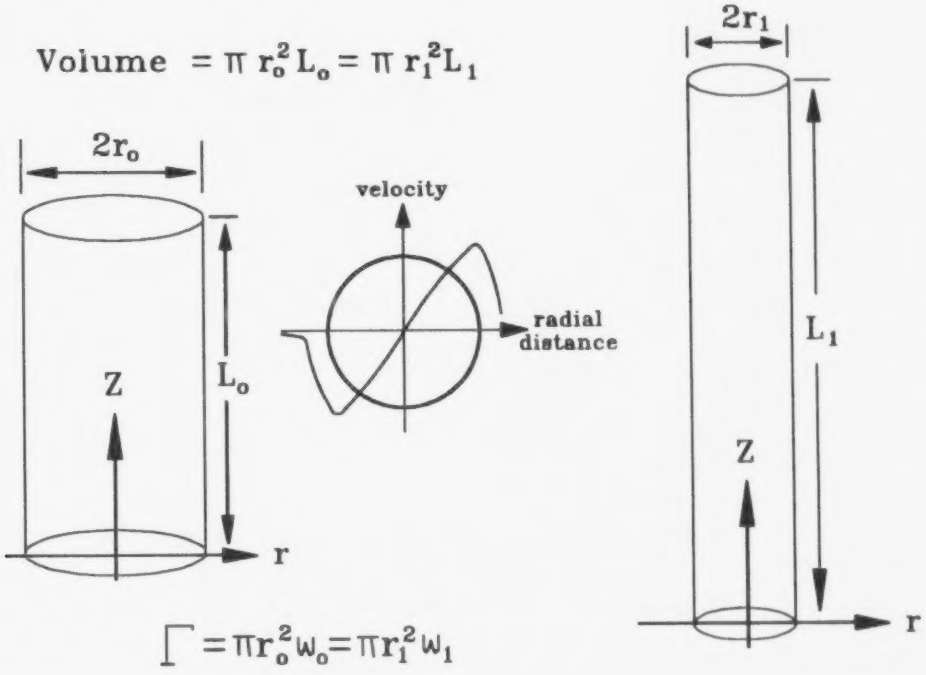
Volume = π $r_o^2 L_o$ = π $r_1^2 L_1$
2r_o
velocity
radial distance
Z
L_o
r
Γ = π$r_o^2 w_o$ = π$r_1^2 w_1$
2r_1
L_1
Z
r

Figure 2.13: The ideal vortex tube.

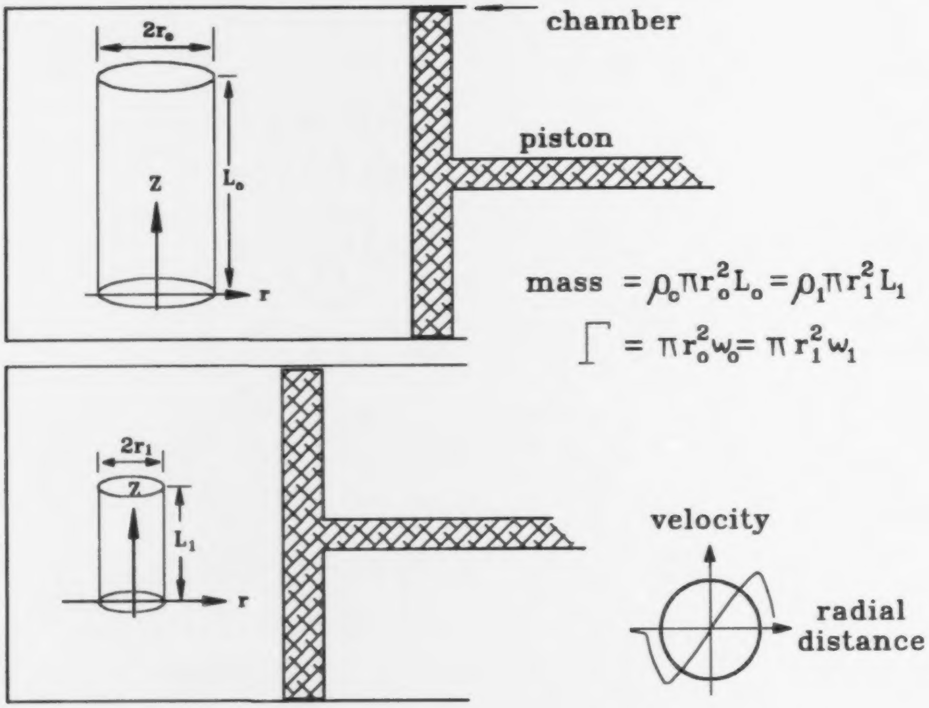
chamber
piston
$2r_o$
L_o
Z
r
mass $= \rho_o \pi r_o^2 L_o = \rho_1 \pi r_1^2 L_1$
$\Gamma = \pi r_o^2 w_o = \pi r_1^2 w_1$
$2r_1$
Z
L_1
r
velocity
radial distance

Figure 2.14: Compressing the ideal vortex tube.

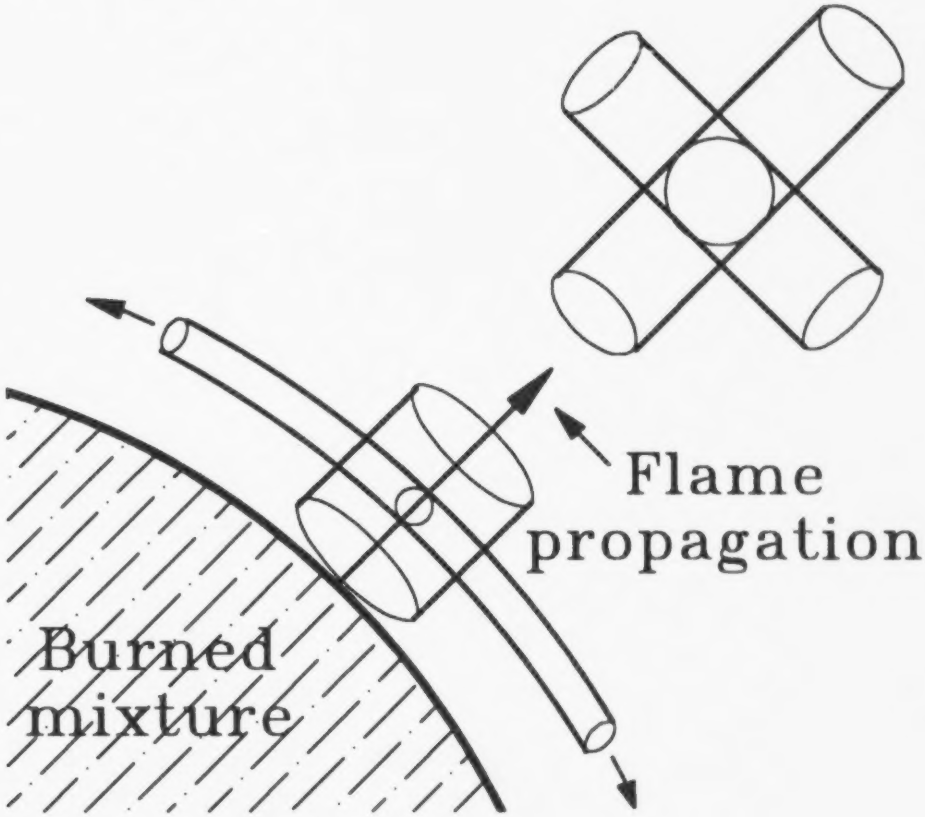
Flame
propagation
Burned
mixture

Figure 2.15: Vortex tube distortion by a spherically advancing flame.

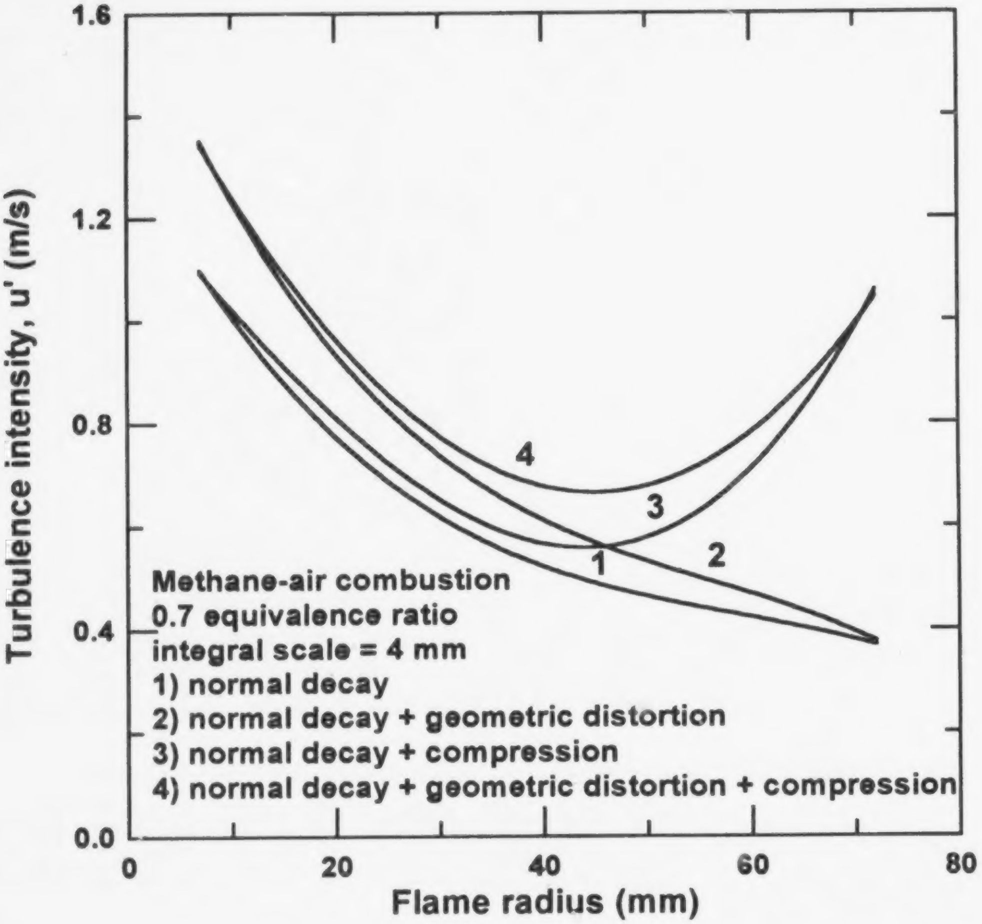

Figure 2.16: The rapid distortion effects on flame front turbulence.

CHAPTER 3

THE NUMERICAL FLAME GROWTH MODEL

This chapter describes the semi-empirical, multi-zone thermodynamic equilibrium, numerical flame growth model. It steps through the numerical algorithm while the programs and other details are given in Appendix B. This chapter investigates the semi-empirical parameters used in the flame growth model. A sensitivity analysis is conducted to check the effects of various parameters on the flame growth in a constant-volume combustion chamber. The model is used to simulate laminar flame growth and turbulent flame growth in Chapter 5 and Chapter 6 respectively.

3.1: NUMERICAL ALGORITHM

A multi-zone thermodynamic equilibrium model is employed to simulate combustion processes in the cubical combustion chamber with known mixture stoichiometry, initial pressure and temperature, initial kernel size, pressure and temperature effects, and initial turbulence along with its decay rate. The model assumes an adiabatic combustion wave of zero thickness which propagates in the radial direction from the ignition point. The code for this multi-zone model is an energy balance and thermodynamic equilibrium solver based on ideal gas property relationships as in Benson [Be77]. The mixture burnt over each time step is treated as a concentric spherical shell element.

3.1.1: QUIESCENT COMBUSTION

Curvature and stretching effects are neglected in the quiescent flame model. These effects as discussed in Chapter 2 are small over the ranges of flame size considered. The cubical chamber confinement shape effects are also omitted as the present model focuses on the early stages of flame growth. The flame is assumed to start from a spark kernel of a size estimated from experiment. The spark kernel starts burning at the experimentally determined, quasi-steady laminar burning velocity, S_l. This quasi-steady laminar burning velocity is the reference laminar burning velocity, S_{lo}, with the pressure and temperature effects accounted for. In other words, the laminar burning velocity, S_l, is calculated according to Equation 2.6. During one time step, the burning mass,

$$\Delta m_u = S_l \, A \, \rho_u \, \Delta t \tag{3.1}$$

where Δt is the time step.

The mass burned during each time step is treated as a concentric shell element. The temperature and specific heat ratio of the reactants in the next element, and of all previously burnt elements are calculated, based on the pressure before the element burns. The chamber pressure after the element burns is guessed and the program then calculates the temperature, specific heat ratio, and volume of every element assuming isentropic compression to this pressure. This is a multi-shell model in which each previously burnt element is chemically and thermally isolated from each other. Knowing the pressure and temperature before and after the element burns, the work of compression on each element is calculated. Then, an equilibrium calculation and energy balance are performed on the burning element to find its temperature, composition and volume after combustion. It should be noted that the present model does not recalculate the equilibrium of previously burnt elements. The improvement when including the equilibrium recalculation is found to be negligible [Ch94].

The equilibrium calculation includes carbon dioxide dissociation and the water-gas reaction. Specifically,

$$CO_2 \rightleftharpoons CO + \frac{1}{2}O_2 \tag{3.2}$$

$$CO + H_2O \rightleftharpoons CO_2 + H_2 \tag{3.3}$$

These five species together with nitrogen and methane are considered in the model. By comparison with STANJAN [Re87], this is found to be adequate for energy analysis of the methane-air mixtures being analyzed. Table 3.1 shows typical comparisons in flame temperature for 0.7 and 0.9 equivalence ratio methane-air mixtures ignited at 300 K. Over the range of conditions considered, the maximum adiabatic flame temperature error is less than 1%.

Table 3.1: Comparison of methane-air adiabatic flame temperatures predicted by the present model with those calculated by STANJAN [Re87].

P (atm)	1.0		1.5		2.0	
Ø	0.7	0.9	0.7	0.9	0.7	0.9
STANJAN T_{ad} (K)	1839	2135	1839	2140	1839	2143
model T_{ad} (K)	1845	2152	1845	2156	1845	2158
% error	0.3	0.8	0.3	0.7	0.3	0.7

The energy balance is

$$Q + U_r = U_p + W_{comp} \tag{3.4}$$

where Q is the element heat transfer to the other elements and/or surroundings, U_r and U_p are the internal energy of the element reactants and products, and W_{comp} is the work done by the burning element in compressing other elements. The element heat transfer can be adjusted for the heat losses to the spark electrodes, unburned mixture and the chamber walls. However, the element heat transfer is assumed to be zero in this study. The compression work done by the burning element in compressing all other elements is calculated as

$$W_{comp} = \sum \frac{P_e\,V_e - P_i\,V_i}{1 - \gamma} \tag{3.5}$$

where P_e and V_e represent pressure and volume after combustion at thermodynamic equilibrium condition, P_i and V_i are pressure and volume before combustion. The guessed pressure after the element burns, P_e, is iterated until the sum of the volume of all elements converges to the volume of the combustion chamber.

3.1.2: TURBULENT COMBUSTION

Beyond the pressure and temperature effects on the underlying laminar burning velocity, the turbulent burning velocity is also subject to turbulence effects. These turbulence effects are expressed as Equation 2.19. The linear coefficient, C_L, is found (from experimental data as discussed in Chapter 6) to be proportional to the flame radius over the square-root of the turbulent integral scale. Specifically,

$$C_L = C_D \frac{r}{\sqrt{\Lambda}} + C_I \qquad 3.6$$

where the dependence coefficient, C_D, illustrates how strongly C_L depends on the flame radius divided by the square-root of the integral scale and C_I designates the spark-induced turbulence enhancement. The values for C_D and C_I are 0.015 $mm^{-0.5}$ and 0.064 respectively as discussed in Chapter 6. Over one time step, the turbulent burning mass is given by:

$$\Delta m_u = S_t A_m \rho_u \Delta t \qquad 3.7$$

The burning mass is considered to be a concentric shell element.

3.2: SEMI-EMPIRICAL PARAMETERS

The pressure exponent of Equation 2.6 is found to be about -0.43 and -0.26 for 0.66 and 0.86 equivalence ratio methane-air flames. As the mixture stoichiometry is only accurate to within ±0.05 equivalence ratio, the 0.66 and 0.86 equivalence ratio mixtures are expressed as 0.7 and 0.9 equivalent ratio mixtures respectively. The temperature exponent, Texp, is about 2 according to [RG80]. The spark kernel radius, r_{spark}, as estimated from schlieren images is about 2 mm. The reference laminar burning velocities, S_{lo}, are 0.12 m/s and 0.25 m/s for 0.7 and 0.9 equivalence ratio methane-air flames respectively. The details of these experimentally determined values are given and discussed in Chapter 5. These empirical parameters are also confirmed by the values in the literature. For the quiescent combustion, Pexp, Texp, r_{spark} and S_{lo} are the only empirical parameters required.

For the turbulent combustion, the relation between the turbulent burning velocity, laminar burning velocity and turbulence intensity are expressed as Equation 2.18. The linear coefficient, C_L, is as expressed in Equation 3.6. Combining Equation 2.18 and Equation 3.6 leads to

$$S_t = S_l + (C_D \frac{r}{\sqrt{\Lambda}} + C_I)\, u' \qquad 3.8$$

The dependence coefficient, C_D, and the ignition coefficient, C_I, are the only two additional empirical parameters required for turbulent combustion.

3.3: SENSITIVITY ANALYSIS

A typical sensitivity analysis for 0.9 equivalence ratio laminar flame initiated at 300 K and 1 atm is summarized in Table 3.2. The default settings are: equivalence ratio of 0.9, initial temperature of 300 K, initial pressure of 1 atm, time step of 0.2 ms, unburned spark radius of 2 mm (expanding to about 4 mm after burning), pressure exponent of -0.26, temperature exponent of 2 and a reference laminar burning velocity of 0.25 m/s. Table 3.2 summarizes the sensitivity results due to ±50% change in time step, spark radius, pressure exponent and temperature exponent, and also due to ±10% variation in initial pressure, initial temperature and equivalence ratio. The effects are expressed in terms of the change of time taken to reach 200 kPa. This particular pressure is chosen because it is very close to the point when part of the flame front touches the walls of the combustion chamber.

The results from the sensitivity analysis tabulated in Table 3.2 show that the change in time step has very little effect on the pressure trace generated. Therefore, a default time step of 0.2 ms is adequate for modelling purposes. The combustion process is most sensitive to error in mixture stoichiometry. A ±10% error in equivalence ratio can lead to up to 42% error in time taken to reach 200 kPa. This mixture stoichiometry error is probably the largest source of experimental errors in the present study. The mixture stoichiometry is estimated to be within ±0.05 equivalence ratio. The second most sensitive parameter is the initial temperature. A 30 K change in initial temperature can result in 11% error in the combustion duration to reach 200 kPa. However, a thermocouple is used to monitor the initial mixture temperature. The initial temperature varied by no more than 5 K during all the experiments.

Table 3.2: Sensitivity analysis on 0.9 equivalence ratio, laminar methane-air flame ignited at 300 K and 1 atm.

Variable	Value	Time taken to reach 200 kPa (ms)
default	default	34.4
Δt (ms)	0.1 0.3	34.2 34.5
spark radius (mm)	1 3	35.4 33.2
Pexp	-0.13 -0.39	33.4 35.2
Texp	1 3	36.2 32.6
P_{init} (atm)	0.9 1.1	35.4 33.2
T_{init} (K)	270 330	38.2 31.2
Ø	0.81 0.99	48.8 26.2

Table 3.3 summarizes a typical sensitivity analysis results for a 0.9 equivalence ratio turbulent flame. The default settings are: 300 K initial temperature, 1 atm initial pressure, 0.2 ms time step, 2 mm unburnt spark radius, pressure exponent of -0.26, temperature exponent of 2, rms turbulence intensity of 0.6, integral scale of 4 mm, C_D of 0.015 $mm^{-0.5}$ and C_I of 0.064. The summary of sensitivity results tabulated in Table 3.3 are due to ±50% change in time step, spark radius, pressure exponent and temperature exponent, and also due to ±10% variation in initial pressure, initial temperature, equivalence ratio, turbulence intensity, integral scale, dependence coefficient and ignition coefficient. The effects are again expressed in term of the change of time taken to reach 200 kPa. The second last column indicates the time duration required to reach 200 kPa when the turbulence level is allowed to decay as in the cold (without

combustion) run. The last column presents time duration results to reach 200 kPa if there was no turbulence decay. In both the last and the second last columns, C_D and C_I are based on the turbulence level just ahead of the flame front. In other words, straining and compression effects are accounted for via the use of the rapid distortion model of [CB92].

The sensitivity results in Table 3.3 show once again that error in mixture stoichiometry causes the largest change in the burning rate. A 10% error in equivalence ratio can lead to 33% error in the combustion duration to reach 200 kPa. This 33% error is lower than the 42% in the laminar flame case as shown in Table 3.2. Maintaining a higher level of turbulence by omitting the turbulence decay results in an even lower error of 24%. This is probably due to the fact that increasing the turbulence level increases the turbulence enhancement. The increase in turbulence enhancement tends to mask the errors in pressure, temperature and mixture stoichiometry.

Table 3.3 also shows that ±50% changes in time step and pressure exponent have very little effect on the combustion duration. Small changes of the order of ±10% in integral scale and ignition coefficient also have insignificant effects on the combustion rate. Changes in spark radius, temperature exponent, initial pressure and temperature, turbulence intensity and the dependence coefficient have small but significant effects on the combustion rate.

Table 3.3: Sensitivity analysis on 0.9 equivalence ratio, turbulent methane-air flame with initial turbulence intensity of 1 m/s and integral scale of 4 mm.

Variable	Value	Time taken to reach 200 kPa (ms)	
default	default	* 21.2	** 18.2
Δt (ms)	0.1	21.0	18.0
	0.3	21.6	18.3
spark radius (mm)	1	22.4	19.0
	3	20.2	17.4
Pexp	-0.13	21.0	18.0
	-0.39	21.6	18.4
Texp	1	21.8	18.4
	3	20.8	17.8
P_{init} (atm)	0.9	22.0	18.6
	1.1	20.6	17.6
T_{init} (K)	270	21.8	18.2
	330	20.8	18.0
ϕ	0.81	28.2	22.6
	0.99	17.2	15.2
u' (m/s)	0.54	22.0	19.0
	0.66	21.6	17.4
Λ	3.6	21.0	17.8
	4.4	21.6	18.4
C_D ($mm^{-0.5}$)	0.014	22.0	18.8
	0.017	20.6	17.6
C_I	0.058	21.6	18.4
	0.071	21.0	18.0

* X/D at ignition is fixed at 10. The turbulence level is allowed to vary according to the normal decay and rapid distortion effects.

** The cold mixture (without combustion) turbulence intensity does not decay. The flame front turbulence level is adjusted for the rapid distortion effects.

CHAPTER 4

EXPERIMENTAL DETAILS

This chapter describes the experimental apparatus used in this study. The experimental details covered in previous theses are referred to while the modifications made since these previous studies are emphasized here.

4.1: EXPERIMENT AND ANALYSIS

Figure 4.1 shows the 125 mm cubical combustion chamber used in this study. The total hydraulic volume is 0.001882 m^3 which leads to a hydraulic cell radius of 76.6 mm. The design of this combustion chamber is based on the original design by Checkel and Thomas [CT83, Ch81]. The evolution of the combustion chamber is described following the chronological sequence of [Ch81, Mc88, Mo90, Ti92].

The chamber is made of 6066-T6 aluminum alloy. All walls are 25 mm thick. Two 30 mm thick, 110 mm diameter PK-7 optical glass windows are mounted on the front and back sides of the chamber. These two windows allow schlieren visualization of the growing flame.

A Norwood model 111 four-active-arm strain gauge pressure transducer was used to trace the combustion chamber pressure during flame propagation. A gain of 500 is used in this study. The pressure transducer is located on the side wall of the combustion chamber as shown in Figure 4.1. A typical pressure transducer calibration is given in Appendix C.

Two spark electrodes pass through the centre of the chamber. The micrometer electrode is adjusted to give a 5.00 mm spark gap at the centre of the chamber. A capacitive discharge/coil ignition with 312.5 mJ (500 V and 2.5 μF) of energy supply is used to form the spark. A detailed circuit drawing of the ignition system can be found in [Ti92].

An ionization probe is located at 60 mm (2 mm from the top wall) from the spark gap. This probe detects the flame front arrival at the top of the chamber. The ionization measurements are not described here because the schlieren images provide a better measure of the flame growth.

A heat flux sensor is placed beside the left spark electrode as shown in Figure 4.1. It is located at the centre in the vertical direction and 25 mm from the left, back edge of the chamber. It measures the propagating flame heat flux. The detailed description of this heat flux sensor and the heat flux analysis are given in [Ji94].

Figure 4.2 shows a typical perforated plate used for generating the pre-ignition turbulence. The plates have holes of diameter, D, placed on alternate intersections of a grid with spacing D to give a 60% solid ratio. The four plates used in this study have 20, 10, 5 and 2.5 mm diameter holes. All perforated plates are 5 mm thick. The turbulence generated by pulling the plate across the chamber prior to ignition is as described in Chapter 2.

A schematic of the overall experimental set-up is shown in Figure 4.3. The five main elements are the 125 mm cubical combustion chamber, the gas mixer, the four channel FM tape recorder, the gas chromatograph and the high speed video camera.

Combustible gas mixtures for this study were produced as required using a gas mixing manifold and choked flow orifices. The choked flow method used in the gas mixing procedure is described in Appendix D. This method was found to be more repeatable and easier to use than the partial pressure method.

A gas chromatograph, model P200 manufactured by Microsensor Technology Inc., was used for analysing the supply gas compositions as described in Appendix E. The analysis of the supply methane and extra dry air are given along with the premixed mixture analysis. The supply methane was found to be 99% pure.

The high speed schlieren video camera is described in Appendix F along with the schlieren image analysis. Details of the schlieren technique can be found in [Ha86, Mo90]. The schlieren image results are discussed in Chapter 5 and Chapter 6.

All experimental data except the schlieren images are recorded on the four channel FM tape recorder, RACAL store 4DS. The recorded data are digitized and analyzed on a IBM compatible 486DX2 computer. The detailed procedure and the digitization programs are presented in Appendix G.

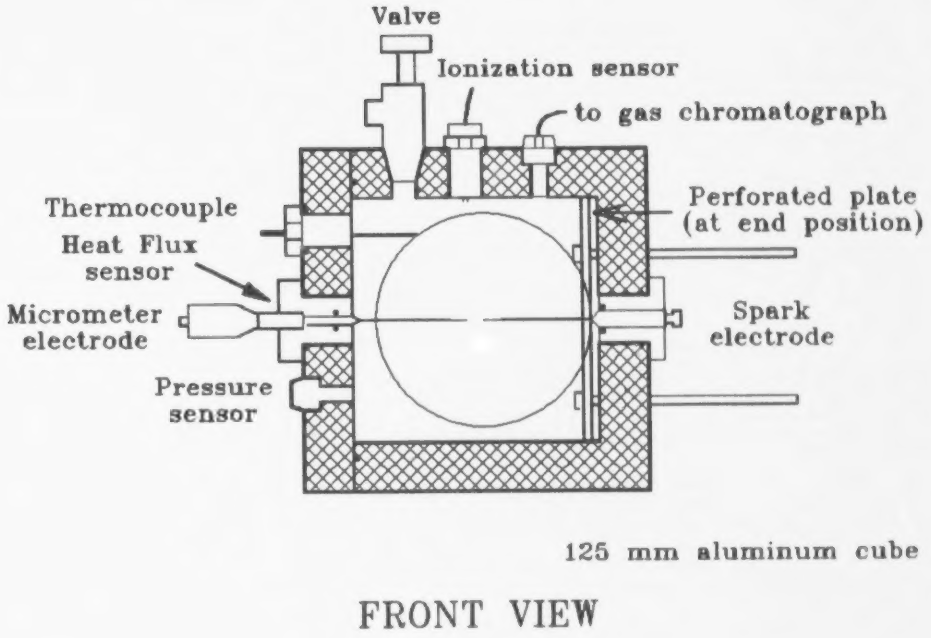
Valve
Ionization sensor
to gas chromatograph
Thermocouple
Heat Flux sensor
Micrometer electrode
Pressure sensor
Perforated plate (at end position)
Spark electrode
125 mm aluminum cube
FRONT VIEW

Figure 4.1: The 125 mm cubical combustion chamber.

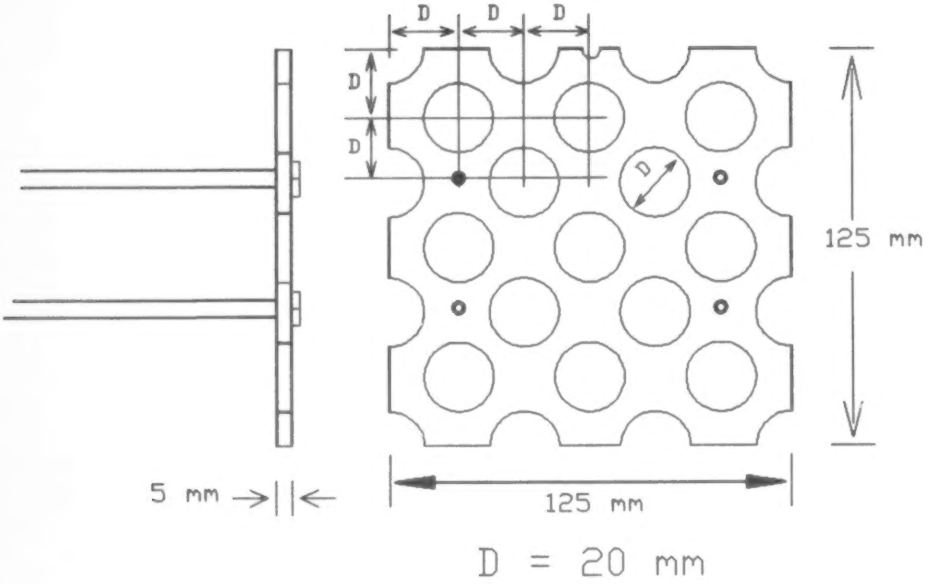
D
D
D
D
D
D
125 mm
5 mm
125 mm
D = 20 mm

Figure 4.2: The 60% solid, perforated plate with 20 mm diameter holes.

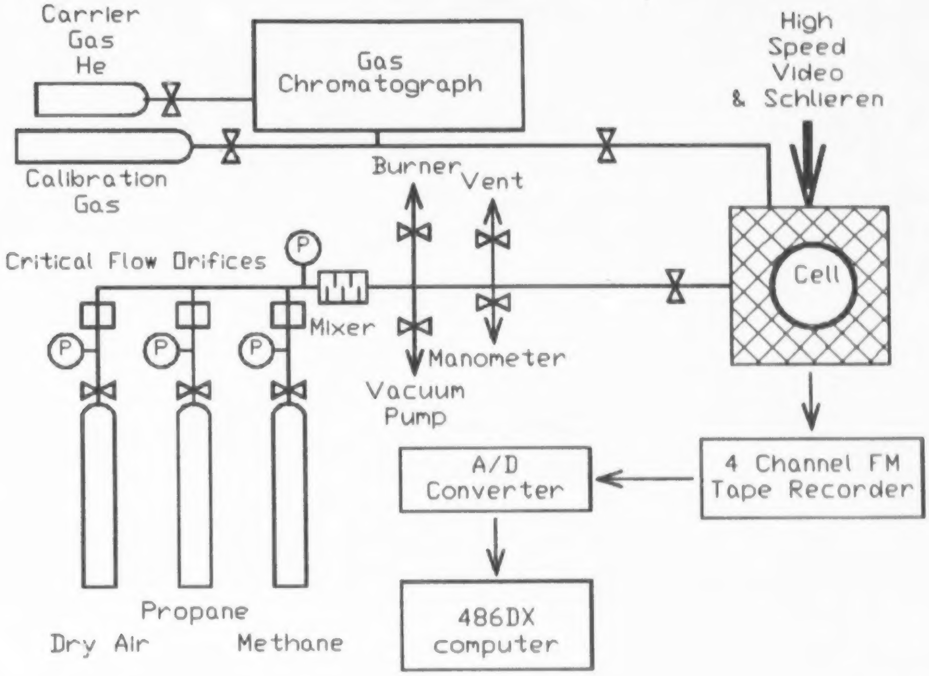
Carrier Gas He
Gas Chromatograph
High Speed Video & Schlieren
Calibration Gas
Burner
Vent
Critical Flow Orifices
P
Cell
Mixer
Manometer
Vacuum Pump
A/D Converter
4 Channel FM Tape Recorder
486DX computer
Propane
Dry Air
Methane

Figure 4.3: A schematic of the experimental apparatus.

CHAPTER 5

LAMINAR FLAME GROWTH RESULTS AND DISCUSSION

This chapter summarizes all major laminar methane-air flame growth results. Further details and tabulations of the experimental data are given in Appendix H. This chapter discusses both experimental and numerical quiescent combustion processes inside the cubical combustion chamber. It also compares the numerical calculations with the experiments. This chapter ends with a summary describing the important features of spark ignited, laminar flame growth in a constant volume combustion chamber.

5.1: EXPERIMENTAL RESULTS

Methane-air mixtures of equivalence ratio from 0.6 to 1.0 were ignited at 300 K and 1 atm. Note that these equivalence ratios are given to one decimal place portraying that they are accurate to within ±0.05. The actual equivalence ratios according to the choked flow method are given up to the second decimal place. The wide range of equivalence ratios were used to study the effect of equivalence ratio on laminar flame growth. For 0.7 and 0.9 equivalence ratio flames, initial pressures of 0.5, 1.0, 1.5 or 2.0 atm were used to investigate the effect of pressure on these flames. The initial temperature and spark gap were fixed at 300 K and 5.00 mm respectively throughout this study. The ignition energy supply was fixed at 312.5 mJ unless otherwise specified.

5.1.1: COMPARISON BETWEEN SCHLIEREN VIDEO AND PRESSURE TRACE ANALYSIS

The flame growth was visualized simultaneously using a schlieren system while monitoring the combustion chamber pressure rise. The flame schlieren edge corresponds closer to the unburnt mixture than the luminous zone [Fr65, RG80, Gl87]. While the luminous zone underestimates the location of the flame front, the outer schlieren edge tends to over-estimates the flame front location slightly. In other words, the use of outer schlieren edge (closest to the unburned mixture) probably leads to the inclusion of a small portion of the preheat zone as the burnt mixture. However, with the relative small flame thickness (~0.5 mm [GM92]), the over-estimation error is expected to be negligible.

Typical 0.7 and 0.9 equivalence ratio laminar flame growth schlieren images are shown in Figure 5.1. These laminar flames were ignited at 300 K and 1 atm. The time durations between two consecutive flame images are 5.0 ms and 2.5 ms for the 0.7 and 0.9 equivalence ratio laminar flames respectively. The figure shows that the flames remained relatively spherical during the early flame growth period.

Figure 5.2 shows typical flame growth comparison between schlieren video and pressure trace analysis. Note that while the combustion chamber is a 125 mm cube the hydraulic radius is 76.6 mm. The 0.7 and 0.9 equivalence ratio methane-air mixtures were ignited at 300 K and 1 atm. While the schlieren video is limited to flames smaller than the circular windows, the pressure trace analysis is noisy at the very early flame growth period. In general, the figure shows close agreement between schlieren images and pressure trace analysis. This agreement validates the use of schlieren video at the very early period of flame growth in which the pressure trace is noisy.

Based on the 0.9 equivalence ratio laminar flame growth shown in Figure 5.2, both the flame growth rate and the burning velocity are determined. The flame growth rate as defined in Chapter 2 is simply the slope of the plot in Figure 5.2. The laminar burning velocity is calculated based on the multi-zone thermodynamic equilibrium model as described in Appendix B. Both laminar flame growth rate and laminar burning velocity are plotted against the flame radius in Figure 5.3. The figure shows that the flame growth rate of a laminar flame with quasi-steady laminar burning velocity is highly transient in a closed chamber. The gas expansion velocity is initially directed away from the ignition point, adding to the laminar burning velocity. As the amount of burned volume increases, the pressure inside the chamber starts to rise. As a consequence, the burning shell of mixture begins to expand in both radially inward and radially outward directions from the ignition point. The outward expansion slows down with further increase in chamber pressure. Therefore, the flame growth rate decreases as the flame grows inside a chamber as shown in Figure 5.3. The laminar burning velocity as plotted in Figure 5.3 remains quasi-steady as the flame grows. While the increase in pressure tends to reduce the burning velocity, the increase in the unburned mixture temperature due to compression has a positive effect. The overall pressure and temperature effects inside the chamber tends to increase the laminar burning velocity slightly as the flame grows. The slight increase in laminar burning velocity is mostly due to the stronger temperature enhancement compared with the smaller pressure diminishment.

5.1.2: THE EFFECTS OF MIXTURE STOICHIOMETRY ON LAMINAR FLAME GROWTH

The schlieren flame images in Figure 5.4 illustrate the effect of mixture stoichiometry on methane-air flame growth. All mixtures were ignited at 300 K and 1 atm. The time step between two consecutive frames of 1.0, 0.9 and 0.8 equivalence ratio flames is 2.5 ms. A larger time step of 5 ms is used for the slower burning, 0.7 equivalence ratio flame. For the very slow burning, 0.6 equivalence ratio flame, a 10 ms time step is employed. The figure shows that 1.0, 0.9, 0.8 and 0.7 equivalence ratio flames propagate swiftly through the chamber maintaining their roughly spherical shape. On the other hand, the very lean, 0.6 equivalence ratio flame is growing too slowly to escape the effects of buoyancy. Part of the 0.6 equivalence ratio flame ball is in contact with the upper wall over a relatively long period of time. Therefore, a significant amount of heat loss via conduction is expected for this very lean flame.

Figure 5.5 shows the typical pressure traces of 1.0, 0.9, 0.8, 0.7 and 0.6 equivalence ratio, laminar methane-air flames ignited at 300 K and 1 atm. From stoichiometric to 60% stoichiometric, the maximum pressure decreases while the time required to reach the maximum pressure increases notably. As the mixture becomes leaner, the amount of heat release decreases and hence a decrease in maximum pressure rise. Leaner mixture also leads to slower reaction rate and hence a longer combustion time. The longer combustion period allows more time for heat losses. This is especially true for the 0.6 equivalence ratio flame as shown in Figure 5.4 where part of the flame is in contact with the upper wall over a long period of time. As a consequence, the maximum pressure rise falls progressively short of the ideal adiabatic maximum pressure rise for leaner mixture. While the stoichiometric to 70% stoichiometric flames reach about 80% of the maximum adiabatic pressures, the 60% stoichiometric flame falls significantly lower than its adiabatic value. Using the present experimental apparatus, Jiang [Ji94] found that the heat flux to the wall increases gradually before flame contact. The heat flux increases sharply as the flame reaches the wall. In short, most of the heat loss occurs after the flame front is in contact with the chamber walls. This happens at the later stages of the combustion process which is outside the scope of this thesis.

Burning velocities as functions of equivalence ratio are compared with others in Figure 5.6. The comparison is made with the 19 mm radius flames measured from the schlieren images in this study. This particular flame size is used for comparison because the corresponding unburnt temperature and pressure are approximately unchanged from the initial settings of 300 K and 1 atm. Therefore, no pressure or temperature adjustment is required. Moreover, at 19 mm, the flame curvature effect is small due to the small flame thickness to flame radius ratio (~ 0.05). There are also enough flame images above and below the 19 mm radius flame for averaging. In general, Figure 5.6 shows that the present laminar burning velocities are lower but within the band of literature values. The somewhat lower laminar burning velocities could be due to discrepancies in actual fuel content or mixture stoichiometry between studies along with conduction heat losses to the spark electrodes and radiation heat losses to the chamber walls. The flame response can be qualitatively reversed when the flame stretch changes from positive to negative, especially for flame with a non-zero Markstein number [TI93, EC89]. The expanding spherical flame undergoes positive flame stretch while a Bunsen flame experiences negative flame stretch. Comparatively, the expanding spherical flame loses more heat to a diverging cold sorrounding than a burner flame. On the other hand, burner flames tend to retain more heat, especially in a heated environment. Therefore, the burning velocity deduced from a spherically expanding flame is generally lower than that deduced from the burner flame. For the current experiment, the radiation heat loss was estimated to cause a 5 to 10% reduction in the actual burning velocity [Ji94].

5.1.3: THE EFFECTS OF PRESSURE ON LAMINAR FLAME GROWTH

Figure 5.7 shows 0.9 equivalence ratio laminar flame growth under the effect of pressure. The time step between two consecutive flame images is 2.5 ms. The flame growth rate is slower with increasing initial pressure.

The pressure effect on 0.7 equivalence ratio laminar flame growth is shown in Figure 5.8. The time step between two consecutive flame images is 5.0 ms. Increasing the initial pressure from 0.5 to 2.0 atm leads to increase in the schlieren image intensity. The flame growth rate decreases by a factor of two when the initial pressure is increased from 0.5 atm to 2.0 atm. Pressure seems to have a much larger effect on leaner flames when comparing Figure 5.8 with Figure 5.7.

The pressure effect was studied explicitly because of a relatively large pressure rise ratio of about seven. The range of flame sizes considered in this thesis is from spark kernels up to 55 mm radius. Over this period of flame growth, the pressure inside the chamber doubled. Figure 5.9 shows the plots of laminar burning velocity measured for different initial pressures. The laminar burning velocity values are calculated from 19 mm radius flames based on schlieren image analysis. The figure shows that the laminar burning velocity decreases with increasing pressure as expected. The pressure effect is stronger for the leaner 0.7 equivalence ratio flame compared with the 0.9 equivalence ratio flame. This agrees with the comparison made between Figure 5.7 and Figure 5.8. The pressure exponents are also tabulated in Table 5.1. These pressure exponents are in approximate agreement with others [Gi56, AG61, BH71, RG80, EC89] drawn from the literature. Part of the discrepancy can be due to the different ranges of pressure used. The trend about more negative pressure exponent for leaner mixture agrees with [EC89].

Table 5.1: Pressure exponent of laminar burning velocity.

Ø	Pexp this study	 other studies
0.7	-0.43	-0.58 [EC89]
0.9	-0.26	-0.47 [EC89]
1.0	-	-0.26 [AG61], -0.27 [Gi56], -0.5 [BH71], -0.265 [RG80]

5.1.4: LAMINAR BURNING VELOCITY AS A FUNCTION OF FLAME RADIUS

This section discusses the quasi-steady burning behaviour of the spark-ignited, premixed, laminar flame. As the premixed laminar flame grows from the spark kernel, the pressure, temperature, flame front curvature and straining alter notably. However, over the flame sizes considered, the combined effect due to pressure, temperature, curvature, straining and chamber geometry is small. In other words, the laminar burning velocity remains roughly constant as the flame grows inside the combustion chamber. This study does not intend to decouple all the effects on the growing flame. However, the purpose behind this laminar flame section is to set a baseline for the turbulent flame growth. Over the range of flame sizes considered, the change in laminar burning velocity is within 10% of the average. On the other hand, the turbulent burning velocity as discussed in Chapter 6 changes by more than a factor of two in most cases.

The average laminar burning velocities as functions of equivalence ratio and flame radius results are summarized in Figure 5.10. All mixtures are ignited at 300 K and 1 atm. The figure shows that over the range of 15 to 69 mm flame radii considered, the laminar burning velocities remain approximately unaltered as the flames grow. Omitting the noise in the early pressure trace results can lead to a few observations. First, the laminar burning velocities for 1.0, 0.9 and possibly 0.8 equivalence ratio flames appear to increase slightly as the flames grow. This as explained before is likely due to the larger temperature enhancement than pressure diminishment. The small increase in laminar burning velocity as the flame grows is less obvious as the flame becomes leaner. The 0.7 and 0.6 equivalence ratio flames indeed show a decrease for flames larger than 55 mm in radius. There are two possible reasons for this decrease in laminar burning velocity. First of all, part of the flame front is in contact with the chamber walls when the flame grows larger than 55 mm in radius. For the 0.6 equivalence ratio flame, the flame ball is in contact with the upper wall way before the flame grows to 55 mm in radius. The second reason is that the negative pressure effect is stronger for leaner flames as shown in the last section.

The variations in laminar burning velocity as shown in Figure 5.10 are of the magnitude of the experimental scatter. Therefore, no attempt is made here to analyze the detailed effects of curvature on laminar burning velocity. However, the geometric stretching due to expanding spherical flame ball is estimated for completeness. The stretch rate can be defined [La88] as

$$k = \frac{1}{A}\frac{dA}{dt} = \frac{2}{r}\frac{dr}{dt} \qquad 5.1$$

for an expanding spherical laminar flame. Figure 5.11 shows the changes in stretch rate as the flames grow. The slower (leaner) the flame, the smaller the stretch rate as expected. The stretch rate initially increases as the flame kernel grows from a spark. This initial increase in stretch rate can be due to the intense spark energy supply which accelerates the flame. The stretch rate then decreases roughly proportional to the inverse of the flame radius as the flame grows larger. For 1.0 to 0.6 equivalence ratio laminar flames ignited at 300 K and 1 atm, the maximum stretch rate is about 530 s^{-1}.

5.2: COMPARING NUMERICAL SIMULATIONS WITH EXPERIMENTS

As discussed in Chapter 3, the present numerical model uses the experimentally determined reference laminar burning velocity, S_{lo}, as the starting point. The underlying chemical kinetics within the reference laminar burning velocity is left outside the scope of this thesis. The next subsection compares the experimental results with numerical calculation with no adjustment for pressure and temperature effects. The experimentally determined pressure and temperature effects are then applied and the comparison is made again.

5.2.1: CONSTANT BURNING VELOCITY LAMINAR FLAME PROPAGATION

Figure 5.12 compares the numerical simulations when assuming no pressure and temperature effects with experiments. In other words, the temperature and pressure exponents are set to zero while using a 0.2 ms time step and a 2 mm radius unburned spark. All mixtures are ignited at 300 K and 1 atm. The figure shows rather good agreements between numerical simulations and experiments even without any temperature and pressure corrections. For a typical 0.9 equivalence ratio flame, the numerical pressure trace takes about 7 ms longer to reach 200 kPa (about 7% error in terms of the time taken to reach 200 kPa). The numerically simulated pressure traces rise slightly slower than the experiments because the overall temperature enhancement over pressure diminishment has been omitted. The very lean, 0.6 equivalence ratio flames show severe disagreement between model prediction and experiments at later time. The actual pressure rise is much slower than the model prediction at later times because of drastic heat loss via conduction to the upper chamber wall.

5.2.2: LAMINAR FLAME GROWTH IN A CLOSED CHAMBER

Using pressure exponents of -0.26, -0.26, -0.35, -0.43 and -0.43 for 1.0, 0.9, 0.8, 0.7 and 0.6 equivalence ratio flames respectively lead to results as shown in Figure 5.13. A temperature exponent of 2 is assumed for all the mixtures considered. All combustion processes shown are initiated from 300 K and 1 atm. Other than the 0.6 equivalence ratio flame, the model predictions agree closely with experiments. For a typical 0.9 equivalence ratio flame, the numerical pressure trace takes about 3 ms longer to reach 200 kPa (about 3% error in terms of the time taken to reach 200 kPa). The agreements shown in Figure 5.13 are better than those in Figure 5.12. The conduction heat loss to the upper wall for the 0.6 equivalence ratio flame is again shown by the substantially lower pressure rise at later time.

5.3: SUMMARY OF LAMINAR FLAME GROWTH IN A CHAMBER

Both high speed schlieren video and pressure trace analysis were used in studying the laminar methane-air flames in a combustion chamber. Methane-air mixtures of 1.0, 0.9, 0.8, 0.7 and 0.6 equivalence ratios were ignited at 300 K in a 125 mm cubical combustion chamber. The study focused on flames ignited at 1 atm. For the 0.7 and 0.9 equivalence ratio flames, the pressure effect was studied by varying the initial pressure from 0.5 to 2.0 atm.

In general, the two-dimensional schlieren flame images show approximately spherical laminar flame growth during the early combustion period. However, for the very lean 0.6 equivalence ratio flame, the flame growth is slow enough to allow buoyancy force to convect the flame upward. The flame convection also causes a large dimple into the bottom of the flame ball.

Flame growths from schlieren flame images agree well with those calculated from pressure trace analysis using a multi-zone thermodynamic equilibrium model. The agreement between these two independent analyses confirm the validity of the experiment.

From stoichiometric to 0.6 equivalence ratio flames, the laminar burning velocity decreases as expected. The quasi-steady laminar burning velocities found in this study are within the band of literature values but somewhat lower than the well-accepted values. The disagreements are probably due to heat losses which are not accounted for in the present study and the discrepancies in fuel compositions and mixture stoichiometry. The sensitivity analysis shows that the largest error can be due to discrepancies in mixture stoichiometry.

Pressure has a negative effect on the methane-air laminar burning velocity. The pressure exponents are found to be -0.26 and -0.43 for 0.9 and 0.7 equivalence ratio methane-air flames respectively over the range of conditions tested. These pressure exponent values and the trend of more negative pressure effect for leaner fuel are in agreements with the literature.

The empirical spark size, reference laminar burning velocity, pressure and temperature exponents are employed in the numerical model. The model is a multi-zone, thermodynamic equilibrium calculation assuming adiabatic thin flame front propagation. With proper temperature and pressure effects accounted for, the numerical predictions agree well with the experiments.

Ø=0.7, Δt=5.0 ms

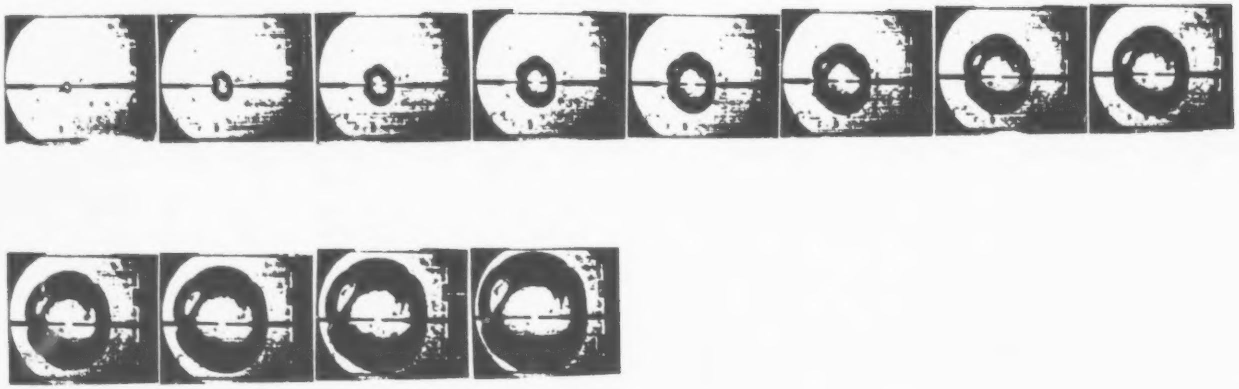

Ø=0.9, Δt=2.5 ms

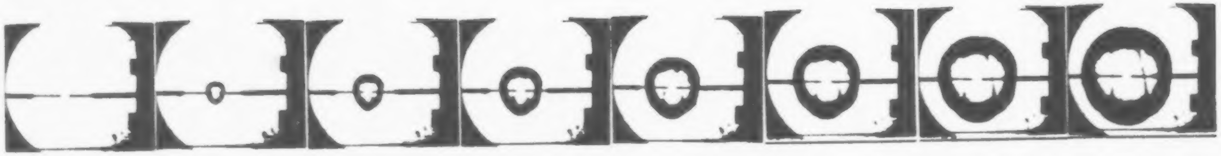

Figure 5.1: Typical laminar flame growth schlieren images.
Ø=0.7, 0.9; P_{init}=1 atm; T_{init}=300 K; Δt=5.0 ms for Ø=0.7 and 2.5 ms for Ø=0.9.

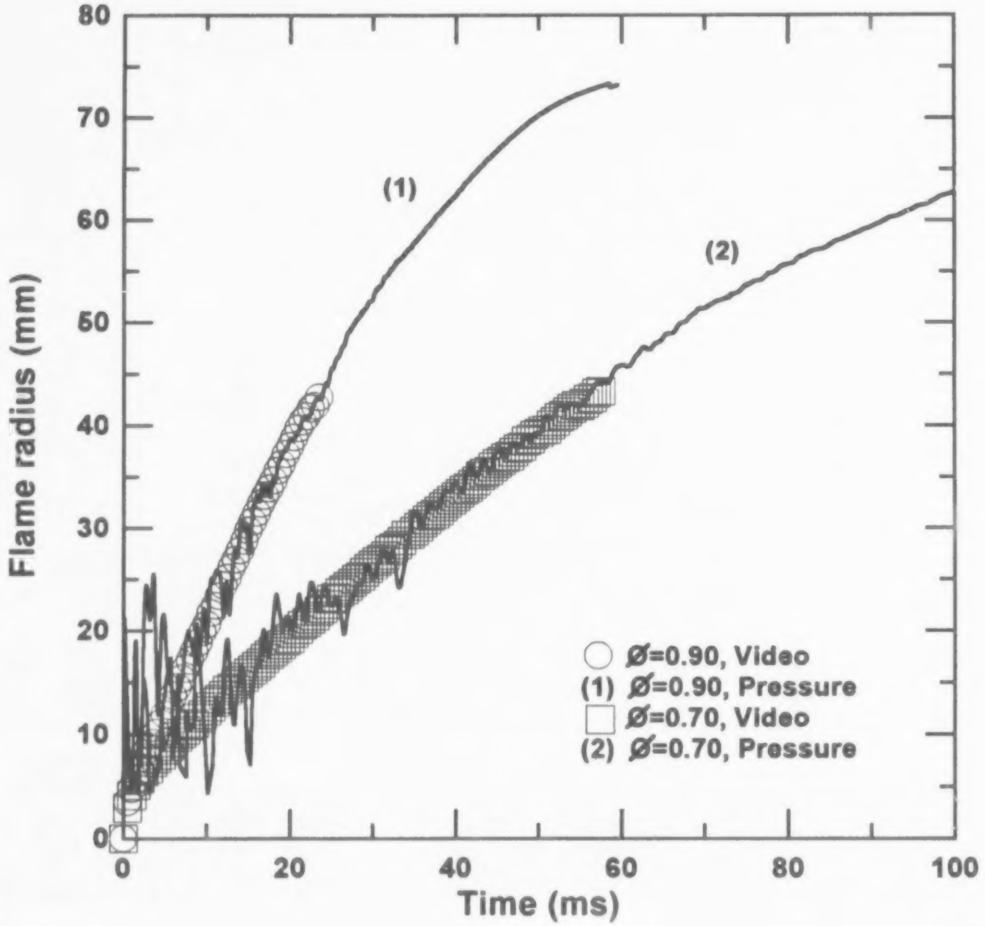

Figure 5.2: Comparison of laminar flame growth measured from schlieren images and the pressure trace.
Ø=0.7, 0.9; P_{init}=1 atm; T_{init}=300 K.

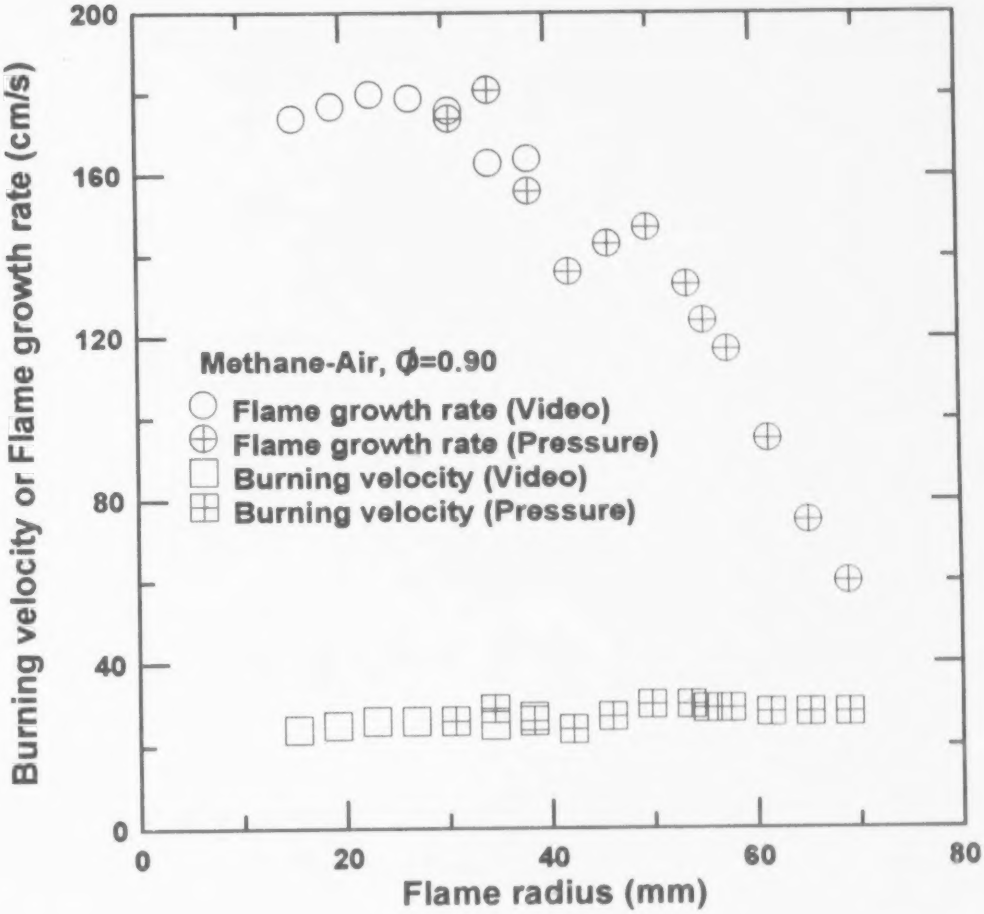

Figure 5.3: Comparison of laminar flame growth rate and laminar burning velocity calculated from schlieren images and the pressure trace.
Ø=0.9; P_{init}=1 atm; T_{init}=300 K.

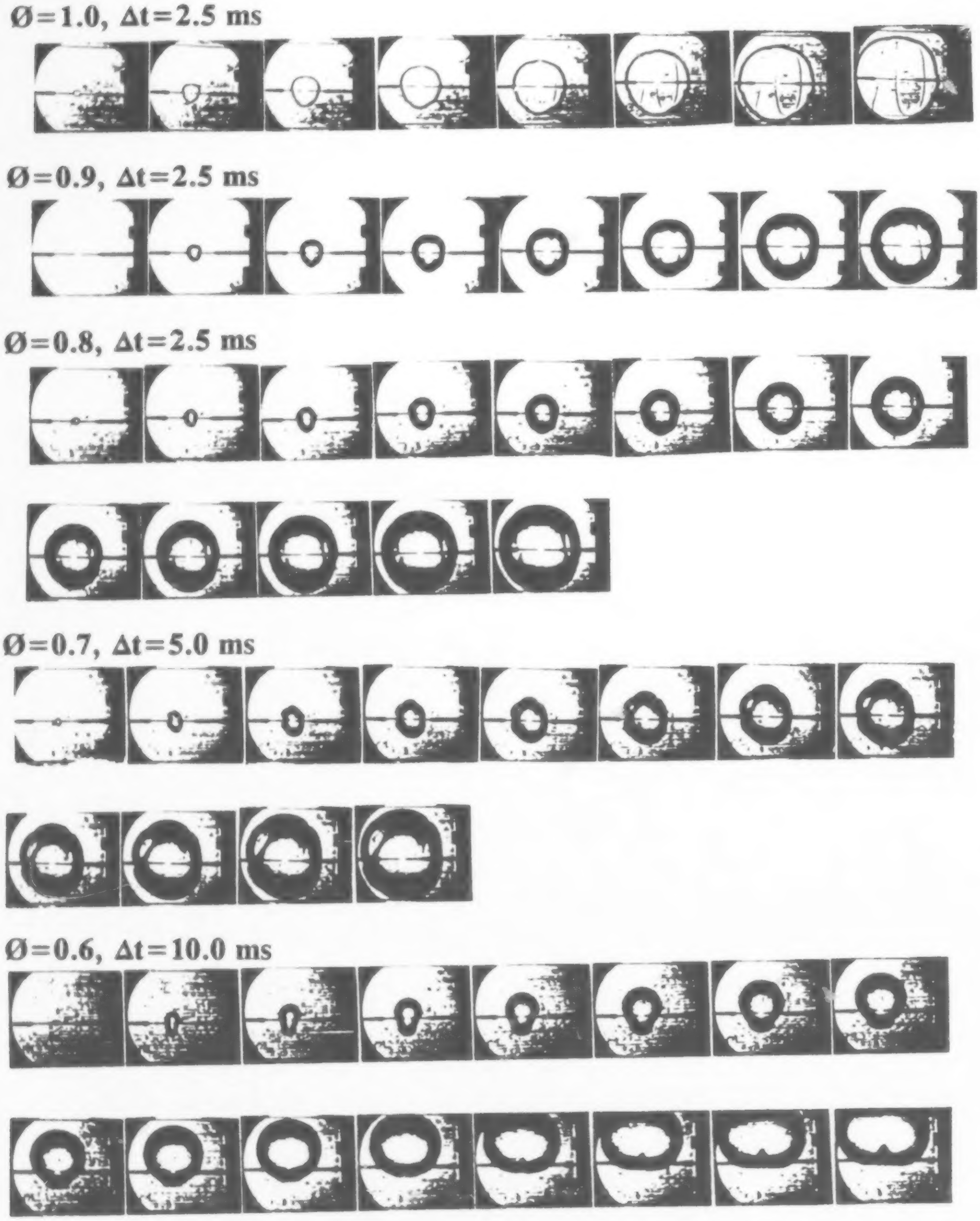

Ø=1.0, Δt=2.5 ms

Ø=0.9, Δt=2.5 ms

Ø=0.8, Δt=2.5 ms

Ø=0.7, Δt=5.0 ms

Ø=0.6, Δt=10.0 ms

Figure 5.4: The effects of mixture stoichiometry on laminar flame growth. Ø=1.0, 0.9, 0.8, 0.7, 0.6; $P_{init}=1$ atm; $T_{init}=300$ K; Δt=2.5 ms for Ø=1.0, 0.9, 0.8; Δt=5.0 ms for Ø=0.7 and 10.0 ms for Ø=0.6.

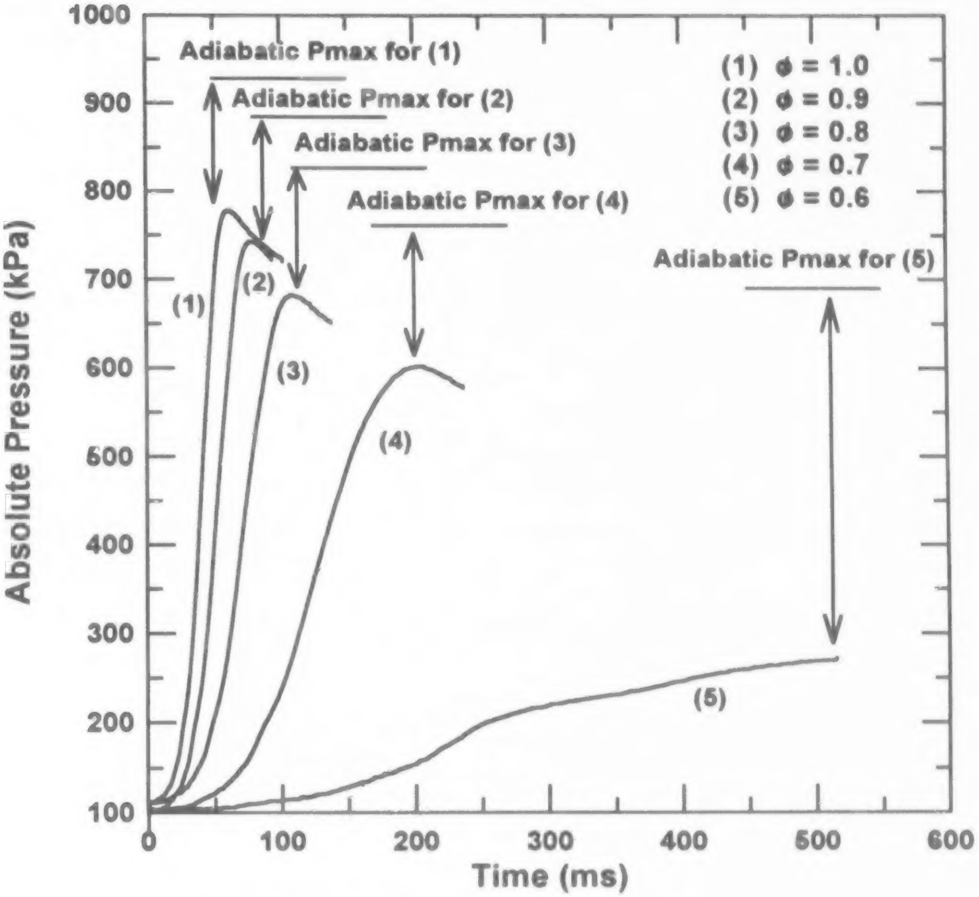

Figure 5.5: The effects of mixture stoichiometry on combustion chamber pressure rise. Ø=1.0, 0.9, 0.8, 0.7, 0.6; P_{init}=1 atm, T_{init}=300 K.

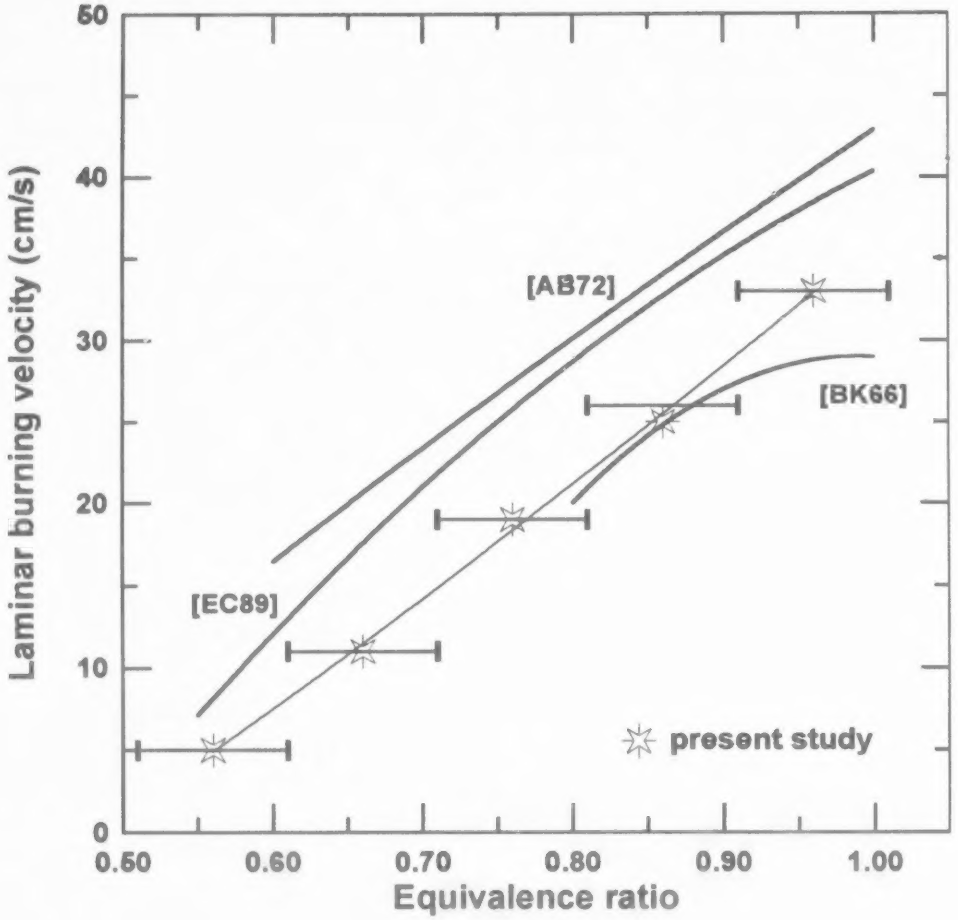

Figure 5.6: Laminar burning velocity as a function of equivalence ratio compared with others.

T_o=300 K, P_o=1 atm; Solid horizontal lines are the error bars due to uncertainty in mixture stoichiometry.

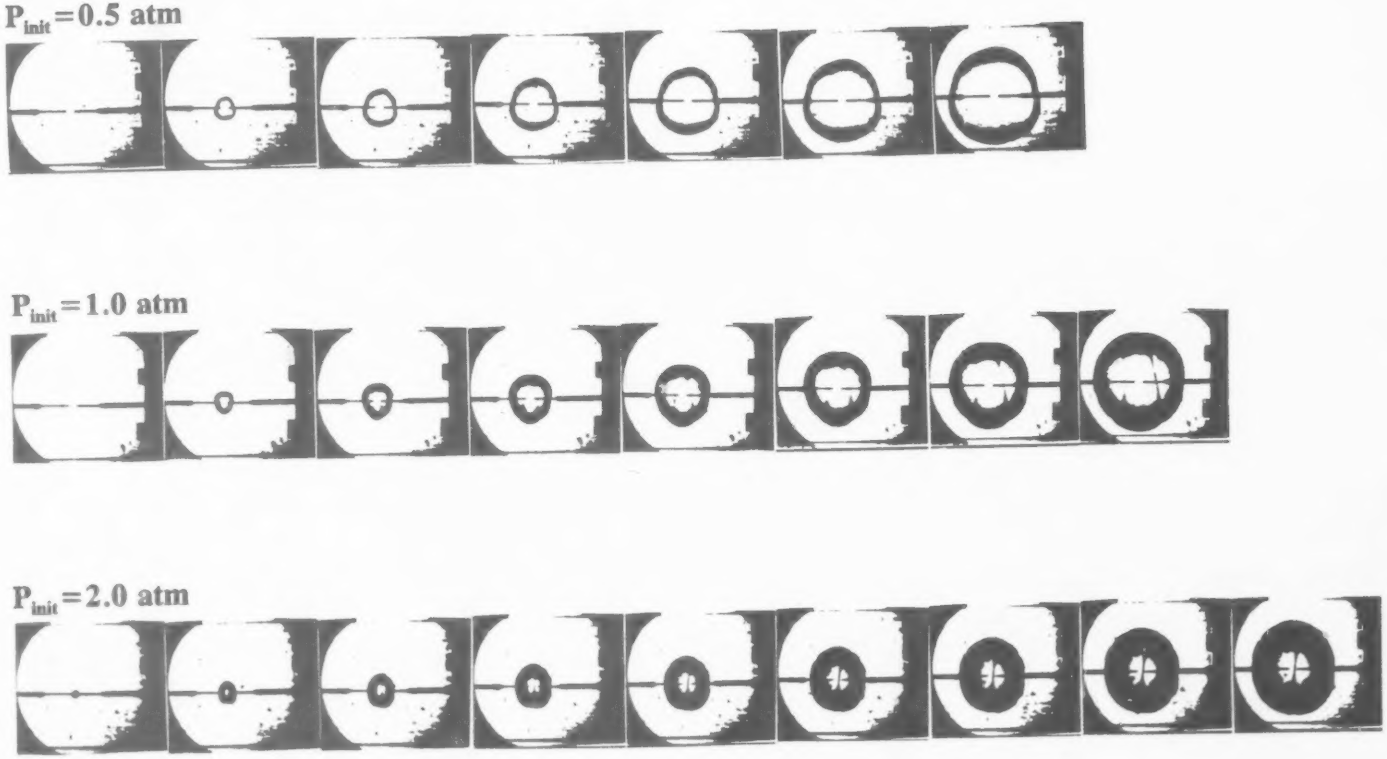
$P_{init} = 0.5$ atm
$P_{init} = 1.0$ atm
$P_{init} = 2.0$ atm

Figure 5.7: The effects of pressure on 0.9 equivalence ratio laminar flame growth. $P_{init} = 0.5, 1.0, 2.0$ atm; $T_{init} = 300$ K; $\Delta t = 2.5$ ms.

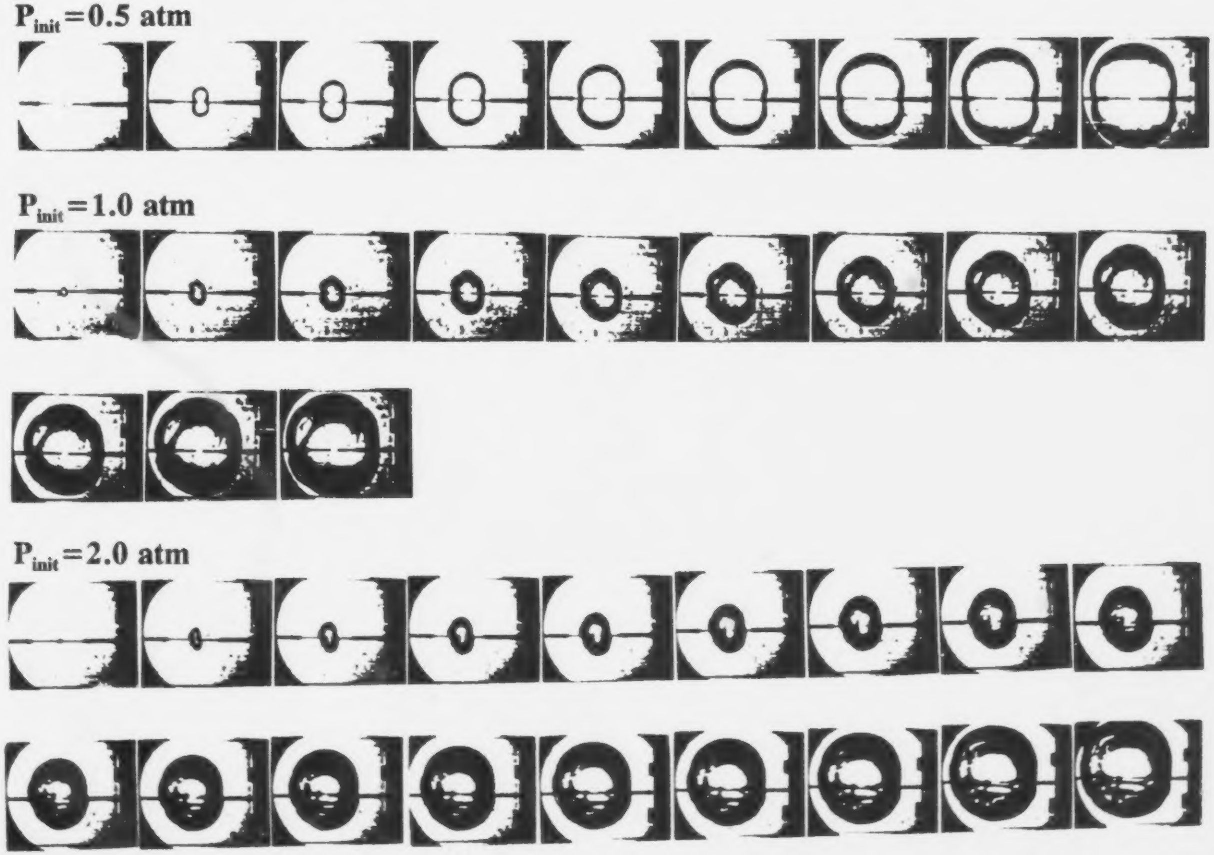
$P_{init}=0.5$ atm
$P_{init}=1.0$ atm
$P_{init}=2.0$ atm

Figure 5.8: The effects of pressure on 0.7 equivalence ratio laminar flame growth. $P_{init}=0.5$, 1.0, 2.0 atm; $T_{init}=300$ K; $\Delta t=5.0$ ms.

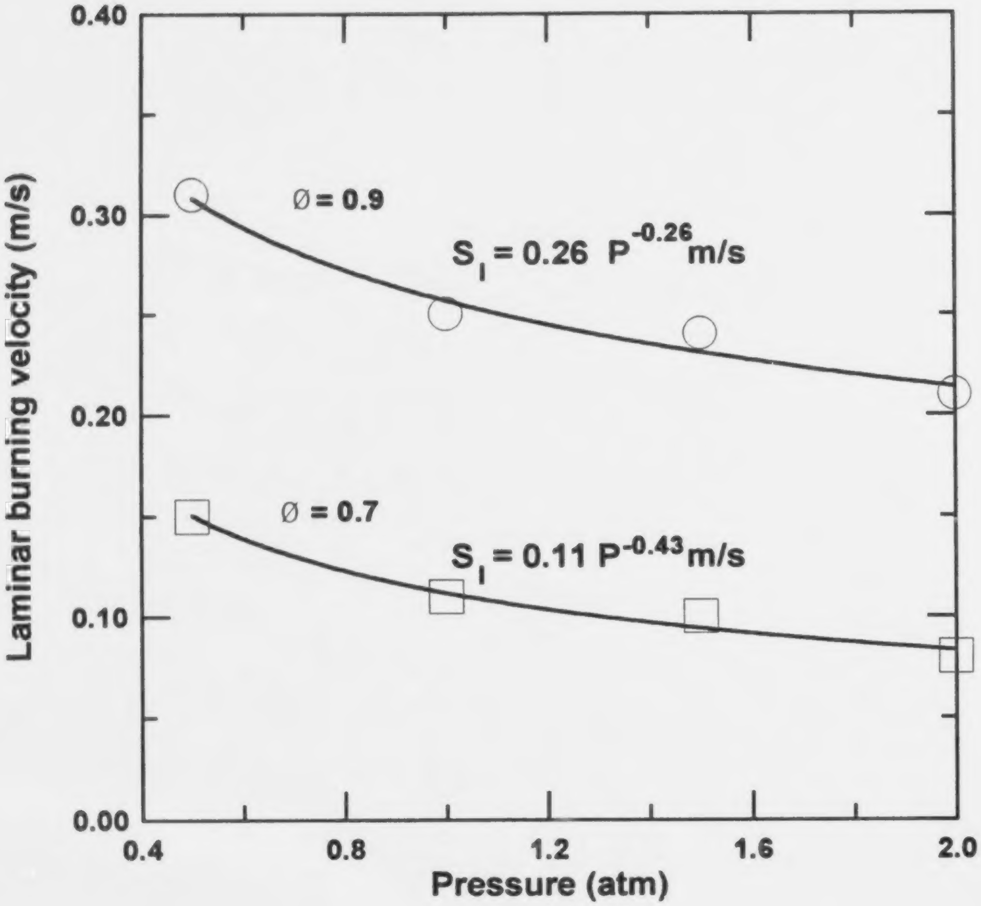

Figure 5.9: The effects of pressure on laminar burning velocity.
Ø=0.9, 0.7; P_{init}=0.5, 1.0, 1.5, 2.0 atm; T_{init}=300 K.

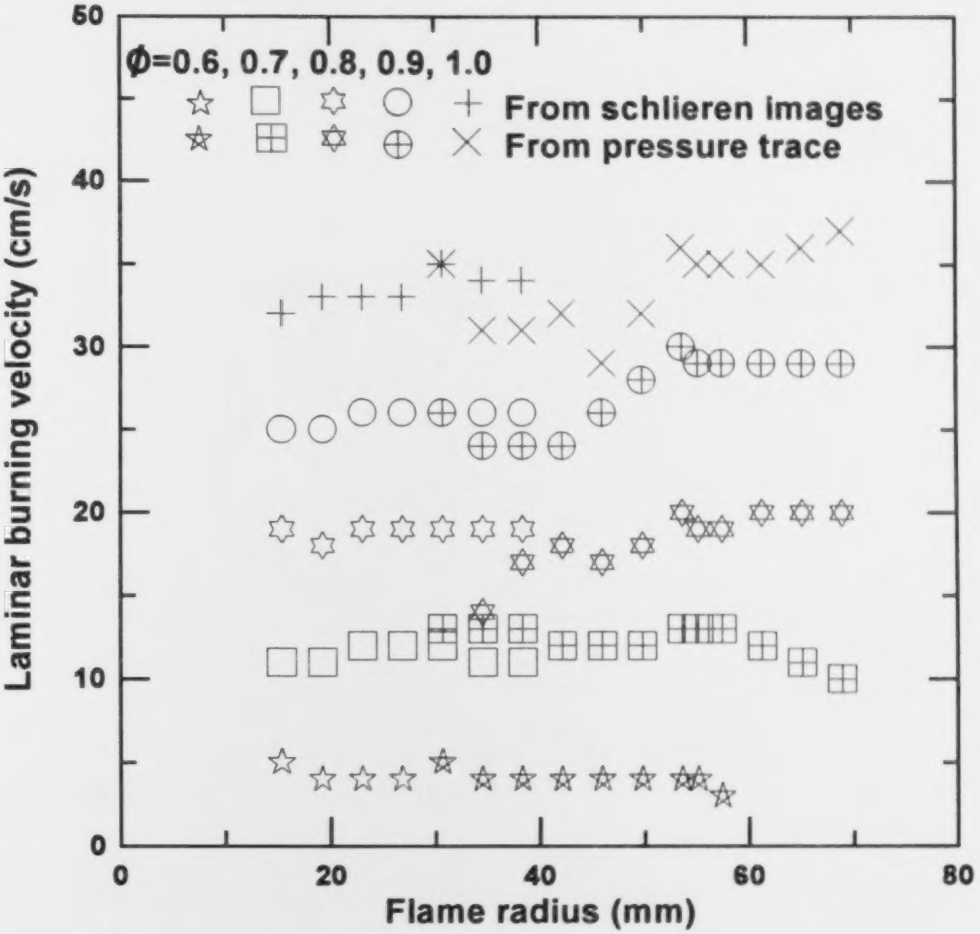

Figure 5.10: Typical laminar burning velocities as functions of flame radius. Ø=1.0, 0.9, 0.8, 0.7, 0.6; P_{init}=1.0 atm; T_{init}=300 K.

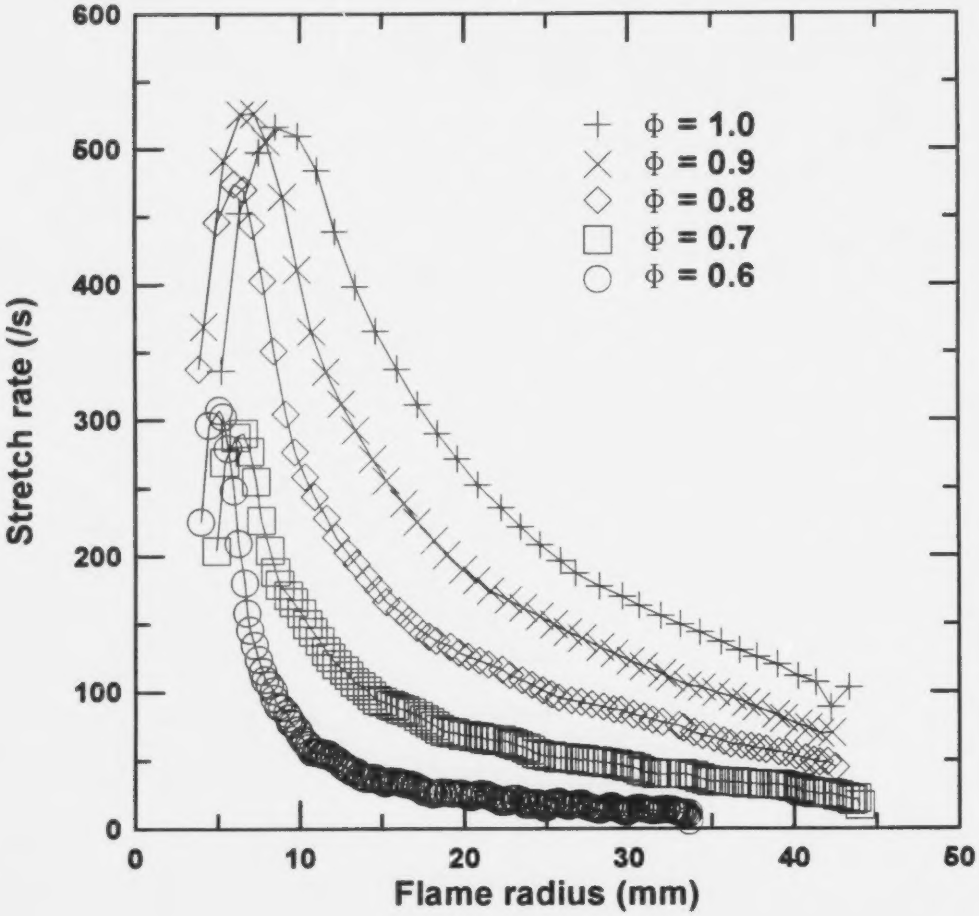

Figure 5.11: Stretch rates for the outwardly propagating spherical flames. Ø=1.0, 0.9, 0.8, 0.7, 0.6; P_{init}=1.0 atm; T_{init}=300 K.

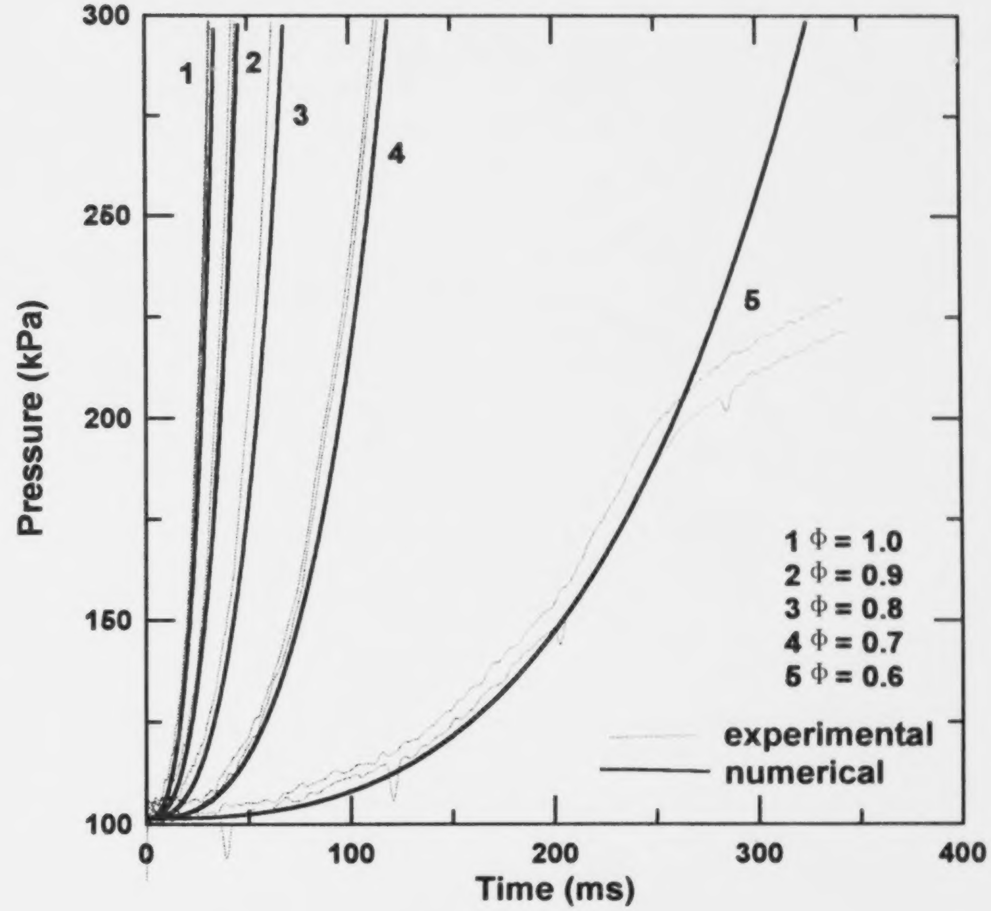

Figure 5.12: Comparing experimental pressure traces with numerical calculations assuming constant laminar burning velocities.
$\emptyset$=1.0, 0.9, 0.8, 0.7, 0.6; P_{init}=1.0 atm; T_{init}=300 K.

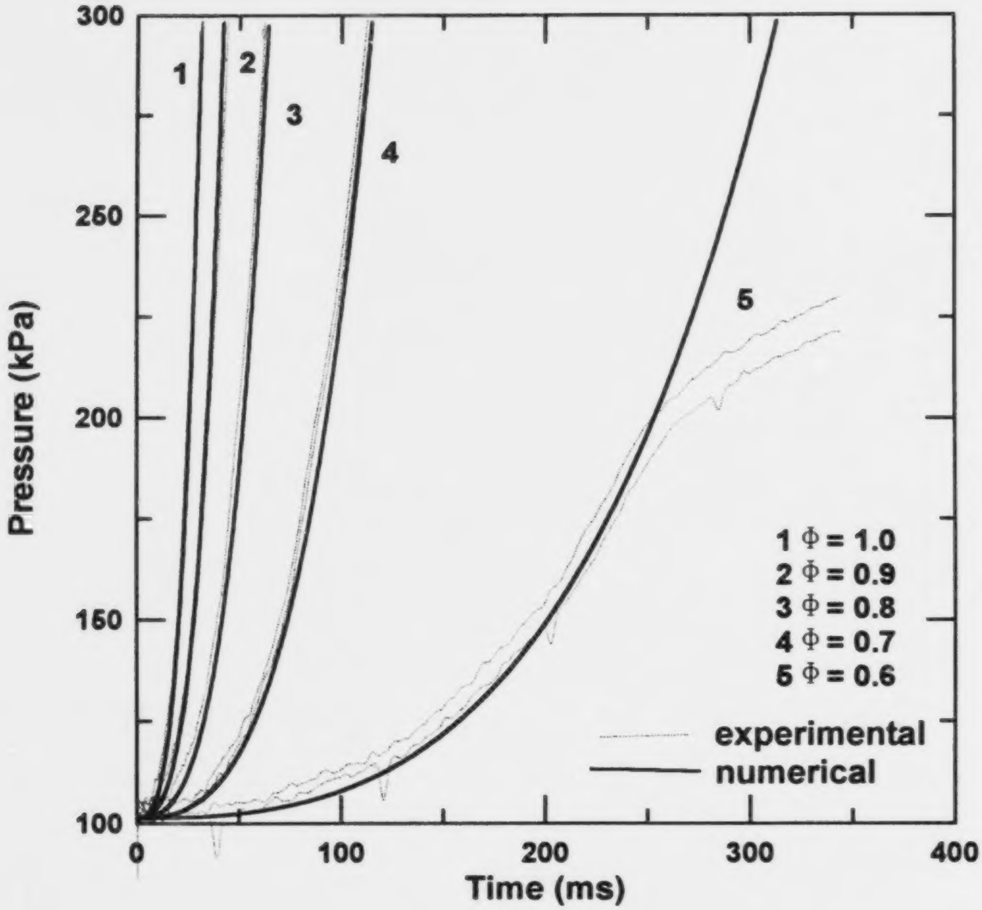

Figure 5.13: Comparing experimental pressure traces with numerical calculations using quasi-steady laminar burning velocities.
Ø=1.0, 0.9, 0.8, 0.7, 0.6 with Pexp=-0.26, -0.26, -0.35, -0.43, -0.43 respectively and Texp=2; P_{init}=1.0 atm; T_{init}=300 K.

CHAPTER 6

TURBULENT FLAME GROWTH RESULTS AND DISCUSSION

This chapter summarizes all major turbulent methane-air flame growth results. Further details and tabulations of the experimental data are given in Appendix I. The first part of this chapter compares the schlieren turbulent flame growth images with the pressure trace analysis. The behaviour of a turbulent flame in the combustion chamber as compared to its laminar partner is discussed. It illustrates the progressive turbulence enhancement as the flame grows. The turbulent burning velocity-turbulence intensity relation, the turbulent burning velocity-mean strain rate relation, the turbulent burning velocity-Karlovitz stretch number relation and the eddy structure model are presented. Based on the experimentally determined relations, a simple numerical model as discussed in Chapter 3 is proposed. The numerical calculations are used to predict the separate effects of turbulence intensity and turbulent length scale.

The turbulent flame growth experiments cover the following range of conditions. The combustion chamber turbulence is up to 2 m/s intensity with 1.5, 2, 4 or 8 mm integral scale. The 1.5 mm integral scale case is occasionally shown as $\Lambda \approx 1$ mm since the ignition-time integral scale is sometimes better estimated as 1 mm. As the turbulence decays, the 1 mm integral scale expands faster than the larger integral scales because of its relatively higher shear and hence, its faster decay rate. Only 0.9 and 0.7 equivalence ratio methane-air flames are considered in the turbulent tests. All turbulent mixtures were ignited at 300 K and 1 atm.

6.1: COMPARING SCHLIEREN IMAGES WITH PRESSURE TRACE ANALYSIS

Figure 6.1 compares a typical turbulent flame schlieren image with the corresponding laminar flame image of the same mixture composition. These are 0.9 equivalence ratio methane-air flames. For the turbulent flame, the ignition-time turbulence intensity is about 1 m/s and the integral scale is about 8 mm. The figure shows that the laminar flame is rather smooth and spherical. On the other hand, the turbulent flame is wrinkled but the shape is still roughly spherical.

Typical 0.9 equivalence ratio turbulent flame growth results obtained from schlieren images are compared with those obtained from the pressure trace analysis. The comparisons for 0.9 equivalent ratio and 8, 4, 2 or 1 mm integral scale turbulence are shown in Figure 6.2a, Figure 6.2b, Figure 6.2c and Figure 6.2d respectively. Typical turbulent flame growths in 0 (laminar) to 2 m/s intensity turbulent flows are illustrated. The pressure trace analysis uses the multi-zone, thermodynamic equilibrium model as discussed in Appendix B to estimate the flame growth rate and the burning velocity. In general, the agreement between schlieren images and pressure trace analysis is good. While the agreement for the laminar case is very good, the turbulent flame growth from schlieren images is somewhat faster than that from pressure trace analysis. The slightly faster schlieren flame growth is due to the inclusion of some unburnt and burning mixture in the schlieren image analysis. The unburnt mixture included is caused by wrinkling of the flame front by turbulent eddies along with the schlieren image interference from the third dimension.

Figures 6.3a, 6.3b, 6.3c and 6.3d show typical 0.7 equivalence ratio turbulent flame growth comparisons between schlieren image and pressure trace analyses. Similar to the 0.9 equivalence ratio case, the schlieren flame growth is slightly faster than the pressure trace flame growth. This trend is especially true for the larger scale turbulence case, $\Lambda \approx 8$ mm. The faster schlieren flame growth is more significant at higher level of turbulence and/or as the flame grows. These trends are in agreement with others [De65, Sm82, HO84, AB86, HT88, KH87, HK91, KH91, KN92]. Part of the reason behind faster schlieren flame growth as the flame grows is due to progressive turbulence wrinkling as discussed in the following section.

Ideally, the pressure trace analysis gives more accurate turbulent flame growth representation because the combustion chamber pressure rise corresponds to the burnt volume. The smooth-surfaced sphere of burnt volume used in the pressure trace analysis does not include burning or unburnt mixture. However, the high noise to signal ratio in the early period of combustion prohibits the accurate use of pressure trace analysis. The initial pressure trace noise is especially high for the high-intensity turbulent flames as illustrated in Figures 6.2a, 6.2b, 6.2c, 6.2d, 6.3a, 6.3b, 6.3c and 6.3d.

On the other hand, schlieren image analysis is most suitable for flames with well-defined flame fronts. Except for very distorted and wrinkled turbulent flames, the schlieren flame growth is not much faster than the pressure trace flame growth. The schlieren image analysis is limited to the early flame propagation period before part of the flame front expands beyond the circular windows. As discussed in section 2.6, the turbulence is less effective in wrinkling the flame front in the early flame growth period. Therefore, the schlieren flame front does not embrace much burning or unburnt mixture. Accordingly, the schlieren analysis is most useful during the early flame growth period when the flame front is not very wrinkled and the pressure traces are still noisy. In short, the limitations of pressure trace analysis during early flame growth period are overcame by the schlieren image analysis.

6.2: TURBULENT FLAME GROWTH VERSUS LAMINAR FLAME GROWTH

It is clear from Figure 6.1 that a turbulent flame can be quite different from its laminar partner. Figure 6.4 shows the plots of typical 0.9 equivalence ratio turbulent flame growth rate as a function of flame radius. Turbulent flames with ignition-time turbulence intensity of 1 and 1.5 m/s, and 4 mm integral scale are shown. The underlying laminar flame growth rate, 0 m/s turbulence intensity, is also plotted for comparison. The figure shows that the turbulent flame growth rate is faster than its laminar partner as expected. In addition, the turbulent flame growth rate increases with increasing turbulence intensity.

Typical 0.7 equivalence ratio turbulent flame growth rates are plotted against the flame radius in Figure 6.5. The 4 mm integral scale turbulent flames with ignition-time turbulence intensity of 1 and 1.5 m/s are plotted along with the underlying laminar flame growth rate. Again, the figure shows that the turbulent flame growths are much faster than the laminar flame growth as expected. The relatively higher u'/S_l ratios as compared to those shown in Figure 6.4 lead to larger and longer turbulent flame acceleration before it is suppressed by the confinement of the combustion chamber. However, the magnitudes of the flame growth rate are lower for the leaner, 0.7

equivalence ratio turbulent flames than the 0.9 equivalence ratio flames.

Typical 0.9 equivalence ratio turbulent burning velocities are plotted as functions flame radius in Figure 6.6. The associated laminar burning velocity of the same mixture is also plotted for comparison purposes. The figure shows that the turbulent burning velocities are larger than the underlying laminar burning velocity. This turbulent burning velocity increases with increasing turbulence intensity. The main reason behind the larger turbulent burning velocity is likely the larger flame surface area caused by turbulence wrinkling as seen in Figure 6.1. This explanation is especially true under conditions of low to moderate intensity, large-scale turbulence. The other turbulence enhancement mode is the increase in transport rate within the reaction zone. The increase in transport rate is more important in small-scale, high-intensity turbulence conditions as discussed in Chapter 2. Most of the present turbulent flame growth results fall into the region of moderate level of turbulence with turbulent eddies larger than the laminar flame front thickness. As a consequence, the transport rate effects on the burning rate are probably small. Most importantly, the figure also shows that the turbulent burning velocity increases as the flame grows. In other words, the turbulent flames accelerate instead of remaining quasi-steady as the laminar flames. The turbulent flame acceleration is mostly caused by progressive turbulence enhancement as discussed in section 2.6 and the next section.

Figure 6.7 shows typical 0.7 equivalence ratio laminar and turbulent burning velocities as functions of flame radius. Similar to those shown in Figure 6.6, the turbulent burning velocity increases with increasing turbulence intensity. In general, the turbulent burning velocity also increases as the flame grows. The turbulent flame acceleration for these leaner mixture explosions appears to be less than that shown in Figure 6.6. The smaller increase in turbulent burning velocity for the leaner flames is mostly due to lower turbulence ahead of the flame front at later stages of combustion. In other words, the slower burning, 0.7 equivalence ratio flame allows a larger amount of turbulence to decay. Moreover, the slower propagating flame enhances the turbulence ahead of the flame front to a lesser degree compared to the faster burning 0.9 equivalence ratio flame. The trend of turbulent flame acceleration and the argument about progressive turbulence enhancement is discussed in more detail in the next section.

6.3: PROGRESSIVE WRINKLING OF A TURBULENT FLAME

Figure 6.8 shows typical flame growth schlieren images along with the corresponding laminar partner. The turbulent integral scale is fixed at approximately 8 mm for all the 0.9 equivalence ratio turbulent flames shown. The figure shows that with increasing turbulence intensity, going down the column, the flame becomes progressively more wrinkled and distorted. Hence, the flame grows faster with increasing turbulence intensity. What is less obvious is the increase in flame front wrinkling as the flame grows. Progressive increases in wrinkling with time or as the flame grows can be deduced by going across the row. This progressive wrinkling trend is not very clear because the flame front turbulence usually decays somewhat as the flame grows. While the amount of wrinkling per unit turbulence intensity increases as the flame grows, the actual amount of flame front wrinkling may increase or decrease depending on the rate of turbulence decay or enhancement.

Typical flame perimeter estimations were performed using the images of Figure 6.8. Each image was zoomed into an 8 inch by 10 inch black and white photograph. The flame perimeters were estimated using a "thread and glue" method as described in Appendix I. The flame perimeter results are summarized in Figure 6.9. The estimated two-dimensional flame perimeter is divided by the circumference of a circle enclosing the two-dimensional flame cross-sectional area. The square of this perimeter ratio is used as an indicator for the flame surface area ratio. This squared ratio which resembles the turbulent flame surface area ratio is plotted against the flame radius in Figure 6.9. The figure shows that the flame surface area ratio increases with increasing turbulence intensity and as the flame grows. The trend about increasing flame surface area ratio is less obvious at higher turbulence intensity. One of the major causes behind this is the larger flame perimeter estimation error at higher turbulence intensity. The wrinkling scales become smaller and more populated with increasing turbulence intensity. The lesser defined flame front along with increased difficulty in estimating the flame perimeter accurately using the thread and glue method contribute to an overall larger flame perimeter error. Moreover, the present schlieren images include the third dimension interference. In other words, the schlieren images obtained from this study do not give the sliced two-dimensional tomography of the flame. It is important to note that both of these errors lead to a lower flame perimeter estimation. Therefore, the actual flame perimeters are larger than the estimated values shown. This is especially true at higher intensities and smaller scale turbulence. However, even when a laser sheet is used to estimate the flame perimeter [KF92, KW92], the accuracy of the technique is limited to relatively large-scale, low-intensity turbulent flames. The other major cause is the faster turbulence decay rate at higher turbulence intensity. With faster decay rate, the turbulence level drops more severely over the range of combustion duration or flame sizes considered. The larger turbulence decay rate can possibly lead to larger error in using rapid distortion in estimating the flame front turbulence. Due to these limitations, the present flame perimeter results only give the qualitative trends. The qualitative results show higher excess flame area at higher turbulence intensities and as the flame grows, agreeing with those in [KF92, KW92].

Further illustration and discussion about progressive wrinkling of a flame front is given in the following sections. More quantitative progressive turbulence enhancement results can be obtained by correlating the turbulence parameters with combustion parameters which can be more accurately measured. The next section illustrates progressive turbulence enhancement by expressing the turbulent burning velocity-turbulence intensity relation in a quantitative manner.

6.4: TURBULENT BURNING VELOCITY-TURBULENCE INTENSITY RELATION

The turbulent burning velocity-turbulence intensity relation can be expressed in various forms. The normalized turbulent burning velocity-turbulence intensity relation as of Equation 2.18,

$$\frac{S_t}{S_l} - 1 = C_L \frac{u'}{S_l} \qquad 6.1$$

is discussed here. It is emphasized here that S_t, S_l, u', r and Λ are the instantaneous values. The turbulence intensity, u', is estimated from the turbulence decay along with compression and geometric distortion according to the rapid distortion as discussed in section 2.8 unless otherwise specified. The instantaneous integral scale is based on normal turbulence decay as shown in Figure 2.12 along with the effects due to compression. In other words, the integral scale is assumed to be unaffected by rapid distortion. As illustrated in Chapter 2, this linear estimation can be used to express the turbulent burning velocity-turbulence intensity relation under moderate levels of turbulence. The effectiveness of turbulence enhancement on the turbulent burning velocity or the linear coefficient, C_L, is of prime interest.

Figure 6.10 shows typical plots of S_t/S_l - 1 against u'/S_l for 0.9 equivalence ratio, 23 mm radius turbulent flames. Linear fits are used to fit the data for the 5, 10 and 20 mm perforated plate hole diameter cases. These 5, 10 and 20 mm hole diameter cases correspond approximately to 2, 4 and 8 mm integral scale respectively. The linear fits for all the cases shown follow Equation 6.1 very closely. This agreement validates that, for the range of experimental conditions considered, the turbulent burning velocity increases approximately linearly with increasing turbulence intensity. The slope of the line is the linear coefficient, C_L. The higher the slope, the more effective the turbulence is in enhancing the turbulent burning velocity. The figure illustrates larger slope for smaller integral length scale. For the same turbulence intensity and the same flame radius, small-scale turbulence is more effective in enhancing the turbulent burning velocity than large-scale turbulence. These more effective small-scale turbulence results confirm the theory given in section 2.7.

Figure 6.11 illustrates typical plots of S_t/S_l - 1 against u'/S_l as the flame grows. The typical case shown is for the 10 mm perforated plate hole diameter, 0.9 equivalence ratio turbulent flames of 23, 46 and 55 mm radii. For clarity of illustration, the data points are fitted using straight lines passing through the origin identical to Equation 6.1. The figure shows progressive turbulence enhancement as the flame grows. In other words, the turbulence becomes progressively more effective in enhancing the turbulent burning velocity as the flame grows. Note that the flame continues to accelerate even when the flame radius is more than ten times larger than the integral scale. This implies that the turbulent flames do not become fully developed within the size range of engine-like combustion.

Figures 6.12a, 6.12b, 6.12c and 6.12d depict the effects of different unburned mixture turbulence estimations on the turbulent burning velocity-turbulence intensity relation. Both the 0.9 equivalence ratio turbulent flame results and the 0.7 equivalence ratio turbulent flame results are plotted. The results shown in these figures are for the 23 mm radius flames calculated from the schlieren images. Crosses designate results obtained when the flame front turbulence is estimated from the normal decay model alone. Diamonds denote results acquired when both the normal turbulence decay and the compression effects are accounted for. Squares are the results when normal decay, compression and geometric distortion effects are accounted for in the unburned turbulence estimation. In general, all figures show that adjusting the turbulence level just ahead of the flame front using normal decay along with compression and/or rapid distortion has no effect on the qualitative trends. In other words, adjusting the turbulence level using the rapid distortion model lowers the slopes slightly. The adjustments do not alter the conclusion that growing flames are progressively more affected by the turbulence.

For the 2.5 mm D case shown in Figure 6.12a, it appears that the change of equivalence ratio from 0.9 to 0.7 has a significant effect on the turbulent burning velocity-turbulence intensity relation. However, the 2.5 mm D plate is more prone to errors as presented and discussed in [Ch86]. The turbulent length scales generated using this 2.5 mm D plate also vary more profoundly over the combustion process compared to larger length scale cases. Moreover, the eddies are closer to the flame front thickness compared with the larger integral length scale cases. Due to these discrepancies, the non-zero y-intercepts for the 0.7 equivalence ratio flames are disregarded. Based on the slope or the linear coefficient alone, turbulence seems to be more effective in enhancing the 0.7 equivalence ratio methane-air flame than the 0.9 equivalence ratio methane-air flame. The more effective turbulence enhancement in the leaner flame is probably due to the difference in Markstein number. According to [TI93], the Markstein number for 0.9 and 0.7 equivalence ratio methane-air flames are about 1.8 and -0.2 respectively.

The respective Markstein numbers imply that the 0.9 equivalence ratio flame turbulent burning velocity decreases with flame stretch while flame stretch has negligible effect on the 0.7 equivalence ratio flame. In other words, the positive Markstein number, 0.9 equivalence ratio turbulent burning velocity is reduced under the influence of stretch. On the other hand, the slightly negative Markstein number, 0.7 equivalence ratio turbulent burning velocity is somewhat enhanced by stretch.

Figure 6.12b shows similar results as those shown in Figure 6.12a. The difference between the 0.9 and 0.7 equivalence ratio flames is less severe for the 5 mm D case in Figure 6.12b. The figure shows that the 0.9 equivalence ratio flame follows Equation 6.1 closely. On the other hand, the y-intercepts for the 0.7 equivalence ratio flame are slightly negative. The slopes of the linear fits seem to indicate that the turbulence is somewhat more effective in enhancing the leaner, 0.7 equivalence ratio flames than the 0.9 equivalence ratio flames. This trend agrees with that deduced from Figure 6.12a.

The 10 mm D case shown in Figure 6.12c illustrates relatively close agreement between the 0.9 and 0.7 equivalence ratio flames. The slopes seem to indicate that turbulence is barely less effective in enhancing the 0.7 equivalence ratio flames. This trend, if true, can be due to the relatively larger u'/S_l for the 0.7 equivalence ratio flames. The high turbulence can reduce the local burning velocity due to the effects of flame front curvature and straining [DM83, AB88, KK91, MP91, RD93, DS94, YS94] and hence, lowers the linear coefficient. However, the difference is of the same order of magnitude as the experimental scatter. Therefore, it is probably more appropriate to say that the change of equivalence ratio from 0.9 to 0.7 does not alter the linear coefficients for this 10 mm D case.

The larger 20 mm diameter perforated plate holes not only lead to larger integral scale but also result in higher turbulence intensity for the same plate speed. Figure 6.12d shows that the slower burning 0.7 equivalence ratio flames give higher relative turbulence intensity and also substantially more scatter than the 0.9 equivalence ratio flames. The high scatter and the high relative turbulence intensities for the 0.7 equivalence ratio flames are possibly related. The 0.7 equivalence ratio flames could be encountering partial local flame quenching at these high intensities. The 0.7 equivalence ratio flame is also more susceptible to mixture stoichiometry error than the 0.9 equivalence ratio flame because of its smaller volume fraction of fuel. The error in equivalence ratio has a greater effect on S_l for 0.7 equivalence ratio flame than for 0.9 equivalence ratio flame. This is due to the progressively larger slope for leaner mixture on the S_l versus equivalence ratio plot such as those in Figure 5.6. Due to the large scatter and much higher relative turbulence intensities for the 0.7 equivalence ratio flames, it is difficult to deduce any concrete conclusion from the comparison between the two different equivalence ratio flames.

Figures 6.13a, 6.13b, 6.13c and 6.13d show similar comparisons between 0.9 and 0.7 equivalence ratio flames at 55 mm radius. These results are acquired from the pressure trace analysis. In general, the same conclusions drawn from Figures 6.12a, 6.12b, 6.12c and 6.12d can be drawn from these figures. The smaller plate hole diameter cases shown in Figures 6.13a and 6.13b appear to show higher slopes for the 0.7 equivalence ratio flames. On the other hand, the more reliable, larger plate hole diameter cases shown in Figures 6.13c and 6.13d show that change in mixture composition from 0.9 to 0.7 equivalence ratio has negligible effect on the turbulent burning velocity-turbulence intensity relation.

Despite the scatter and uncertainties in the experiments, two trends are obvious about the turbulent burning velocity-turbulence intensity relation. The turbulence becomes progressively more effective in enhancing the turbulent burning velocity as the flame grows. This trend is shown by the larger slopes for the 55 mm radius flames in Figures 6.13a, 6.13b, 6.13c and 6.13d than those for the 23 mm radius flames in Figures 6.12a, 6.12b, 6.12c and 6.12d, for the same integral scales. This progressive turbulence enhancement as the flame grows is in agreement with other findings in the scientific literature [PS69, AB86, TG90, KF92, KW92]. For the same turbulence intensity and the same flame size, smaller length scale turbulence is more effective in amplifying the turbulent burning velocity. This is shown by the decreasing slope with increasing integral scale in Figures 6.12a, 6.12b, 6.12c, 6.12d, 6.13a, 6.13b, 6.13c and 6.13d. There are both agreements and disagreement about this trend as discussed in section 2.7. Studies such as [GM80, AB83, CT83, KW83, HI89, Br92, CV92, BH94, Jo94] agree with the present results about more effective small-scale turbulence.

An estimate of the effects of flame radius and integral scale on the general turbulent burning velocity-turbulence intensity relation can be investigated. For this purpose, it is assumed that the change in equivalence ratio has negligible effect on the turbulent burning velocity-turbulence intensity relation. With this assumption, the corresponding linear coefficient results are summarized in Table 6.1. The details along with other plots of S_t/S_l - 1 against u'/S_l are given in Appendix I.

Table 6.1: Summary of linear coefficient results.

D (mm)	Λ (mm)	r (mm)	source	C_L	R^2
2.5	≈1.5	23	video	0.48	0.95
		38	pressure	0.56	0.88
		46	pressure	0.86	0.93
		55	pressure	0.72	0.98
5	≈2	23	video	0.28	0.98
		38	pressure	0.47	0.90
		46	pressure	0.49	0.93
		55	pressure	0.65	0.97
10	≈4	23	video	0.24	0.99
		38	pressure	0.36	0.86
		46	pressure	0.41	0.96
		55	pressure	0.54	0.99
20	≈8	23	video	0.21	0.96
		38	pressure	0.23	0.85
		46	pressure	0.29	0.92
		55	pressure	0.36	0.99

Figure 6.14 shows that the linear coefficient can be expressed according to Equation 3.6 as

$$C_L = C_D \frac{r}{\sqrt{\Lambda}} + C_I \qquad 6.2$$

where the dependence coefficient, C_D, is the slope of the line and the initial dependence coefficient, C_I, is the y-intercept. The dependence coefficient illustrates how sensitive the linear coefficient is to changes in flame size and integral scale, $r/\sqrt{\Lambda}$. The initial dependence coefficient designates the turbulence enhancement present at the time of spark initiation. The linear coefficient results of 23 mm (schlieren images) and 55 mm (pressure traces) radius flames for the 2 mm, 4 mm and 8 mm integral scale are plotted in the figure. The 1 mm integral scale case is not included because of its potential for larger errors. Using best linear fit, the values for C_D and C_I are 0.015 $mm^{-0.5}$ and 0.064 respectively as shown in the figure.

An alternative way to express the linear coefficient relation is to replace the square-root of integral scale in Equation 6.2 with Taylor microscale. This will normalize the equation without introducing other parameters. However, as Taylor microscale can not be measured directly, a turbulence flow field relation is required to replace integral scale with Taylor microscale. The use of the turbulence flow field relation may introduce other errors.

It is worth mentioning that Figure 6.14 only portrays the average effects of flame radius and integral scale on the averaged turbulent burning velocity-turbulence intensity relation. In other words, the effects of r and Λ on the developing turbulent flames are indirectly deduced from the average of the linear fits of S_t/S_l and u'/S_l relations. A more direct way to examine the effects of flame radius and integral scale on the turbulent burning velocity-turbulence intensity relation is to plot S_t as a function of r, Λ, u' and S_l directly. From Equation 6.1 and Equation 6.2, the turbulent burning velocity-turbulence intensity relation can be expressed as

$$\frac{S_t}{S_l} - 1 = C_D \frac{r}{\sqrt{\Lambda}} \frac{u'}{S_l} \qquad 6.3$$

The initial dependence coefficient, C_I, is omitted for convenience. By doing so, this equation assumes that the effects of initial turbulence resulting from spark ignition are negligible.

The normalized turbulent burning velocity, S_t/S_l-1, is plotted as a function of $(r/\sqrt{\Lambda})(u'/S_l)$ in Figures 6.15a, 6.15b and 6.15c. Only the 23 mm (schlieren images) and 55 mm (pressure traces) flame radius results are used because these flames sizes correspond to the most accurate schlieren and pressure analyses respectively. The results for $\Lambda \approx 2$, 4 and 8 mm are combined. The $\Lambda \approx 1$ mm results are not included due to the larger potential errors. Instantaneous values for S_t, S_l, r, Λ and u' are used. The integral scale is estimated based on compression and normal turbulence decay for all cases. The turbulence intensity, u', in Figure 6.15a is estimated from the normal turbulence decay only. In Figure 6.15b, u' is adjusted for the effects due to compression along with the normal turbulence decay. The instantaneous turbulence intensity, u', in Figure 6.15c is estimated based on normal turbulence decay, compression and rapid distortion effects. The least-squares procedure is applied to fit the data points using straight lines. The standard deviations of the slope and the y-intercept are calculated according to equations given in [Do90]. The linear fit results are summarized in Table 6.2.

From the deviations of the slope and of the y-intercept as shown in Table 6.2, the least-squares fit appears to become progressively better when the compression effects and the rapid distortion effects are accounted for. This trend seems to validate the flame front turbulence adjustments using the rapid distortion model as described in Chapter 2. However, the improvement is small and direct flame front turbulence measurements would be required to further justify the rapid distortion model.

All three turbulence estimation models shown in Table 6.2 appear to portray relatively larger slopes for the leaner, 0.7 equivalence ratio flames than the 0.9 equivalence ratio flames. This could be due to the difference in Markstein number as discussed earlier. There is also the possibility of a time duration influence. The slower burning, 0.7 equivalence ratio flames allow a much longer time for flame-turbulence interaction compared to the faster burning, 0.9 equivalence ratio flames. As mentioned in Chapter 2, the instantaneous turbulent burning velocity-turbulence intensity relation may depend on the previous turbulence interaction as well as the present turbulence interaction. Solving this discrepancy requires experiments using both large-positive and large-negative Markstein number mixtures along with independently varying the flame-turbulence interaction duration. This is beyond the scope of the present thesis. However, possible experiments tackling this problem are recommended in Chapter 7.

Table 6.2: Summary of least-squares fit results.

u' model	Ø	slope ($mm^{-0.5}$)	standard deviation of slope ($mm^{-0.5}$)	y-intercept	standard deviation of y-intercept
normal decay	0.7	0.0404	5.89e-6	-0.429	2.48e-2
	0.9	0.0293	5.40e-6	0.076	1.03e-2
	0.7+0.9	0.0368	2.56e-6	-0.217	8.02e-3
normal decay + compression	0.7	0.0234	2.21e-6	0.175	1.71e-2
	0.9	0.0162	2.94e-6	0.403	1.06e-2
	0.7+0.9	0.0221	1.28e-6	0.193	7.41e-3
normal decay + compression + distortion	0.7	0.0182	1.43e-6	0.279	1.67e-2
	0.9	0.0148	2.11e-6	0.321	1.05e-2
	0.7+0.9	0.0181	7.82e-7	0.208	6.68e-3

It is worth mentioning that the positive y-intercept likely implies some sort of turbulence effects at spark ignition. The negative y-intercept portrayed by Figure 6.15a is probably due to the under-estimation of the flame front turbulence. In other words, the normal turbulence decay model alone seems to under-estimate the flame front turbulence.

6.5: TURBULENT BURNING VELOCITY-MEAN STRAIN RATE RELATION

As discussed in Chapter 2, the turbulent burning velocity is commonly correlated using the rate of strain of the flow ahead of the flame. This section verifies that there is indeed a roughly linear relation between the turbulent burning velocity and the rate of strain. However, as the rate of strain in a flow can not be measured directly, the turbulent burning velocity-rate of strain relation depends heavily on the model used in estimating the rate of strain.

The unburnt mixture turbulence is adjusted for decay and compression effects only for the results presented in this section. While the normal decay has been measured during the cold runs without combustion, the combustion pressure rise increases the turbulence level as discussed in section 2.8. Most studies [RA89, RB90] measured similar sort of increase in the unburnt mixture. Moreover, the adjustment for decay and compression effects lead to turbulence in between the two extremes. In other words, turbulence according to decay and compression effects only falls above the normal decay curve but below the decaying with rapid distortion curve, as illustrated in Figure 2.16.

Figures 6.16a, 6.16b and 6.16c show the plots of S_t/S_l-1 against the rate of strain for integral scale of 2, 4 and 8 mm cases respectively. For lucidity of depiction, linear fits through the origin are used. The results at 19 and 27 mm flame radius are from the schlieren images while those at r of 55 mm are from the pressure analysis. The rate of strain is estimated based on Equation 2.15 as discussed in Chapter 2. The kinematic viscosity is calculated using the dynamic viscosity of air from [IL84] assuming ideal gas. Only the effects of decay and compression on the turbulence are accounted for. In general, these figures show that the slope increases as the flame becomes larger. This implies that for the same rate of strain, the flow becomes progressively more effective in enhancing the burning rate as the flame grows. This is especially true for the 0.7 equivalence ratio flames. It appears that, for the same strain rate, the flow is more effective in enhancing the burning rate of the leaner, 0.7 equivalence ratio flames than the 0.9 equivalence ratio flames. This trend seems to be caused by the slightly less than unity Lewis number and somewhat negative Markstein number as discussed in Chapter 1 and the last section. Moreover, as discussed in the preceding section, the longer flame-turbulence interaction period for the slower burning, leaner flames may also lead to more effective turbulence. It requires further and better experimental evidence to justify the trend. The trend is larger than expected because the fit used is $S_t=C(u'/\lambda)S_l+S_l$. A plot showing $S_t=C(u'/\lambda)+S_l$ should be used instead and this would reduce the effect due to mixture stoichiometry notably.

It is deduced from Figures 6.16a, 6.16b and 6.16c that the change in the turbulence scale does not seem to affect the turbulent burning velocity-rate of strain relation much, especially for larger flames. All the 55 mm radius results can be plotted on the same graph to study the effect of strain rate estimation model on the turbulent burning velocity-rate of strain results. Figures 6.17a and 6.17b show the 0.9 and 0.7 equivalence ratio results respectively. Comparison is made between the results based on Equation 2.14 [AB81] and Equation 2.15 [KW83]. It can be seen that the model used to estimate the rate of strain has a significant effect of the quantitative results but not the qualitative results. In other words, both models lead to a roughly linear relation between the turbulent burning velocity and the rate of strain. However, the model based on [AB81] results in lower slopes and more scatter. Therefore, the model from [KW83] is used in estimating the strain rate in the subsequent paragraphs. In short, while the rate of strain can be used to correlate the burning rate, some accurate means of determining true strain rate is necessary for general agreements from one study to the other.

Alternatively, the rate of strain can be expressed in the normalized form called the Karlovitz stretch factor according to Equation 2.16. Figure 6.18 shows a plot of S_t/S_l-1 as a function of the stretch factor. The laminar flame front thickness used here is estimated from [GM92]. The laminar flame front thicknesses are 0.30 and 0.46 mm for 0.9 and 0.7 equivalence ratio flames respectively. The figure displays a roughly linear relation between the normalized turbulent burning velocity and the Karlovitz stretch factor. For stretch factors up to 1.2 considered, there appears to be no levelling off of turbulent burning velocity at high stretch. The stretch appears to be marginally more effective in enhancing the richer, 0.9 equivalence ratio flames than the 0.7 equivalence ratio flames. This trend, if true, is in contradiction with the expected trend due to the effects of Markstein number. However, this discrepancy probably lies within the model for estimating the stretch factor. It is worth emphasizing that for these near-zero Markstein number flames, stretch is not expected to alter the local burning velocity significantly. Therefore, stretch acts mostly by increasing the flame front surface area and hence, the turbulent burning velocity.

The effects of flame size on the turbulent burning velocity-Karlovitz stretch factor relation are also examined. These effects are shown in Figures 6.19a and 6.19b for the 0.9 and 0.7 equivalence ratio flames respectively. Figures 6.19a and 6.19b demonstrate the change in the turbulent burning velocity-Karlovitz stretch factor relation as the flame grows. Both 0.9 and 0.7 equivalence ratio flames become progressively more effectively enhanced by the flow stretch factor as the flame grows. The increase in the stretch effectiveness in enhancing the flame as the flame grows is more substantial for the leaner flames. This could be due to the fact that the leaner, 0.7 equivalence ratio flames take a much longer time to grow from 19 to 55 mm radius. The longer propagation time allows for prolonged flame-stretch interaction which may lead to the more effective stretch effect.

The rate of strain or the Karlovitz stretch factor appears to be a useful parameter in correlating the burning rate. As the rate of strain and the Karlovitz stretch factor can not be measured directly, the value depends on the model used in deriving it from the measurable turbulence parameters. The quantitative results can vary significantly depending on the model used to estimate the rate of strain or the Karlovitz stretch factor. In general, the turbulent burning velocity increases roughly linearly with the rate of strain or the Karlovitz stretch factor. The turbulent flame development process shown is because the strain becomes progressively more effective in increasing the turbulent burning velocity as the flame grows. This progressive straining effect appears to be greater for the leaner 0.7 equivalence ratio flames.

The turbulent length scale effects are incorporated in the rate of strain or the Karlovitz stretch factor. In other words, when correlating the burning rate with the rate of strain or the Karlovitz stretch factor the turbulent length scale effect on the developing turbulent flame disappears. The effects due to laminar burning velocity and the laminar flame front thickness are also included in the Karlovitz stretch factor correlation.

6.6: EDDY STRUCTURE MODEL

According to Ashurst's eddy structure model discussed in Chapter 2, the instantaneous turbulent burning velocity can be related to the instantaneous turbulence intensity and the instantaneous laminar burning velocity expressed by Equation 2.17. In the idealized case, the constants, C_3 and C_4, are equal to $1+0.82\lambda/\Lambda$ and $1-\lambda/\Lambda$ respectively [AC94]. It is assumed that the turbulence properties relation expressed by Equation 2.15 is valid in the present combustion chamber. Then, Equation 2.17 can be re-written as

$$\frac{S_t}{S_l} = \frac{1 + \dfrac{u'}{S_l}}{\left(1 + 1.220\ Re_\Lambda^{\ -0.2} \right) + \left(1 - 1.484\ Re_\Lambda^{\ -0.2} \right) \dfrac{u'}{S_l}} \qquad 6.4$$

where S_t, S_l, u', λ and Λ are the instantaneous values.

Figures 6.20a and 6.20b show the comparison between the eddy structure model predictions and the experimental data for 0.9 and 0.7 equivalence ratio flames respectively. The figures plot S_t/S_l-1 as a function of u'/S_l. The crosses (schlieren images for 19 mm radius flames) and the squares (pressure trace results for 55 mm radius flames) are the experimental data while the solid and dotted lines are the model prediction. In Figure 6.20a, the constants, C_3 and C_4, are multiplied by pre-factors in order for the model prediction to agree with the experiments. The pre-factor for C_3 is 0.91 while the pre-factor for C_4 changes from 10/19 to 10/55 as the flame grows from 19 mm to 55 mm in radius. In other words, the progressive turbulence enhancement has to be accounted for in order for the model to predict the experimental trend. The same pre-factors used in the 0.9 equivalence ratio flames are employed for the 0.7 equivalence ratio flames shown in Figure 6.20b. It appears that these pre-factors have to be re-adjusted for the leaner flames. Some modification of these pre-factors so that the flow turbulence is more effective in enhancing the 55 mm radius flames would be required. This adjustment appears to agree with the somewhat more effective slower burning, leaner, 0.7 equivalence ratio flames. Due to the scatter of the data points these alterations are not performed here. It is worth noting the eddy structure model's ability in predicting the levelling off of the increase in turbulent burning velocity with increasing turbulence intensity at higher turbulence intensities. This feature is based on the turbulence flow structure and it is not due to the partial quenching flame front at high strain [AC94].

6.7: OVERALL COMBUSTION RATE

As discussed in section 2.8, the combustion chamber turbulence decays notably over the period of combustion. The decay process is partially countered by the rapid distortion effect in the presence of a propagating flame. The level of turbulence enhancement due to rapid distortion is dependent on the rate at which the flame propagates. Therefore, the overall combustion rate which is the inverse of the overall combustion duration is an important parameter.

Both higher turbulence intensity and smaller turbulent length scale provide better turbulence enhancement in spark-ignited, premixed combustion. The ideal fast-burn engine would utilize small-scale, high-intensity turbulence. However, both higher turbulence intensity and smaller turbulent length scale lead to faster turbulence decay. Therefore, unless the level of turbulence can be maintained, small-scale turbulence may not lead to faster overall combustion rate in an engine. In other words, there appears to be an optimum turbulence level for the fastest overall combustion rate in a given combustion chamber size. These points are further illustrated in the next section using the numerical flame growth model simulations. In real engines, a combination of swirl and tumble seems to be beneficial in terms of fast burning. While swirl generates additional turbulence, tumble can break the large-scale turbulence into smaller eddies which are more beneficial in terms of both faster burning and possibly lower cyclic variation [Hi88, HK89].

6.8: NUMERICAL FLAME GROWTH MODEL CALCULATIONS

Typical flame growth model simulations for 0.7 equivalence ratio laminar and turbulent mixtures ignited at 1 atm and 300 K are compared with the experiments in Figure 6.21. The comparisons are illustrated by the combustion chamber pressure traces. The ignition-time turbulence is 0 (laminar), 1.0 or 2.0 m/s with about 8 mm integral scale. The numerical simulations are based on a constant integral scale of 8 mm over the combustion period considered. The combustion period considered is up to 300 kPa chamber pressure. This period corresponds to the time from ignition spark up to the point where the flame reached the chamber walls. The solid lines are those obtained from the numerical calculations while dashed lines are the experimental results. The figure shows that numerical simulations agree reasonably well with the experiments. The spark kernel size or the temperature and pressure exponents could be adjusted to better match the simulations with experiments. This was not done as the current agreements are about the same magnitude as the experimental scatter. The main purpose here is to examine the qualitative trends and the effects of turbulence intensity, turbulent length scale and the flame size on the combustion process.

Figure 6.22 displays the effects of turbulence intensity on the combustion pressure traces calculated using the numerical model. The ignition-time turbulence intensity was 0, 0.5, 1.0, 1.5 or 2.0 m/s while keeping the integral scale fixed at 4 mm. The turbulence is allowed to decay and undergo the effects of compression and rapid distortion. The noise-free pressure traces simulated by the model show increasing pressure rise rate with increasing turbulence intensity as expected.

The underlying burning velocities of the pressure traces in Figure 6.22 are plotted in Figure 6.23. Figure 6.23 portrays that the higher the turbulence intensity the higher the burning velocity as expected. For the range considered, the turbulent burning velocities increase as the flames grow. With increasing turbulence intensity, the increase of turbulent burning velocity per unit increase in turbulence intensity becomes progressively smaller. This is especially true as the flames grow larger. The succeeding figures illustrate this point further.

Figure 6.24 depicts the effects of turbulence intensity on the combustion process using numerical simulations. The unburned mixture turbulence intensity is fixed at 0, 0.5, 1.0, 1.5 or 2.0 m/s and the integral scale is fixed at 4 mm. The figure shows the expected trend of increasing pressure rise rate with increasing turbulence intensity. Comparing these pressure traces with those shown Figure 6.22, the pressure rises faster when the turbulence intensity is held constant throughout the combustion process. There is also a larger increase in pressure rise rate per unit increase in turbulence intensity as shown in Figure 6.24. This is because the higher intensity turbulence is forced not to decay and hence the trend of faster decaying turbulence at higher intensities is arbitrarily suppressed.

The underlying burning velocities for the combustion processes shown in Figure 6.24 are plotted in Figure 6.25. The figure portrays the faster turbulent burning velocity trend with increasing turbulence intensity. The turbulent burning velocities shown are higher than those shown in Figure 6.23, especially at higher turbulence intensities.

Figure 6.26 illustrates the effects of integral scale on the rate of pressure rise. The numerical simulations are based on 0.7 equivalence ratio methane-air flames with 1 m/s ignition-time turbulence. The integral scale is fixed at either 8, 4, or 2 mm. The figure shows that the decrease in integral scale from 8 mm to 4 mm has a very small effect on the combustion rate. Further decrease in integral scale from 4 mm to 2 mm has a somewhat larger effect on the combustion rate. Over the range of combustion period considered, the 8 mm integral scale turbulence leads to the fastest overall combustion rate. The 8 mm integral scale turbulence starts by being relatively less effective in enhancing the initial flame kernel. However, the 8 mm integral scale turbulence decays slower than the other two cases. Therefore, the 8 mm integral scale turbulence becomes more effective compared to the smaller-scale turbulence as the flame grows. The 2 mm integral scale turbulence begins effectively wrinkling the flame kernel right after ignition. However, it decays relatively faster than larger-scale turbulence due to its higher shear in the flow.

Figure 6.27 shows the underlying burning velocity for the combustion processes described in Figure 6.26. The figure more clearly illustrates the trend about initially more effective 2 mm integral scale turbulence. The 2 mm integral scale turbulence quickly becomes less effective due to faster turbulence decay and hence progressively lower turbulence level. On the other hand, the initially less effective 8 mm integral scale turbulence becomes progressively more effective due to slower turbulence decay.

Figure 6.28 illustrates the effects of integral scale with fixed turbulence intensity on the combustion rate. The 0.7 equivalence ratio methane-air flames are under the influence of fixed turbulence intensity of 1 m/s. The integral scale is fixed at either 8, 4 or 2 mm. The decrease in integral scale from 8 mm to 2 mm has very profound effects of the combustion rate. With fixed turbulence intensity, the smaller the eddies the faster the combustion rate. In other words, smaller-scale turbulence is much more effective in enhancing the overall combustion rate in an engine if it is prohibited from decaying. The underlying burning velocities are plotted against the flame radius in Figure 6.29.

Other than using the flow turbulence, enhanced ignition is an alternative approach to improve engine combustion [DO81, GT83, BB84, LA87, HS88, MC91, CS92]. The underlying science of the enhanced ignition process is very complicated [BD88, Ki88, BD91, AH92]. However, the faster combustion rate resulting from an enhanced ignition spark is generally due to two factors. Enhanced ignition usually leads to larger spark size and higher turbulence. Figure 6.30 shows the effects of spark size on the rate of combustion. For the laminar case, the increase in spark size results in a shorter combustion duration as expected. Even with the relatively constant laminar burning velocity, a larger spark kernel can reduce the overall combustion duration significantly. This is because a relatively larger amount of time is required to travel the same radial distance from a smaller sphere compared to a larger sphere. For the turbulence case, the same increase in spark size results in a much larger percentage decrease in the overall combustion duration. While the absolute decrease in combustion duration is about the same as that in the laminar case, the much shorter overall turbulent combustion duration leads to a much larger relative effect on combustion duration. Moreover, a larger spark also leads to a more effective turbulence enhancement right after ignition as the effectiveness of turbulence enhancement, the linear coefficient, varies linearly with the flame size. It is worth noting that the effects due to any additional turbulence caused by enhanced ignition are not included in Figure 6.30.

6.9: SUMMARY OF DEVELOPING TURBULENT FLAME IN A COMBUSTION CHAMBER

It has been shown that the spark-ignited turbulent flame develops as it propagates. Under engine-like combustion conditions, the turbulent flame continues to develop even when the flame is much larger than the integral length scale. The progressive turbulence enhancement as the flame grows has been illustrated using the excess two-dimensional flame perimeters estimated from the schlieren images, the normalized turbulent burning velocity-turbulence intensity (S_t/S_l-1 and u'/S_l) relation and the normalized turbulent burning velocity-rate of strain or Karlovitz stretch factor (S_t/S_l-1 and u'/λ or K) relation.

There is a roughly linear relation between S_t/S_l-1 and u'/S_l. The linear coefficient from the normalized turbulent burning velocity-turbulence intensity relation varies linearly with flame radius and inversely proportional to the square-root of the integral scale. The normalized turbulent burning velocity, S_t/S_l-1, also varies approximately linearly with the rate of strain and/or the Karlovitz stretch factor. The slopes from these relationships increase with increasing flame size showing the development of the turbulent flame.

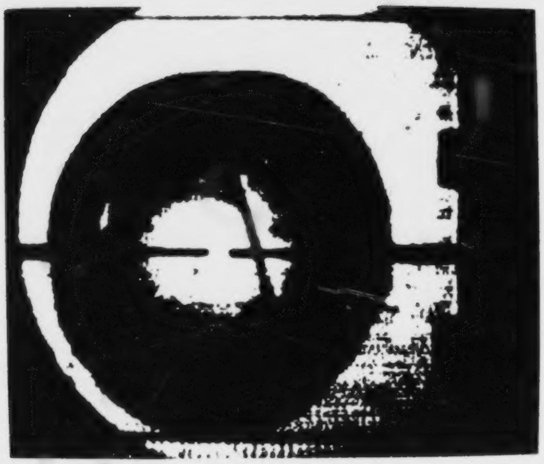

Quiescent

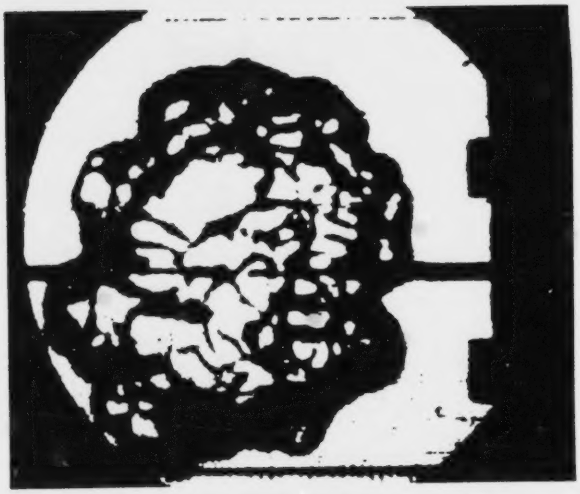

Turbulent, u' ≈ 1 m/s, Λ ≈ 8 mm

Figure 6.1: Typical turbulent and laminar flame schlieren images. Ø=0.9; P_{init}=1 atm; T_{init}=300 K.

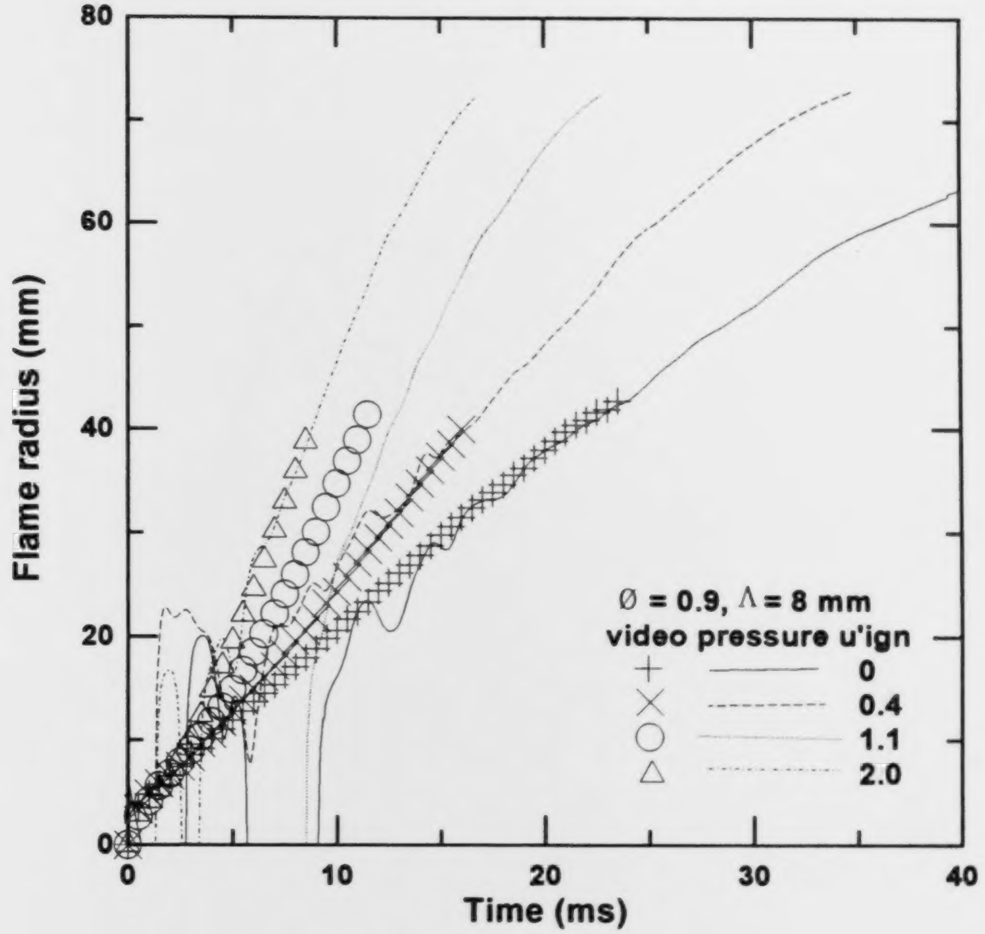

Figure 6.2a: Typical 0.9 equivalence ratio turbulent and laminar flame growths from schlieren images compared with pressure trace analysis.
Λ≈8 mm; P_{init}=1 atm; T_{init}=300 K.

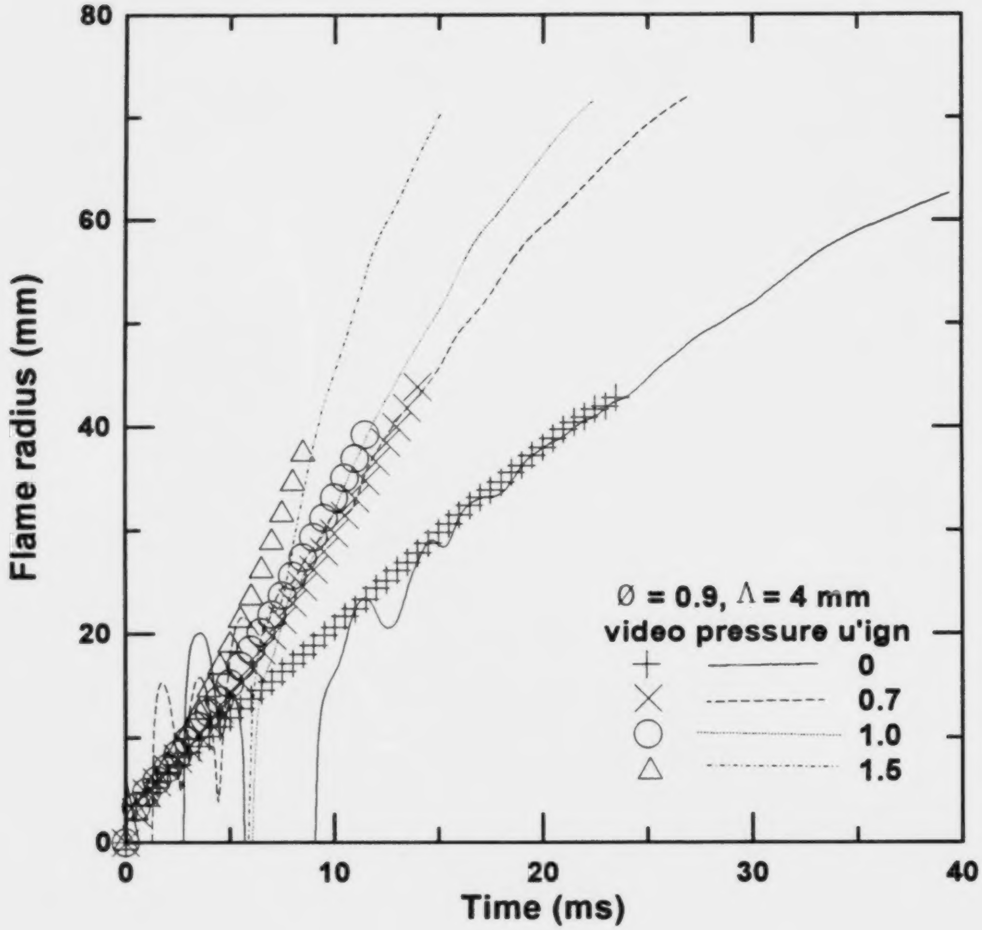

Figure 6.2b: Typical 0.9 equivalence ratio turbulent and laminar flame growths from schlieren images compared with pressure trace analysis.
Λ≈4 mm; P_{init}=1 atm; T_{init}=300 K.

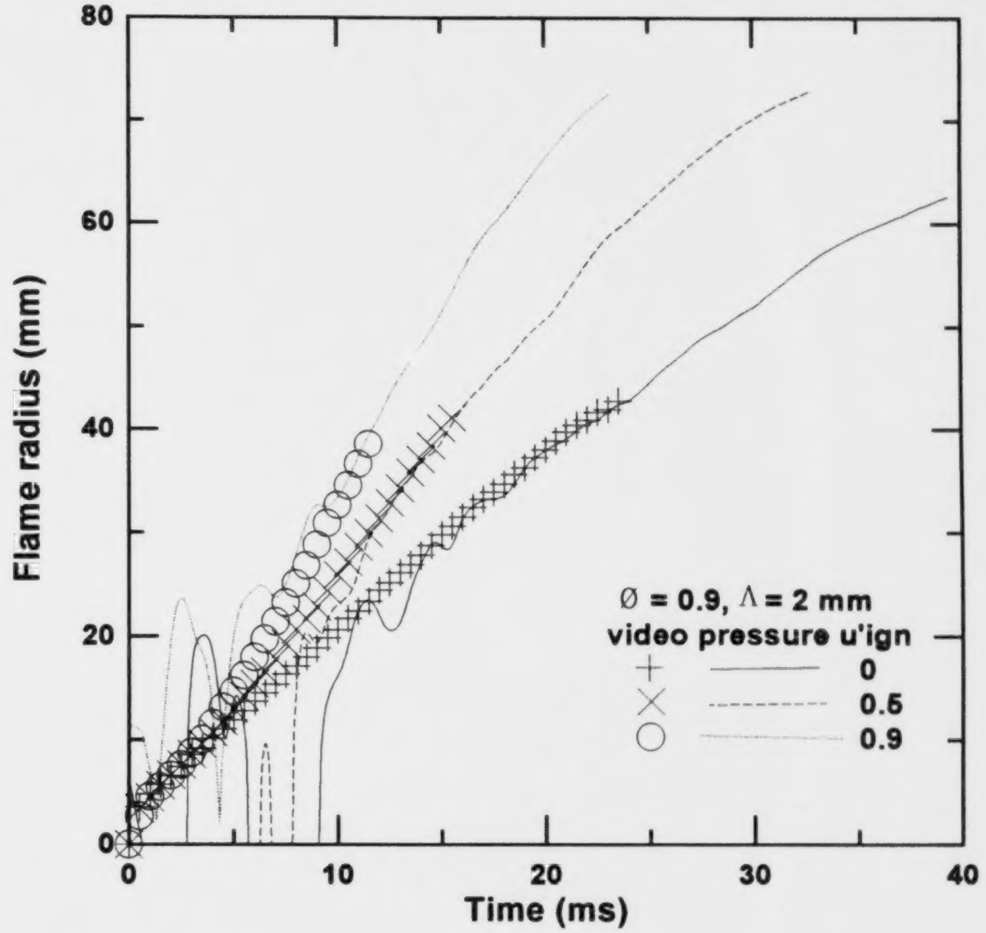

Figure 6.2c: Typical 0.9 equivalence ratio turbulent and laminar flame growths from schlieren images compared with pressure trace analysis.
$\Lambda \approx 2$ mm; $P_{init} = 1$ atm; $T_{init} = 300$ K.

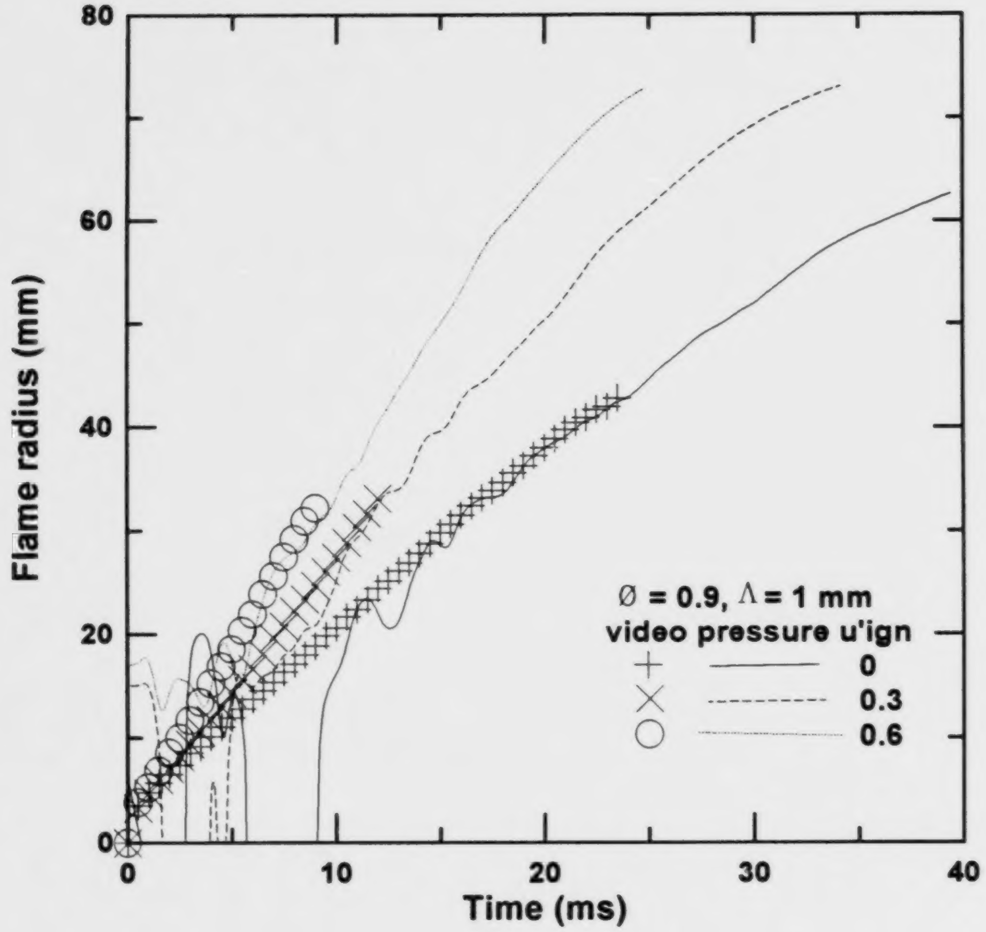

Figure 6.2d: Typical 0.9 equivalence ratio turbulent and laminar flame growths from schlieren images compared with pressure trace analysis.
$\Lambda \approx 1$ mm; $P_{init}=1$ atm; $T_{init}=300$ K.

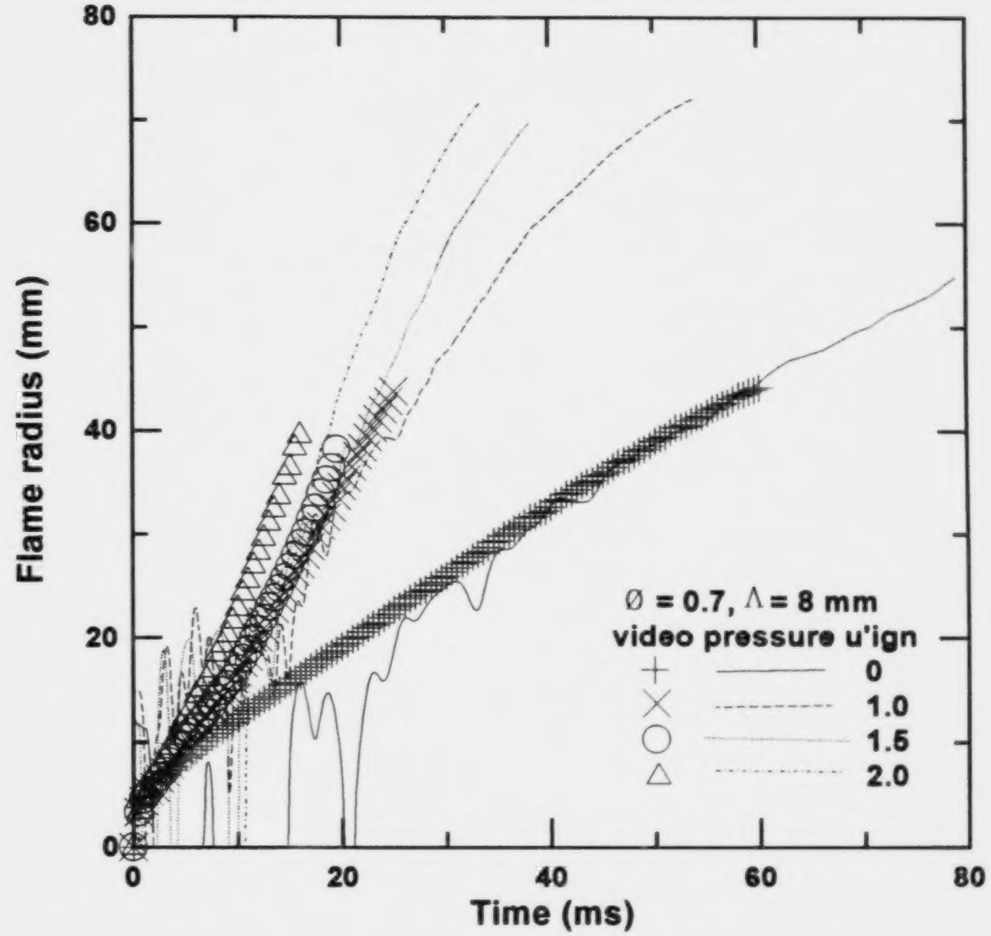

Figure 6.3a: Typical 0.7 equivalence ratio turbulent and laminar flame growths from schlieren images compared with pressure trace analysis.
Λ≈8 mm; P_{init}=1 atm; T_{init}=300 K.

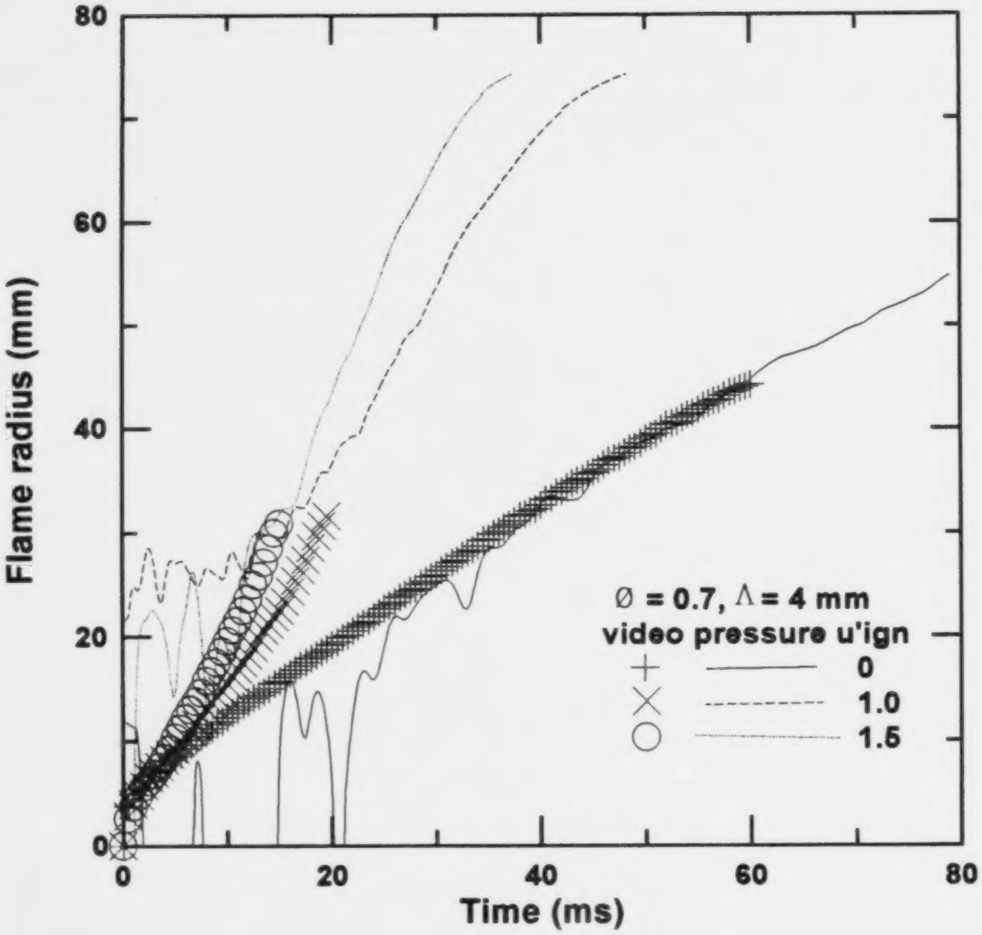

Figure 6.3b: Typical 0.7 equivalence ratio turbulent and laminar flame growths from schlieren images compared with pressure trace analysis.
Λ≈4 mm; P_{init}=1 atm; T_{init}=300 K.

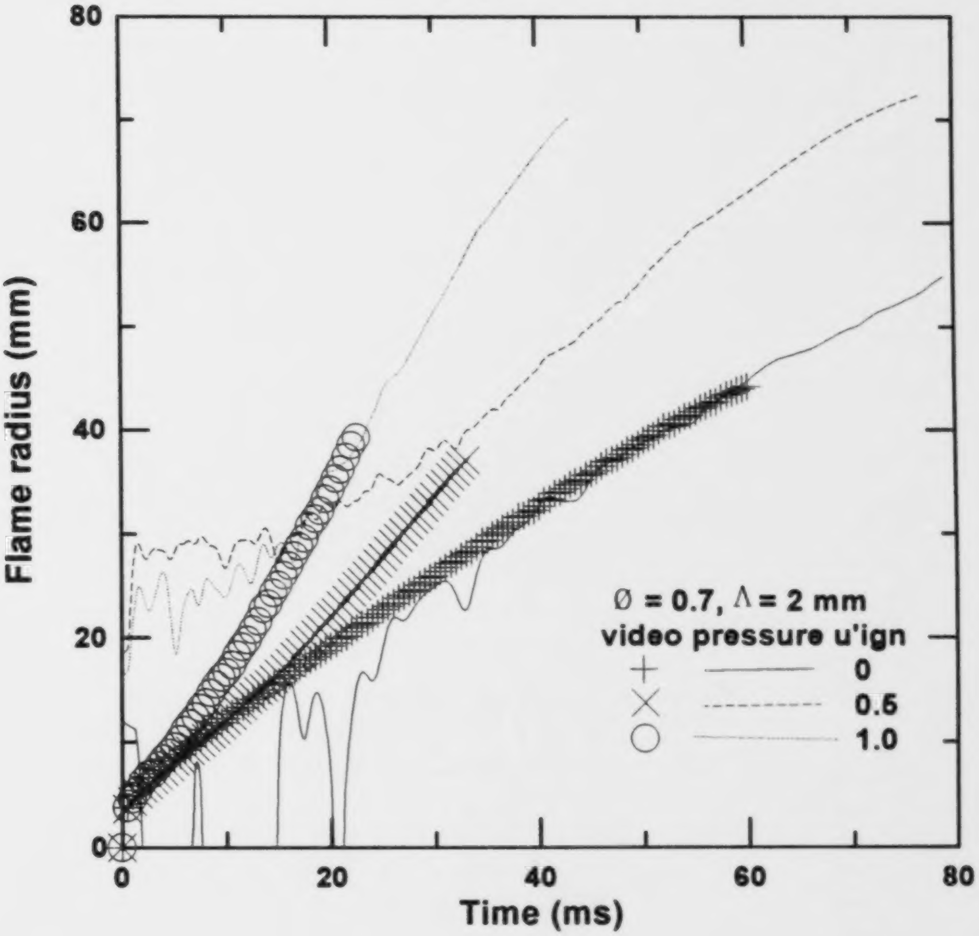

Figure 6.3c: Typical 0.7 equivalence ratio turbulent and laminar flame growths from schlieren images compared with pressure trace analysis.
$\Lambda \approx 2$ mm; $P_{init}=1$ atm; $T_{init}=300$ K.

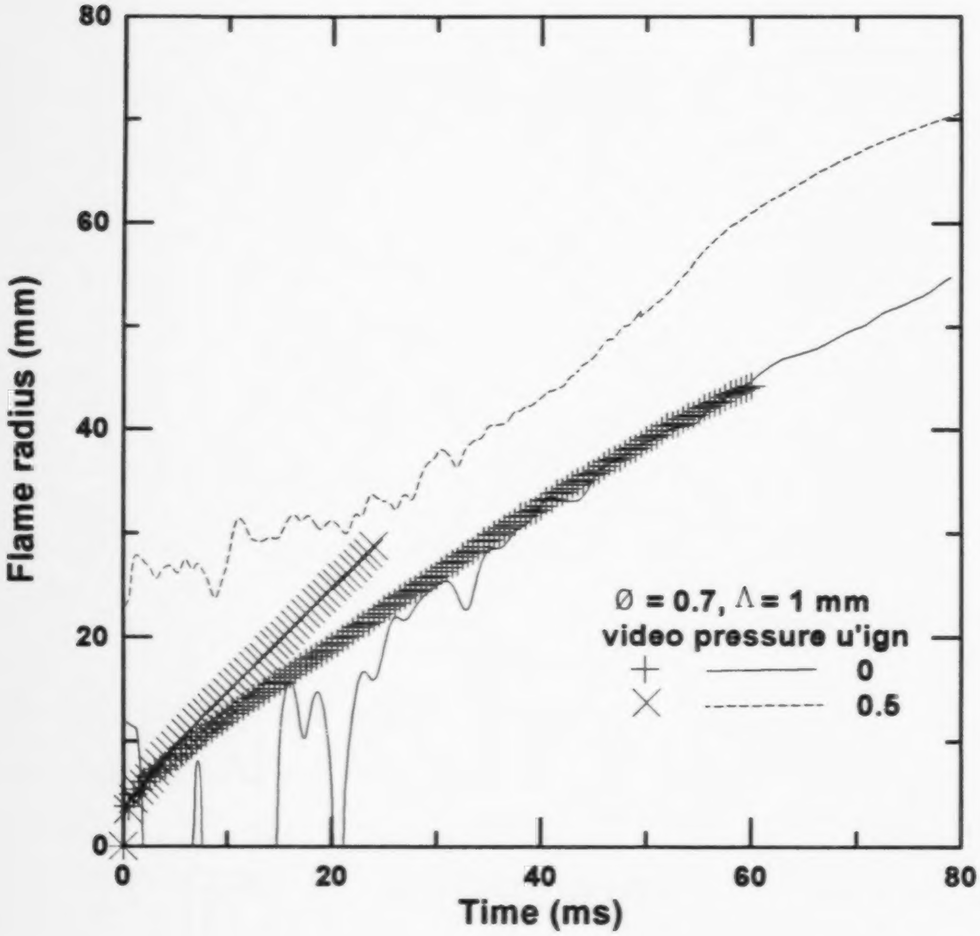

Figure 6.3d: Typical 0.7 equivalence ratio turbulent and laminar flame growths from schlieren images compared with pressure trace analysis.
Λ≈1 mm; P_{init}=1 atm; T_{init}=300 K.

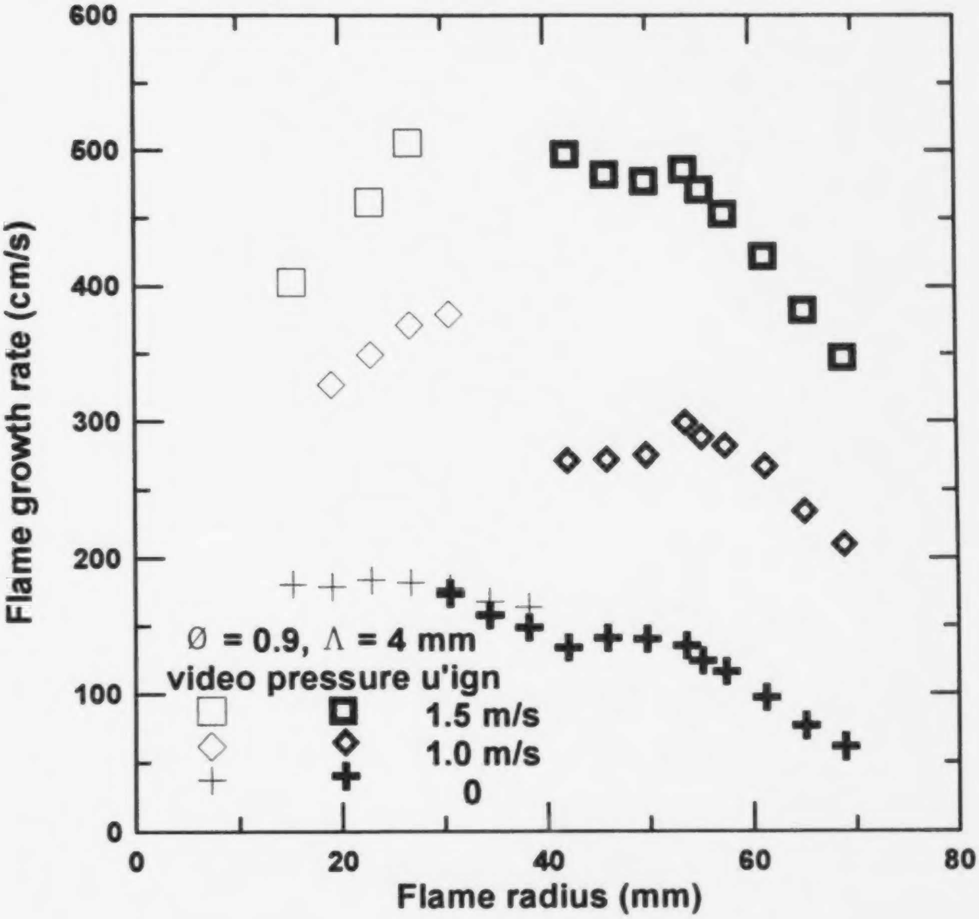

Figure 6.4: Effects of turbulence level on typical 0.9 equivalence ratio flame growth rate as a function of flame size.
Ø=0.9; Λ=4 mm; u'_{ign}=0, 1.0, 1.5 m/s; P_{init}=1 atm; T_{init}=300 K.

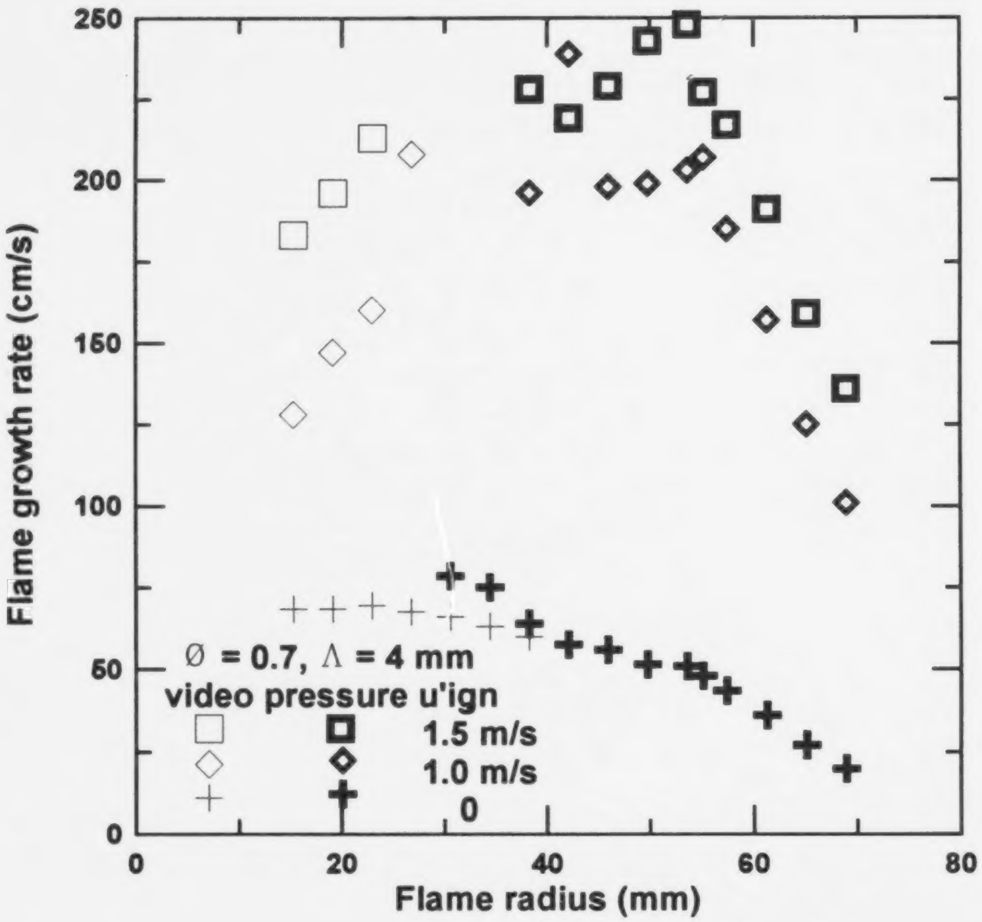

Figure 6.5: Effects of turbulence level on typical 0.7 equivalence ratio flame growth rate as a function of flame size.
Ø=0.7; Λ=4 mm; u'_{ign}=0, 1.0, 1.5 m/s; P_{init}=1 atm; T_{init}=300 K.

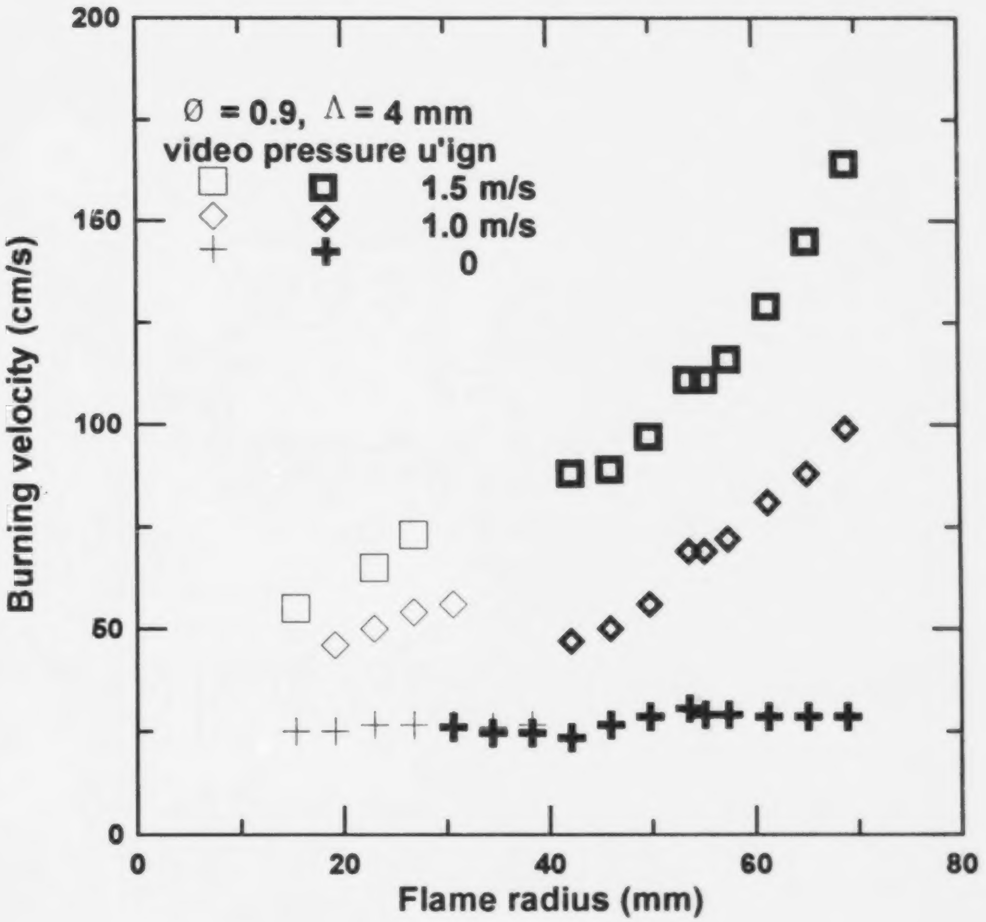

Figure 6.6: Effects of turbulence intensity on typical 0.9 equivalence ratio burning velocity as a function of flame size.
Ø=0.9; Λ=4 mm; u'_{ign}=0, 1.0, 1.5 m/s; P_{init}=1 atm; T_{init}=300 K.

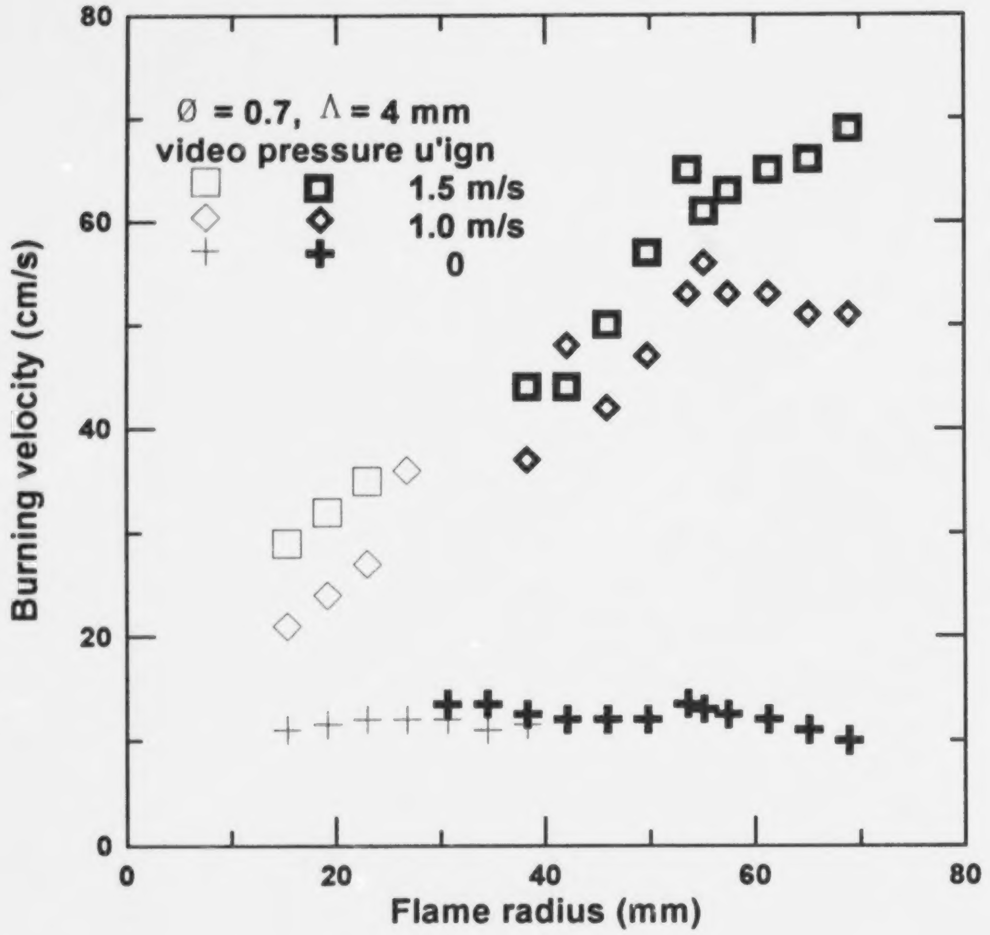

Figure 6.7: Effects of turbulence intensity on typical 0.7 equivalence ratio burning velocity as a function of flame size.
$\emptyset$=0.7; Λ=4 mm; u'_{ign}=0, 1.0, 1.5 m/s; P_{init}=1 atm; T_{init}=300 K.

Quiescent (No Turbulence).

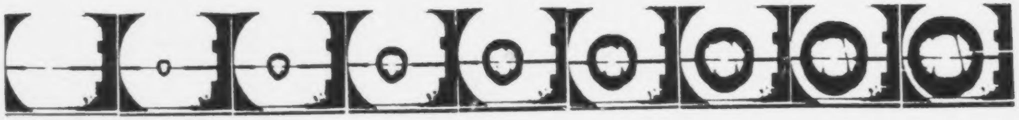

Low Turbulence, u' ≈ 0.4 m/s.

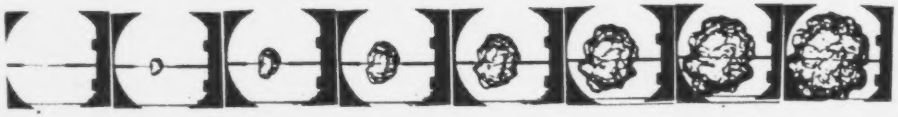

Moderate Turbulence, u' ≈ 1.3 m/s.

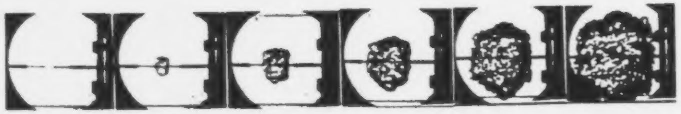

High Turbulence, u' ≈ 2.0 m/s.

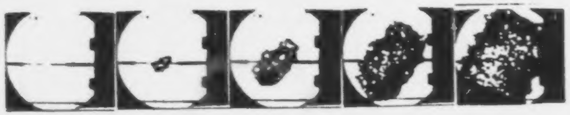

Time Step = 2.5 ms
Initial Pressure = 1 atm
Initial Temperature = 300 K
$\Lambda \approx 8$ mm, X/D ≈ 12

Spark Condition:
5.0 mm spark gap
2.5 μF, 500 V (312.5 mJ)

Figure 6.8: Progressive turbulence enhancement illustrated by schlieren flame growth images.
$\emptyset=0.9$; $\Lambda \approx 8$ mm; $P_{init}=1$ atm; $T_{init}=300$ K.

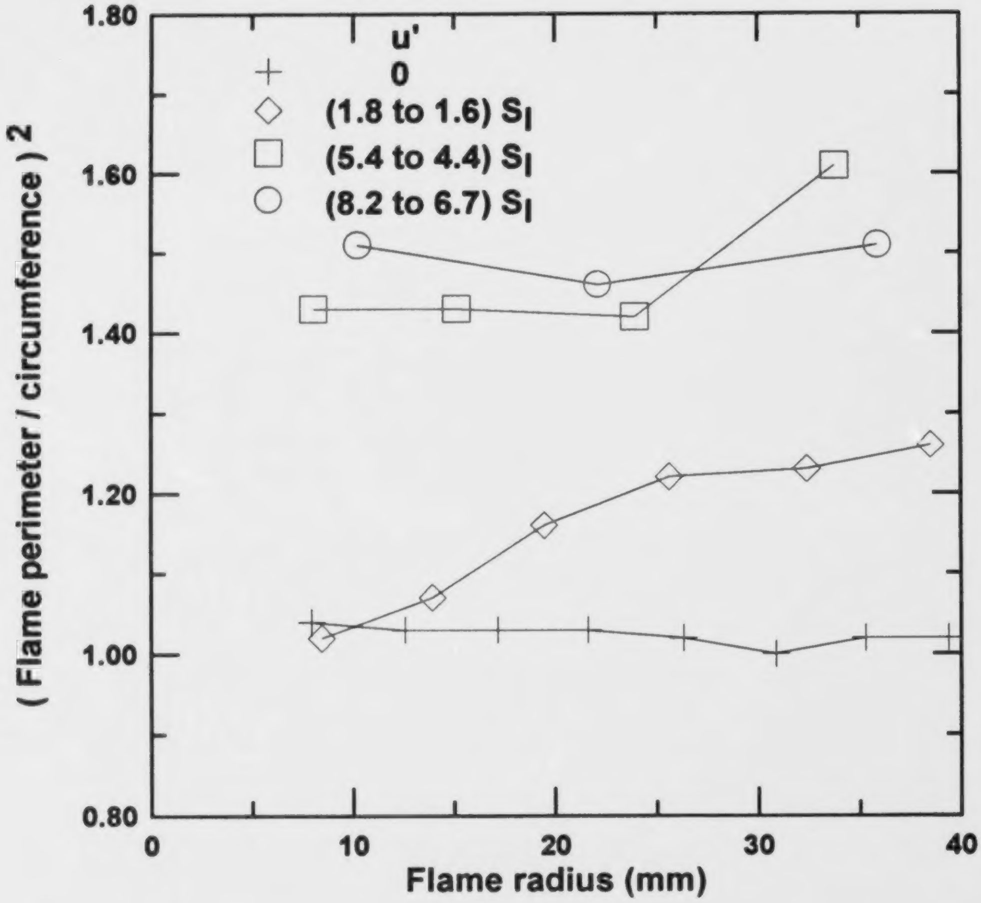

Figure 6.9: The square of flame perimeter ratio as functions of flame radius and turbulence intensity.
Ø=0.9; Λ≈8 mm; P_{init}=1 atm; T_{init}=300 K.

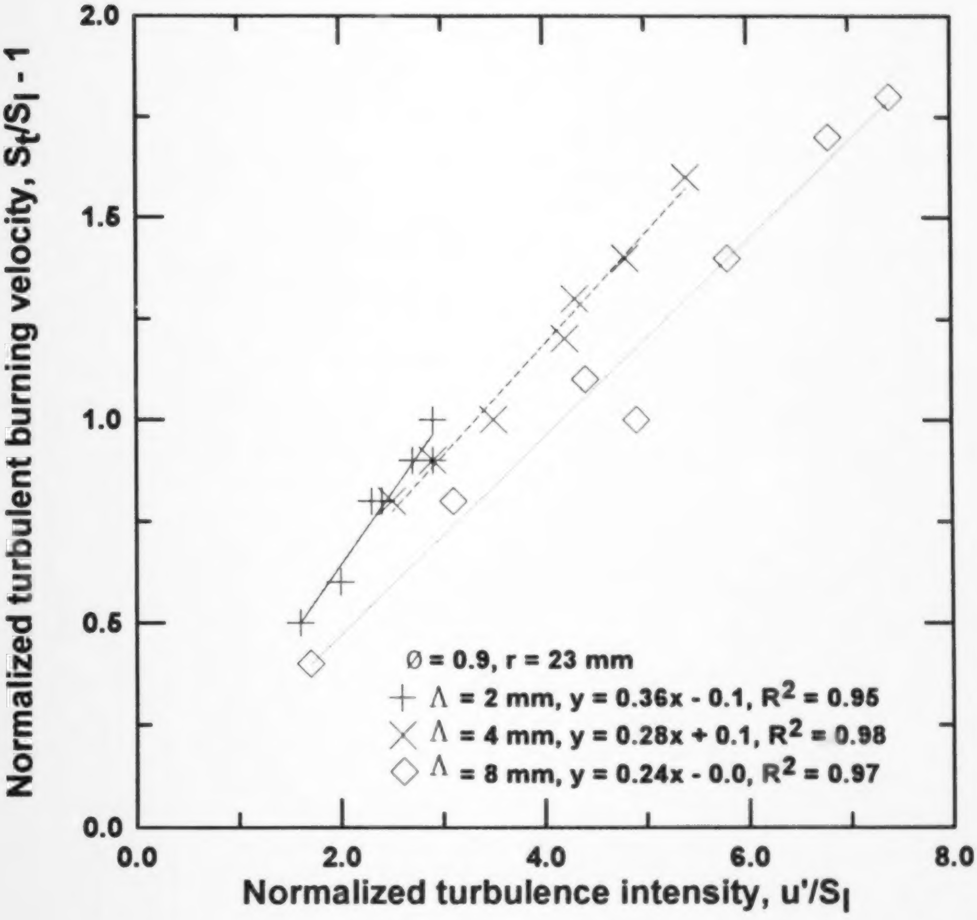

Figure 6.10: Normalized turbulent burning velocities as functions of normalized turbulence intensities, S_t/S_l - 1 = C_L u'/S_l, for typical 23 mm radius, 0.9 equivalence ratio turbulent flames.
Ø=0.9; Λ≈2, 4, 8 mm; P_{init}=1 atm; T_{init}=300 K.

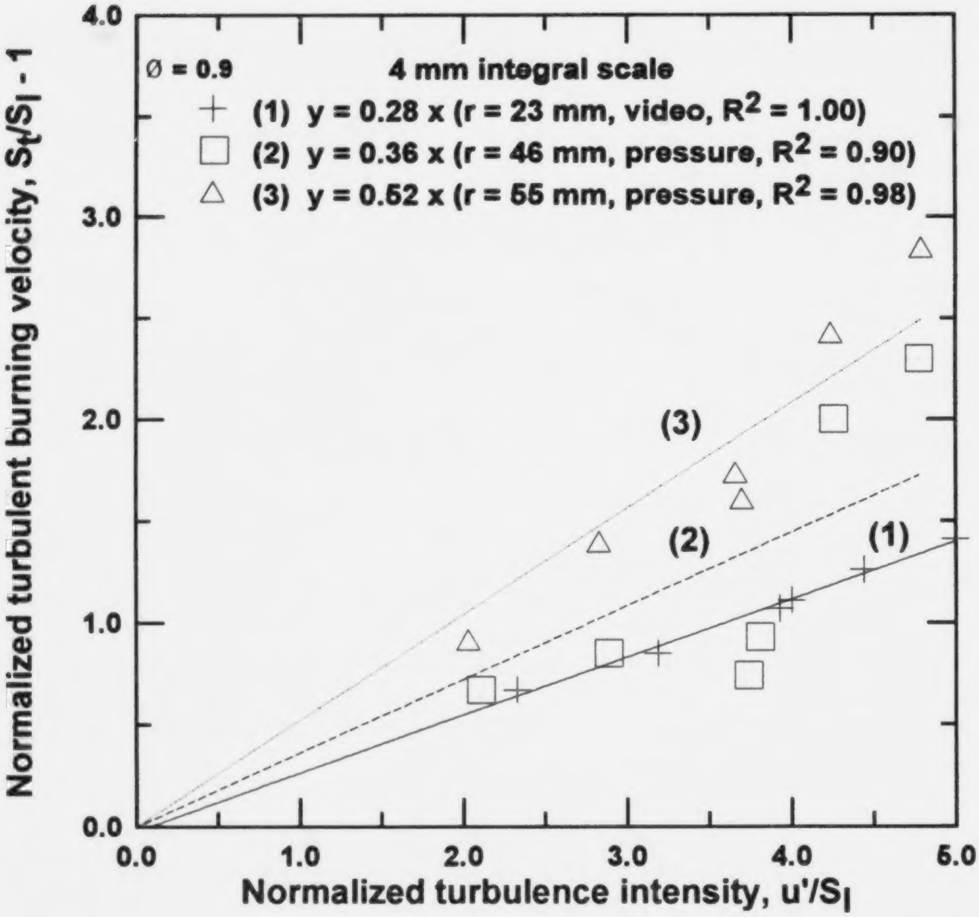

Figure 6.11: Typical plots of S_t/S_l - 1 against u'/S_l as the flame grows. Ø=0.9; Λ≈4 mm; r=23, 46, 55 mm; P_{init}=1 atm; T_{init}=300 K.

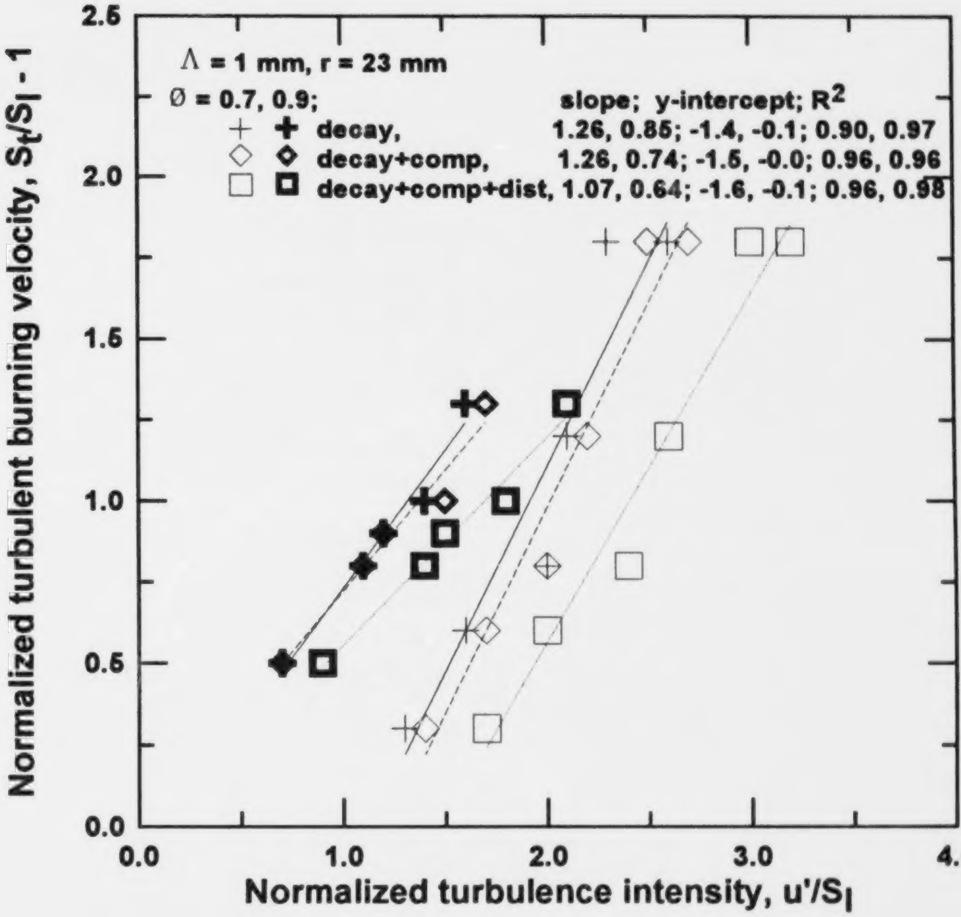

Figure 6.12a: Plots of normalized turbulent burning velocity, S_t/S_l - 1, against normalized turbulence intensity, u'/S_l, for typical 23 mm radius, fine scale, turbulent flames. Ø=0.7, 0.9; Λ≈1 mm; P_{init}=1 atm; T_{init}=300 K.

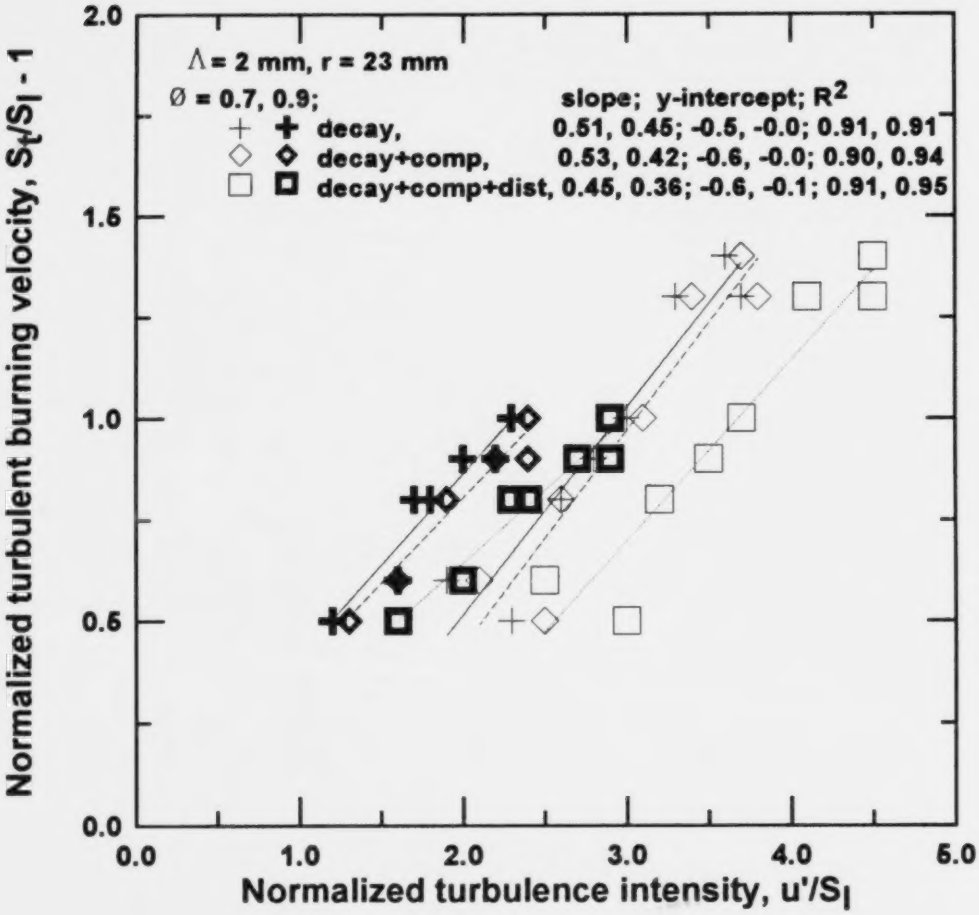

Figure 6.12b: Plots of normalized turbulent burning velocity, S_t/S_l - 1, against normalized turbulence intensity, u'/S_l, for typical 23 mm radius, small scale, turbulent flames. Ø=0.7, 0.9; Λ≈2 mm; P_{init}=1 atm; T_{init}=300 K.

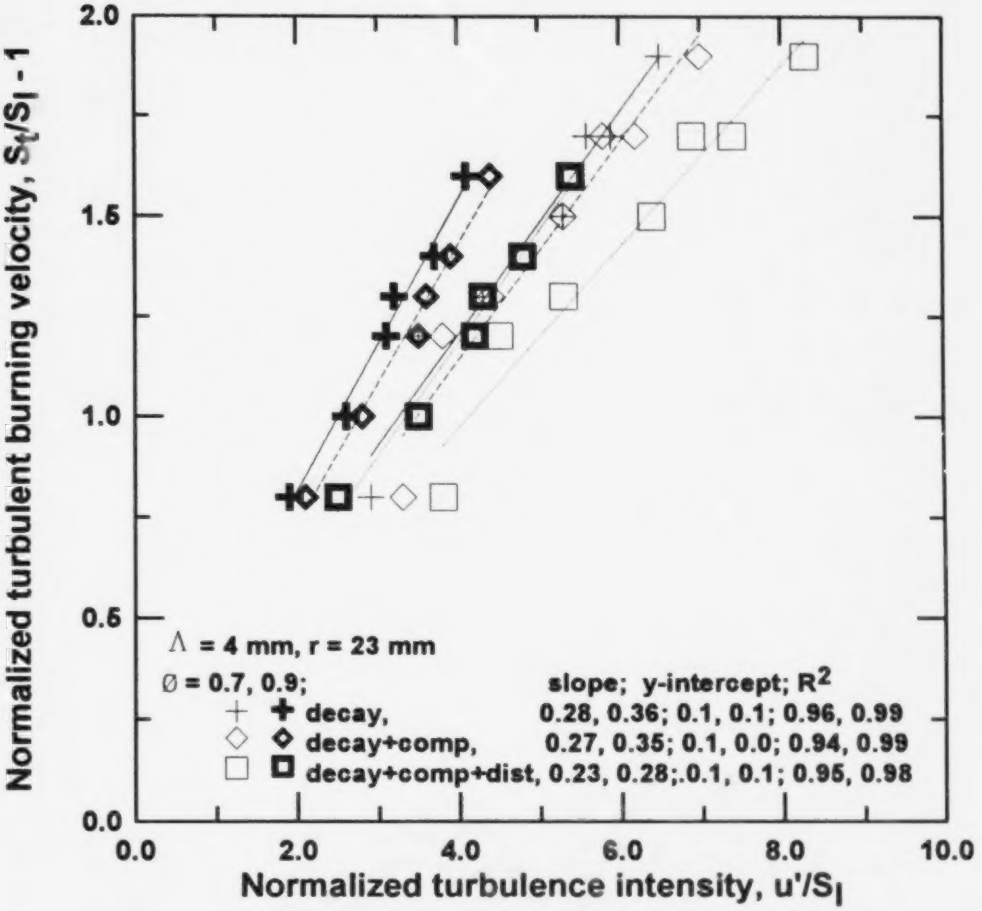

Figure 6.12c: Plots of normalized turbulent burning velocity, S_t/S_l - 1, against normalized turbulence intensity, u'/S_l, for typical 23 mm radius, medium scale, turbulent flames. Ø=0.7, 0.9; Λ≈4 mm; P_{init}=1 atm; T_{init}=300 K.

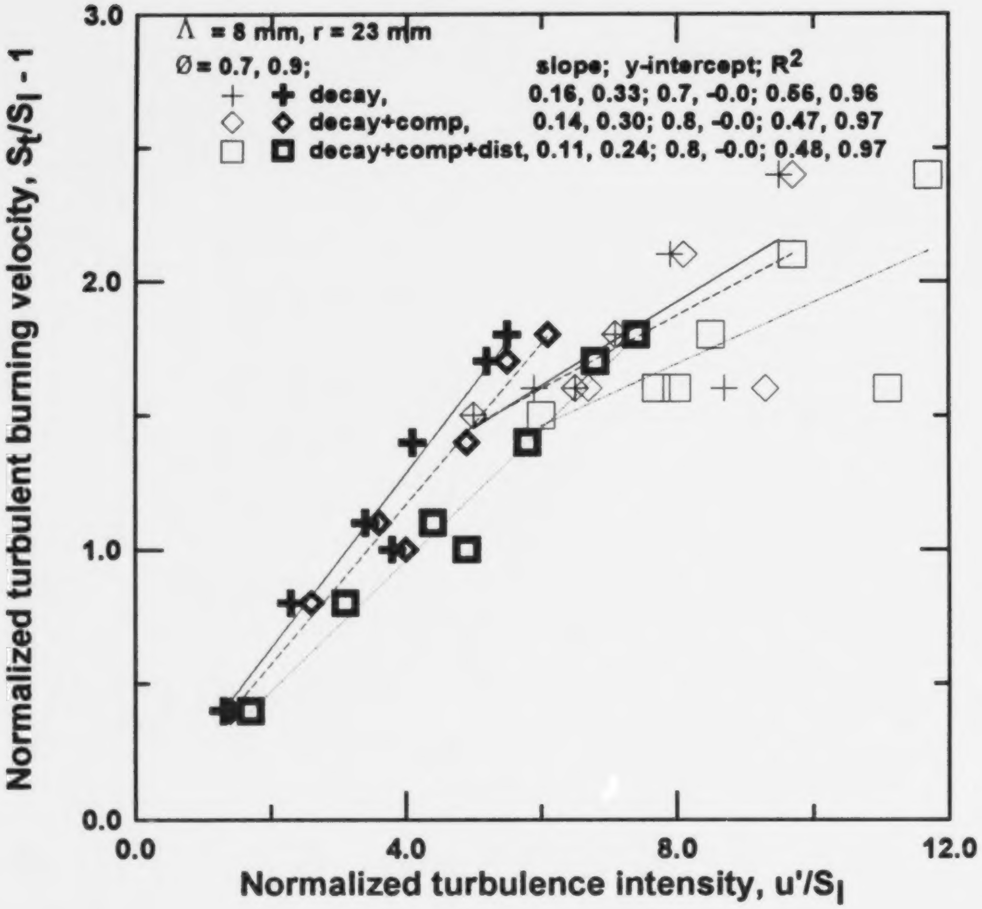

Figure 6.12d: Plots of normalized turbulent burning velocity, S_t/S_l - 1, against normalized turbulence intensity, u'/S_l, for typical 23 mm radius, large scale, turbulent flames. Ø=0.7, 0.9; Λ≈8 mm; P_{init}=1 atm; T_{init}=300 K.

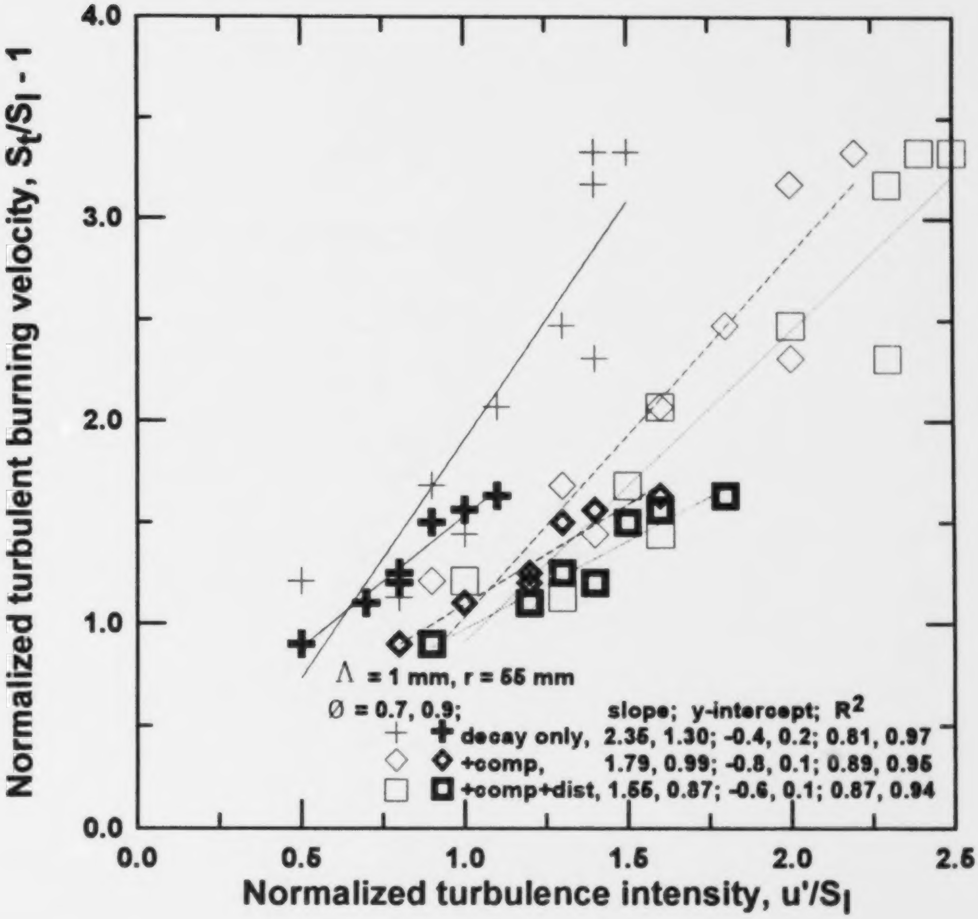

Figure 6.13a: Plots of normalized turbulent burning velocity, S_t/S_l - 1, against normalized turbulence intensity, u'/S_l, for typical 55 mm radius, fine scale, turbulent flames. $Ø=0.7$, 0.9; $\Lambda \approx 1$ mm; $P_{init}=1$ atm; $T_{init}=300$ K.

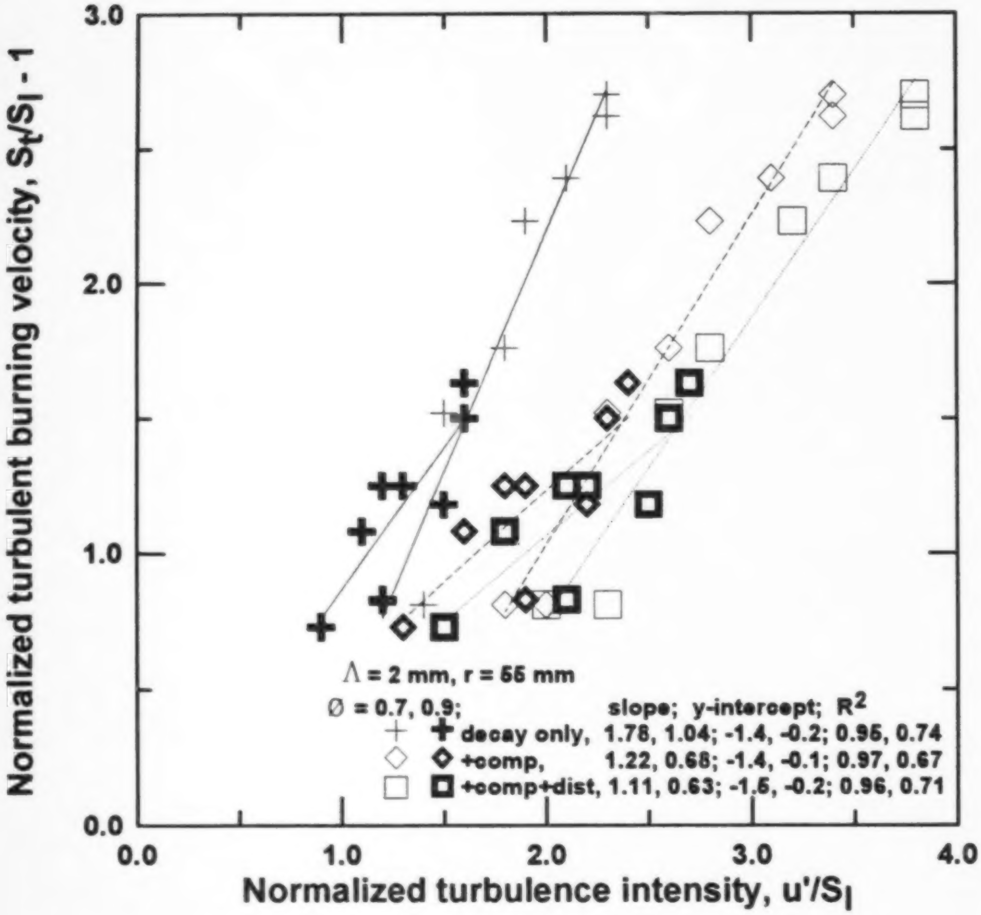

Figure 6.13b: Plots of normalized turbulent burning velocity, $S_t/S_l - 1$, against normalized turbulence intensity, u'/S_l, for typical 55 mm radius, small scale, turbulent flames. $\varnothing = 0.7$, 0.9; $\Lambda \approx 2$ mm; $P_{init} = 1$ atm; $T_{init} = 300$ K.

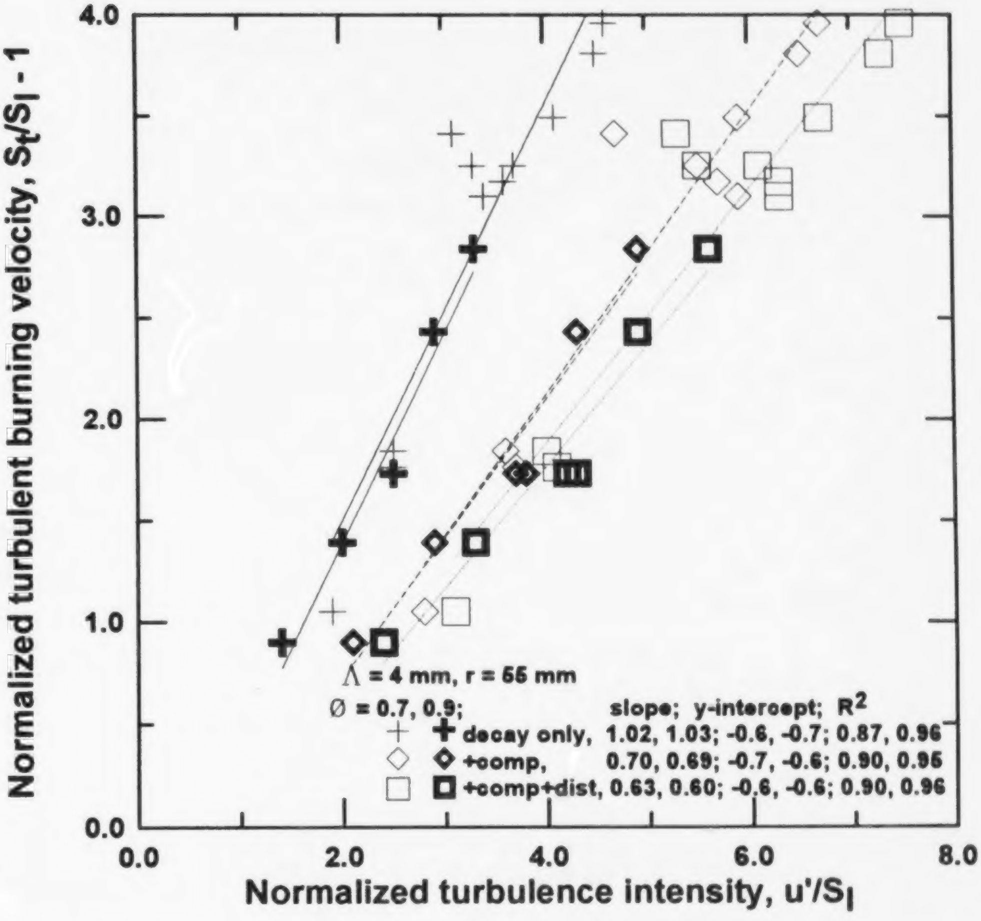

Figure 6.13c: Plots of normalized turbulent burning velocity, S_t/S_l - 1, against normalized turbulence intensity, u'/S_l, for typical 55 mm radius, medium scale, turbulent flames. Ø=0.7, 0.9; Λ≈4 mm; P_{init}=1 atm; T_{init}=300 K.

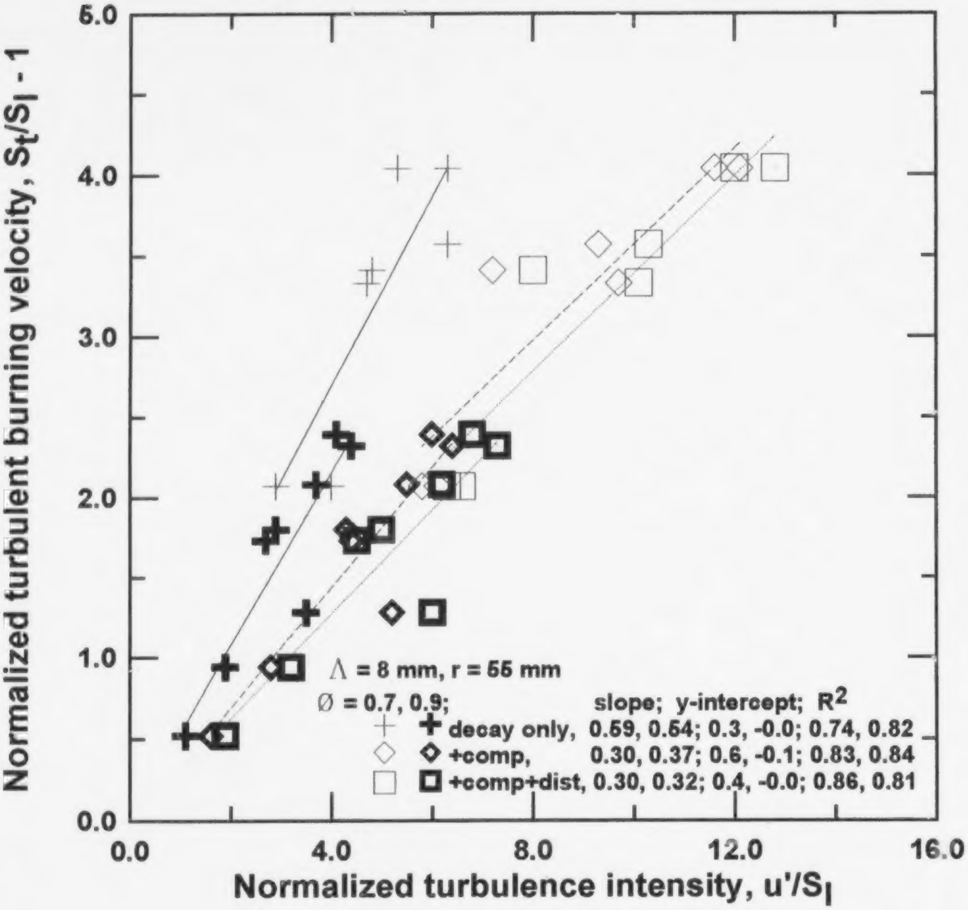

Figure 6.13d: Plots of normalized turbulent burning velocity, S_t/S_l - 1, against normalized turbulence intensity, u'/S_l, for typical 55 mm radius, large scale, turbulent flames. Ø=0.7, 0.9; $\Lambda \approx 8$ mm; P_{init}=1 atm; T_{init}=300 K.

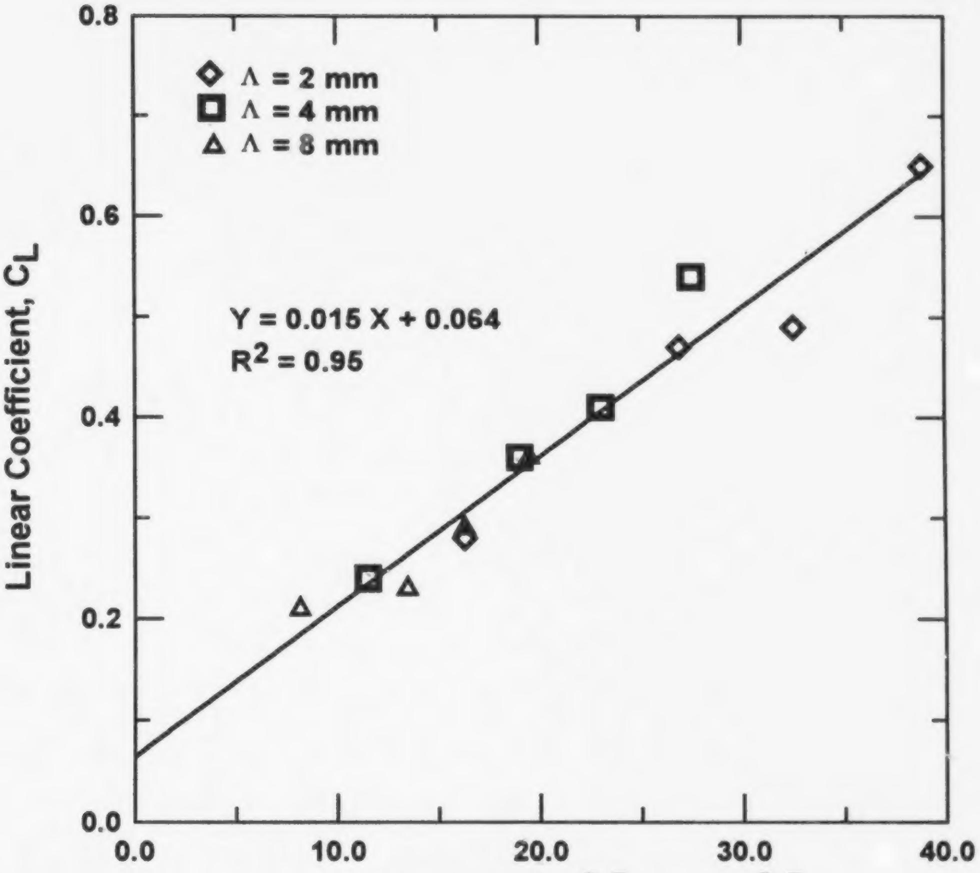

Figure 6.14: Linear coefficient as a function of flame radius and the square-root of integral scale.

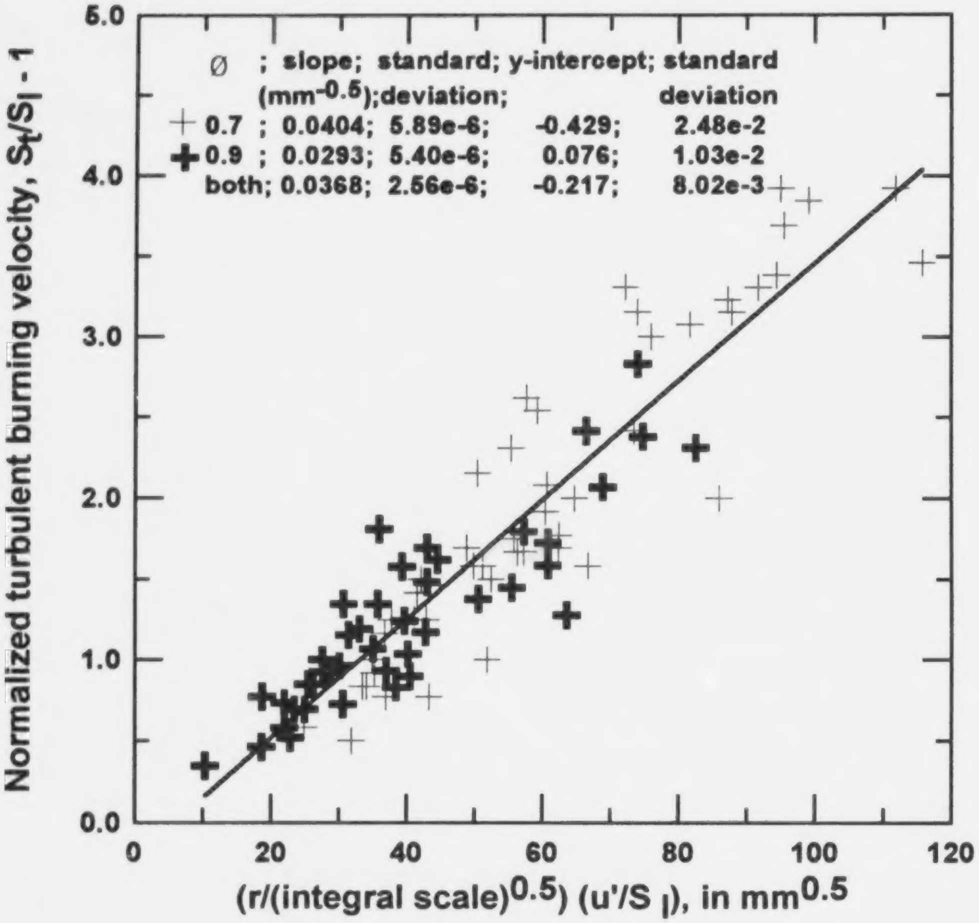

Figure 6.15a: Normalized turbulent burning velocity, S_t/S_l-1, as a function of $(r/\sqrt{\Lambda})(u'/S_l)$. The turbulence intensity, u', is based on normal turbulence decay.

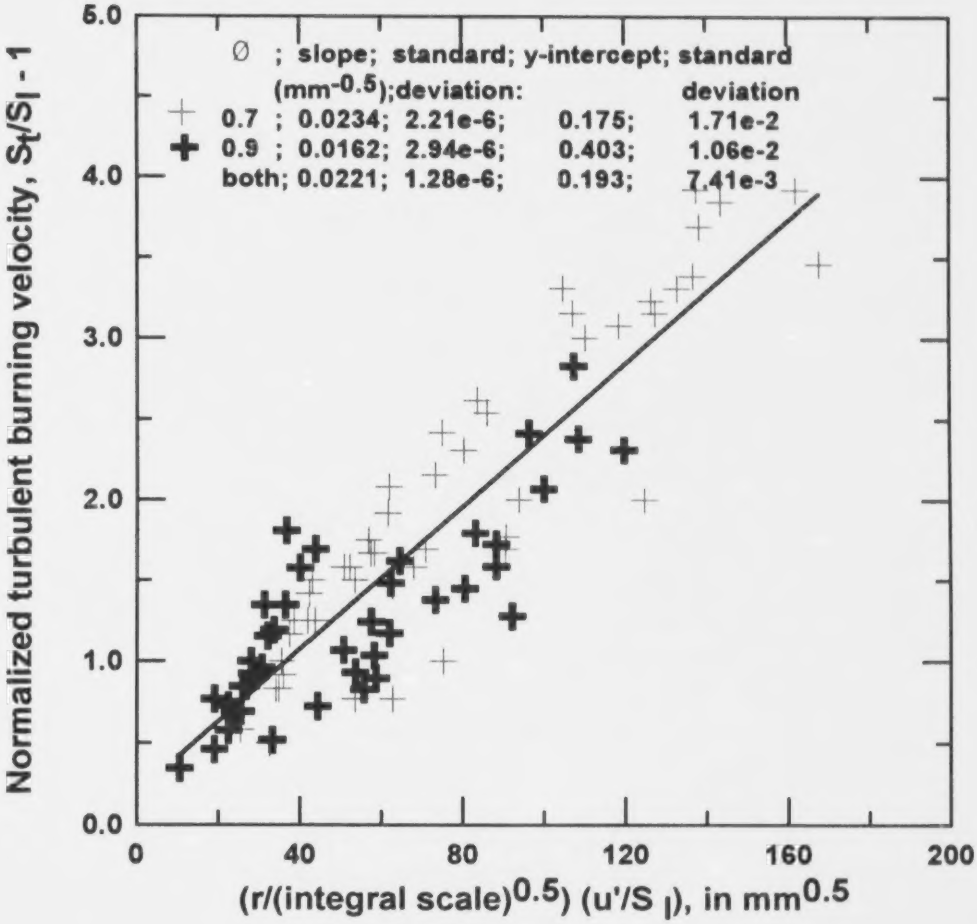

Figure 6.15b: Normalized turbulent burning velocity, S_t/S_l-1, as a function of $(r/\sqrt{\Lambda})(u'/S_l)$. The turbulence intensity, u', is based on normal turbulence decay and compression.

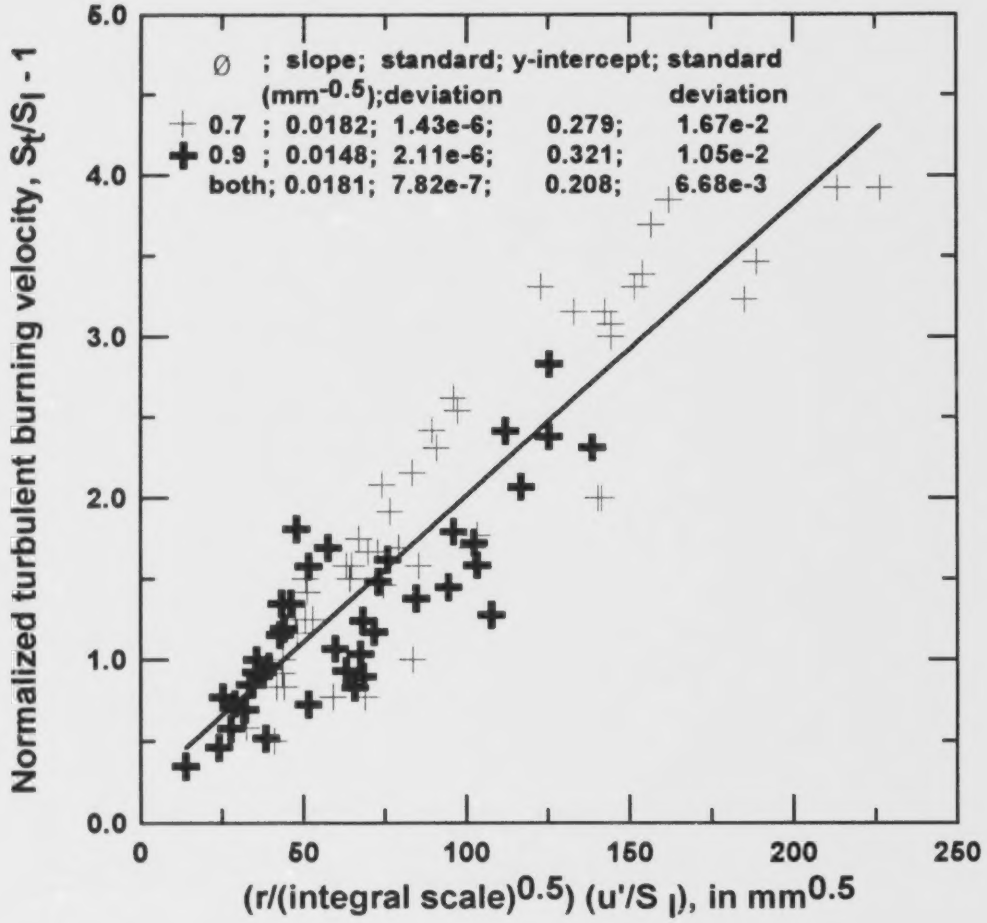

Figure 6.15c: Normalized turbulent burning velocity, S_t/S_l-1, as a function of $(r/\sqrt{\Lambda})(u'/S_l)$. The turbulence intensity, u', is based on normal turbulence decay, compression and rapid distortion.

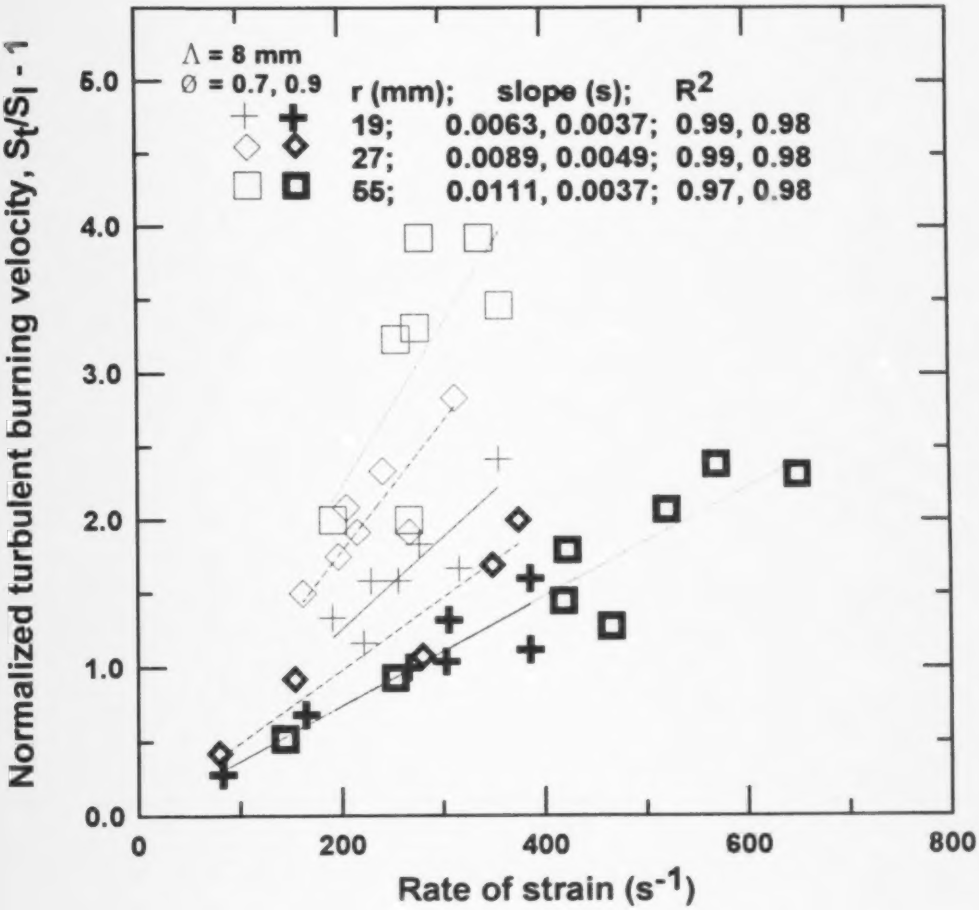

Figure 6.16a: Normalized turbulent burning velocity, S_t/S_l-1, as a function of the rate of strain. Λ≈8 mm; Ø=0.7, 0.9; r=19 mm (schlieren images), 27 mm (schlieren images), 55 mm (pressure traces).

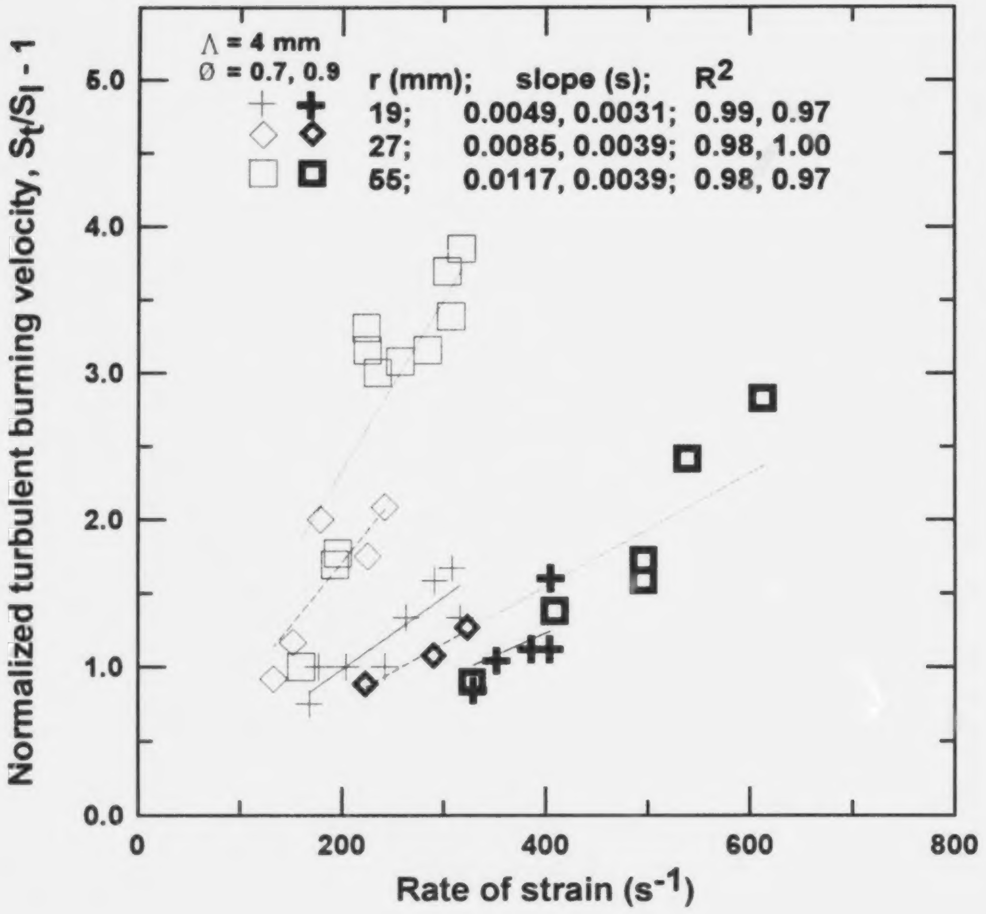

Figure 6.16b: Normalized turbulent burning velocity, S_t/S_l-1, as a function of the rate of strain. Λ≈4 mm; Ø=0.7, 0.9; r=19 mm (schlieren images), 27 mm (schlieren images), 55 mm (pressure traces).

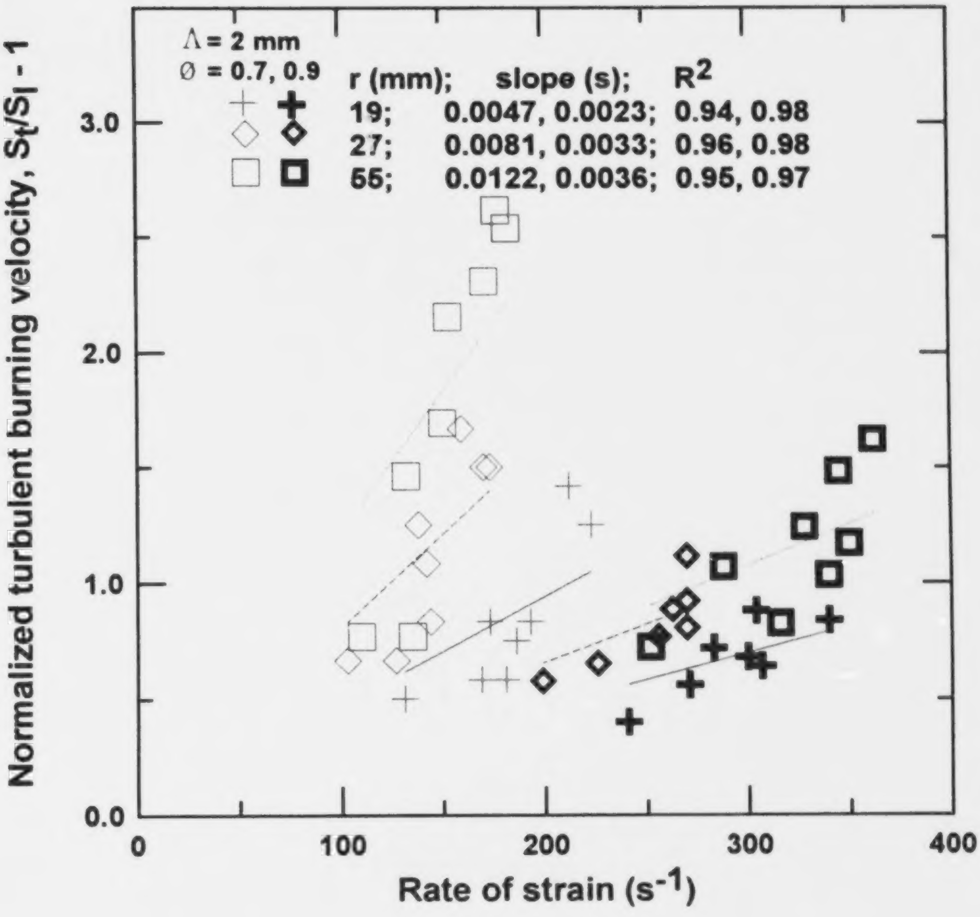

Figure 6.16c: Normalized turbulent burning velocity, S_t/S_l-1, as a function of the rate of strain. Λ≈2 mm; Ø=0.7, 0.9; r=19 mm (schlieren images), 27 mm (schlieren images), 55 mm (pressure traces).

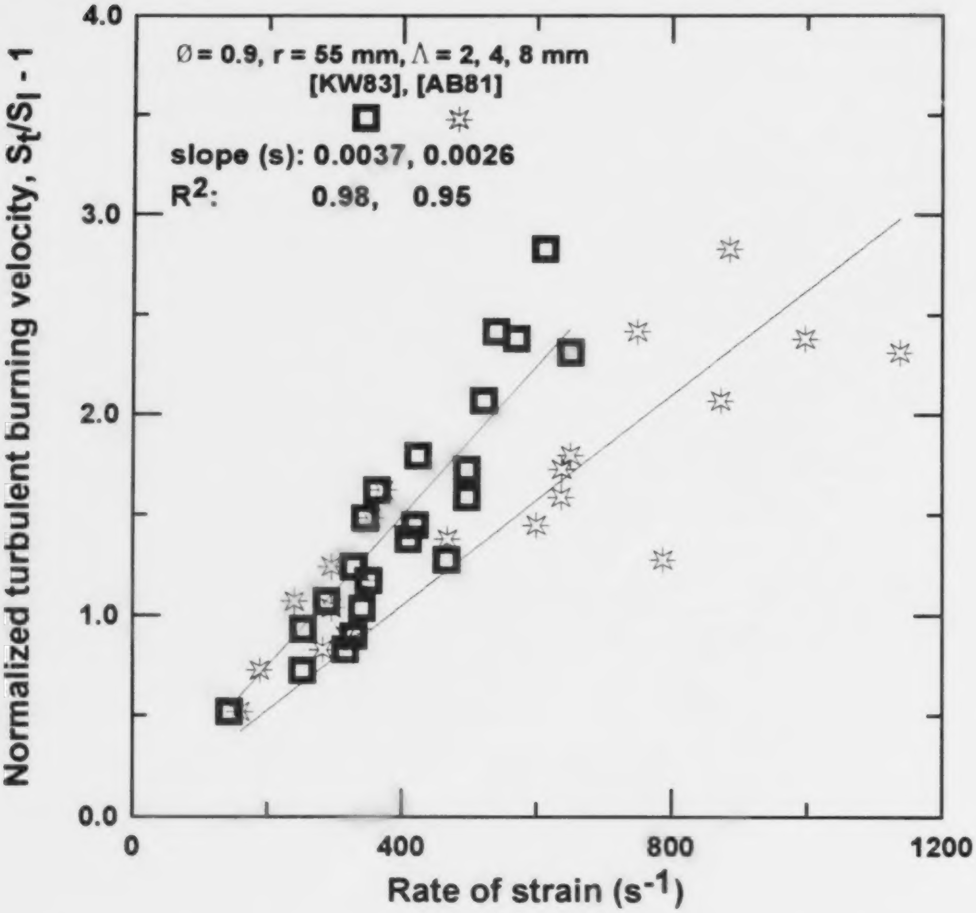

Figure 6.17a: Normalized turbulent burning velocity, S_t/S_l-1, as a function of the rate of strain. Λ≈2, 4, 8 mm; Ø=0.9; r=55 mm (pressure traces).

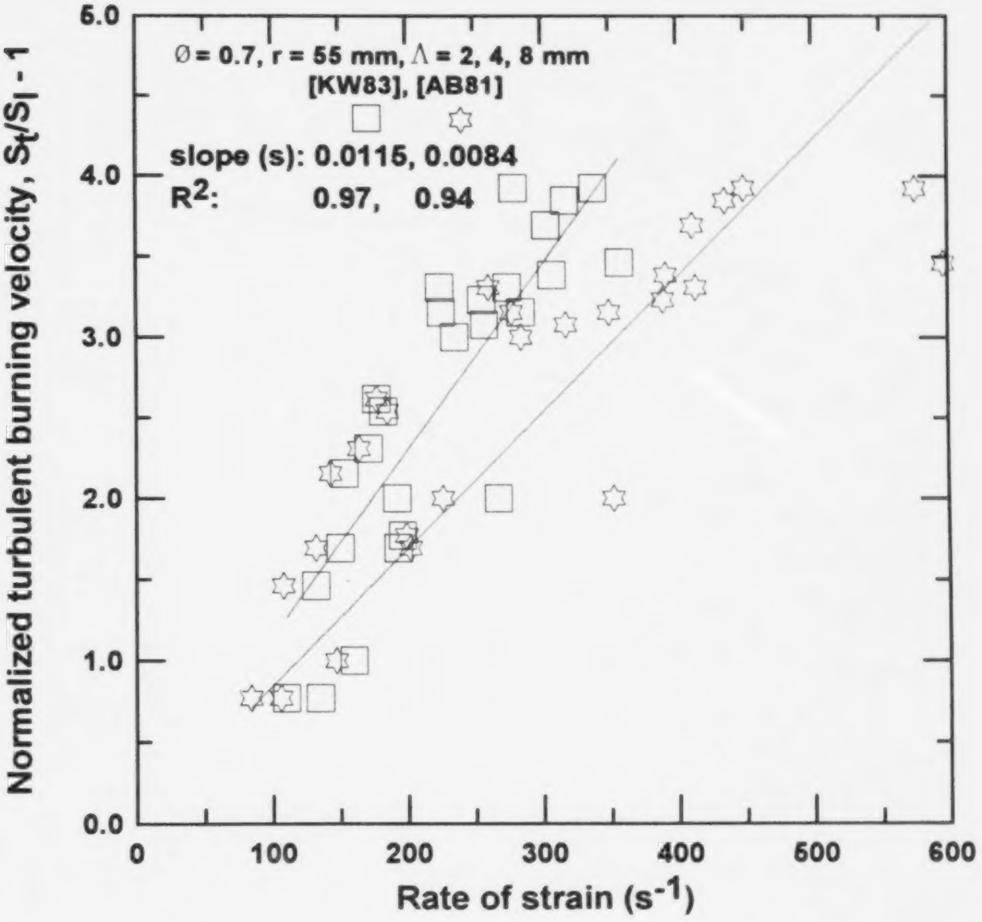

Figure 6.17b: Normalized turbulent burning velocity, S_t/S_l-1, as a function of the rate of strain. Λ≈2, 4, 8 mm; Ø=0.7; r=55 mm (pressure traces).

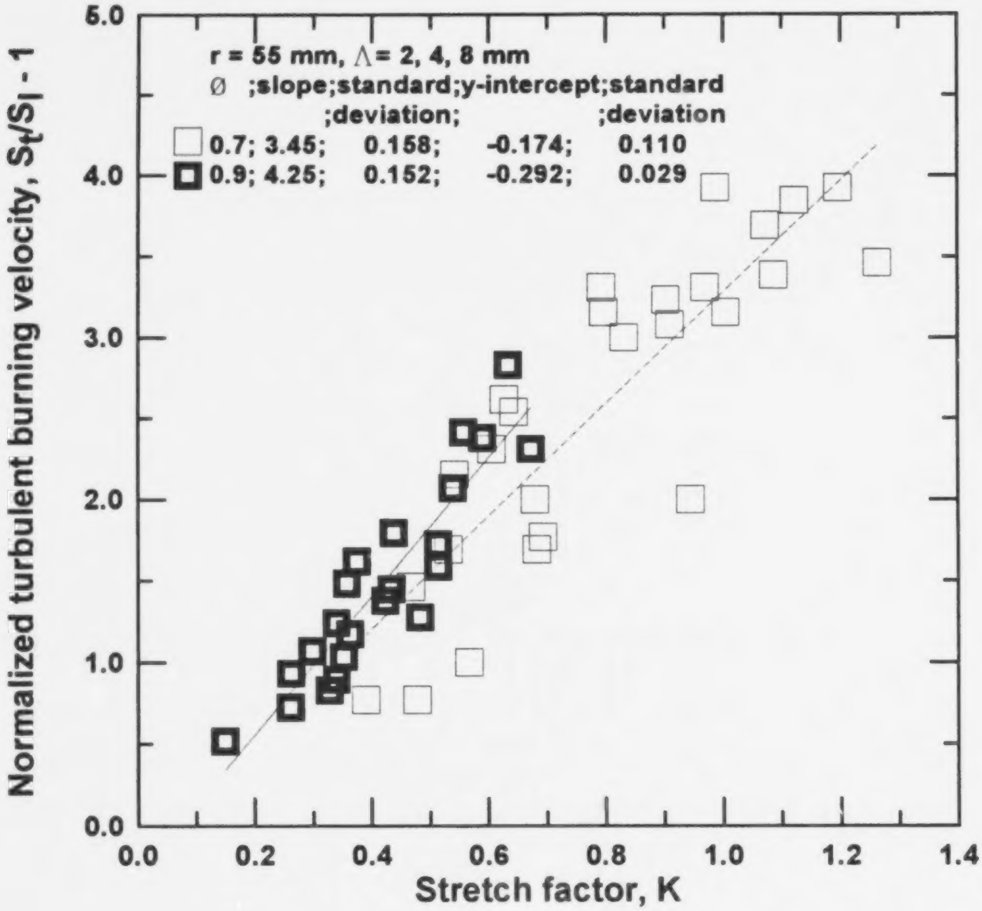

Figure 6.18: Normalized turbulent burning velocity, S_t/S_l-1, as a function of Karlovitz stretch factor. Λ≈2, 4, 8 mm; Ø=0.7, 0.9; r=55 mm (pressure traces).

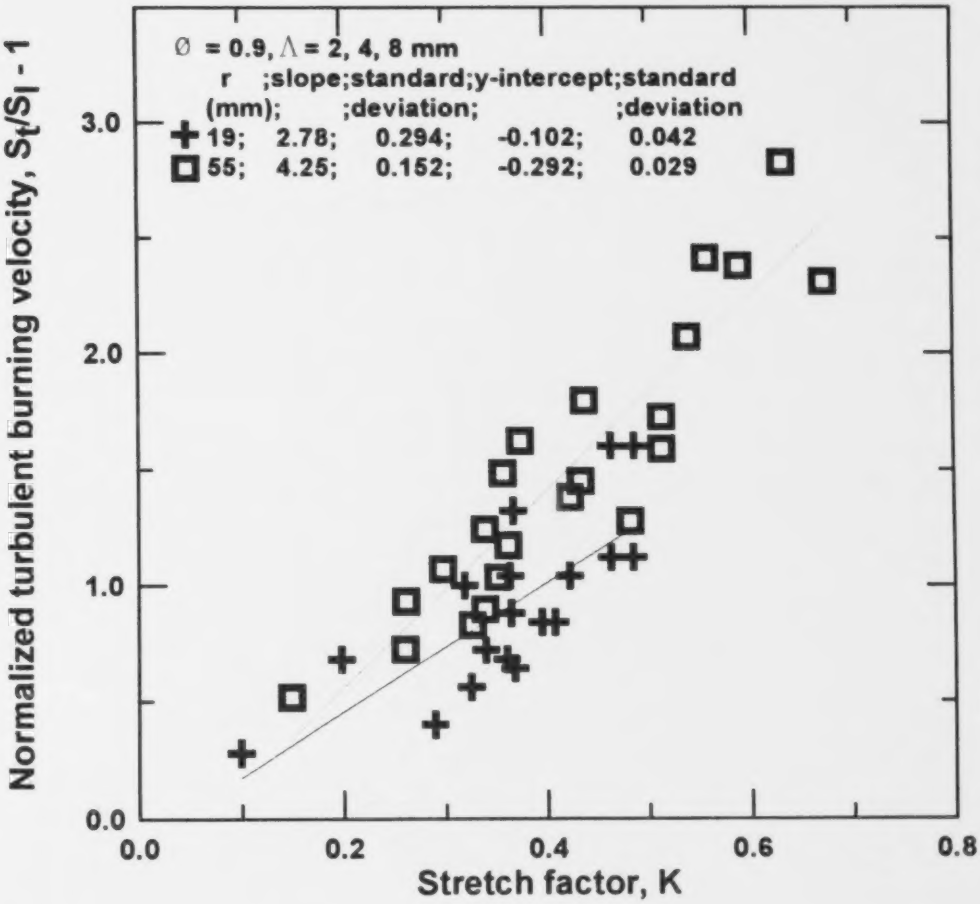

Figure 6.19a: The normalized turbulent burning velocity, S_t/S_l-1, as a function of Karlovitz stretch factor and flame size. Λ≈2, 4, 8 mm; Ø=0.9; r=19 mm (schlieren images), 55 mm (pressure traces).

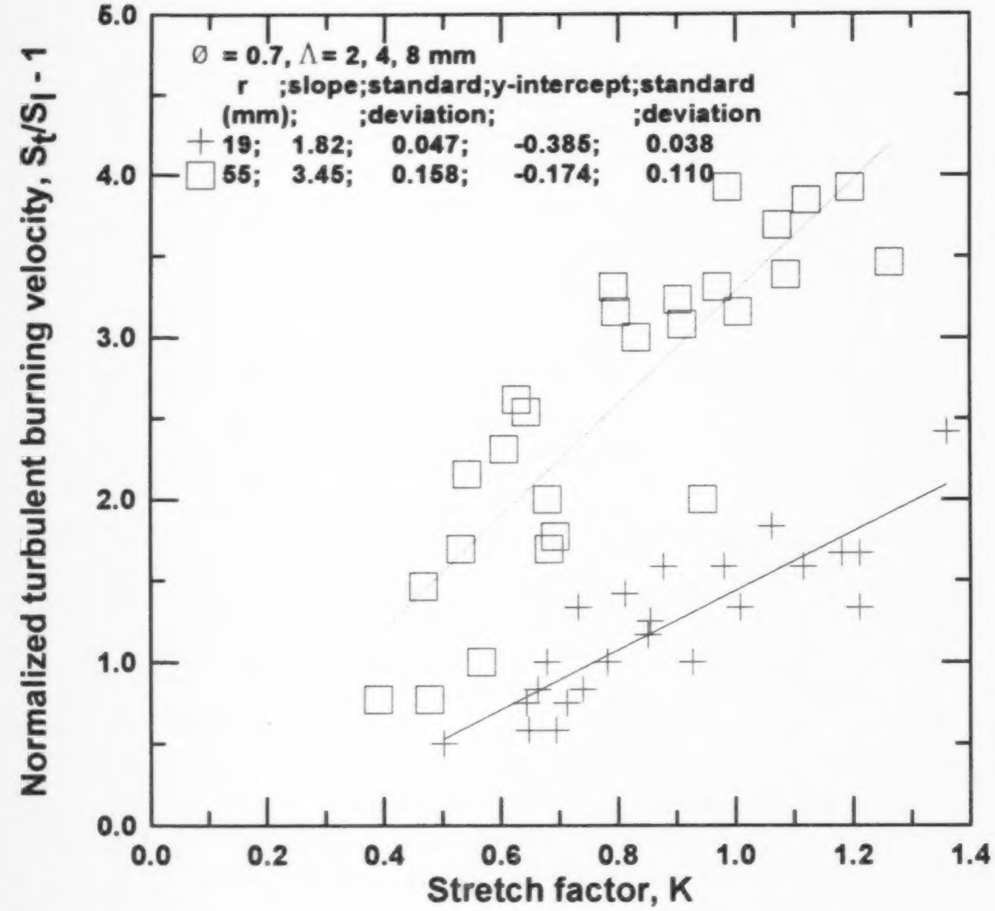

Figure 6.19b: The normalized turbulent burning velocity, S_t/S_l-1, as a function of Karlovitz stretch factor and flame size. Λ≈2, 4, 8 mm; Ø=0.7; r=19 mm (schlieren images), 55 mm (pressure traces).

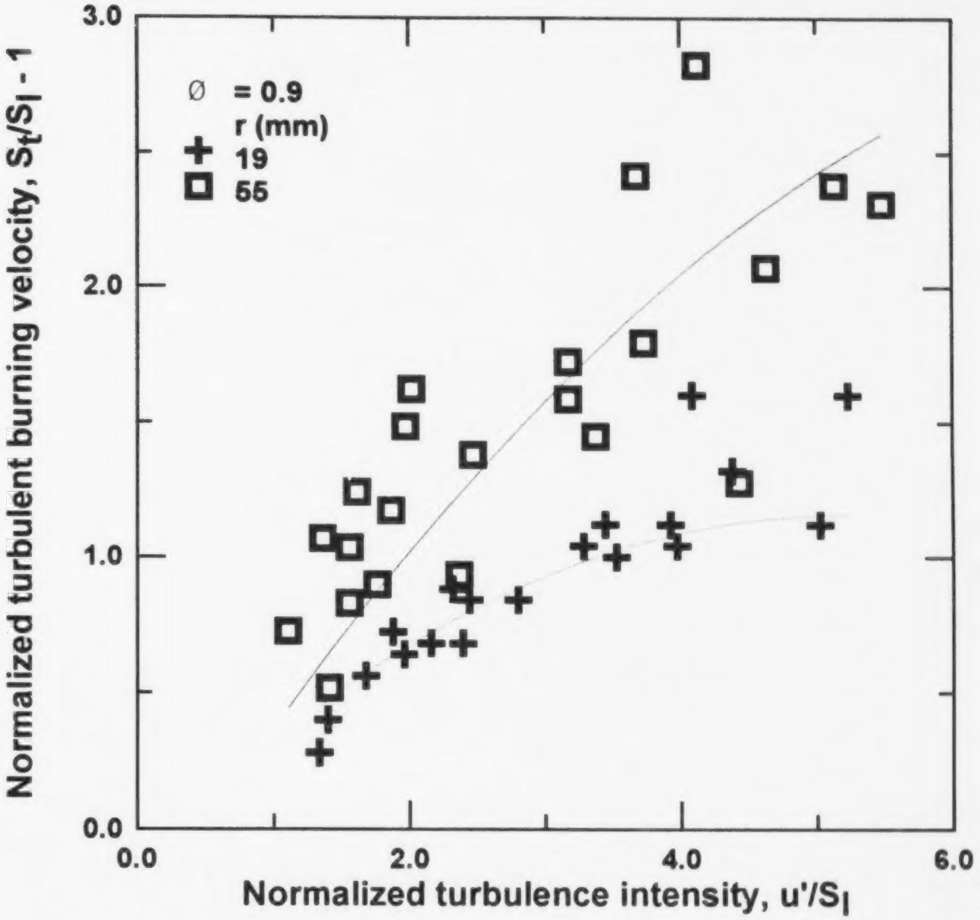

Figure 6.20a: Comparing eddy structure model predictions with experiments. Ø=0.9; Λ≈2, 4, 8 mm; r=19 mm (schlieren images), 55 mm (pressure traces).

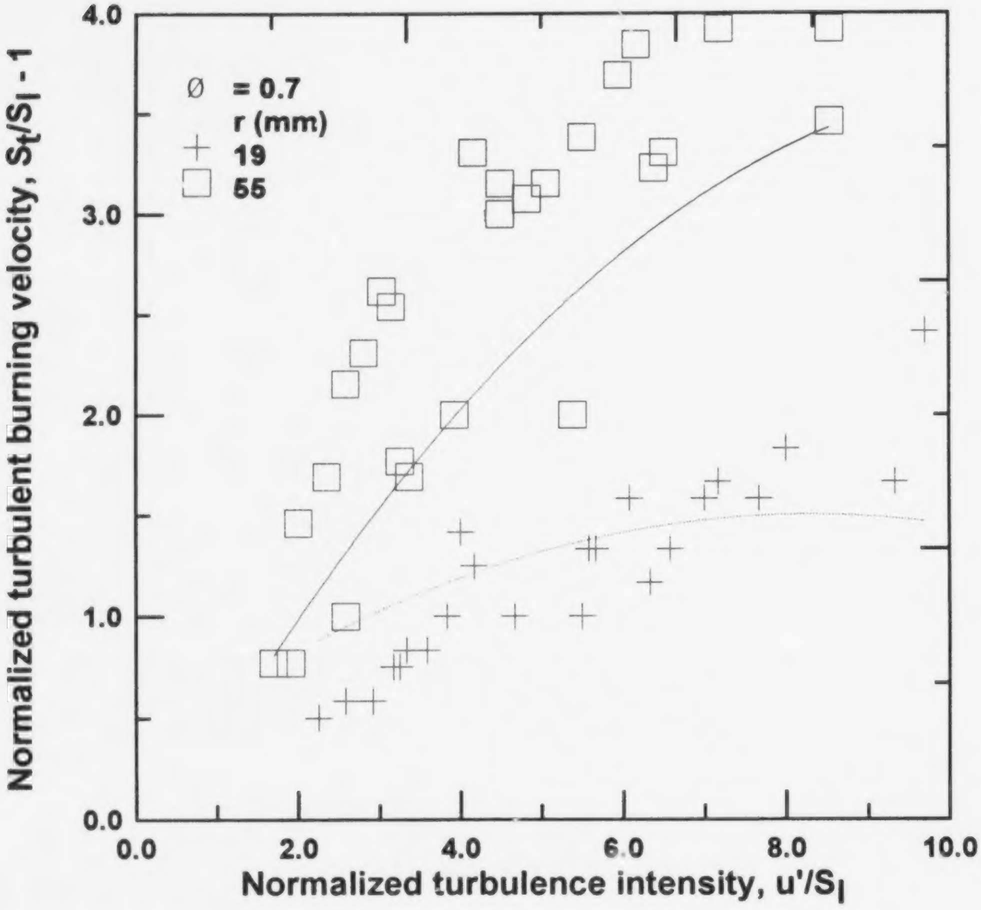

Figure 6.20b: Comparing eddy structure model predictions with experiments. Ø=0.7; Λ≈2, 4, 8 mm; r=19 mm (schlieren images), 55 mm (pressure traces).

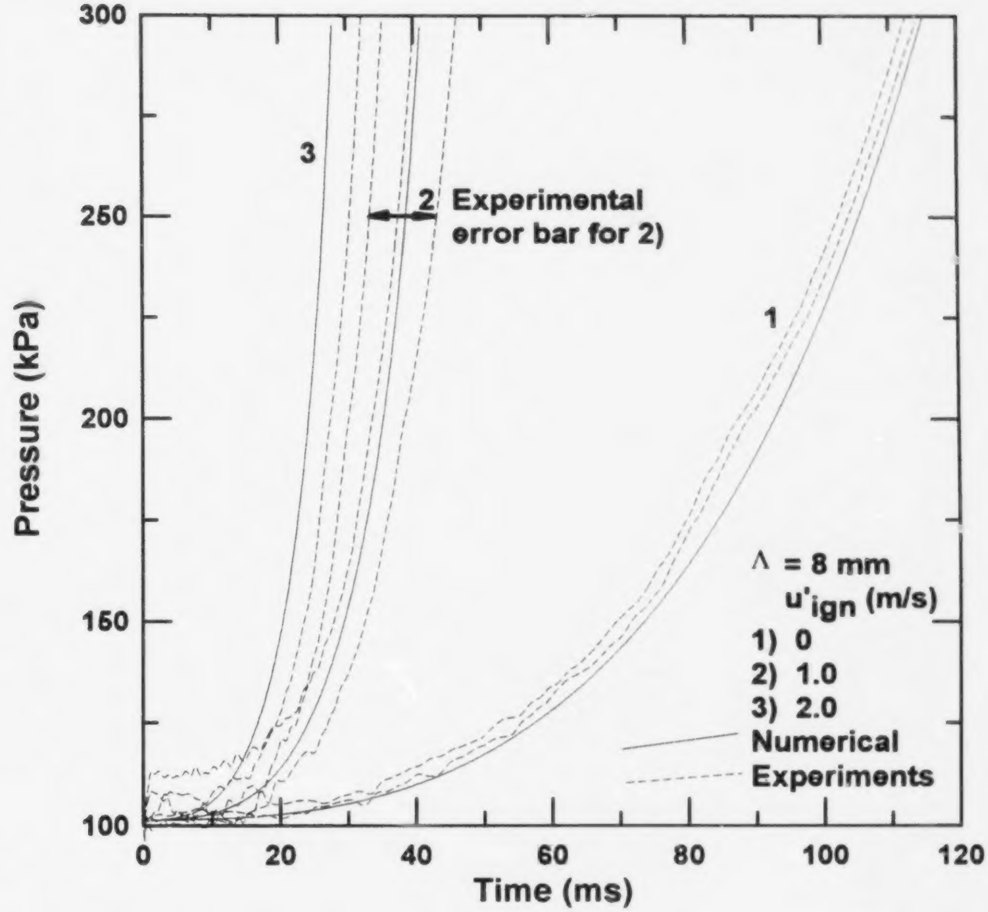

Figure 6.21: Comparing turbulent flame pressure rise simulations with experiments. Ø=0.7; Λ≈8 mm; u'_{ign}=0, 1.0, 2.0 m/s; P_{init}=1 atm; T_{init}=300 K.

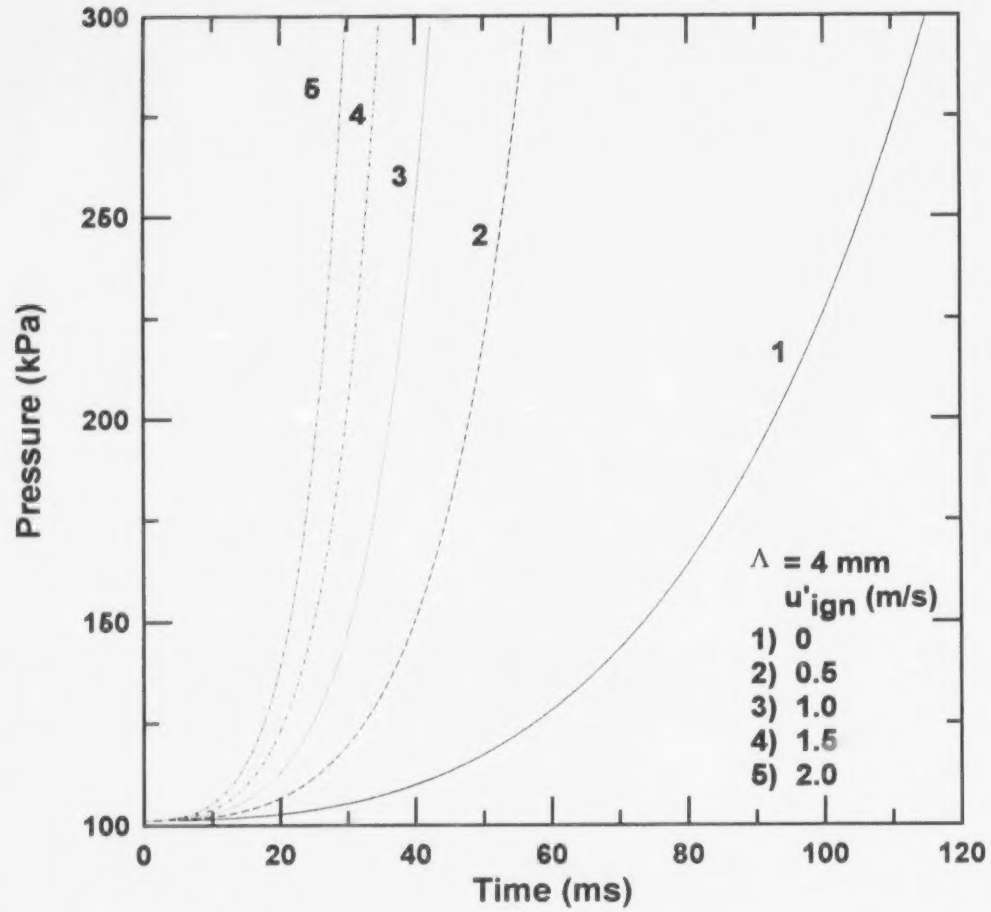

Figure 6.22: Numerical simulations of u' effects on combustion chamber pressure rise. Ø=0.7; Λ≈4 mm; u'_{ign}=0, 0.5, 1.0, 1.5, 2.0 m/s; P_{init}=1 atm; T_{init}=300 K.

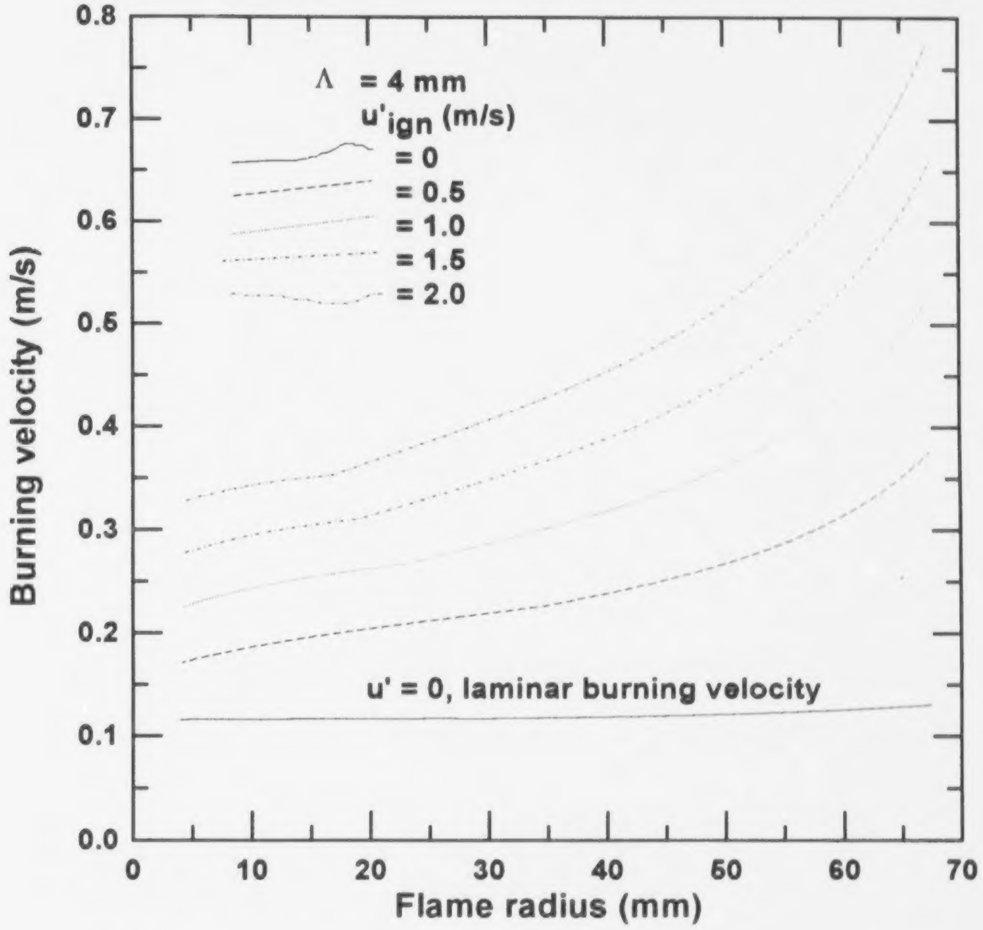

Figure 6.23: Numerical simulations of u' effects on burning velocity as a function of flame radius.
Ø=0.7; Λ≈4 mm; u'_{ign}=0, 0.5, 1.0, 1.5, 2.0 m/s; P_{init}=1 atm; T_{init}=300 K.

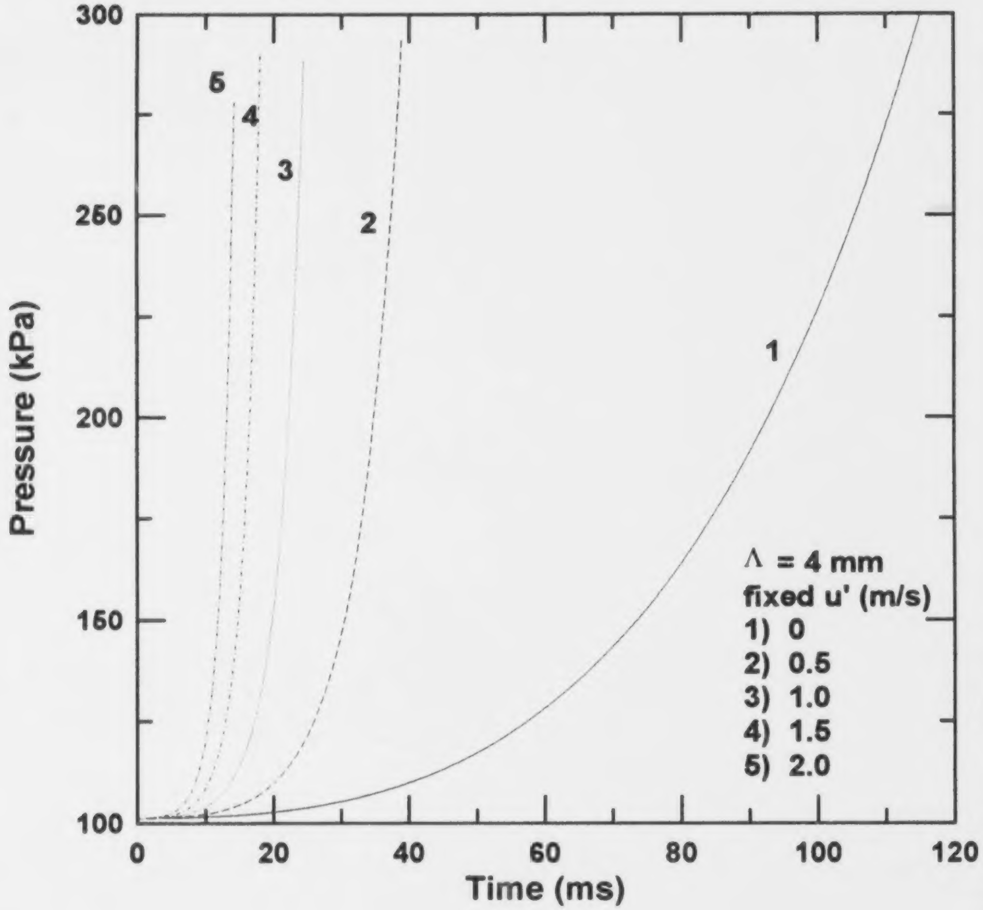

Figure 6.24: Numerical simulations of fixed u' effects on combustion chamber pressure rise.

Ø=0.7; Λ≈4 mm; u' fixed at 0, 0.5, 1.0, 1.5, 2.0 m/s; P_{init}=1 atm; T_{init}=300 K.

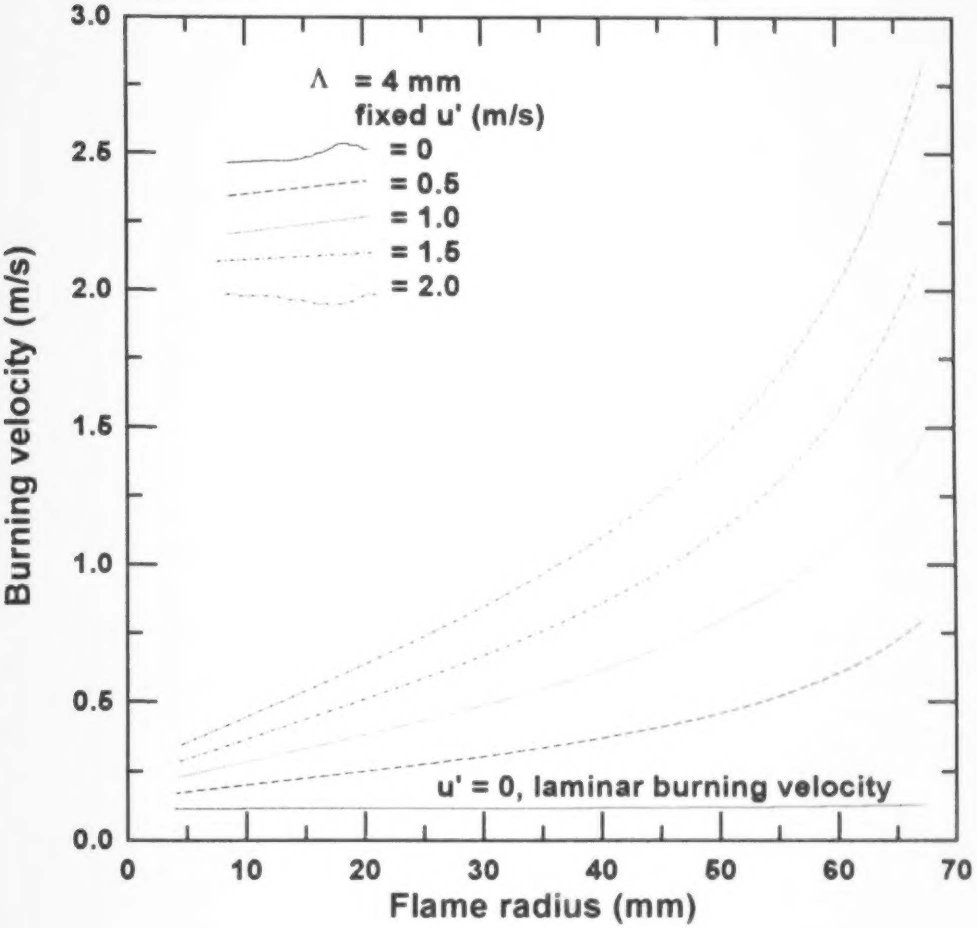

Figure 6.25: Numerical simulations of fixed u' effects on burning velocity as a function of flame radius.
Ø=0.7; Λ≈4 mm; u' fixed at 0, 0.5, 1.0, 1.5, 2.0 m/s; P_{init}=1 atm; T_{init}=300 K.

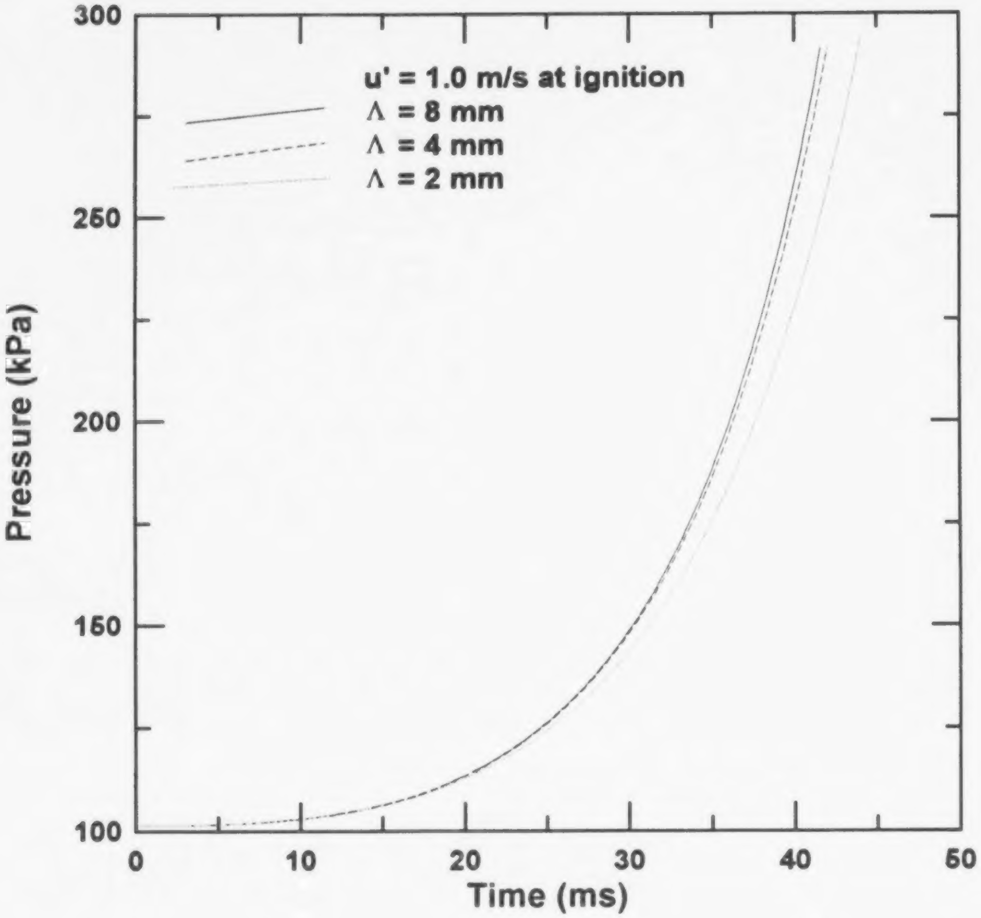

Figure 6.26: Numerical simulations of integral scale effects on combustion chamber pressure rise.
Ø=0.7; Λ≈2, 4, 8 mm; u'_{ign}=1.0 m/s; P_{init}=1 atm; T_{init}=300 K.

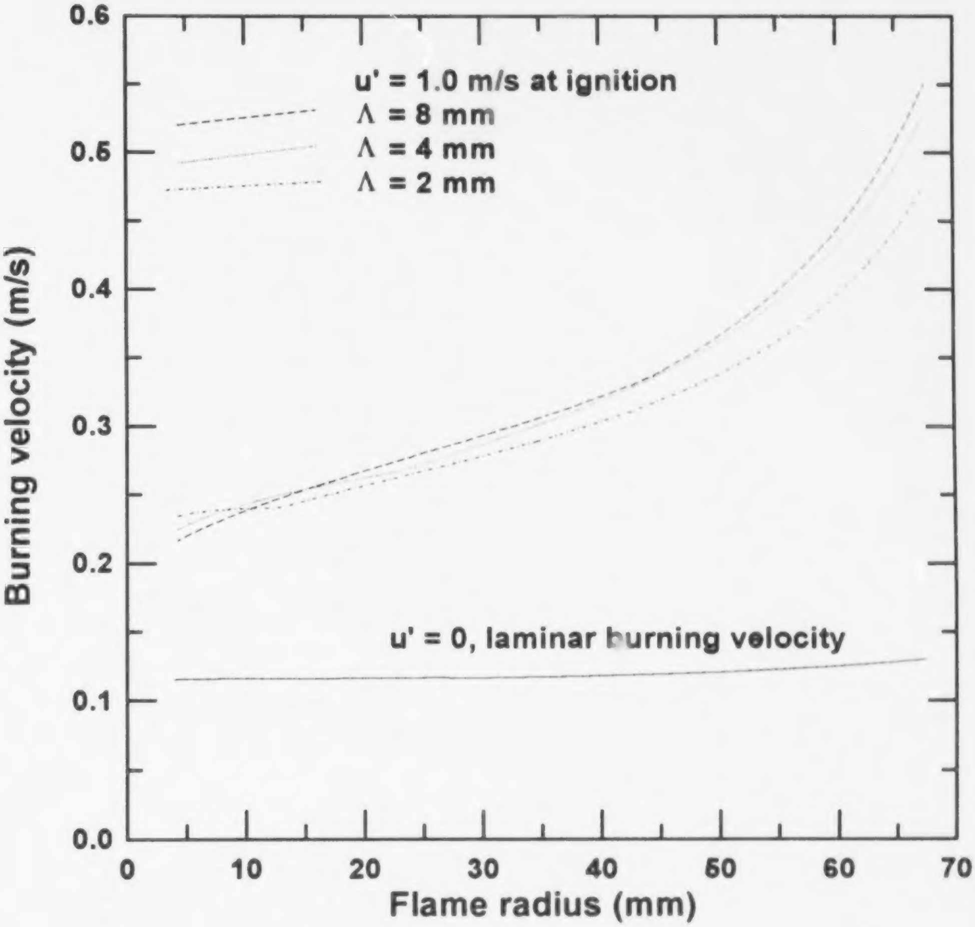

Figure 6.27: Numerical simulations of integral scale effects on burning velocity as a function of flame radius.
$\emptyset=0.7$; $\Lambda\approx2, 4, 8$ mm; $u'_{ign}=1.0$ m/s; $P_{init}=1$ atm; $T_{init}=300$ K.

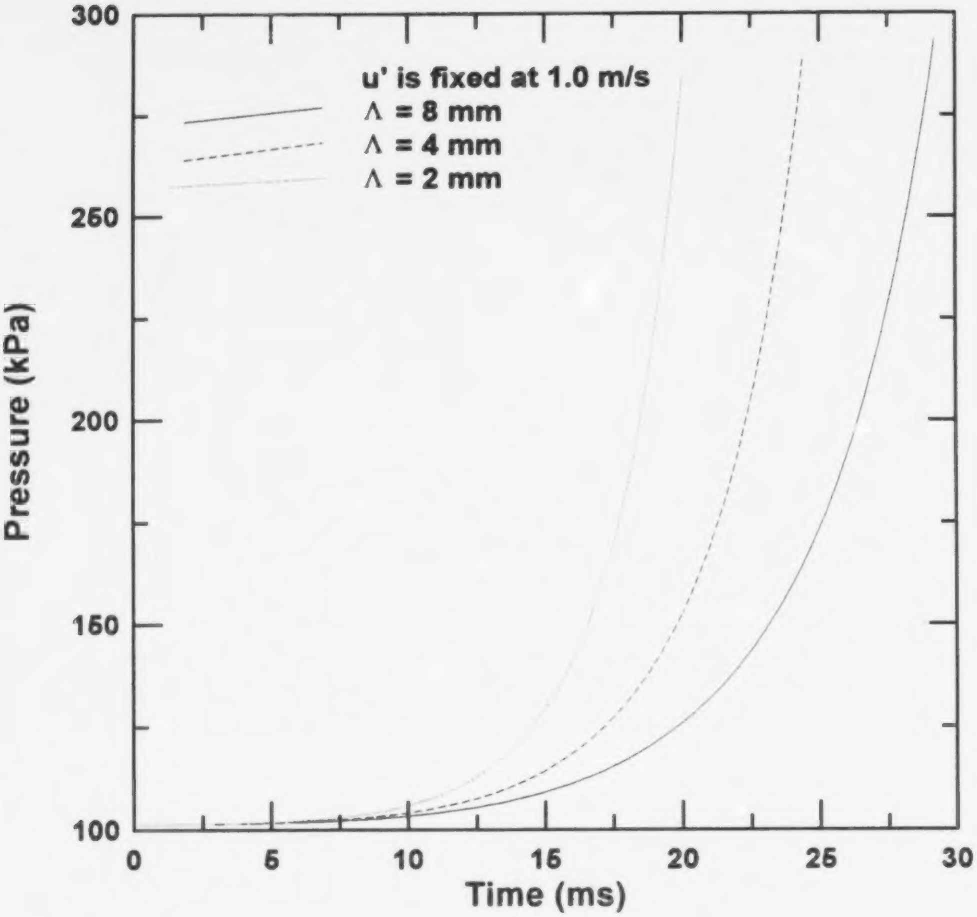

Figure 6.28: Numerical simulations of integral scale effects with fixed u' on combustion chamber pressure rise.
Ø=0.7; Λ≈2, 4, 8 mm; u' fixed at 1.0 m/s; P_{init}=1 atm; T_{init}=300 K.

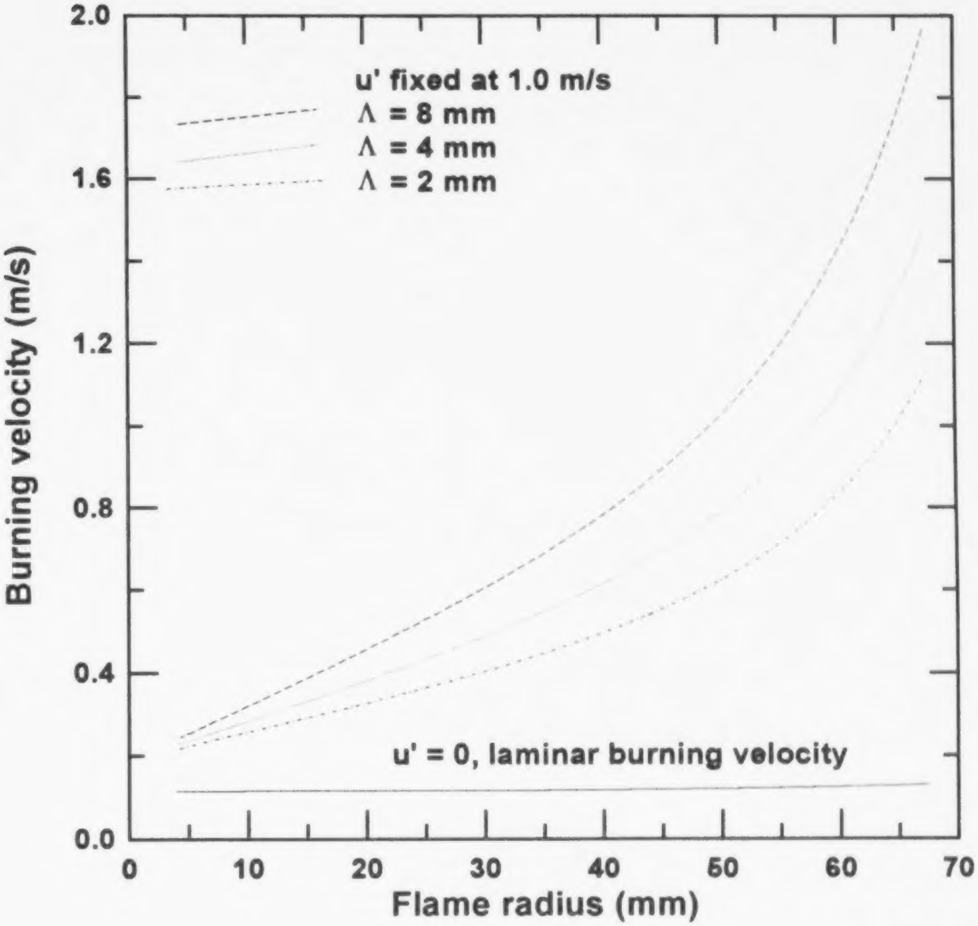

Figure 6.29: Numerical simulations of integral scale effects with fixed u' on burning velocity as a function of flame radius.
Ø=0.7; Λ≈2, 4, 8 mm; u' fixed at 1.0 m/s; P_{init}=1 atm; T_{init}=300 K.

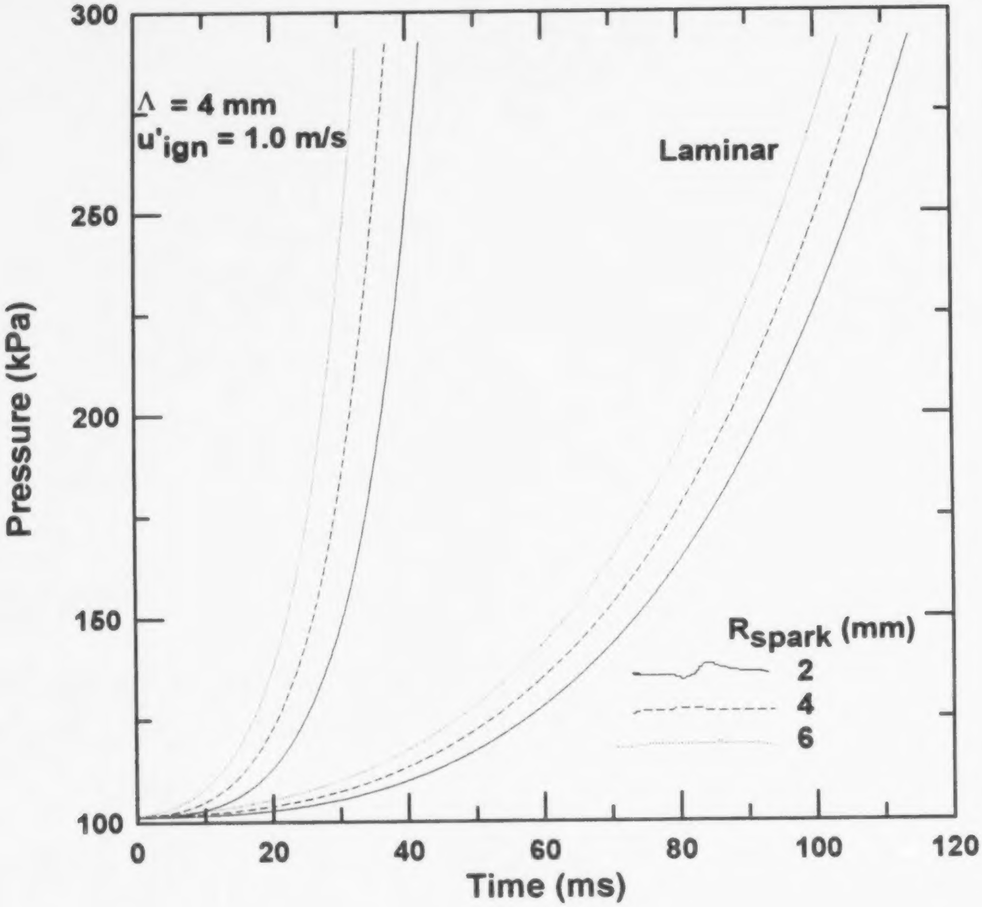

Figure 6.30: Numerical simulations of spark size effects on combustion chamber pressure rise.

Ø=0.7; Λ≈4 mm; u'_{ign}=1.0 m/s; r_{spark}≈2, 4, 6 mm; P_{init}=1 atm; T_{init}=300 K.

CHAPTER 7

CONCLUSIONS AND RECOMMENDATIONS

This chapter draws all major methane-air flame growth conclusions. The laminar flame conclusions are deduced followed by the turbulent flame conclusions. Various recommendations are suggested for possible future work.

7.1: SUMMARY AND CONCLUSIONS

Both high speed schlieren video and pressure trace analyses were used to study the methane-air flame growth in a 125 mm cubical combustion chamber. Equivalence ratio was varied from 1.0 to 0.6 while the initial temperature was fixed at 300 K. The initial pressure for 0.7 and 0.9 equivalence ratio laminar flames was varied from 0.5 to 2.0 atm in order to estimate the effects of pressure on the flame growth. Only the 0.7 and 0.9 equivalence ratio mixtures ignited at 1 atm and 300 K are considered in the turbulent flame growth study. The ignition-time turbulence intensity was up to 2 m/s with 1 to 8 mm integral scale.

7.1.1: LAMINAR FLAME GROWTH IN A CLOSED CHAMBER

The schlieren flame growth agrees well with the flame growth deduced from the pressure trace analysis using a multi-zone thermodynamic equilibrium model. Right after spark ignition, there is a high noise to signal ratio in the pressure traces. The agreement between the schlieren video and the pressure trace allows the use of schlieren video results in the noisy pressure trace region. The agreement indirectly confirms that the laminar flame front is thin with completely burnt mixture at thermodynamic equilibrium behind the flame front.

For very lean, slow burning mixtures, the effects of buoyancy can convect the flame upward creating a dimple on the lower side of the flame ball. The 0.6 equivalence ratio flame ignited at 300 K and 1 atm has shown this phenomenon.

Pressure has a slight negative effect on the methane-air flame growth rate. Over the range of pressures from 0.5 to 2.0 atm, the pressure exponents for 0.7 and 0.9 equivalence ratio methane-air flames at 300 K are -0.43 and -0.26 respectively. These pressure exponents agree with those in the literature. The trend of more negative pressure exponent for leaner methane-air flame is in agreement with [EC89].

While the flame growth rate changes significantly in a closed chamber, the laminar burning velocity remains quasi-steady. The initial outwardly propagating flame is slowed down due to compression as the combustion chamber pressure rises. The compression also heats up the unburnt mixture and this temperature rise has a positive effect on burning velocity. This positive effect tends to cancel the negative pressure effect. Hence, the laminar burning velocity remains quasi-steady in the chamber.

With the empirically determined r_{spark}, S_{lo}, Pexp and Texp, the numerical flame growth model can calculate the combustion process based on given initial conditions. The numerically simulated combustion processes are in close agreement with the experiments. The numerical flame growth model is used to analyze the sensitivity of various parameters on the burning rate. It is found that the combustion process is most sensitive to changes in the mixture stoichiometry. For a mixture ignited at 300 K and 1 atm, a $\pm 10\%$ error in equivalence ratio can lead to 42% error in time taken to reach 200 kPa. The second most sensitive parameter is the initial temperature followed by the initial pressure.

7.1.2: TURBULENT FLAME GROWTH IN A CLOSED CHAMBER

Turbulent flame growth measured by schlieren video is slightly faster than the turbulent flame growth calculated from the pressure trace. The somewhat faster schlieren flame growth can be due to the inclusion of a small amount of unburnt mixture brought into the flame front by the eddies. The schlieren analysis is most accurate at the early stages of combustion where the flame front is less wrinkled and the amount of unburnt mixture included in the schlieren image is small. On the other hand, there is a high noise-to-signal ratio in the pressure trace during the early combustion period and hence the pressure trace analysis is more accurate when the combustion pressure rise is significant. Therefore, the short-coming of the pressure trace analysis is over-come by the schlieren analysis and vice versa.

Turbulent flames are wrinkled compared to smooth laminar flames. At higher turbulence intensities, the turbulent flame is distorted as well as corrugated. The wrinkled and distorted turbulent flames grow faster than the laminar flames. Over the range of turbulence conditions considered, the higher the turbulence intensity the faster the flame growth. These wrinkled turbulent flames grow faster mostly due to the larger flame front surface area.

Depending on the turbulence decay rate and the flame growth rate, the turbulent burning velocity can increase or decrease as the flame grows. For a frozen turbulence level, the turbulent burning velocity increases dramatically as the flame grows. In other words, the turbulent burning velocity / turbulence intensity ratio increases as the flame grows. This accelerating turbulent flame is found to be caused by progressive turbulence enhancement as the flame grows. Progressive turbulence enhancement in spark-ignited flames is critical in engine-like combustion. The classical explanation argues that the progressive turbulence enhancement as the flame grows is caused by progressively larger eddies become effective as the initial flame kernel grows larger. According to the classical reasoning, the flame becomes fully developed when it grows somewhat larger than the energy-containing, integral length scale. This classical logic alone is inadequate in explaining the evidence of developing turbulent flame even when the flame is much larger than the integral scale. It is postulated that as well as the classical theory, the accelerating turbulent flame is also caused by increasing flame-turbulence interaction. The instantaneous flame behaviour appears to depend on both the instantaneous parameters as well as the history of flame-turbulence interaction.

There is a roughly linear relation between the normalized turbulent burning velocity, S_t/S_l-1, and the normalized turbulence intensity, u'/S_l. The slope of the linear relation, the linear coefficient, designates the effectiveness of turbulence enhancement on the burning velocity. The linear coefficient is found to be proportional to the flame radius and inversely proportional to the square-root of integral scale. In other words, the turbulent burning velocity-turbulence intensity relation results show progressive turbulence enhancement as the flame grows. The turbulent burning velocity-turbulence intensity relation results also demonstrate that small-scale turbulence is more effective. The more effective small-scale turbulence is due to a few reasons. First of all, for the same turbulence intensity, small-scale turbulence leads to higher shear than large-scale turbulence. Smaller eddies also become effective in wrinkling the flame ball earlier in the combustion process. For the same turbulence intensity, there are many more small eddies in a small-scale turbulence flow compared to the number of eddies in a large-scale turbulence flow.

The normalized turbulent burning velocity, S_t/S_l-1, varies linearly with the normalized turbulence intensity, u'/S_l. In addition, the linear coefficient changes with $r/\sqrt{\Lambda}$. Hence, the results imply that S_t/S_l-1 is a linear function of $(r/\sqrt{\Lambda})(u'/S_l)$. From the least-squares linear fits for the S_t/S_l-1 versus $(r/\sqrt{\Lambda})(u'/S_l)$ plots, normal turbulence decay alone seems to under-estimate the flame front turbulence. Normal turbulence decay along with compression and geometric distortion effects appear to lead to somewhat better fits. This appears to validate the rapid distortion model. However, direct flame front turbulence measurements are required to justify this result.

Alternatively, S_t/S_l-1 can be correlated with the rate of strain or the Karlovitz stretch factor. There is an approximately linear relation between S_t/S_l-1 and the rate of strain or the Karlovitz stretch factor. However, the rate of strain can not be measured directly using turbulence flow measurement techniques. Therefore, the validity of the results relies heavily on the accuracy of the model used in predicting the rate of strain. The available strain rate models in the literature lead to substantially different quantitative results. On the other hand, the different models agree on the qualitative results about roughly linear turbulent burning velocity-rate of strain or Karlovitz stretch factor relation. Most importantly, the results of turbulent burning velocity-rate of strain or Karlovitz stretch factor correlations depict progressive turbulence enhancement similar to that demonstrated by the turbulent burning velocity-turbulence intensity results. The effects of turbulent length scale are included in the rate of strain and the Karlovitz stretch factor. Therefore, the turbulent burning velocity-rate of strain or Karlovitz stretch factor correlations do not seem to be affected by a change in turbulent length scale.

With the empirically determined r_{spark}, S_{lo}, Pexp, Texp and the turbulent burning velocity relations, the numerical flame growth model can simulate the turbulent combustion processes for given initial conditions. The numerically simulated turbulent combustion processes agree with the experiments. The numerical simulations show that, similar to the laminar combustion process, the turbulent combustion process is most sensitive to changes in the mixture stoichiometry. When maintaining a constant turbulence level over the combustion process, smaller-scale turbulence leads to dramatically faster burning. In real combustion, however, smaller-scale turbulence also means faster decaying turbulence. The simulations portray that the more efficient, small-scale turbulence effects are hindered by its faster decay rate in real combustion. For the same eddy-size turbulence, an increase in turbulence intensity increases the combustion rate. Numerical simulations demonstrate that the increase in combustion rate is more substantial when the turbulence level is maintained throughout the combustion process. In other words, the faster turbulence decay at higher turbulence intensities results in a lesser increase in overall combustion rate per unit increase in turbulence intensity in real combustion processes.

7.2: RECOMMENDATIONS

The current study has lead to many important qualitative conclusions. The quantitative results might be improved significantly with an improved experimental set-up. Wider ranges of experimental parameters could be used to provide better understanding of turbulent flame propagation.

7.2.1: IMPROVEMENTS IN THE EXPERIMENTAL APPARATUS AND ANALYSIS

Similar combustion chambers of different sizes can be used. The use of larger combustion chambers may resolve the turbulent flame development phase. In other words, larger combustion chambers can allow much larger flame size to turbulent length scale ratios. As methane-air flames do not detonate, the developing methane-air flames are expected to become fully developed eventually. Larger chambers also permit a longer pre-pressure combustion period. Use of schlieren imaging or flame tomography in these larger chambers can resolve the problem of high noise-to-signal ratio in the pressure trace analysis.

A better estimate of the unburnt mixture turbulence is needed to improve the current quantitative results, especially the values for the linear coefficient. The best available technique for measuring the flame front turbulence is probably particle image velocimetry as used by Reuss et al [RA89, RAa89, RB90]. However, a more cost-effective method would be laser Doppler velocimetry as used in many turbulent combustion studies such as [TG90, VS90]. Whenever possible, the Taylor microscale and the Kolmogorov scale should also be estimated.

The current circular windows can be replaced with square windows that expose the whole cavity of the chamber. This will allow schlieren flame growth analysis up to a much larger flame size. This will permit a larger combustion period in which both flame visualization and pressure trace analysis are both reasonably accurate. Flame tomography can be measured using the technique as described in [KW92]. The use of flame tomography can minimize the third dimensional interference encountered in the present schlieren images. Hence, a better two-dimensional flame cross-sectional area can be estimated. Laser interferometry as described in [HS89] may be used in conjunction to the present pressure transducer. This laser interferometry can measure the very early combustion chamber pressure rise, which is too low and too noisy for the strain gauge pressure transducer. The two-dimensional flame perimeter can also be better estimated using flame tomography. Another pair of windows, mounted on the top and bottom sides of the chamber, can be used along with the front and back windows in order to better estimate the three-dimensional flame shape.

Open-atmosphere, spark-ignited turbulent flames, such as those in [PS69], can be used to further justify the progressive turbulent flame growth results. As these flames propagate in an open atmosphere, there is no pressure rise. Therefore, the pressure and temperature effects encountered in the closed chamber combustion are not present.

7.2.2: WIDER RANGES OF EXPERIMENTAL PARAMETERS

Lean to rich methane-air and propane-air mixtures can be used to study the effects of Lewis number and Markstein number on the turbulent burning velocity. Rich methane-air and lean propane-air flames have larger than unity Lewis numbers and positive Markstein numbers. On the other hand, very lean methane-air and rich propane-air flames have less than unity Lewis numbers and negative Markstein numbers. The burning behaviour of these non-unity Lewis number and non-zero Markstein number flames may resolve the discrepancy of the effects of change in equivalence ratio from 0.7 to 0.9.

The pressure [Fi58] and temperature effects on a turbulent flame can be investigated. These pressure and temperature effects on a turbulent flame can be quite different from those on a laminar flame. Phenomena of turbulent flame growth at higher pressures and temperatures are most important in engine-like combustion.

REFERENCES

AA84 R.G. Abdel-Gayed, K.J. Al-Khishali and D. Bradley, "Turbulent burning velocities and flame straining in explosions", Proc. R. Soc. Lond., A 391: 393-414, 1984.

AB75 G.E. Andrews, D. Bradley and S.B. Lwakabamba, "Turbulence and Turbulent Flame Propagation - A Critical Appraisal", Combustion and Flame 24: 285-304, 1975.

AB81 R.G. Abdel-Gayed and D. Bradley, "A Two-Eddy Theory of Premixed Turbulent Flame Propagation", Phil. Trans. R. Soc. Lond., A 301: 1-25, 1981.

AB83 W.T. Ashurst and P.K. Barr, "Stochastic Calculation of Laminar Wrinkled Flame Propagation via Vortex Dynamics", Combust. Sci. and Tech., Vol. 34, 227-256, 1983.

AB83a K.J. Al-Khishali, P.M. Boston, D. Bradley, M. Lawes and M.J. Pegg, "The influence of fluctuations in turbulence upon fluctuations in turbulent burning velocity", International Conference on Combustion in Engineering, Volume I, I Mech E Conference Publications 1983-3, C49/83, 175-180, 1983.

AB84 R.G. Abdel-Gayed, D. Bradley, M.N. Hamid and M. Lawes, "Lewis Number Effects on Turbulent Burning Velocity", Twentieth Symposium (International) on Combustion, 505-512, 1984.

AB85 J. Abraham, F.V. Bracco and R.D. Reitz, "Comparisons of Computed and Measured Premixed Charge Engine Combustion", Combustion and Flame 60: 309-322, 1985.

AB86 R.G. Abdel-Gayed, D. Bradley, M. Lawes and F.K-K. Lung, "Premixed Turbulent Burning During Explosions", Twenty-First Symposium (International) on Combustion, 497-504, 1986.

AB87 R.G. Abdel-Gayed, D. Bradley and M. Lawes, "Turbulent burning velocities: a general correlation in terms of straining rates", Proc. R. Soc. Lond., A 414: 389-413, 1987.

AB88 R.G. Abdel-Gayed, D. Bradley and A.K.C. Lau, "The Straining of Premixed Turbulent Flames", Twenty-Second Symposium (International) on Combustion, 731-738, 1988.

AB89 R.G. Abdel-Gayed and D. Bradley, "Combustion Regimes and the Straining of Turbulent Premixed Flames", Combustion and Flame 76: 213-218, 1989.

AC93 W.T. Ashurst, M.D. Checkel and D.S-K. Ting, "The Eddy Structure Model of Turbulent Flamelet Propagation, the Expanding Spherical and Steady Planar Cases", presented at the Fall Technical Meeting, The Combustion Institute, Western States Section and Eastern States Section, USA, October 1993.

AC94 W.T. Ashurst, M.D. Checkel and D.S-K. Ting, "The Eddy Structure Model of Turbulent Flamelet Propagation, the Expanding Spherical and

Steady Planar Cases", Combust. Sci. and Tech., Vol. 99, 51-74, 1994.

AE91 C. Arcoumanis, A.C. Enotiadis and J.H. Whitelaw, "Frequency analysis of tumble and swirl in motored engines", Proc. Instn. Mech. Engrs., Part D, Vol. 205, 177-184, 1991.

AG61 J.T. Agnew and L.B. Graiff, "The Pressure Dependence of Laminar Burning Velocity by the Spherical Bomb Method", Combustion and Flame 5: 209-219, 1961.

AH92 S. Au, R. Haley and P.R. Smy, "The Influence of the Igniter-Induced Bast Wave Upon the Initial Volume and Expansion of the Flame Kernel", Combustion and Flame 88: 50-60, 1992.

Al92 R.C. Aldredge, "The Propagation of Wrinkled Premixed Flames in Spatially Periodic Shear Flow", Combustion and Flame 90: 121-133, 1992.

AM89 W.T. Ashurst and P.A. Mcmurtry, "Flame Generation of Vorticity: Vortex Dipoles from Monopoles", Combust. Sci. and Tech., Vol. 66, 17-37, 1989.

As78 W.T. Ashurst, "Vortex Dynamic Calculation of Fluid Motion in a Four Stroke Piston "Cylinder" - Planar and Axisymmetric Geometry", SAND78-8229, 1978.

As87 W.T. Ashurst, "Vortex Simulation of Unsteady Wrinkled Laminar Flames", Combust. Sci. and Tech., Vol. 52, 325-351, 1987.

As93 W.T. Ashurst, "Flame Propagation Through Swirling Eddies, A Recursive Pattern", Combust. Sci. and Tech., Vol. 92, 87-103, 1993.

As94 W.T. Ashurst, "Constant-Density Markstein Flamelet in Navier-Stokes Turbulence", Combust. Sci. and Tech., in press, 1994.

As94a W.T. Ashurst, "Modelling Turbulent Flame Propagation", Topical Review, Twenty-Fifth Symposium (International) on Combustion, 1994.

As95 W.T. Ashurst, "A Simple Illustration of Turbulent Flame Ball Growth", Comb. Sci. and Tech., in press, 1995.

AW85 J. Abraham, F.A. Williams and F.V. Bracco, "A Discussion of Turbulent Flame Structure in Premixed Charges", SAE paper 850345, 1985.

Ba52 G.K. Batchelor, "The effect of homogeneous turbulence on material lines and surfaces", R. Soc. Lond., A 213: 349-366, 1952.

Ba79 D.R. Ballal, "The structure of a premixed turbulent flames", Proc. R. Soc. Lond., A 367: 353-380, 1979.

Ba79a D.R. Ballal, "The influence of laminar burning velocity on the structure and propagation of turbulent flames", Proc. R. Soc. Lond., A 367: 485-502, 1979.

Ba79b D.R. Ballal, "Further development of the three-region model of a premixed turbulent flame: III. Eddy entrainment, combustion in depth process of region 3", Proc. R. Soc. Lond., A 368: 294-304, 1979.

Ba89 T.A. Baritaud, "Combustion and Fluid Dynamic Measurements in a Spark Ignition Engine: Effects of Thermochemistry and Velocity Field; Turbulent Flame Speeds", SAE paper 892098, 1989.

BB84 P.M. Boston, D. Bradley, F.K-K. Lung, I.M. Vince and F.J. Weinberg, "Flame Initiation in Lean, Quiescent and Turbulent Mixtures with various Igniters", Twentieth Symposium (International) on Combustion, 141-149, 1984.

BC91 K.N.C. Bray and R.S. Cant, "Some applications of Kolmogorov's turbulence research in the field of combustion", Proc. R. Soc. Lond., A 434: 217-240, 1991.

BC91a Y. Bianco, W.K. Cheng and J.B. Heywood, "The Effects of Initial Flame Kernel Conditions on Flame Development in SI Engine", SAE paper 912402, 1991.

BC94 B. Bedat and R.K. Cheng, "Experimental Study of Premixed Flames in Intense Isotropic Turbulence", Twenty-Fifth Symposium (International) on Combustion, 1994.

BD88 A. Borghese, A. D'Alessio, M. Diana and C. Venitozzi, "Development of Hot Nitrogen Kernel, produced by a very fast Spark Discharge", Twenty-Second Symposium (International) on Combustion, 1651-1659, 1988.

BD91 A. Borghese, M. Diana, V. Moccia and R. Tamai, "Early Growth of Flames, Ignited by Fast Sparks", Combust. Sci. and Tech., Vol. 76, 219-231, 1991.

Be77 R.S. Benson, Advanced Engineering Thermodynamics, Pergamon Press Ltd., 2nd Ed., 1977.

BG86 T.A. Baritaud and R.M. Green, "A 2-D Flame Visualisation Technique Applied to the I.C. Engine", SAE paper 860025, 1986.

BG94 D. Bradley, P.H. Gaskell and X.J. Gu, "Application of a Reynolds Stress, Stretched Flamelet, Mathematical Model to Computations of Turbulent Burning Velocities and Comparison with Experiments", Combustion and Flame 96: 221-248, 1994.

BH71 D. Bradley and G.F. Hundy, Thirteenth Symposium (International) on Combustion, 575-, 1971.

BH94 M.R. Belmont, J. Hacohen and P.W. Carpenter, "Tumble and swirl: are they a mixed blessing?", Proc. Instn. Mech. Engrs., Part D, Vol. 208, 223-226, 1994.

BK66 V.S. Babkin and L.S. Kozachenko, "Study of normal burning velocity in methane/air mixtures at high pressures", Combustion, Explosion and Shock Waves, Vol. 2, 46-52, 1966.

BK94 U. Bielert, M. Klug and G. Adomeit, "Numerical Simulation of the Turbulent Combustion Process in a Rapid Compression Device", SAE paper 940211, 1994.

BL75 D.R. Ballal and A.H. Lefebvre, "The structure and propagation of turbulent flames", Proc. R. Soc. Lond., A 344: 217-234, 1975.

BL92 D. Bradley, A.K.C. Lau and M. Lawes, "Flame stretch rate as a determinant of turbulent burning velocity", Phil. Trans. R. Lond., A 338: 359-387, 1992.

BL93 S.R. Bell, G.A. Loper and M. Gupta, "Combustion Characteristics of Natural Gas Fuelled Spark Ignited Engine", ASME paper 93-ICE-17, 1993.

Br90 K.N.C. Bray, "Studies of the turbulent burning velocity", Proc. R. Soc. Lond., A 431: 315-335, 1990.

Br92 D. Bradley, "How Fast Can We Burn?", Twenty-Fourth Symposium (International) on Combustion, 247-262, 1992.

BS94 K. Boulouchos, T. Steiner and P. Dimopoulos, "Investigation of Flame Speed Models for the Flame Growth Period During Premixed Engine Combustion", SAE paper 940476, 1994.

BT37 C.L. Bouchard, C.F. Taylor and E.S. Taylor, "Variables Affecting Flame Speed in the Otto-Cycle Engine", SAE Journal, Vol. 41, No. 5, 514-520, 1937.

CB88 R.S. Cant and K.N.C. Bray, "Strained Laminar Flamelet Calculations of Premixed Turbulent Combustion in a Closed Vessel", Twenty-Second Symposium (International) on Combustion, 791-799, 1988.

CB89 R.S. Cant and K.N.C. Bray, "A Theoretical Model of Premixed Turbulent Combustion in Closed Vessel", Combustion and Flame 76: 243-263, 1989.

CB92 T.C. Chew and R.E. Britter, "Effect of Flame-Induced Geometrical Straining on Turbulence Levels in Explosions and Common Burner Configurations", Int. J. Engng. Sci., Vol. 30, No. 8, 983-1002, 1992.

CB94 R.S. Cant, K.N.C. Bray, L.W. Kostiuk and B. Rogg, "Flow Divergence Effects in Strained Laminar Flamelets for Premixed Turbulent Combustion", Combust. Sci. and Tech., in press, 1994.

CC49 J.M. Campbell, D.F. Caris and L.L. Withrow, "Increasing the Thermal Efficiencies of Internal-Combustion Engines", SAE Transactions, Vol. 3, No. 2, 341-380, April 1949.

CD91 W.K. Cheng and J.A. Diringer, "Numerical Modelling of SI Engine Combustion with a Flame Sheet Model", SAE paper 910268, 1991.

Ch81 M.D. Checkel, Turbulence Enhanced Combustion of Lean Mixtures, Ph.D. Thesis, Cambridge University, 1981.

Ch86 M.D. Checkel, "Measurements of Turbulence Generated by 60% Solid Perforated Plates", ASME paper 85-WA/FE-2, 1986.

Ch94 M.D. Checkel, private communication, 1994.

CK92 M.E. Crane and S.R. King, "Emission Reductions Through Pre-combustion Chamber Design in a Natural Gas, Lean Burn Engine", Journal of Engineering for Gas Turbines and Power, Transactions of the ASME, Vol. 114, 466-474, July 1992.

Cl13 D. Clerk, "The Working Fluid of Internal-Combustion Engines", Engineering, 28-63, July 4, 1913.

Cl21 D. Clerk, "Cylinder Actions in Gas and Gasoline Engines", SAE Journal, Vol. 8, No. 6, 523-539, June 1921.

CL28 J.M. Campbell, W.G. Lovell and T.A. Boyd, "Importance of Mixture

Ratio in Rating Fuels for Knock", Industrial and Engineering Chemistry, Vol. 20, No. 10, 1045-1048, October 1928.

Cl85 P. Clavin, "Dynamic Behaviour of Premixed Flame Fronts in Laminar and Turbulent Flows", Prog. Energy Combust. Sci., Vol. 11, 1-, 1985.

Cl94 P. Clavin, "Premixed Combustion and Gas-dynamics", Ann. Rev. Fluid Mech., 26: 321-352, 1994.

CM56 D.F. Caris, B.J. Mitchell, A.D. McDuffie and F.A. Wyczalek, "Mechanical Octanes for Higher Efficiency", SAE Transactions, Vol. 64, 76-100, 1956.

CN59 D.F. Caris and E.E. Nelson, "a new look at High Compression Engines", SAE Transactions, Vol. 67, 112-124, 1959.

CS88 E.L. Chau, F.W. Schipperijn, R. Nagasaka, R.F. Sawyer and A. Liyama, "Effect of Intake Valve Configuration on Lean Combustion", SAE paper 88020, 1988.

CS92 Y.S Cho, D.A. Santavicca and R.M. Sonntag, "The Effect of Spark Power on Spark-Ignited Flame Kernel Growth", SAE paper 922168, 1992.

CT83 M.D. Checkel and A. Thomas, "Turbulent explosions in closed vessels", International Conference on Combustion in Engineering, Volume I, I Mech E Conference Publications 1983-3, C57/83, 181-189, 1983.

CT92 M.D. Checkel and D.S-K. Ting, "Measuring Turbulent Flame Growth by Visualization", SAE paper 920184, 1992.

CT92a M.D. Checkel and D.S-K. Ting, "Turbulence Effects on Developing Flames", presented at 1992 Spring Technical Meeting, The Combustion Institute, Canadian Section, May 1992.

CT93 M.D. Checkel and D.S-K. Ting, "Turbulence Effects on Developing Turbulent Flames in a Constant Volume Combustion Chamber", SAE paper 930867, 1993.

CT94 M.D. Checkel and A. Thomas, "Turbulent Combustion of Premixed Flames in Closed Vessels", Combustion and Flame 96: 351-370, 1994.

CV91 C. Chen and A. Veshagh, "A Premixed Turbulent Flame Velocity Model Based on Dimensional Reasoning", SAE paper 910077, 1991.

CV92 C. Chen and A. Veshagh, "A Refinement of Flame Propagation Combustion Model for Spark-Ignited Engines", SAE paper 920679, 1992.

Da40 G. Damkohler, "The Effect of Turbulence on the Flame Velocity in Gas Mixtures", National Advisory Committee for Aeronautics, NACA, Technical Memorandum, No. 1112, April 1947; translated from "Der Einfluss der Turbulenz auf die Flammengeschwindigkeit in Gasgemischen", Zeitschrift fur Elektrochemie und angewandte Physikalische Chemie, Vol. 46, No. 11, 601-626, 1940.

De65 G. De Soete, "A Survey of the Effects of Turbulence on Engine Combustion", Cranfield International Symposium Series, Vol. 8, Advances in Automobile Engineering, Part IV, Combustion Processes in the Spark Ignition Engine, Proceedings of a Symposium held at the Advanced School of Automobile Engineering, Edited by D. Hodgetts, 35-

58, July 1965.

DE94 A.K. Das and R.L. Evans, "A Fractal Analysis of Lean Premixed Turbulent Flames", presented as work-in-progress poster at the Twenty-Fifth Symposium (International) on Combustion, 1994.

DM83 H. Daneshyar, J.M.C. Mendes-Lopes, G.S.S. Ludford and P.S. Tromans, "The influence of straining on a premixed flame and its relevance to combustion in SI engines", International Conference on Combustion in Engineering, Volume I, I Mech E Conference Publications 1983-3, C50/83, 191-199, 1983.

DN90 S. Dhandapani, B. Nagalingam and K.V. Gopalakrishnan, "Effect of Swirl Due to Squish Height on the Performance of Lean Burn SI Engine", Journal of The Institution of Engineers (India), Vol. 70, Part MC 6, 108-110, March 1990.

DO81 J.D. Dale and A.K. Oppenheim, "Enhanced Ignition for I.C. Engines with Premixed Gases", SAE paper 810146, 1981.

Do90 E.O. Doebelin, MEASUREMENT SYSTEMS APPLICATION AND DESIGN, McGraw-Hill Publishing Company, 4th Ed., 1990.

DS94 J.F. Driscoll, D.J. Sutkus, W.L. Roberts, M.E. Post and L.P. Goss, "The Strain Exerted by a Vortex on a Flame-Determined from Velocity Field Images", Combust. Sci. and Tech., Vol. 96, 213-229, 1994.

DV93 J.M. Duclos, D. Veynante and T. Poinsot, "A Comparison of Flamelet Models for Premixed Turbulent Combustion", Combustion and Flame 95: 101-117, 1993.

Dy79 T.M. Dyer, "Characterization of One- and Two-Dimensional Homogeneous Combustion Phenomena in a Constant Volume Bomb", SAE paper 790353, 1979.

EC89 F.N. Egolfopoulos, P. Cho and C.K. Law, "Laminar Flame Speeds of Methane-Air Mixtures Under Reduced and Elevated Pressures", Combustion and Flame 76: 375-391, 1989.

EN92 H. Endres, H-J. Neuber and R. Wurms, "Influence of Swirl and Tumble on Economy and Emissions of Multi Valve SI Engines", SAE paper 920516, 1992.

ET90 R.L. Evans and E.C. Tippett, "The Effects of Squish Motion on the Burn-Rate and Performance of a Spark-Ignition Engine", SAE paper 901533, 1990.

Ev92 R.L. Evans, "Combustion Chamber Design for a Lean-Burn SI Engine", SAE paper 921545, 1992.

Fi58 B. Fine, "Effect of Pressure on Turbulent Burning Velocity", Combustion and Flame 2: 109-116, 1958.

FL93 F. Fichot, F. Lacas, D. Veynante and S. Candel, "One-Dimensional Propagation of a Premixed Turbulent Flame With a Balance Equation for the Flame Surface Density", Combust. Sci. and Tech., Vol. 90, 35-60, 1993.

FO85 R.D. Fleming and G.B. O'Neal, "Potential for Improving the Efficiency of a Spark Ignition Engine for Natural Gas Fuel", SAE paper 852073, 1985.

Fr65 R.M. Fristrom, "Definition of Burning Velocity and a Geometric Interpretation of the Effects of Flame Curvature", The Physics of Fluids, Vol. 8, No. 2, 273-280, 1965.

GE93 Z. Gete and R.L. Evans, "An Experimental Investigation of Jet-Enhanced Turbulent Combustion", Combust. Sci. and Tech., Vol. 92, 349-365, 1993.

GH84 J.A. Gatowski, J.B. Heywood and C. Deleplace, "Flame Photographs in a Spark-Ignition Engine", Combustion and Flame 56: 71-81, 1984.

GH88 F.C. Gouldin, S.M. Hilton and T. Lamb, "Experimental Evaluation of the Fractal Geometry of Flamelets", Twenty-Second Symposium (International) on Combustion, 541-550, 1988.

Gi20 H.C. Gibson, "Bettering the Efficiency of Existing Engines", SAE Journal, Vol. 6, No. 1, 7-13, 1920.

Gi56 M. Gilbert, "The Influence of Pressure On Flame Speed", Sixth Symposium (International) on Combustion, 74-83, 1956.

Gl87 I. Glassman, COMBUSTION, ACADEMIC PRESS, INC., 2nd edition, 1987.

GM80 E.G. Groff and F.A. Matekunas, "The Nature of Turbulent Flame Propagation in a Homogeneous Spark-Ignited Engine", SAE paper 800133, 1980.

GM92 J. Gottgens, F. Mauss and N. Peters, "Analytic Approximations of Burning Velocities and Flame Thicknesses of Lean Hydrogen, Methane, Ethylene, Ethane, Acetylene, and Propane Flames", Twenty-Fourth Symposium (International) on Combustion, 129-135, 1992.

Go87 F.C. Gouldin, "An Application of Fractals to Modelling Premixed Turbulent Flames", Combustion and Flame 68: 249-266, 1987.

GT83 L.E. Gettel and K.C. Tsai, "The Effect of Enhanced Ignition on the Burning Characteristics of Methane-Air Mixtures", Combustion and Flame 54: 183-193, 1983.

Gu90 O.L. Gulder, "Turbulent Premixed Flame Propagation Models for Different Combustion Regimes", Twenty-Third Symposium (International) on Combustion, 743-750, 1990.

Ha86 R.F. Haley, A SCHLIEREN STUDY OF FLAME INITIATION, MSc Thesis, Department of Electrical Engineering, University of Alberta, 1986.

HB88 R. Herweg, Ph. Begleris, A. Zettlitz and G.F.W. Ziegler, "Flow Field Effects on Flame Kernel Formation in a Spark-Ignition Engine", SAE paper 881639, 1988.

HD91 O. Hadded and I. Denbratt, "Turbulence Characteristics of Tumbling Air Motion in Four-Valve S.I. Engines and their Correlation with Combustion Parameters", SAE paper 910478, 1991.

HD92 M.J. Hall, W. Dai and R.D. Matthews, "Fractal Analysis of Turbulent

Premixed Flame Images from SI Engines", SAE paper 922242, 1992.

He88 J.B. Heywood, Internal Combustion Engine Fundamentals, McGraw-Hill, Inc., 1988.

HF50 S.D. Heron and A.E. Felt, "Cylinder Performance-Compression Ratio and Mechanical Octane-Number Effects", SAE Transaction, Vol. 4, No. 4, 455-, 1950.

Hi88 P.G. Hill, "Cyclic Variations and Turbulence Structure in Spark-Ignition Engines", Combustion and Flame 72: 73-89, 1988.

HI89 Y. Hamamoto, M. Izumi and E. Tomita, "Turbulent Premixed Flames in a Closed Vessel Studied Through Analysis of Flame Photographs", JSME International Journal, Series II, Vol. 32, No. 3, 443-448, 1989.

HI90 Y. Hamamoto, M. Izumi and E. Tomita, "Effects of Swirl and Air-Fuel Ratio on Premixed Combustion in a Closed Vessel", JSME International Journal, Series II, Vol. 33, No. 2, 370-376, 1990.

HI91 Y. Hamamoto, M. Izumi, E. Tomita and O. Miyamoto, "Direct Measurement of Burning Velocity of Flame Propagating in Fuel-Air Homogeneous Mixtures in a Closed Vessel", JSME International Journal, Series II, Vol. 34, No. 2, 253-257, 1991.

HK89 P.G. Hill and A. Kapil, "The Relationship Between Cyclic Variations in Spark-Ignition Engines and the Small Structure of Turbulence", Combustion and Flame 78: 237-247, 1989.

HK91 S. Huang and H. Kido, "Experimental Study of the Structure of Premixed Turbulent Flames Using the Schlieren Photography and a Micro-Probe Method", Memoirs of the Faculty of Engineering, Kyushu University, Vol. 51, No. 4, 243-266, 1991.

HK92 J.O. Han and S.S. Kim, "Effects of swirl on high-speed combustion in a single-shot optical SI engine", Proc. Instn. Mech. Engrs., Part D, Vol. 206, 237-247, 1992.

HM92 R. Herweg, R.R. Maly, "A Fundamental Model for Flame Kernel Formation in S.I. Engines", SAE paper 922243, 1992.

HN92 K. Horie, K. Nishizawa, T. Ogawa, S. Akazaki and K. Miura, "The Development of a High Fuel Economy and High Performance Four-Valve Lean Burn Engine", SAE paper 920455, 1992.

Ho21 H.L. Horning, "Turbulence", SAE Journal, Vol. 8, No. 6, 579-587, June 1921.

HO84 Y. Hamamoto, H. Ohkawa, H. Yamamoto and R. Sugahara, "Effects of Turbulence on Combustion of Homogeneous Mixture of Fuel and Air in Closed Vessel", Bulletin of JSME, Vol. 27, No. 226, April 1984.

HS87 C.M. Ho and D.A. Santavicca, "Turbulence Effects on Early Flame Kernel Growth", SAE paper 872100, 1987.

HS88 R.F. Haley and P.R. Smy, "Electrically induced turbulence - the short duration spark", J. Phys. D: Appl. Phys. 22, 258-265, 1989.

HS89 R. Haley and P.R. Smy, "Combustion Chamber Pressure Measurement at Very Early Times: Comparison of Plasma Jet Ignition with

Conventional Ignition", Combust. Sci. and Tech., Vol. 63, 1989.

HT88 Y. Hamamoto, E. Tomita and M. Izumi, "The Effect of Swirl on the Combustion of a Homogeneous Mixture in a Closed Vessel", JSME International Journal, Series II, Vol. 31, No. 1, 78-86, 1988.

HT94 Y. Hamamoto, E. Tomita and D. Jiang, "Temperature measurement of end gas under knocking condition in a spark-ignition engine by laser interferometry", JSAE Review 15, 117-122, 1994.

HW82 Y. Hamamoto, T. Wakisaka and M. Ohnishi, "Cycle-to-Cycle Fluctuation of Lean Mixture Combustion in Spark-Ignition Engines", Bulletin of the JSME, Vol. 25, No. 199, Paper No. 199-9, 61-67, January 1982.

IL84 T.F. Irvine and P.E. Liley, Steam and Gas Tables with Computer Equations, Academic Press, Inc., 1984.

Je92 M.J. Jennings, "Multi-Dimensional Modelling of Turbulent Premixed Charge Combustion", SAE paper 920589, 1992.

Ji94 M. Jiang, HEAT FLUX MEASUREMENTS IN A CUBICAL COMBUSTION CELL, MSc Thesis, Department of Mechanical Engineering, University of Alberta, 1994.

Jo93 B. Johansson, "Influence of the Velocity Near the Spark Plug on Early Flame Development", SAE paper 930481, 1993.

Jo94 B. Johansson, "The Influence of Different Frequencies in the Turbulence on Early Flame Development in a Spark Ignition Engine", SAE paper 940990, 1994.

JW93 J. Jimenez, A.A. Wray, P.G. Saffman and R.S. Rogallo, "The structure of intense vorticity in isotropic turbulence", J. Fluid Mech., Vol. 255, 65-90, 1993.

Ka52 B. Karlovitz, "Open Turbulent Flames", Fourth Symposium (International) on Combustion, 60-67, 1952.

Ka83 G.A. Karim, "Some Considerations of the Safety of Methane, (CNG), as an Automotive Fuel - Comparison with Gasoline, Propane and Hydrogen Operation", SAE paper 830267, 1983.

Ka85 G.T. Kalghatgi, "Early Flame Development in a Spark-Ignition Engine", Combustion and Flame 60: 299-308, 1985.

Ke20 C.F. Kettering, "Combustion of Fuels in Internal-Combustion Engines", SAE Journal, Vol. 7, No. 3, 224-227, 1920.

Ke47 C.F. Kettering, "More Efficient Utilization of Fuels", SAE transactions, Vol. 1, No. 4, 669-679, 1947.

KF92 S. Kwon and G.M. Faeth, "Stochastic Simulation of Free Turbulent Premixed Flames in Isotropic Turbulence", Twenty-Fourth Symposium (International) on Combustion, 451-460, 1992.

KH87 J.C. Keck, J.B. Heywood and G. Noske, "Early Flame Development and Burning Rates in Spark Ignition Engines and Their Cyclic Variability", SAE paper 870164, 1987.

KH91 H. Kido, S. Huang and K. Nakashima, "A Premixed Turbulent Flame Structure Model Having Reactant Islands and Fractal Flame Surfaces:

Formulation and Test of the Model", JSME International Journal, Series II, Vol. 34, No. 4, 509-519, 1991.

KH93 H. Kido and S. Huang, "Comparison of Premixed Turbulent Burning Velocity Models Taking Account of Turbulence and Flame Spatial Scales", SAE paper 930218, 1993.

KH94 H. Kido and S. Huang, "A Discussion of Premixed Turbulent Burning Velocity Models Based on Burning Velocity Diagrams", Combust. Sci. and Tech., Vol. 96, 409-418, 1994.

Ki88 I. Kimura, "Promotion of Combustion by Electric Discharges: The Role of Vibrationally Excited Species", JSME Series II, Vol. 31, No. 3, 376-386, 1988.

KK91 H. Kobayashi and M. Kitano, "Flow Fields and Extinction of Stretched Cylindrical Premixed Flames", Combust. Sci. and Tech., Vol. 75, 227-239, 1991.

KK92 H. Kido, T. Kitagawa, K. Nakashima and J-H. Kim, "Refinement of the Spectral Model of Turbulent Burning Velocity", JSME International Journal, Series II, Vol. 35, No. 3, 421-427, 1992.

KK93 S.S. Kim and S.S. Kim, "Effects of Swirl on Early Flame Development and Late Combustion Characteristic in a High-Speed Single-Shot Visualized SI Engine", JSME International Journal, Series B, Vol. 36, No. 4, 711-722, 1993.

KN92 H. Kido, K. Nakashima, J-H. Kim and M. Kataoka, "Observation of the premixed turbulent propagating flame by laser tomography", Proceedings of the 2nd JSME-KSME thermal engineering conference, 1, 231-236, October 19-21, 1992.

Ko94 L.W. Kostiuk, "Burning Rate of Premixed Laminar Flames", presented at the 1994 Spring Technical Meeting, The Combustion Institute, Canadian Section, paper 55, March 1994.

KW83 H. Kido, Y. Wakuri and K. Nakashima, "Experiments and a correlation of turbulent burning velocities", Proceedings of ASME-JSME Thermal Engrg. Joint Conference, Vol. 4, 183-190, 1983.

KW92 S. Kwon, M-S. Wu, J.F. Driscoll and G.M. Faeth, "Flame Surface Properties of Premixed Flames in Isotropic Turbulence: Measurements and Numerical Simulations", Combustion and Flame 88: 221-238, 1992.

La17 A. Lavoisier, "Great discoveries in science. 3. Combustion: Antoine Lavoisier (1743-1794) [filmstrip]". Detroit: Produced by the Jam Handy Organization, c 1967.

LA87 M.T. Lim, R.W. Anderson and V.S. Arpaci, "Prediction of Spark Kernel Development in Constant Volume Combustion", Combustion and Flame 69: 303-316, 1987.

La88 C.K. Law, "Dynamics of Stretched Flames", Twenty-Second Symposium (International) on Combustion, 1381-1402, 1988.

LA93 D.L. Lord, R.W. Anderson, D.D. Brehob and Y. Kim, "The Effects of Charge Motion on Early Flame Kernel Development", SAE paper 930463, 1993.

LB82 G.G. Lucas and M.F.J. Brunt, "The Effect of Combustion Chamber Shape on the Rate of Combustion in a Spark Ignition Engine", SAE paper 820165, 1982.

Le92 J.F. Le Coz, "Cycle-to-Cycle Correlations Between Flow Field and Combustion Initiation in an S.I. Engine", SAE paper 920517, 1992.

Li75 C.D. Lind, "What Causes Unconfined Vapour Cloud Explosions?", Loss Prevention, Vol. 9, 101-105, 1975.

LK76 D.R. Lancaster, R.B. Krieger, S.C. Sorenson and W.L. Hull, "Effects of Turbulence on Spark-Ignition Engine Combustion", SAE paper 760160, 1976.

LL88 Y. Liu and B. Lenze, "The Influence of Turbulence on the Burning Velocity of Premixed CH_4-H_2 Flames with Different Laminar Burning Velocities", Twenty-Second Symposium (International) on Combustion, 747-754, 1988.

LL93 T-W Lee, J.G. Lee, D. A. Nye and D.A. Santavicca, "Local Response and Surface Properties of Premixed Flames During Interactions with Karman Vortex Streets", Combustion and Flame 94: 146-160, 1993.

LN90 W. Leuckel, W. Nastroll and N. Zarzalis, "Experimental Investigation of the Influence of Turbulence on the Transient Premixed Flame Propagation inside Closed Vessels", Twenty-Third Symposium (International) on Combustion, 729-734, 1990.

LS93 T.W. Lee and D.A. Santavicca, "Flame Front Geometry and Stretch During Interactions of Premixed Flames with Vortices", Combust. Sci. and Tech., Vol. 90, 211-229, 1993.

LV67 B. Lewis and G. Von Elbe, COMBUSTION, FLAMES and EXPLOSIONS of GASES, Academic Press Inc., 3rd Ed., 1967.

LW77 C.D. Lind and J.C. Whitson, "Explosion hazards associated with spills of large quantities of hazardous materials, Phase II", Department of Transportation, United States Coast Guard, Report No. CG-D-85-77, Final report ADA-047585, November 1977.

Ma34 C.F. Marvin, "Observations of Flame in an Engine", SAE Journal, Vol. 35, No. 5, 391-462, November 1934.

Ma64 G. Markstein, NON-STEADY FLAME PROPAGATION, The MacMillan Company, Pergamon Press Ltd., 1964.

Ma75 J. Mayo, "The Effect of Engine Design Parameters on Combustion Rate in Spark-Ignited Engines", SAE paper 750335, 1975.

Ma75a B.B. Mandelbrot, "On the geometry of homogeneous turbulence, with stress on the fractal dimension of the iso-surfaces of scalars", J. Fluid Mech., Vol. 72, Part 2, 401-416, 1975.

MB94 T. Mantel and R. Borghi, "A New Model of Premixed Wrinkled Flame Propagation Based on a Scalar Dissipation Equation", Combustion and Flame 96: 443-457, 1994.

Mc88 B.J. McDonell, Burning Rates of Propane-Air Mixtures in Homogeneous

Decaying Turbulence, M.Sc. Thesis, Department of Mechanical Engineering, University of Alberta, 1988.

MC91 R.M. Modien, M.D. Checkel and J.D. Dale, "The Effect of Enhanced Ignition Systems on Early Flame Development in Quiescent and Turbulent Conditions", SAE paper 910564, 1991.

MF88 J. Mantzaras, P.G. Felton and F.V. Bracco, "Three-Dimensional Visualization of Premixed-Charge Engine Flames: Islands of Reactants and Products; Fractal Dimensions; and Homogeneity", SAE paper 881635 or SP-759, 1988.

MH20 D. MacKenzie and R.K. Honaman, "The Velocity of Flame Propagation in Engine Cylinders", SAE Journal, Vol. 6, No. 2, 119-122, 1920.

MI85 S. Matsushita, T. Inoue, K. Nakanishi, K. Kato and N. Kobayashi, "Development of the Toyota Lean Combustion System", SAE paper 850044, 1985.

MK80 M. Metghalchi and J.C. Keck, "Laminar Burning Velocity of Propane-Air Mixtures at High Temperature and Pressure", Combustion and Flame 38: 143-154, 1980.

ML83 E.MM. Mallard and H.L. Le Chatelier, "Recherches Experimentales et theoriques sur la combustion des melanges gazeux explosifs", Annales des Mines, 8, 3, 274-378, 1883.

Mo90 R.M. Modien, The Effects of Enhanced Ignition Systems and Turbulence on Flame Development, M.Sc. Thesis, Department of Mechanical Engineering, University of Alberta, 1990.

MP91 C. Meneveau and T. Poinsot, "Stretching and Quenching of Flamelets in Premixed Turbulent Combustion", Combustion and Flame 86: 311-332, 1991.

MT88 M. Murayama and T. Takeno, "Fractal-Like Character of Flamelets in Turbulent Premixed Combustion", Twenty-Second Symposium (International) on Combustion, 551-559, 1988.

NH80 M. Namazian, S. Hansen, E. Lyford-Pike, J. Sanchez-Barsse, J. Heywood and J.Rife, "Schlieren Visualization of the Flow and Density Fields in the Cylinder of a Spark-Ignition Engine", SAE paper 800044, 1980.

NS90 G.L. North and D.A. Santavicca, "The Fractal Nature of Premixed Turbulent Flames", Combust. Sci. and Tech., Vol. 72, 215-232, 1990.

NT83 A. Nagao and K. Tanaka, "The effect of swirl control on combustion improvement of spark ignition engine", International Conference on Combustion in Engineering, Volume I, I Mech E Conference Publications 1983-3, C54/83, 153-161, 1983.

Op93 A.K. Oppenheim, "Perspective - Aerodynamic Control of Combustion", Transactions of the ASME, Journal of Fluids Engineering, Vol. 115, 561-567, December 1993.

Pe92 N. Peters, "A spectral closure for premixed turbulent combustion in the flamelet regime", J. Fluid Mech., Vol. 242, 611-629, 1992.

PS69 A. Palm-Leis and R.A. Strehlow, "On the Propagation of Turbulent Flames", Combustion and Flame 13: 111-129, 1969.

RA89 D.L. Reuss, R.J. Adrain, C.C. Landreth, D.T. French and T.D. Fansler, "Instantaneous Planar Measurements of Velocity and Large-Scale Vorticity and Strain Rate in an Engine Using Particle-Image Velocimetry", SAE paper 890616, 1989.

RA89a D.L. Reuss, R.J. Adrain and C.C. Landreth, "Two-Dimensional Velocity Measurements in a Laminar Flame Using Particle Image Velocimetry", Combust. Sci. and Tech., Vol. 67, 73-83, 1989.

RB90 D.L. Reuss, M. Bardsley, P.G. Felton, C.C. Landreth and R.J. Adrian, "Velocity, Vorticity, and Strain-Rate Ahead of a Flame Measured in an Engine Using Particle Image Velocimetry", SAE paper 900053, 1990.

RC93 T.W. Ryan III, T.J. Callahan and S.R. King, "Engine Knock Rating of Natural Gases - Methane Number", Journal of Engineering for Gas Turbines and Power, Transactions of the ASME, Vol. 115, 769-776, October 1993.

RD91 W.L. Roberts and J.F. Driscoll, "A Laminar Vortex Interacting with a Premixed Flame: Measured Formation of Pockets of Reactants", Combustion and Flame 87: 245-256, 1991.

RD93 W.L. Roberts, J.F. Driscoll, M.C. Drake and L.P. Goss, "Images of the Quenching of a Flame by a Vortex - To Quantify Regimes of Turbulent Combustion", Combustion and Flame 94: 58-69, 1993.

Re87 W.C. Reynolds, "STANJAN, An Interactive Program for Equilibrium Analysis by the Method of Element Potentials", v.3.81, Mechanical Engineering Department, Stanford University, 1987.

RF90 C.J. Rutland and J.H. Ferziger, "Unsteady Strained Premixed Laminar Flames", Combust. Sci. and Tech., Vol. 73, 305-326, 1990.

RF90a C.J. Rutland, J.H. Ferziger and S.H. El Tahry, "Full Numerical Simulations and Modelling of Turbulent Premixed Flames", Twenty-Third Symposium (International) on Combustion, 621-627, 1990.

RF91 C.J. Rutland and J.H. Ferziger, "Simulations of Flame-Vortex Interactions", Combustion and Flame 84: 343-360, 1991.

RG80 C.J. Rallis and A.M. Garforth, "The Determination of Laminar Burning Velocity", Prog. Energy Combust. Sci., Vol. 6, 303-329, 1980.

RS94 P.D. Ronney, M. Shoda, S.T. Waida and E.J. Durbin, "Throttle-less premixed-charge engines: concept and experiment", Proc. Instn. Mech. Engrs., Part D, Vol. 208, 13-24, 1994.

RT93 C.J. Rutland and A. Trouve, "Direct Simulations of Premixed Turbulent Flames with Non-unity Lewis Numbers", Combustion and Flame 94: 41-57, 1993.

Sc34 K. Schnauffer, "Engine-Cylinder Flame-Propagation Studied by New Methods", SAE Journal, Vol. 34, No. 1, January 1934.

SC93 C.R. Stone, T.R. Carden and I. Podmore, "Analysis of the effect of inlet valve disablement on swirl, combustion and emissions in a spark ignition engine", Proc. Instn. Mech. Engrs., Part D, Vol. 207, 295-305, 1993.

SG52 A.C. Scurlock and J.H. Grover, "Propagation of Turbulent Flames", Fourth Symposium (International) on Combustion, 645-658, 1952.

Sh43 K.I. Schelkin, "On Combustion in a Turbulent Flow", NACA Technical Memorandum No. 1110, 1947; translated from Journal of Technical Physics (USSR) Vol. XIII, Nos 9-10, 1943.

SJ90 Z-S. She, E. Jackson and S.A. Orszag, "Intermittent vortex structures in homogeneous isotropic turbulence", NATURE, Vol. 344, 226-228, 1990.

SJ91 Z-S. She, E. Jackson and S.A. Orszag, "Structure and dynamics of homogeneous turbulence: models and simulations", Proc. R. Lond., A 434: 101-124, 1991.

SK94 I.G. Shepherd and L.W. Kostiuk, "The burning rate of premixed turbulent flames in divergent flows", Combustion and Flame 96: 371-380, 1994.

SL90 D.A. Santavicca, D. Liou and G.L. North, "A Fractal Model of Turbulent Flame Kernel Growth", SAE paper 900024, 1990.

Sm82 J.R. Smith, "Turbulent Flame Structure in a Homogeneous-Charge Engine", SAE paper 820043, 1982.

Sp21 S.W. Sparrow, "Compression Ratio and Thermal Efficiency of Airplane Engines", SAE Journal, Vol. 8, No. 3, 266-281, March 1921.

TC93 D.S-K. Ting and M.D. Checkel, "Modelling Turbulent Flame Growth in a Combustion Chamber", presented at 1993 Spring Technical Meeting, The Combustion Institute, Canadian Section, May 1993.

TC94 D.S-K. Ting, M.D. Checkel, R. Haley and P.R. Smy, "Early Flame Acceleration Measurements in a Turbulent Spark-Ignited Mixture", SAE paper 940687, 1994.

TC94a D.S-K. Ting and M.D. Checkel, "Modelling Turbulent Flame Propagation in a Chamber", presented at the 1994 Spring Technical Meeting, The Combustion Institute, Canadian Section, May 1994.

TC94b D.S-K. Ting and M.D. Checkel, "A Study of Progressive Turbulence Enhancement on Growing Flames", CSME Bulletin, May 1994.

TC94c D.S-K. Ting and M.D. Checkel, "Spark Ignited Flame Propagation in a Turbulent Flow Field", presented at the Eleventh Canadian Symposium on Fluid Dynamics, June 1994.

TC94d D.S-K. Ting, M.D. Checkel and W.T. Ashurst, "Turbulent Burning Velocity: Dependence upon flame size, flow length scale and velocity intensity", presented as work-in-progress poster at the Twenty-Fifth Symposium (International) on Combustion, July 1994.

TG90 S.E. Trautwein, A. Grudno and G. Adomeit, "The Influence of Turbulence Intensity and Laminar Flame Speed on Turbulent Flame Propagation under Engine Like Conditions", Twenty-Third Symposium (International) on Combustion, 723-728, 1990.

Th86 A. Thomas, "The Development of Wrinkled Turbulent Premixed Flames", Combustion and Flame 65: 291-312, 1986.

Ti92 D.S-K. Ting, Turbulent Flame Growth in a Combustion Chamber with

Homogeneous Decaying Turbulence, MSc Thesis, Department of Mechanical Engineering, University of Alberta, 1992.

TI93 L-K. Tseng, M.A. Ismail and G.M. Faeth, "Laminar Burning Velocities and Markstein Numbers of Hydrocarbon/Air Flames", Combustion and Flame 95: 410-426, 1993.

TK90 T. Takahashi, M. Katsuki and Y. Mizutani, "Observation of the Distributed Reaction Zone in Turbulent Premixed Flames", JSME International Journal, Series II, Vol. 33, No. 2, 349-354, 1990.

TL72 H. Tennekes and J.L. Lumley, A First Course in Turbulence, The MIT Press, 1972.

UB93 A. Unich, R.M. Bata and D.W. Lyons, "Natural Gas: A Promising Fuel for I.C. Engines", SAE paper 930929, 1993.

VH92 J.C. Vassilicos and J.C.R. Hunt, "Turbulent Flamelet Propagation", Combust. Sci. and Tech., Vol. 87, 291-327, 1992.

VM94 A. Vincent and M. Meneguzzi, "The dynamics of vorticity tubes in homogeneous turbulence", J. Fluid Mech., Vol. 258, 245-254, 1994.

VS78 G.J. Van Wylen and R.E. Sonntag, Foundamentals of Classical Thermodynamics, John Wiley and Sons, 2nd Ed., 1978.

VS90 B.D. Videto and D.A. Santavicca, "Flame-Turbulence Interactions in a Freely-Propagating Premixed Flame", Combust. Sci. and Tech., Vol. 70, 47-73, 1990.

WD92 M-S. Wu and J.F. Driscoll, "A Numerical Simulation of a Vortex Convected Through a Laminar Premixed Flame", Combustion and Flame 91: 310-322, 1992.

Wh19 R.V. Wheeler, "The Inflammation of Mixtures of Ethane and Air in a Closed Vessel: The Effects of Turbulence", Journal of The Chemical Society, Vol. 115, 81-94, 1919.

WH90 P.O. Witze, M.J. Hall and M.J. Bennett, "Cycle-Resolved Measurements of Flame Kernel Growth and Motion Correlated with Combustion Duration", SAE paper 900023, 1990.

Wi76 F.A. Williams, "Criteria for Existence of Wrinkled Laminar Flame Structure of Turbulent Premixed Flames", Combustion and Flame 26: 269-270, 1976.

Wi85 F.A. Williams, Combustion Theory, The Benjamin/Cummings Publishing Company, Inc., 2nd Ed., 1985.

Wi92 F.A. Williams, "The Role of Theory in Combustion Science", Twenty-Fourth Symposium (International) on Combustion, 1-17, 1992.

Wi93 F.A. Williams, "Advances in Modelling of Turbulent Combustion", Turbulence and Molecular Processes in Combustion, T. Takeno (Editor), 1-12, 1993.

WK91 M.S. Wu, S. Kwon, J.F. Driscoll and G.M. Faeth, "Preferential Diffusion Effects on the Surface Structure of Turbulent Premixed Hydrogen/Air Flames", Combust. Sci. and Tech., Vol. 78, 69-96, 1991.

WL21 C.A. Woodbury, H.A. Lewis and A.T. Canby, "The Nature of Flame

Movement in a Closed Cylinder", SAE Journal, Vol. 8, No. 3, 209-218, March 1921.

YA92 A. Yoshida, Y. Ando, T. Yanagisawa and H. Tsuji, "Fractal Behaviour of Wrinkled Laminar Flame", Combustion Science and Technology (in Japanese), Vol. 1, 37-43, 1992.

Ya93 V. Yakhot, "Theory and Modelling of Premixed Turbulent Combustion", Turbulence and Molecular Processes in Combustion, T. Takeno (Editor), 13-33, 1993.

YA93a A. Yoshida, Y. Ando, T. Yanagisawa and H. Tsuji, "Effect of Laminar Burning Velocity on Fractal Behaviour and Turbulent Burning Velocity of Wrinkled Laminar Flame", Combustion Science and Technology (in Japanese), Vol. 1, 103-109, 1993.

YN92 A. Yoshida, M. Narisawa and H. Tsuji, "Structure of Highly Turbulent Premixed Flames", Twenty-Fourth Symposium (International) on Combustion, 519-525, 1992.

YN92a A. Yoshida and M. Narisawa, "High-Efficiency and High-Intensity Turbulent Premixed Combustion", Tokyo Denki University, Res. Inst. for Tech. Annual Report, No. 11, 151-156, 1991-92.

YN93 A. Yoshida, M. Narisawa and H. Tsuji, "Effect of turbulence on NO_x formation in premixed turbulent flames", Turbulence and Molecular Processes in Combustion, 339-354, 1993.

Yo90 A. Yoshida, "Recent Advances in Experimental Studies of Turbulent Premixed Flames", JSME International Journal, Series II. Vol 33, No. 3, 424-435, 1990.

YS94 K.M. Yu, C.J. Sung and C.K. Law, "Some Aspects of the Freely Propagating Premixed Flame in a Spatially Periodic Flow Field", Combustion and Flame 97: 375-383, 1994.

ZB87 A.O. Zur Loye and F.V. Bracco, "Two-Dimensional Visualization of Ignition Kernels in an IC Engine", Combustion and Flame 69: 59-69, 1987.

APPENDIX A: IDEALIZED TURBULENT FLOWS OF SINGLE-SIZE VORTEX TUBES

This appendix shows the effects of change in vortex core radius on the number of vortex tubes required for a fixed turbulent kinetic energy. The flow considered is an idealized turbulent flow in which all eddies are assumed to be vortex tubes of the same core radius and unit length. These vortex tubes are assumed to behave as if they are solid rods with a fixed rotation speed. In other words, solid body rotation is assumed for the fluid within the vortex tubes.

Consider a two-dimensional flow in which all vortex tubes have a core radius of R. With an angular velocity of Ω the maximum tangential velocity at R is then ΩR. This maximum tangential velocity is often considered to be the root-mean-square turbulence intensity, u'. The turbulent kinetic energy of one of these eddies is,

$$KE = \frac{\rho}{2} \int_0^R (\Omega\ r)^2\, dV \qquad \text{A.1}$$

where ρ is the density which is assumed to be constant, r is the radial distance from the centre of the core and V is the volume of the vortex tube. The integration results in

$$KE = \frac{\rho \pi \Omega^2}{4} R^4 \qquad \text{A.2}$$

where KE is the turbulent kinetic energy per unit depth.

An increase in turbulent length scale is illustrated here by doubling the vortex core radius from R to 2R. Keeping the maximum tangential velocity at ΩR requires a reduction in the angular velocity from Ω to Ω/2. In other words, the angular velocity is reduced to Ω/2 so that the tangential velocity at the core radius, 2R, is maintained at ΩR. This is done to fix the root-mean-square turbulence intensity at u'. For an unit depth, the turbulent kinetic energy of on of these larger vortex tubes is

$$KE = \frac{\rho}{2} \int_0^{2R} \left(\frac{\Omega}{2}\ r\right)^2 2\pi r\, dr \qquad \text{A.3}$$

which leads to

$$KE = \rho \pi \Omega^2 R^4 \qquad \text{A.4}$$

This shows that the turbulent kinetic energy of the larger vortex tube with core radius of 2R is four times the turbulent kinetic energy of the smaller vortex tube with core radius of R, for the same u'.

In summary, the effects due to a change in vortex core size is portrayed here by considering two idealized turbulent flows. One flow is made up of R core radius vortex tubes of unit length while the other flow consists of 2R core radius vortex tubes of unit length. In order to maintain the same turbulent kinetic energy in the two flows, the number of vortex tubes in the small-scale turbulent flow has to be four times the number of vortex tubes in the large-scale turbulent flow.

APPENDIX B: MULTI-ZONE THERMODYNAMIC EQUILIBRIUM FLAME GROWTH MODEL

This appendix details the semi-empirical, multi-zone thermodynamic equilibrium flame growth model. The program in the QuickBasic format is attached at the end of the appendix along with a simplified flow-chart describing the numerical algorithm.

The main program for flame growth model is called P-BV93.bas. This program shares the common variables listed in CMBCOM.bas and it uses subroutines in CMBSUB.bas. Programs CMBCOM.bas and CMBSUB.bas are included in Appendix G. The whole program simulates a pressure trace of a laminar or a turbulent flame based on user specified fuel (can be either methane or propane), mixture stoichiometry, spark kernel size, pressure and temperature effects in terms of pressure and temperature exponents, initial pressure and temperature, and the flow field motion.

The program simulates flame growth starting from the specified spark kernel. The kernel burns at the laminar burning velocity with the pressure and temperature effects accounted for. At the present stage, the model uses the experimentally determined reference laminar burning velocity at 300 K and 1 atm with the specified fuel and mixture stoichiometry. The present model can be improved to include detailed chemical kinetics for calculating the reference laminar burning velocity. The effects due to curvature, stretching, heat losses can also be accounted but these adjustments are not included in the present model.

For the turbulent flame growth simulation, the turbulence intensity level along with its decay rate, and the integral scale must be specified. The model at the present stage estimate the turbulence decay rate based on the ignition-time turbulence intensity and integral scale along with the perforated plate hole diameter. This turbulence decay rate estimation can easily be modified to take other forms of decay expression.

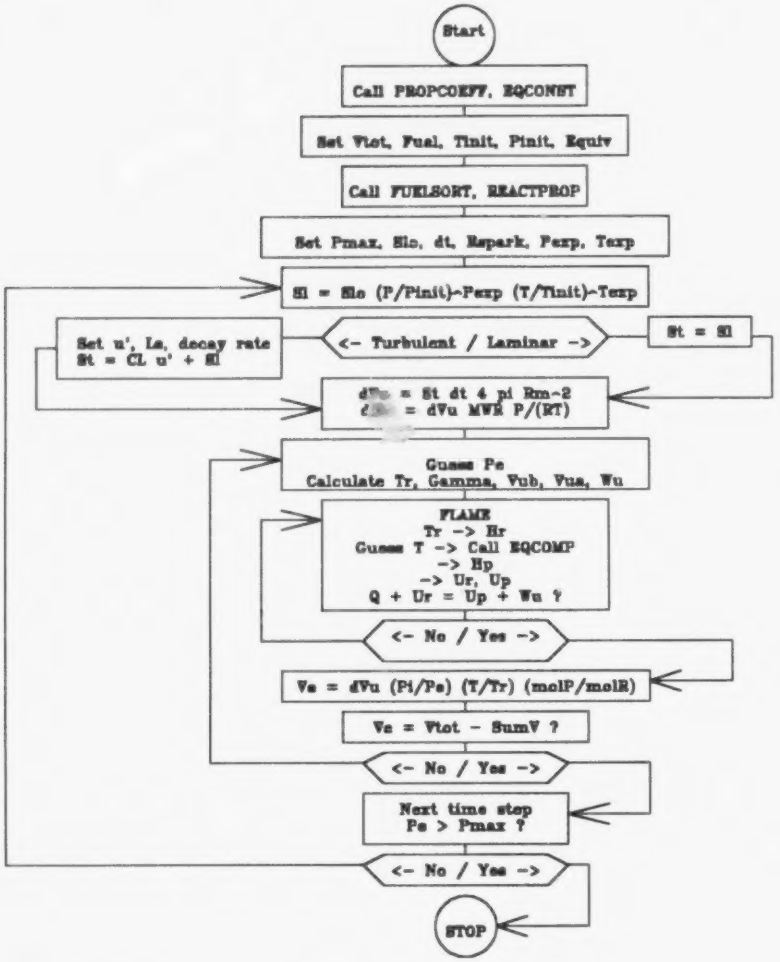
Start
Call PROPCOEFF, EQCONST
Set Vtot, Fuel, Tinit, Pinit, Equiv
Call FUELSORT, REACTPROP
Set Pmax, Slo, dt, Rspark, Pexp, Texp
Sl = Slo (P/Pinit)^Pexp (T/Tinit)^Texp
Set u', Ls, decay rate
St = CL u' + Sl
<- Turbulent / Laminar ->
St = Sl
dVu = St dt 4 pi Rm^2
dmu = dVu MWR P/(RT)
Guess Pe
Calculate Tr, Gamma, Vub, Vua, Wu
FLAME
Tr -> Hr
Guess T -> Call EQCOMP
-> Hp
-> Ur, Up
Q + Ur = Up + Wu ?
<- No / Yes ->
Ve = dVu (Pi/Pe) (T/Tr) (molP/molR)
Ve = Vtot - SumV ?
<- No / Yes ->
Next time step
Pe > Pmax ?
<- No / Yes ->
STOP

Figure B.1: A simplified flow-chart for P-BV93.bas program.

EQCONST, FLAME, FUELSORT, PROPCOEFF and REACTPROP are subroutines as described in the program listing. CL=linear coefficient, dmu=element mass, dt=time step, dVu=element volume before it burns, Equiv=equivalent ratio, Gamma=specific heat ratio, Hp=enthalpy of products, Hr=enthalpy of reactants, Ls=integral length scale, molP=moles of products/mole of fuel, molR=moles of reactants/mole of fuel, MWR=molar mass of the reactants, P=pressure, Pe=pressure at thermodynamic equilibrium, Pexp=pressure exponent, pi=3.1416, Pi=pressure before the element burns, Pinit=initial pressure before ignition, Pmax=maximum pressure to simulate, Q=heat losses, R=ideal gas constant, Rm=mean flame radius, Rspark=spark radius, Sl=laminar burning velocity, Slo=Sl at 300 K and 1 atm, SumV=total volume of all other elements, St=turbulent burning velocity, T=temperature, Texp=temperature exponent, Tinit=initial temperature before ignition, Tr=temperature of the reactants, Up=internal energy of the products, Ur=internal energy of reactants, u'= turbulence intensity, Ve=element volume at equilibrium, Vtot=total cell volume, Vua=volume after the element burns, Vub=volume before the element burns, Wu=compression work done by the burning element.

```
DECLARE SUB EQCONST ()
DECLARE SUB FUELSORT (FUEL%, FUEL$(), FCA!, FHA!, FMW!)
DECLARE SUB FLAME (x, Q!, W!, PE!, FCA!, FHA!, FMW!, S!, Tr!, t!, MWR!, MWP!, FLAG%)
DECLARE SUB PROPCOEFF ()
DECLARE SUB REACTPROP (Equiv!, FCA!, FHA!, FMW!, MF!, MOXY#, MN2#, MWR!)
DECLARE SUB Sturb (Iscalei!, Urms!, Iscale!, Rf!, Sl!, St!)
DECLARE SUB Turb (D!, Urmsi!, Iscalei!, I%, dt!, Urms!, Iscale!, Rfb!, Mfb!, Pinit!, Tinit!, P!, Tu!)
'
'     P-BV93.BAS
'     25-May-92     MD CHECKEL
'     06-Dec-93     DSK TING
'
' This program simulates a pressure trace of a LAMINAR/TURBULENT FLAME from
' known FUEL, EQUIVALENCE RATIO, PRESSURE EXPONENT, TEMPERATURE EXPONENT,
' INITIAL PRESSURE, INITIAL TEMPERATURE and FLOW FIELD (LAMINAR or TURBULENT
' with known PERFORATED PLATE HOLE DIAMETER, IGNITION-TIME TURBULENCE
' INTENSITY and IGNITION-TIME INTEGRAL SCALE).
'
' The mean geometric flame radius used in this "Geometric Method" accounts for
' the flame expansion during combustion of the Ith element.
'----------------------------------------------------------------------
' PROGRAM HISTORY:
'
' Based on BOMB.BAS per Alun Thomas's BOMB.BAS with corrections re units, etc
'
' The subroutines that are called in the CMBSUB subroutine file are fairly
' well tested and proven.  Please do NOT change them.
' Read CMBSUB.DOC for an understanding of the program and subroutines.
'
' Thermodynamic properties and methods are used as described in:
'                 Rowland S. Benson,
'                 "Advanced Engineering Thermodynamics"
'                 Pergammon Press, 1977, 2nd Edition
'----------------------------------------------------------------------
' Include common statements and routines.
'
        REM $INCLUDE: 'C:\QB\COMB\CMBCOM.BAS'
        REM $INCLUDE: 'C:\QB\LIB\PLOTCOM.BAS'
        REM $INCLUDE: 'C:\QB\LIB\COLORset.BAS'
        REM $INCLUDE: 'C:\QB\COMB\CMBFN-RP.BAS'
        REM $DYNAMIC
'
        VERDAT$ = "06-Dec-93"
'
        REDIM I$(8), W(8), IC(8, 7), CC(6), CW(6), R(7), P(7), M#(6)
        REDIM FUEL$(2)
        DIM STORE(600, 15)
'----------------------------------------------------------------------
' Ideal gas constant in J/kmol.K
        rmol = 8314.3
```

```
   '
   ' The subroutine PROPCOEFF fills an array with coefficients used in
   ' calculating enthalpy and Gibbs function for CO, CO2, H2, H2O, N2, O2,
   ' and fuel.  (See CMBSUB for details.)
   ' I$() is the alphanumeric name.
   ' W() is the molecular weight.
   ' IC() is the coefficient array.
   '
          CALL PROPCOEFF
   '
   ' The subroutine EQCONST calculates chemical equilibrium constants used
   ' for CO2 and CO2-H2O dissociation reactions.  The IC() array is used for
   ' this.  (See CMBSUB for details.)
   '
          CALL EQCONST
   '
   ' INPUT SECTION:
   ' ************************************************************************
   '-----------------------------------------------------------------------
   ' Set the fuel and cell volume.
   '
   ' V# is the bomb volume in m^3.  It remains constant.
   ' FUEL% is an integer constant to indicate which fuel is present.
   ' FUEL$() contains the alphanumeric fuel names.
   '
          V# = .001882#: FUEL% = 2
          FUEL$(1) = "C3H8"
          FUEL$(2) = " CH4"
   '-----------------------------------------------------------------------
   ' Initial conditions.
   '
          Tinit = 300.15               ' pre-combustion temperature in K
          Pinit = 101325               ' pre-combustion pressure in Pa
          Equiv = .9                   ' equivalence ratio
   '-----------------------------------------------------------------------
   ' Print a bit of a header and verify some parameters with user.
   ' These are the INSCRN variables.
          x% = 5
          REDIM D$(x%), t%(x%), P$(x%), LG%(x%), l%(x%), c%(x%)
          REDIM IP$(x%), IP%(x%), IP!(x%), IP#(x%)
INPUTSECTION:
          COLOR 10, 1: PRINT
          PRINT "P-BV version of "; VERDAT$; ", run at "; TIME$; " on "; DATE$
   '
          D$(1) = STR$(V#): t%(1) = 2: LG%(1) = 9: l%(1) = 12: c%(1) = 10
          P$(1) = "Enter volume of bomb in m3 (0=" + D$(1) + ") >"
          D$(2) = STR$(Tinit): t%(2) = 1: LG%(2) = 7: l%(2) = 14: c%(2) = 10
          P$(2) = "Enter initial temperature  (0=" + D$(2) + ") >"
          D$(3) = STR$(Pinit): t%(3) = 1: LG%(3) = 15: l%(3) = 16: c%(3) = 10
          P$(3) = "Enter initial pressure in Pa (0=" + D$(3) + ") >"
          D$(4) = STR$(Equiv): t%(4) = 1: LG%(4) = 7: l%(4) = 18: c%(4) = 10
```

```
        P$(4) = "Enter equivalence ratio (0<E<=1), (0=" + D$(4) + ") >"
        D$(5) = STR$(FUEL%): t%(5) = 0: LG%(5) = 5: 1%(5) = 20: c%(5) = 10
        P$(5) = "Enter FUEL code (1=propane, 2=methane, default=" + D$(5) + ") >"
'
        CALL inscrn(5, 1, t%(), P$(), LG%(), D$(), 1%(), c%(), IP$(), IP%(), IP!(), IP#(), FX$)
'----------------------------------------------------------------------
' Echo back some of the initial parameters for the user.
'
        CLS : PRINT "INPUT VALUES:": PRINT
        IF IP#(1) > 0 THEN V# = IP#(1)
                PRINT "Bomb Volume is "; V#; " m^3"
                Rbomb = (.75 * V# / 3.141592654#) ^ (1! / 3!)
        IF IP!(2) > 0 THEN Tinit = IP!(2)
                PRINT "Initial Temperature is "; Tinit; " K"
        IF IP!(3) > 0 THEN Pinit = IP!(3)
                PRINT "Initial Pressure is "; Pinit; " Pa"
        IF IP!(4) > 0 AND IP!(4) <= 1 THEN Equiv = IP!(4)
        IF IP%(5) > 0 THEN FUEL% = IP%(5)
        IF FUEL% = 1 THEN AFRSTOIC = 15.5797 ELSE AFRSTOIC = 17.12
                AFR = AFRSTOIC / Equiv
                PRINT USING "Equivalence ratio is #.###  (A/F=##.#)"; Equiv; AFR
'----------------------------------------------------------------------
' Get some of the fuel properties from the FUELSORT subroutine.
' This routine is attached to the bottom of this program.
' (Returns FCA, FHA, and FMW.)
'
        CALL FUELSORT(FUEL%, FUEL$(), FCA, FHA, FMW)
'----------------------------------------------------------------------
' Set time step, spark kernel radius, pressure coefficient and temperature
' coefficient.
'
        Pquit = 3                ' quit when P = Pquit * Pinit
        dt = .0002               ' time step (sec)
        Rspark = .002             ' initial flame radius (m)
        Pexp = -.3               ' pressure coefficient
        Texp = 2                 ' temperature coefficient
        P0 = 101325               ' reference pressure in Pa
        T0 = 300.15               ' reference temperature in K
' initial burning velocity as a function of equivalence ratio (m/s)
        IF FUEL% = 1 THEN           ' propane-air mixture
                Sl0 = -5.26 * Equiv ^ 4 + 16! * Equiv ^ 3 - 18.15 * Equiv ^ 2
                Sl0 = Sl0 + 9.8 * Equiv - 1.96
        ELSE                     ' methane-air mixture
                Sl0 = 7.14274 * Equiv ^ 2 + 59.5716 * Equiv - 33.5715
                Sl0 = Sl0 / 100
        END IF

        PRINT : PRINT "Enter maximum pressure build up ratio (default = "; Pquit;
        INPUT ")> "; Pqjk
        IF Pqjk > 0 THEN Pquit = Pqjk
```

```
    PRINT : PRINT USING "Initial burning velocity =##.## m/s."; Sl0

    PRINT : PRINT "Enter time step between pressure points (default = "; dt;
    INPUT " s) >"; dtjk
    IF dtjk > 0 THEN dt = dtjk

    PRINT : PRINT "Enter spark radius before expansion (def = "; Rspark;
    INPUT " m) >"; Rspjk
    IF Rspjk > 0 THEN Rspark = Rspjk
    Vspark = 4 / 3 * 3.141593 * Rspark ^ 3     'volume of spark (m^3)

    PRINT : PRINT "Enter pressure exponent (default = "; Pexp;
    INPUT " ) >"; Pejk
    IF Pejk <> 0 THEN Pexp = Pejk

    PRINT : PRINT "Enter temperature exponent (default = "; Texp;
    INPUT " ) >"; Tejk
    IF Tejk > 0 THEN Texp = Tejk

    PRINT : PRINT "Enter reference pressure (default = "; P0;
    INPUT " Pa) >"; P0jk
    IF P0jk <> 0 THEN P0 = P0jk

    PRINT : PRINT "Enter reference temperature (default = "; T0;
    INPUT " K) >"; T0jk
    IF T0jk > 0 THEN T0 = T0jk
'---------------------------------------------------------------------------
' Heat Losses.
    CLS : LOCATE 10, 1: PRINT "Heat Losses": PRINT "************": PRINT
    INPUT "Consider Heat Losses ? (Enter=No, 1=Yes) >"; HtAns1%
    IF HtAns1% = 1 THEN
        PRINT : PRINT "Consider Both Conduction and Radiation ?"
        INPUT "(Enter=Both, 1=Conduction Only, 2=Radiation Only) >"; HtCR%
        IF HtCR% <> 1 THEN
            Emis = .2
            PRINT : PRINT "Enter Emissivity (default = "; Emis;
            INPUT " ) >"; Emisjk
            IF Emisjk > 0 THEN Emis = Emisjk
        END IF
    END IF
'---------------------------------------------------------------------------
' Set the turbulence parameters?
    CLS : LOCATE 10, 1: PRINT "Laminar Flame Or Turbulent Flame ?"
    PRINT "***********************************": PRINT
    INPUT "Turbulent Flame ? (Enter=No, 1=Yes) >"; LTans1%
    IF LTans1% = 1 THEN
        Dia = .02       ' plate hole diameter (m)
        Urmsi = 1       ' ignition-time rms turbulence intsnsity (m/s)
        Iscalei = .0076' ignition-time integral scale (m)

        PRINT "Enter perforated plate hole diameter (default = "; Dia;
                INPUT " m) > "; Diajk
                IF Diajk > 0 THEN Dia = Diajk

                PRINT : PRINT
                PRINT "Enter ignition-time turbulence intensity (default = "; Urmsi;
                INPUT " m/s) > "; Urmsijk
                IF Urmsijk > 0 THEN Urmsi = Urmsijk

                PRINT : PRINT
                PRINT "Enter ignition-time integral scale (default = "; Iscalei;
                INPUT " m) > "; Iscaleijk
                IF Iscaleijk > 0 THEN Iscalei = Iscaleijk
        END IF
'------------------------------------------------------------------------
' Entering the MAIN LOOP.
' ----------------------
'
' REACTPROP determines the reactant properties (See CMBSUB).
' MPR = kmol of fuel / element
'
        CALL REACTPROP(Equiv, FCA, FHA, FMW, MF, MOXY#, MN2#, MWR)
        GMR = fngamR(Tinit)
        Mass = MWR * Pinit * V# / rmol / Tinit

' Dimension arrays for burning velocity calculation.
        REDIM Rb(600), dVu(600)

' Pressure before burning element I% is set to Pinit if I%=1 or to PE,
' the pressure after burning the last element, if I% is greater than 1.
' PI is pressure before this element burns (not to be confused with Pinit).
        Tr = Tinit
        PE = Pinit
        Mb = 0          ' nothing is burnt yet
'------------------------------------------------------------------------
' MAIN LOOP:
'!!!!!!!!!!!!!!!!!!!!!!!!!!!!!!!!!!!!!!!!!!!!!!!!!!!!!!!!!!!!!!!!!!!!!!!!
FOR I% = 1 TO 600
        Pi = PE

' dVbg is the volume burnt in the next time step in m^3.
' It is given by:
'     Sl0 * (Pi/P0)^Pexp * (Tr/T0)^Texp * dt * geometric flame area
'        where
'             P0 = 101.325 kPa
'             T0 = 300.15 K
' Laminar burning velocity (m/s)
        Sl = Sl0 * (Pi / P0) ^ Pexp * (Tr / T0) ^ Texp
        IF LTans1% = 0 THEN St = Sl
        dVbg = St * dt * 4 * 3.141593 * Rbnow ^ 2
        IF I% = 1 THEN dVbg = Vspark
CalcdMbg:
```

```
' dMbg is the mass burning in the next time step in kg
        dMbg = dVbg * MWR * Pi / rmol / Tr

' MPR is the moles of fuel per element in this element in kmol/element
        MPR = dMbg / MWR / (MF + MOXY# + MN2#)

' Treactants and GAMMAreactants are evaluated at the current PI.
        Tr = Tinit * (Pi / Pinit) ^ ((GMR - 1) / GMR)
        GMR = fngamR(Tr)

' Estimate PE, the end pressure after this element burns. (just a guess now).
' Flag IFLP is set to 0 to indicate that P is only a guess.
        PE = Pi + Equiv * dMbg / Mass * Pinit
        IFLP = 0
'----------------------------------------------------------------------
CALCVOLUMES:
'@@@@@@@@@@@@@@@@@@@@@@@@@@@@@@@@@@@@@@@@@@@@@@@@
'
' This section now calculates the volume of the remaining unburnts before and
' after combustion of this element. The work done to compress the unburnts is
' evaluated and then a loop adds the work done to compress each previously
' burned element.  If the correct pressure has been selected, the work done
' on all elements will equal the work done by the burning element during its
' combustion and expansion.  When this happens, the selected pressure will
' be the correct pressure after this element burns.
'
' If the correct pressure is guessed, the sum of the volumes will equal the
' total volume.
'
' VUB is the total volume of all the unburnt gases in m^3 BEFORE combustion
' of the Ith element (excluding the Ith element which is about to burn).
' VUA is the total volume of all the unburnt gases in m^3 AFTER combustion
' of the Ith element.
        VUB = (Mass - Mb - dMbg) / Mass * V# * (Pinit / Pi) ^ (1 / GMR)
        VUA = VUB * (Pi / PE) ^ (1 / GMR)
' Calculate the work of compression  (VUB -> VUA) on unburnt elements in J.
' negative => work done By the burning element
        WU = -(PE * VUA - Pi * VUB) / (1 - GMR)
'
' Volume sum and work sum are set equal to the volume of unburned gas and
' work done to compress the unburned gas in m^3 and joules respectively.
'
        SUMW = WU
'
' If there are previously burned elements, calculate the volume of each before
' and after compression to new pressure, PE. Then calculate the work done to
' compress each one and add it to the work sum done by the burning element.
'
' VB is the volume of the Jth element before compression.
' VA is the volume of the Jth element after compression.
' WB is the compression work of the Jth element in Joules.
' negative => work done By the burning element
' SUMVBA is the volume of the burnt gases after combustion of element I.
'
' STORE(J,3) is the volume of the Jth element after combustion.
' STORE(J,1) is the pressure of the Jth element after combustion.
' STORE(J,9) is the specific heat ratio of products in element J. (=FNGAMP(T))
        IF I% > 1 THEN
                SUMVBA = 0!
                FOR J = 1 TO I% - 1
                        VB = STORE(J, 3) * (STORE(J, 1) / Pi) ^ (1 / STORE(J, 9))
                        VA = STORE(J, 3) * (STORE(J, 1) / PE) ^ (1 / STORE(J, 9))
                        WB = -(PE * VA - Pi * VB) / (1 - STORE(J, 9))
                        SUMVBA = SUMVBA + VA
                        SUMW = SUMW + WB
                NEXT J
        END IF
        SUMV = VUA + SUMVBA

' SUMW is total work done in joules for one burning element.
' Dividing by mpr (kmol fuel/element) converts to J/kmol fuel and negative
' sign implies that it is work done BY the burning element.
        WORK = SUMW / MPR        ' J/(kmol of fuel/element)
'
' Use subroutine FLAME to find the temperature of combustion of the burning
' element knowing its starting conditions and work output, SUMW.  Note that
' for a normal element which loses heat and does work on its surroudings,
' HEAT and WORK are both negative numbers, ie not the usual sign convention
' for work OUT of an element or control volume.
'--------------------------------------------------------------------------
HEATLOSS:
IF HtAns1% = 0 THEN GOTO NoHeatL
        Qmass = (1424 * Equiv - 774.5) * 1000  'maximum heat flux in W/m^2
        IF I% > 1 THEN dRbg = dVbg / (4 * 3.1415927# * Rbnow ^ 2)
        Rbnext = Rbnow + dRbg
        Rflame = SQR((Rbnow ^ 2 + Rbnext ^ 2) / 2)
        dRfc = Rflame - .003
        IF dRfc > 0 AND dRfc < .02 THEN
                Afc = 2 * 3.1415927# * .001 * 2 * dRfc
        ELSEIF dRfc > .02 THEN
                Afc = 2 * 3.1415927# * (.001 * .04 + .003 * 2 * (Rflame - .023))
        END IF
        IF I% > 1 THEN Qrad = Emis * 5.67E-08 * (STORE(I% - 1, 7) ^ 4 - Tinit ^ 4)
        dQr = 4 * 3.1415927# * Rflame ^ 2 * Qrad * dt
        dQc = Qmass * Afc * dt
        IF HtCR% = 1 THEN dQr = 0
        IF HtCR% = 2 THEN dQc = 0
        dQtot = dQr + dQc
        HEAT = -dQtot / MPR
NoHeatL:
        CALL FLAME(1, HEAT, WORK, PE, FCA, FHA, FMW, Equiv, Tr, t, MWR, MWP, FLAG%)
'
```

```
' Calculate the volume this element would have if it burned to temperature T
' at pressure PE. (MOLP is number of moles of products per mole of fuel, MOLR
' is moles of reactants per mole of fuel.  Hence VE is in m^3 like V).
'
        VE = dVbg * Pi / PE * t / Tr * molP / molR
'
' Compare this with volume left over from unburned gas and all previous burned
' elements at this pressure, PE.
'
        ERV = VE - (V# - SUMV)
'
' If the error is greater than .01% or (3/I%)%, then make a new estimate of
' pressure and go back to try again.
'
        ERRLIM = .0001
        IF I% < 300 THEN ERRLIM = .03 / I%
        IF ABS(ERV) > VE * ERRLIM THEN
'
' IFLP is a flag which determines whether a previous estimate has been made.
' If it has, extrapolate/interpolate to get a new estimate.
' Otherwise, simply make a small step in pressure.
'
                IF IFLP > 0 THEN
                        PE3 = (PE * ERV1 - PE1 * ERV) / (ERV1 - ERV)
                        PE1 = PE
                        PE = PE3
                ELSE
                        PE1 = PE
                        IFLP = 1
                        IF ERV > 0 THEN
                                PE = Pi + 1.2 * (PE - Pi)
                        ELSE
                                PE = PE + (PE - Pi) / 1.2
                        END IF
                END IF
'
' Having established this estimate for pressure after combustion,
' record the current volume error and go back to re-calculate the
' volumes and compression work with the new pressure value.
'
                ERV1 = ERV
                GOTO CALCVOLUMES
        END IF

'@@@@@@@@@@@@@@@@@@@@@@@@@@@@@@@@@@@@@@@@@@@@@@@@
'
' Calculation of volumes having converged, enter values for the I%th element
' into the storage arrays, STORE and STORE2.  Since this program has been
' through many changes, some of the items below are now meaningless but are
' kept in place rather than risking total confusion by reordering the
' storage arrays.
```

```
'
        STORE(I%, 1) = PE           'pressure after element I% burns
        RR = ((V# - VUA) / V#) ^ (1 / 3)
        STORE(I%, 2) = RR           'relative flame radius after element I% burns
        Rbnext = RR * Rbomb         'flame radius after the element burns (m)
        STORE(I%, 3) = VE           'volume of element after combustion (m^3)
        STORE(I%, 4) = VUB          'volume of unburned element before it burns (m^3)
        STORE(I%, 5) = VUA          'volume of unburned element after it burns (m^3)
        STORE(I%, 6) = Tr           'temperature of the reactants (K)
        STORE(I%, 7) = t            'temperature of element after combustion (K)
        STORE(I%, 8) = fngamR(Tr)   'specific heat ratio of reactants in element I%
        STORE(I%, 9) = fngamP(t)    'specific heat ratio of products in element I%
        STORE(I%, 10) = MWP         'molecular weight of products
'------------------------------------------------------------------------
' Calculate the turbulence parameters and then the turbulent burning velocity.
'
        Mjkb = Mb + dMbg            'total mass burnt (kg)
        ROR = (Mjkb / Mass) ^ (1 / 3)
        IF LTans1% = 0 THEN GOTO SkipTurb
        CALL Turb(Dia, Urmsi, Iscalei, I%, dt, Urms, Iscale, RR, ROR, Pinit, Tinit, PE, Tr)
        CALL Sturb(Iscalei, Urms, Iscale, Rbnow, Sl, St)
SkipTurb:
'------------------------------------------------------------------------
' Account for the flame expansion.
        IF I% < 2 THEN GOTO SkipdVbg2
        dVbg2 = St * dt * 4 * 3.1415927# * (Rbnow ^ 2 + Rbnext ^ 2) / 2
        IF dVbg2 / dVbg < .995 OR dVbg2 / dVbg > 1.005 THEN
                dVbg = dVbg2
                GOTO CalcdMbg
        END IF
SkipdVbg2:

        Rbnow = RR * Rbomb          'flame radius after the element burns (m)
        Mb = Mb + dMbg              'total mass burnt (kg)
        STORE(I%, 11) = Mb / Mass   'mass fraction burnt
        ROR = (Mb / Mass) ^ (1 / 3)
        STORE(I%, 12) = ROR         'relative radius of this element at spark time
        STORE(I%, 13) = Sl          'laminar burning velocity (m/s)
        STORE(I%, 14) = Urms        'rms turbulence intensity (m/s)
        STORE(I%, 15) = Iscale      'integral scale (m)
        Rb(I%) = Rbnow
        dVu(I%) = dVbg

'
' Print out a running listing to let the user know the progress of the
' calculations that are going on.
'
        PRINT USING "###: P=######Pa, Tb=####k, "; I%; PE; t;
        PRINT USING "Tu=####k, r/R=#.###, "; Tr; RR;
        PRINT USING "r0/R=#.###, mb/M=#.###"; ROR; Mb / Mass
        PRINT
        IF PE >= Pquit * Pinit THEN GOTO Outloop

NEXT I%
'
' The end of MAIN LOOP.
'!!!!!!!!!!!!!!!!!!!!!!!!!!!!!!!!!!!!!!!!!!!!!!!!!!!!!!!!!!!!!!!!!!!!!!!!!!
'-------------------------------------------------------------------------
Outloop: nb% = I%
'-------------------------------------------------------------------------
' Make a warbling sound to notify user that the calculations are done.
'
        FOR Nsd = 1 TO 10
                FREQ = 100 + 50 * Nsd
                SOUND FREQ, 1
        NEXT Nsd
'
'-------------------------------------------------------------------------
' Calculate and plot the burning velocity.
'##########################################################################
'
        INPUT "Burning Velocity Calculation. (Enter=Continue) >"; caljk
'-------------------------------------------------------------------------
' Geometric method for calculating burning velocity.
        REDIM SuGeo(nb%), SuOrg(600), SLam(600), rmsU(600), scale(600)
        rlast = Rspark: onethird = 1! / 3!

        FOR I = 2 TO nb%
                Rb = Rb(I)
                deltavi = dVu(I)
                Rflame = SQR((rlast ^ 2 + Rb ^ 2) / 2)
                Ri = (.75 / 3.141593 * (4 / 3 * 3.141593 * Rflame ^ 3 + deltavi)) ^ onethird
                dri = Ri - Rflame
                SuGeo(I) = dri / dt              '"Geometric" burning velocity (m/s)
                SuOrg(I) = dVu(I) / 4 / 3.14159 / Rb(I - 1) ^ 2 / dt

        '"Original" burning velocity (m/s)
                SLam(I) = STORE(I, 13)           'laminar burning velocity (m/s)
                rmsU(I) = STORE(I, 14)           'rms turbulence intensity (m/s)
                scale(I) = STORE(I, 15) * 1000   'compressed integral scale (mm)
                rlast = Rb
        NEXT I
' Convert flame radius from m to mm
FOR I = 1 TO nb%: Rb(I) = Rb(I) * 1000: NEXT
'
' Plotting the burning velocity (Geometric method).
Plotter:
        CALL PINI(12, 1): c% = 15
        CALL XAXIS(0!, 70!, 10!, 0, 2, "Flame Radius (mm)", c%)
        CALL YAXIS(0!, 2!, .4, 0, 2, "Burning", "Velocity", " (m/s) ", c%)
        CALL LINPLT(Rb(), SuGeo(), nb%, 0, 1, 5!, c%)
        CALL LINPLT(Rb(), SuOrg(), nb%, 0, 2, 5!, 10)
        CALL LINPLT(Rb(), SLam(), nb%, 0, 3, 5!, 12)
        CALL LINPLT(Rb(), rmsU(), nb%, 0, 4, 5!, 14)
        LOCATE 1, 1: PRINT SPACE$(70)
        LOCATE 1, 1: INPUT "Enter=Continue, 1=PHCOPY"; BVP1
        IF BVP1 = 1 THEN CALL PHCOPY(xyz$)
'#############################################################################
'----------------------------------------------------------------------
' Save the pressure trace to a file.
SAVEDATA:
        run$ = "1M9P"
        f$ = "C:\QB\PHD\BOMB\TEMP\" + run$ + ".dat"
Filename:
        CLS : PRINT "ABOUT TO WRITE TO "; f$
        INPUT "HIT ENTER TO GO ON, ELSE ENTER A NEW FILE NAME.>"; junk$
        IF junk$ <> "" THEN
                run$ = junk$
                f$ = "C:\QB\PHD\BOMB\TEMP\" + run$ + ".dat"
                PRINT : GOTO Filename
        END IF
        FUEL$ = "Methane"
        INPUT "Fuel (Enter = Methane)"; Fl$
        IF Fl$ <> "" THEN FUEL$ = Fl$

        REDIM com$(8), D!(nb%, 10), par!(8), par$(8), col1$(10), col2$(10)
        FOR I = 1 TO nb%
                D!(I, 1) = (I) * dt * 1000        'time in ms
                D!(I, 2) = STORE(I, 1) / 1000     'pressure in kPa
                D!(I, 3) = STORE(I, 2)            'relative flame radius
                D!(I, 4) = STORE(I, 11)           'mass fraction burnt
                D!(I, 5) = STORE(I, 6)            'Tu (K)
                D!(I, 6) = STORE(I, 7)            'Tb (K)
                D!(I, 7) = STORE(I, 13)           'laminar burning velocity (m/s)
                D!(I, 8) = SuGeo(I)               'Geometric burning velocity (m/s)
                D!(I, 9) = STORE(I, 14)           'rms turbulence intensity (m/s)
                D!(I, 10) = STORE(I, 15) * 1000   'integral scale (mm)
        NEXT I
        com$(1) = "Stimulation of pressure trace"
        com$(2) = "DSK TING " + DATE$ + "  " + TIME$
        com$(3) = "Pressure generated by P-BV.BAS"
        com$(4) = "Filename = " + f$
        com$(5) = "Fuel = " + FUEL$
        com$(6) = ""
        com$(7) = ""
        com$(8) = ""
        par!(1) = Equiv: par$(1) = " Equivalence Ratio "
        par!(2) = dt: par$(2) = " dt (sec) "
        par!(3) = Sl0: par$(3) = " Initial Burning Velocity (m/s) "
        par!(4) = Pexp: par$(4) = " Pressure Coefficient "
        par!(5) = Texp: par$(5) = " Temperature Coefficient "
        par!(6) = Pinit / 1000: par$(6) = " Initial Pressure (kPa) "
        par!(7) = Tinit: par$(7) = " Initial Temperature (K) "
        par!(8) = Dia * 1000: par$(8) = " Plate Hole Diameter (mm) "

        col1$(1) = " TIME": col2$(1) = "ms"
        col1$(2) = " PRESS": col2$(2) = "  kPa"
        col1$(3) = "Fl Radius": col2$(3) = "rb/R"
        col1$(4) = "Mass Brnt": col2$(4) = "mb/M"
        col1$(5) = "Tu before": col2$(5) = "K"
        col1$(6) = "Tb after": col2$(6) = "K"
        col1$(7) = " Sl  ": col2$(7) = "m/s"
        col1$(8) = "Su(Geo)": col2$(8) = "m/s"
        col1$(9) = " Urms ": col2$(9) = "m/s"
        col1$(10) = "Iscale": col2$(10) = "mm"

        CALL dwrite(nb%, 10, 8, 8, f$, com$(), D!(), par!(), par$(), col1$(), col2$())

END

REM $STATIC
SUB FUELSORT (FUEL%, FUEL$(), FCA, FHA, FMW)
'
'  FUELSORT.BAS
'
' Fuelsort is a subroutine which switches the correct fuel into the
' property array and sets up correct fuel molecule variables.
'----------------------------------------------------------------------
' If fuel = propane.
'
        IF FUEL% = 1 THEN
                FCA = 3             'fuel has FCA carbon atoms per atom
                FHA = 8             'fuel has FHA hydrogens per atom
                FMW = 44.09           'fuel molar mass in kg/kgmol
'----------------------------------------------------------------------
' If fuel = methane.
'
        ELSE
                FCA = 1
                FHA = 4
                FMW = 16.043
        END IF
'----------------------------------------------------------------------
' If we don't have the current fuel in I$(7) then swap with I$(8).
'
        IF FUEL$(FUEL%) < > I$(7) THEN
                FOR I = 1 TO 7
                        TEMP = IC(7, I)
                        IC(7, I) = IC(8, I)
                        IC(8, I) = TEMP
                NEXT I
                TEMP$ = I$(7)
                I$(7) = I$(8)
                I$(8) = TEMP$
        END IF
        PRINT "Fuel is " + I$(7) + " and coefficients are:"
        FOR I = 1 TO 7
                PRINT SPACE$(10); IC(7, I)
        NEXT I

END SUB

SUB Sturb (Iscalei, Urms, Iscale, Rf, Sl, St)
'
' STURB.BAS
' 25-Nov-93     DSK TING
'
' This subroutine calculates the turbulent burning velocity given the
' turbulence intensity, integral scale and the laminar burning velocity.
'
' Turbulent burning velocity, St, is obtained from the correlation :
'    St = cL * Urms + Sl
'    where cL = Linear Coefficient
'        Urms = rms Turbulence Intensity
'          Sl = Laminar Burning Velocity
'-----------------------------------------------------------------------
' Calculate the Dependence Coefficient, the Linear Coefficient and the
' Turbulent Burning Velocity.
        pfac = 1
        cD = .01569                   ' dependence coefficient (/(mm)^.5)
        scale = Iscalei               ' integral scale (mm)
        cL = cD * Rf * 1000 / SQR(scale * 1000) + .06423  ' linear coefficient
        cL = cL * pfac
        St = cL * Urms + Sl            ' turbulent burning velocity (m/s)

END SUB

SUB Turb (D, Urmsi, Iscalei, I%, dt, Urms, Iscale, RR, R0R, Pinit, Tinit, P, Tu)
'
' TURB.BAS
' 25-Nov-93     DSK TING
'
' This subroutine generates turbulence parameters (rms turbulence intensity,
' integral scale etc) as a function of time given the plate hole diameter, D,
' the ignition-time turbulence intensity, Urmsi, and the ignition-time
' integral scale.
'-----------------------------------------------------------------------
' power law fits :  Urms/U = c1 (X/D) ^ c2
'                  Iscale/D = c3 (X/D) ^c4
        c1 = 1.984: c2 = -1.081: c3 = .1659: c4 = .3645

        XDi = (Iscalei / D / c3) ^ (1 / c4) ' X/D at ignition
        U = Urmsi / (c1 * XDi ^ c2)        ' plate speed in m/s
        TIME = dt * I%                     ' time after ignition in s
        XD = XDi + TIME * U / D               ' X/D as a function of time
```

```
' First calculate Iscale and Urms assuming normal decay Only.
        Iscale = .38 * D                    ' integral scale in m
        IF XD > 14.3 THEN Iscale = .1 * D * SQR(XD)
        IF XD <= 10 THEN Urms = U * 10.96 / (XD ^ 1.812)
        IF XD > 10 AND XD <= 20 THEN
                Urms = U * 2.627 / (XD ^ 1.191)
        END IF
        IF XD > 20 THEN Urms = U * .773 / (XD ^ .783)

' Rapid Distortion Effects.
        ' RR = radius fraction burned
        ' R0R = initial radius fraction burned
        z = (Pinit / P) * (Tu / Tinit)      ' unburned gas density ratio
        IF RR <= 0 THEN GOTO NextE
        c = (R0R / RR) ^ 2                  ' expansion ratio
        IF c > 1 THEN PRINT "Error in Expansion Ratio": STOP

' Mui = ratio of turbulent kinetic energy after distortion to that
'      before in direction i
'      i=1 is has axis perpendicular to flame front
'      i=2, 3 has axis in flame front
        b = SQR(1! / (z ^ 2) / (c ^ 3) - 1)
        mu1 = .75 * ((b * b - 1) / b ^ 3 * ATN(b) + 1! / b / b) / z ^ 3 / c / c
        mu2 = .75 * c / z
        mu2 = mu2 + .375 * (ATN(b) / b ^ 3 - 1 / b / b / (b * b + 1)) / z ^ 5 / c ^ 5
        mu3 = mu2

        Uratio = SQR((mu1 + mu2 + mu3) / 3!)
        Urms = Uratio * Urms
        Iscale = SQR(z) * Iscale

NextE:

END SUB
```

APPENDIX C: PRESSURE TRANSDUCER CALIBRATION

This appendix details the calibration of the Norwood model 111 four-active-arm strain gauge pressure transducer. It also illustrates the limitation of the present pressure transducer.

The combustion chamber pressure rise is measured using a Norwood model 111 four-active-arm strain gauge pressure transducer with a gain of 500. A calibration of the pressure transducer is performed using an OMEGA Digital Pressure Indicator Model PCL-601 in conjunction with a dead weight tester. While the dead weight tester is limited to pressure larger than 10 psig, the OMEGA digital pressure indicator enables calibration from 0 to 35 psig. The overlapping region between the two pressure indicators illustrates the agreement between the two sensors. The dead weight tester is used as a quick check prior to each series of tests.

The results of a typical pressure transducer calibration are tabulated in Table C.1. The room temperature was 20°C and the pressure, P_{atm}, was 692 mmHg. These results are plotted in term of absolute pressure as a function of pressure transducer output as shown in Figure C.1. Figure C.1 shows that the pressure transducer sensitivity remained relatively constant at 1/299 V/kPa for pressure higher than 200 kPa. The pressure transducer sensitivity becomes progressively smaller (larger slope) as the pressure approaches 100 kPa. The pressure transducer approaches zero sensitivity for pressure less than 100 kPa. The present pressure transducer fails to sense negative gauge pressure properly.

In the pressure trace analysis, the varying pressure transducer sensitivity for pressure between 100 and 200 kPa is accounted for. The change in the pressure transducer sensitivity is continuous adjusted according to the non-linear equation and the linear equation in the figure. For pressure less than 200 kPa,

$$Y = 1038\ X^3 - 4186\ X^2 + 5881\ X - 2606 \qquad \text{C.1}$$

where Y is pressure in kPa and X is voltage in V. For pressure equal or greater than 200 kPa,

$$Y = 299.5\ X \qquad \text{C.2}$$

For sub-atmospheric tests, flame growth and/or burning velocity calculations can not be determined from the pressure trace analysis.

Table C.1: Calibration of the Norwood Model 111 four-active-arm strain gauge pressure transducer (P_{atm} = 692 mmHg).

OMEGA Digital Pressure Indicator		Dead Weight Tester	
Output Voltage (V)	Pressure (psig)	Output Voltage (V)	Pressure (psig)
0.952	0	1.072	10
0.962	1.24	1.162	15
0.969	1.89	1.270	20
0.975	2.52	1.378	25
0.988	3.75	1.480	30
1.008	5.88	1.588	35
1.030	8.37	1.701	40
1.058	10.31	1.814	45
1.097	13.19	1.931	50
1.150	16.07	2.041	55
1.203	18.27	2.162	60
1.272	21.00	2.292	65
1.432	27.30	2.420	70
1.562	32.37	2.550	75
1.612	34.37	2.680	80

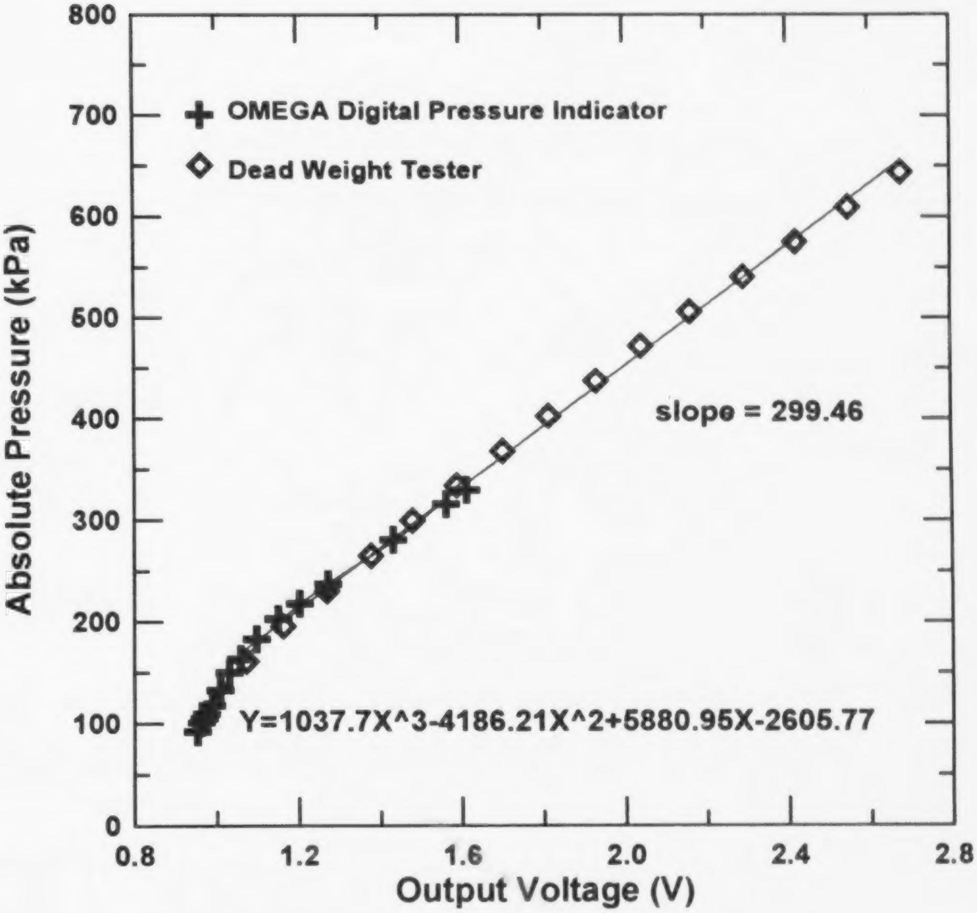

Figure C.1: The strain gauge pressure transducer calibration.

APPENDIX D: GAS MIXING USING CHOKED FLOW METHOD

This appendix describes the gas mixing procedure. It details the calibration of air and methane flow rates using the choked flow method conducted on November 18th, 1992. On November 18th, 1992, the room temperature was 23°C and the room pressure was 705 mmHg.

Figure D.1 shows a schematic of the air-fuel mixer used. This apparatus regulates the volumetric flow rate of the gases through critical flow orifices. The mixer then mixes the gases to produce homogeneous mixtures.

The critical flow orifices for controlling the flow rate are made of brass orifice plates with diameters of 0.1 mm for the fuel and 0.456 mm for the air. With a constant room temperature of 23°C, maintaining a critical flow leads to a linear relation between the flow rate and the upstream gas pressure. When the upstream (before the orifice) pressure is sufficiently larger than the downstream pressure, critical flow is achieved. For a given upstream pressure, the critical downstream pressure is the maximum pressure downstream of the orifice for which the flow is critical. Specifically,

$$\frac{P^*}{P_{up}} = \left(\frac{2}{\gamma + 1}\right)^{\frac{\gamma}{\gamma - 1}} \qquad \textbf{D.1}$$

where γ is the specific heat ratio, P^* is the critical pressure (pressure downstream of the orifice or combustion chamber pressure) and P_{up} is the upstream gas pressure.

Fixing the fuel supply pressure at 220 kPa, the upstream air pressure can be adjusted to obtain the required mixture stoichiometry. For a downstream or combustion chamber pressure of 1 atm, Table D.1 shows the specific heat ratio at 300 K and the corresponding minimum upstream pressure for each gas.

The upstream air pressure is calibrated as a function of flow rate using a rotameter from Century Flowmeter Kit, Tube Catalog No 448-324 with 0.25 inch diameter of Black CD Glass float. The flow rate is corrected to the room conditions of 23°C and 705 mmHg and plotted as a function of upstream air pressure as shown in Figure D.2. The uncertainty in the rotameter is estimated to be ±0.1 l/min.

The methane flow rate, being too low for practical rotameter application, is calibrated using the "Bubble in Burette" technique as shown in Figure D.3. The rubber ball is squeezed until the level of the bubble fluid is above the mouth of the tube through which the mixer gas passes through. The rise of the bubble through the 100 ml burette is timed to obtain the flow rate. The methane flow rate expressed as a function of upstream pressure is shown in Figure D.4. The uncertainty is about ±0.01 l/min.

The program used for tabulating the air to fuel ratios for the choked flow method based on the calibration flow rates is called Mixer.bas. A listing of the program is attached here. Mixer.bas tabulates air supply pressure for the corresponding equivalence ratio. The calibration results are listed in Table D.2. Note that for mixtures richer than 0.9 equivalence ratio and for higher pressure runs, the methane supply pressure setting has to be increased to maintain the critical flow conditions.

Table D.1 : Properties For Critical Flow At 300 K

Gas	Specific heat ratio γ	P^*/P_{up}	P_{up} for $P^*=1$ atm
Air	1.400	0.528	1.893
Methane	1.299	0.546	1.832
Propane	1.126	0.579	1.726

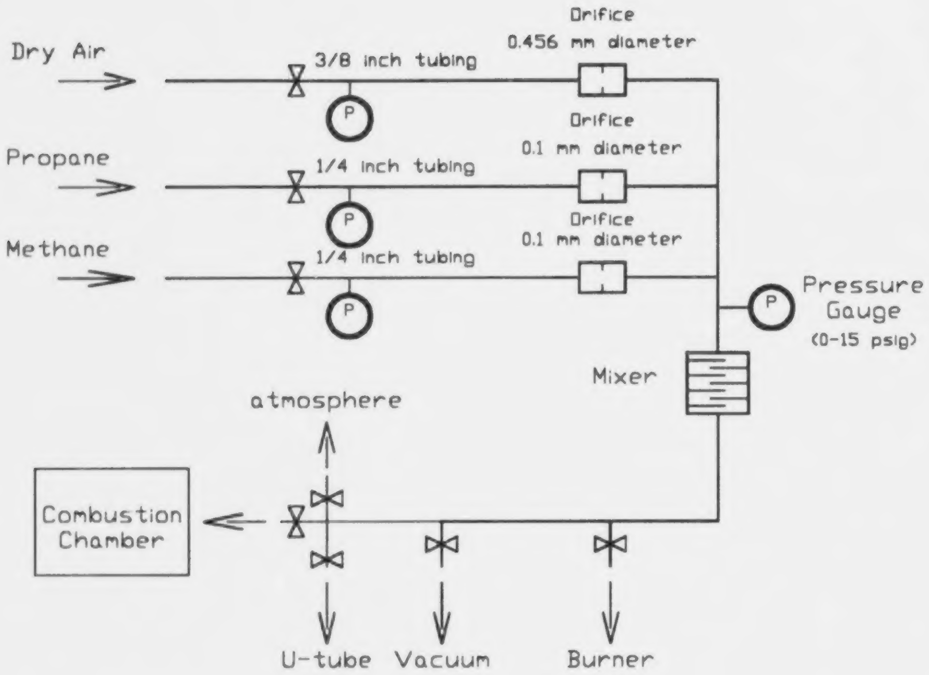
Dry Air
3/8 inch tubing
Orifice
0.456 mm diameter
Propane
1/4 inch tubing
Orifice
0.1 mm diameter
Methane
1/4 inch tubing
Orifice
0.1 mm diameter
P
Pressure Gauge
(0-15 psig)
Mixer
atmosphere
Combustion Chamber
U-tube
Vacuum
Burner

Figure D.1: The choked flow fuel-air mixer.

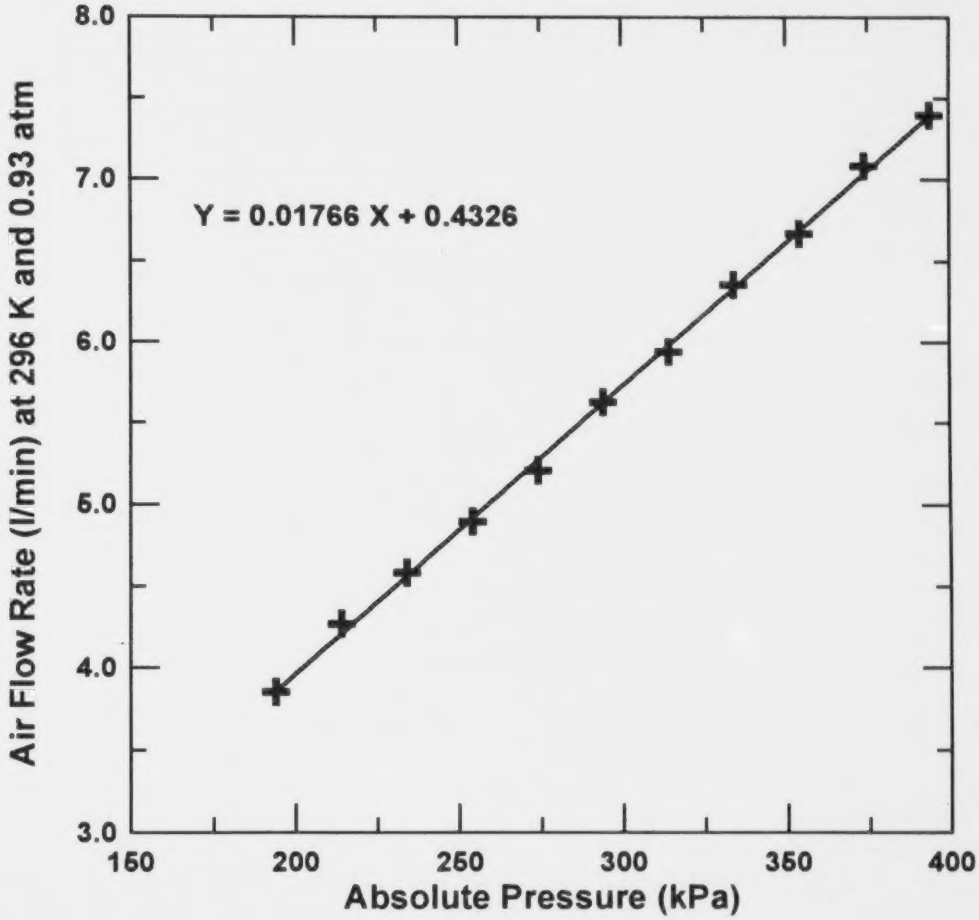

Figure D.2: Air flow rate calibration at 23°C and 705 mmHg.

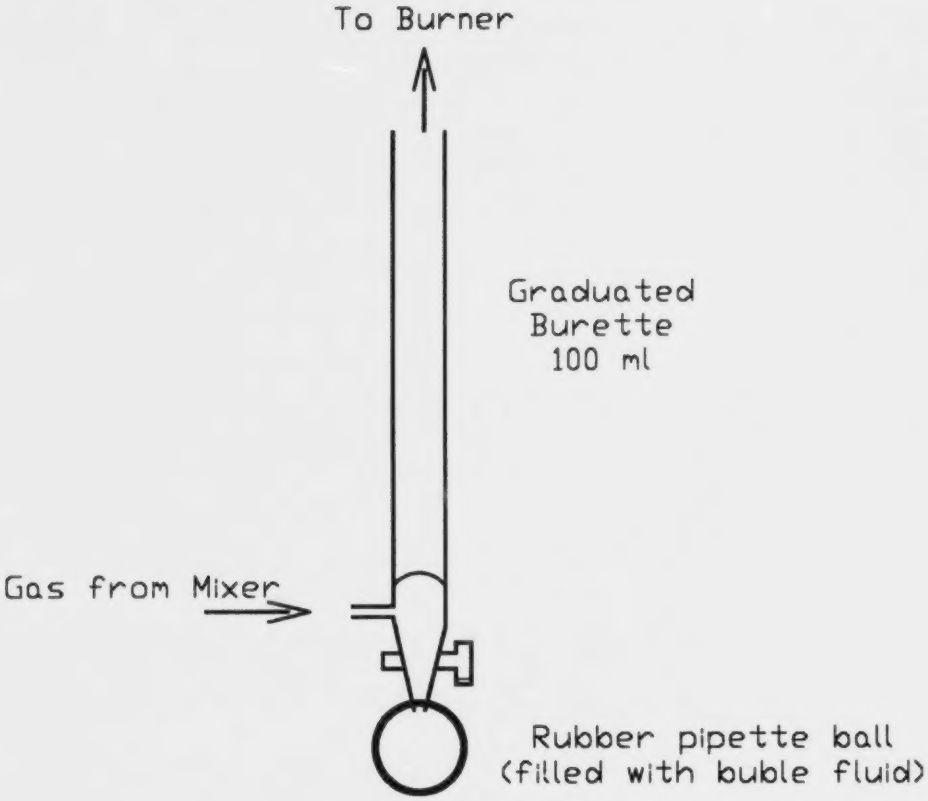
To Burner
Graduated Burette 100 ml
Gas from Mixer
Rubber pipette ball (filled with buble fluid)

Figure D.3: The bubble in burette technique.

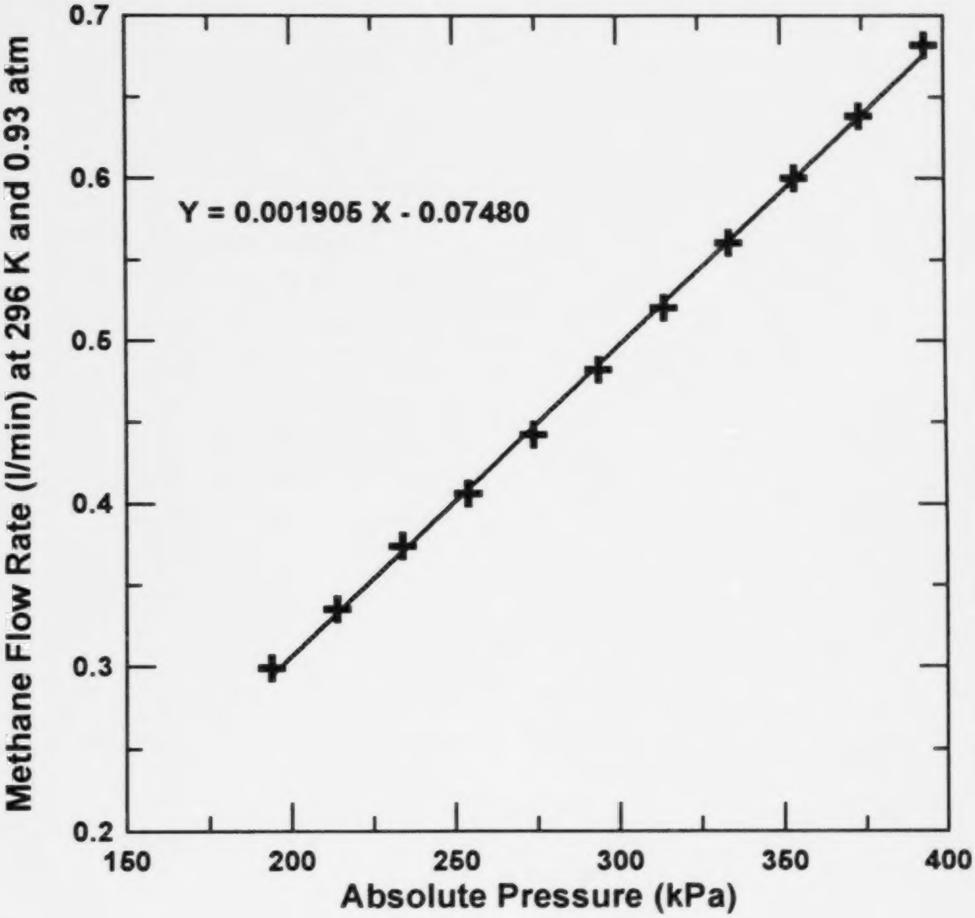

Figure D.4: Methane flow rate calibration corrected to 23°C and 705 mmHg.

```
'
'    Mixer.bas
'    *********
'
'    October 18th 1994    DSK Ting
'
' This program tabulates A/F ratios for the gas mixer based on the calibrated
' flowrates. (Based on the original Fortran Program by B. McDonell)
'
    DIM phi(11), Qair(20), AirP(20), Barom(10)

    OPEN "c:\qb\msc94\data1.dat" FOR OUTPUT AS #1
    PRINT #1, "          Table D.2 : Table of Methane Equivalence Ratios"
    PRINT #1,
    PRINT #1, "          Methane supply pressure setting at 220 kPa"
    PRINT #1,
    PRINT #1, "          stoichiometric A/F = 17.19 (mass basic)"
    PRINT #1,
' Range of barometric pressures to be considered:
    PRINT #1, "          Barometer:"
    PRINT #1, "          (mmHg)";
    FOR i = 1 TO 9
        Barom(i) = 680! + 5 * (i - 1)
        PRINT #1, USING "######"; Barom(i);
    NEXT i
    PRINT #1, : PRINT #1,
    PRINT #1, "          Equiv ratio          AIR supply pressure setting (kPag) :"
' Range of equivalence ratios to be considered:
    FOR i = 1 TO 11
        phi(i) = .5 + (i - 1) * .05
    NEXT i
' Calculate air pressures for methane using Nov 1992 calibration data
' stoichiometric A/F ratio (volume basic) for methane
    AFstoi = 9.52
    FOR i = 1 TO 11
        PRINT #1,
        PRINT #1, "          ";
        PRINT #1, USING "####.##"; phi(i);
        FOR j = 1 TO 9
            QCH4 = .001905 * (220 + .133322 * Barom(j)) - .0748
            Qair(j) = (AFstoi * QCH4) / phi(i)
            AirP(j) = (Qair(j) - .4326) / .01766 - (Barom(j) * .133322)
            PRINT #1, USING "####.#"; AirP(j);
        NEXT j
    NEXT i
END
```

Table D.2 : Table of Methane Equivalence Ratios

Methane supply pressure setting at 220 kPa

stoichiometric A/F = 17.19 (mass basic)

Barometer: (mmHg)	680	685	690	695	700	705	710	715	720
Equiv ratio	AIR supply pressure setting (kPag) :								
0.50	442.3	443.0	443.7	444.4	445.1	445.8	446.5	447.2	447.9
0.55	391.6	392.2	392.7	393.3	393.9	394.5	395.0	395.6	396.2
0.60	349.3	349.8	350.3	350.8	351.2	351.7	352.2	352.7	353.1
0.65	313.6	314.0	314.4	314.8	315.2	315.6	315.9	316.3	316.7
0.70	283.0	283.3	283.6	283.9	284.2	284.5	284.9	285.2	285.5
0.75	256.4	256.7	256.9	257.2	257.4	257.7	257.9	258.2	258.4
0.80	233.2	233.4	233.6	233.8	234.0	234.2	234.4	234.5	234.7
0.85	212.7	212.9	213.0	213.1	213.3	213.4	213.6	213.7	213.8
0.90	194.5	194.6	194.7	194.8	194.9	195.0	195.1	195.2	195.3
0.95	178.2	178.3	178.3	178.4	178.4	178.5	178.5	178.6	178.6
1.00	163.5	163.6	163.6	163.6	163.6	163.6	163.7	163.7	163.7

APPENDIX E: GAS ANAIYSIS USING MTI GAS CHROMATOGRAPH

This appendix reports the gas mixture analysis. It also describes the characteristics of the thermal conductivity gas chromatograph used.

The gas chromatograph used is a Model P200 GC manufactured by Microsensor Technology Inc. The two columns are Mol Sieve 5A and Pora Plot Q 2M. Helium of more than 99.99% purity is used as the carrier gas. The thermal conductivity detector responds to the difference in thermal conductivity between the carrier gas and the sample components eluting through the detector.

The room air is analyzed to check the accuracy and the repeatability of the gas chromatograph. All room air analysis results are obtained from Column A (Mol Sieve 5A) because Column B (Pora Plot) does not separate nitrogen, N_2 from oxygen, O_2. The two methods used are the "External Standard" method and the "Relative Volume" method. The external standard method is used when high quality external calibration gases are available. The relative volume method can be used if the corresponding gas response factors are known. All gases must separate and elute out of the column within the specified elution time when using the relative volume method. The area under a peak relative to the total area is used to calculate the relative proportion of each component.

In the external standard method the absolute areas for O_2 and N_2 peaks have repeatability uncertainty of $\pm 0.5\%$. The first analysis using the relative volume method assumes relative response factor, RRF, of unity for all gases. This leads to $21.57 \pm 0.02\%$ O_2 and $78.43 \pm 0.02\%$ N_2. The repeatability uncertainty is $\pm 0.1\%$ which is 5 times smaller than that of the external standard method.

The atmospheric air is known to consist of 21.8% O_2 (including 1% argon) and 78.2% N_2. According to [Di67, RB73], the RRF of N_2, O_2 and argon are 42, 40 and 42 respectively. With these values, fixing the RRF of N_2 at 42 leads to O_2 RRF of 41.4. The 1% argon in air which can not be separated from the O_2 has a 5% larger RRF of 42. This larger RRF argon is likely to increase the combined RRF of the 21.8% O_2 (20.8% O_2 + 1% argon) in air by the volume-weighted amount. Therefore, an alternative estimate would be a RRF of 41.2 for the 21.8% O_2 (20.8% O_2 + 1% argon) in air. With this alternative estimate, the room air analysis suggests a RRF of 41.8 for N_2. These

RRF values are within the ±3% accuracy for the RRF given in [Di67, RB73]. However, the commercial extra dry air contains no argon. Therefore, the RRF values from [Di67, RB73] may be used directly when analyzing the combustible mixtures.

E.1: THE EXTRA DRY AIR SUPPLY

All results are obtained from Column A (Mol Sieve 5A) because Column B (Pora Plot) does not separate N_2 from O_2. Only Relative Volume Method's results are presented here. With unity RRF for all gases, the extra dry air is found to made up of 21.09±0.02% O_2 and 78.91±0.02% N_2. Using RRF of 41.2 for O_2 and 41.8 for N_2, the extra dry air consists of 21.33±0.02% O_2 and 78.67±0.02% N_2.

E.2: THE METHANE SUPPLY

Column A is used to check for the presence of O_2. No O_2 is presence in the methane supply. Column B is used to analyze the methane supply compositions. Assuming unity RRF for all gases results in 0.56±0.02% N_2, 98.51±0.02% methane, 0.02± 0.01% ethane and 0.91±0.01% propylene.

The RRF values from [Di67, RB73] are 42, 36, 51 and 65 for N_2, methane, ethane and propylene respectively. With these RRF values, the methane supply is found to consist of 0.49±0.02% N_2, 99.00±0.02% methane, 0.01±0.01% ethane, and 0.50±0.01% propylene.

E.3 PARTIAL PRESSURE METHANE-AIR MIXTURE ANALYSIS

Column A is used to analyze the ratio of O_2 and N_2. Column B is used to analyze air, methane and traces of propylene. For 95% stoichiometric methane-air mixtures (9% methane and 91% air), a typical set of results is tabulated in Table E.1. The uncertainty within a prepared gas mixture is low at about ±0.3%, for example 20.00±0.05% O_2. The uncertainty due to mixing is relatively high at about ±5%, for example 10.0±0.5% methane). For this particular case, 7.54% of methane is analyzed by Column A. This is Lower than the expected 9% methane. The 10.13% methane as analyzed by Column B is higher than the expected 9% methane, if the mixture is made up of exactly 9% methane and 91% Air. It is believed that Column B gives more accurate results partly because 10.13% is closer to 9% than 7.54%.

For 50% Methane and 50% Extra Dry Air gas mixtures, a typical set of gas analysis results is tabulated in Table E.2. The uncertainty of a prepared gas mixture is low at about ±0.4%, that is, 51.0±0.2% air. The uncertainty due to mixing is relatively high at about ±2%, for example, 51±1% air. Column A gives 47.63% methane which is lower than the expected 50% (including 0.3% N_2 and 0.3% propylene). The 51% air and 49% fuel as analyzed by Column B are close to the expected values of 50% air and 50% fuel.

Table E.1: Typical results for 95% stoichiometric methane-air mixtures (9% methane and 91% extra dry air).

	Column A			Column B		
	O_2	N_2	methane	air	methane	propylene
RRF %	1 19.32	1 74.10	1 6.58	1 91.19	1 8.81	1 0
RRF %	41.2 19.35	41.8 73.12	36 7.54	42 89.87	36 10.13	65 0

Table E.2: Typical results for 50% methane and 50% extra dry air

	Column A			Column B		
	O_2	N_2	methane	air	methane	propylene
RRF %	1 11.29	1 44.72	1 43.99	1 55.10	1 44.55	1 0.35
RRF %	41.2 10.68	41.8 41.70	36 47.63	42 51.35	36 48.44	65 0.21

REFERENCES

Di67 W.A. Dietz, "Response Factors for Gas Chromatographic Analyses", Journal of Gas Chromatography, February, 1967.

RB73 D.M. Rosie and E.F. Barry, "Quantitative of Thermal Conductivity Detectors", Journal of Chromatographic Science, Vol. 11, 1973.

APPENDIX F: HIGH SPEED SCHLIEREN VIDEO

This appendix describes the high speed video camera used. It also explains the schlieren flame image analysis.

The high speed video camera used along with the schlieren system is a SP2000 Motion Analysis System. The high speed video camera is manufactured by EASTMAN KODAK COMPANY Spin Physics Division. It can record 2000, 1000, 500, 200 and 60 frames per second in full frame format. It is capable of taking up to 12000 pictures per second in partial frame format. In this study, the 2000 frames per second in full frame format is used to give the best resolution for flame image digitization. There are 192 X 238 picture elements on one picture frame. The camera scans 32 lines at one time. At 2000 frames per second, it takes 0.5/6 or 0.0833 ms to scan 32 lines.

The schlieren flame images recorded by the high speed video camera are digitized using programs developed at the University of Alberta Mechanical Engineering Department. After going through a Data Translation DT2789 Frame Grabber, the images go through PASS, AUSAVE1 and FLASH programs.

The flame area finding algorithm in the image processing program called FLASH can be described as:

1) The user selects the centre of the flame ball, which becomes an origin for the polar coordinate system used in finding the two-dimensional flame front.

2) The user then marks off two small sectors which the flame finding algorithm will omit. These sectors are selected to block out the two spark electrodes which intrude into the flame ball.

3) Then, the user marks a vertical distance of 90 mm between two horizontal, parallel lines marked on the front window of the combustion chamber. This vertical distance is used to calibrate the area of each pixel. Due to the non-unity aspect ratio of the screen and the characteristics of the video digitizing hardware, the horizontal dimension of the pixel is 4/3 times 480/512 of the vertical dimension.

4) The user then marks the inside and outside limits of the flame front. The programs assumes that the flame front is within these limits.

5) A set of rays are extracted using the user defined origin. These rays start from the outer limit to the inner limit of the flame front. The rays are taken in a counter-clockwise direction starting from 0 degree angle. The angle increment used is fixed at 0.02 radians. The rays skip the sectors marked by the user. Straight lines are assumed over the skipped sectors.

6) In each ray, the edge is found by looking for a large negative value in the derivative on the ray. The initial threshold to look for is arbitrarily set at -5.5. If the initial threshold is not found, its value will be increased by 0.5. The search is repeated until a match is found. The initial threshold and the increment value are selected based on calibration results using perfect circles of known radii.

7) The edge at each point is saved for later use.

8) When the entire flame has been covered, the screen is wiped blank. The computer-determined flame area is redrawn and filled with white pixels. The pixels are then counted, and their number multiplied by the calibration constant to give the two-dimensional flame cross-sectional area.

APPENDIX G: DATA COLLECTING AND ANALYSIS

This appendix details the procedure of data collecting and analysis. It describes the path from a four channel FM tape recorder to the burning velocity results. The QuickBasic programs used for digitization and analysis of pressure traces are attached at the end of this appendix.

The pressure rise, spark ignition, ionization, heat flux and plate motion are recorded using the 4 channel FM tape recorder. The signal recording and digitizing processes for the laminar runs are summarized in Figure G.1. The pressure trace recorded on channel 1 is used to calculate the burning velocity. Channel 2 is used to measure the maximum pressure rise for the higher pressure runs when the input range of channel 1 is inadequate. The spark ignition is recorded on channel 3 along with flame front ionization at 60 mm from the spark gap (2 mm from the top wall). The heat flux to the side wall (20 mm from an edge, centre in the vertical dimension) is recorded on channel 4.

Figure G.2 summarizes the signal recording and digitization processes for the turbulent case. All channels record the corresponding parameters similar to the laminar case except channel 2. Instead of measuring the maximum pressure rise (which for atmospheric runs can be obtained from channel 1), channel 2 is used to measure the plate motion in the turbulent case.

In both laminar and turbulent cases, the FM tape was set at 30 in/s when recording data. The RACAL wide-band option giving a low-pass filter cutoff frequency of 20 kHz was used in all tests. All four channel were calibrated from 0 to 9 V. The calibration results are summarized in Table G.1 and plotted in Figure G.3.

The path from the digitized pressure trace to burning velocity is shown in Figure G.4. The corresponding programs and procedure are described as follows.

G.1: DIGITIZATION - 4CD16G.BAS

A Metrabyte DAS16G A/D converter board is used for digitization. During digitization the replay speed is set at 1.875 in/s (16 times slower than the recording speed), while the digitization program, 4CD16G.BAS, is taking data at a rate of 4000 Hz.

Therefore, the effective digitization rate is 16 kHz on each channel. For the slower burning tests (such as 0.7 and 0.6 equivalence ratio methane-air laminar flames), the data were digitized at slower rate of 2000 Hz or 1000 Hz. As a result, the slowest effective digitization rate was 4 kHz. The effective digitization rate for all turbulence runs was 16 kHz except the 0.6 equivalence ratio methane-air turbulent runs.

All four channels and time are recorded. The actual plate speed and spark delay, time for the plate to move from the centre of the spark gap (also the centre of the combustion chamber) to spark ignition, are calculated. The plate motion is measured using optical sensors to record the passage of stirrup which is attached to the perforated plate. The plate motion is sensed by a phototransistor focused on alternating black and white markers at 10 mm intervals on the stirrup. The average plate speed from 10 mm to 110 mm is calculated. The first 10 mm of plate acceleration and the last 10 mm of plate deceleration (after hitting the damper) are omitted. This plate speed calculation is double checked with estimates from the schlieren video plate motion.

G.2: PRESSURE UNIT CONVERSION - 4CHPLT.BAS

A program called 4CHPLT.BAS is used to read the data file saved by 4CD16G.bas. It detects the spark from column 4 (channel 3 on the FM tape recorder) and set the time to zero at this point. The maximum pressure rise and the time to reach this pressure are estimated from column 3 (channel 2 on the FM tape recorder).

The pressure trace from column 3 or column 2 (channel 2 or channel 1 on the FM tape recorder) in digital unit is filtered by averaging each value with three preceding and three succeeding values. A second round of filtering uses two preceding and two succeeding values for averaging.

The filtered pressure trace in digital unit is converted to Volts and then to pressure in kPa. After plotting the pressure trace in kPa as a function of time, the pressure trace from column 2 (channel 1 on the FM tape recorder) is saved along with the time.

G.3: MULTI-ZONE THERMODYNAMICS EQUILIBRIUM MODEL

G.3.1: BOMB-A.BAS and CMBSUB.BAS

BOMB-A.bas is used along with the subroutines in CMBSUB.bas (and CMBCOM.bas) for generating the theoretical model of a propagating flame in a closed vessel. A multi-zone thermodynamic model is used. This model assumes an adiabatic combustion wave of zero flame front thickness, which propagates isotropically in the radial direction from the spark kernel.

In this multi-zone model, the premixed mixture is divided into 1500 elements of equal cross-sectional area fraction. The elements are treated as concentric spherical shells which react sequentially starting from the ignition point. All mixture elements are treated as ideal gas. During combustion of the n^{th} element, its equilibrium composition of six species is calculated. The six species considered are CO, CO_2, O_2, N_2, H_2 and H_2O. These species are from the carbon dioxide and water-gas dissociations considered.

The program starts by guessing the pressure after the n^{th} element burns. It then calculates the temperature and the specific heat ratio of the reactants assuming isentropic compression to this pressure. From these values the total unburnt volume before and after combustion of the n^{th} element is calculated. The same calculation is done on all burnt elements to find their current temperature and volume at this pressure. Then, an equilibrium calculation and energy balance are performed on the burning element. The energy balance assumes adiabatic combustion and includes the energy used by the burning element to compress all unburnt and previously burnt elements. The energy balance is:

$$Q + U_r = U_p + W_{comp} \tag{G.1}$$

where element heat transfer, Q, is assumed to be zero. U_r and U_p are the internal energy of element reactants and products. W_{comp} is the work done by the element on the other elements. This work is the sum of the work done in compressing all other elements,

$$W_{comp} = \sum \frac{(P_e V_e - P_i V_i)}{(1-\gamma)} \tag{G.2}$$

where P_e is the pressure after the element burns, V_e is the element volume after burning, P_i is the pressure before the element burns, V_i is the element volume before burning and

γ is the specific heat ratio. Using the calculated temperature and composition, the volume of the burning element is calculated after combustion. If the original pressure guess was right, the total volume of all elements is equal to the volume of the combustion chamber. If not, the pressure guess is refined and the calculation repeated until the correct pressure is found. Concurrently, the flame radius at each mass burnt increment is obtained by assuming the total burnt volume occupies a sphere of that radius.

G.3.2: BP2-93.BAS - interpolating the theoretical values onto the experimental pressure trace

The theoretical results generated by Bomb-A.bas are interpolated onto the experimental pressure trace using a program called BP2-93.bas. The pressure rise, relative flame radius, mass fraction burnt, unburnt mixture temperature and the flame temperature generated from the theoretical model are interpolated onto the experimental pressure trace. The interpolations lead to time (experiment), pressure (experiment / model), relative flame radius (model), mass fraction burnt (model), unburnt temperature (model) and flame temperature (model).

G.3.3: BV-93.BAS - calculating the burning velocity

A program called BV-93.bas is used for calculating the burning velocities from results generated by BP2-93.bas. The burning velocity is strictly defined as the velocity of flame wave relative to the unburned gas mixture in the direction normal to the flame surface.

BV-93.bas uses a geometric method for calculating the burning velocity. The geometric mean flame radius is defined as

$$r = \sqrt{\frac{r_{last}^2 + r_b^2}{2}} \qquad \text{G.3}$$

where r_{last} is the flame radius after burning the last element and r_b is the flame radius after the present element burns. Over a time interval Δt, ΔV_{ub} is the volume consumed by the flame. The flame radius before burning the present element is

$$r_i = \left[\frac{3}{4\pi}\left(\frac{4}{3}\pi r^3 + \Delta V_{ub}\right)\right]^{\frac{1}{3}} \qquad \text{G.4}$$

The burning velocity based on the geometric method is then calculated as

$$S_u = \frac{r_i - r}{\Delta t} \qquad \text{G.5}$$

where Δt is the time step.

Table G.1: FM tape recorder calibration.

Input (V)	Channel 1 0 to 4 V (unit)	Channel 2 0 to 10 V (unit)	Channel 3 0 to 10 V (unit)	Channel 4 0 to 2 V (unit)
0.347	184.4	75.43	78.78	352.3
0.803	417.8	168.1	173.5	812.2
1.309	675.6	270.8	278.7	1323
1.883	967.2	387.0	397.4	1905
2.793	1433	572.2	586.5	2030
3.505	1799	715.5	733.0	2030
3.810	1954	776.9	795.7	2030
5.132	2059	1044	1068	2029
7.060	2059	1434	1466	2030
8.583	2059	1744	1781	2029

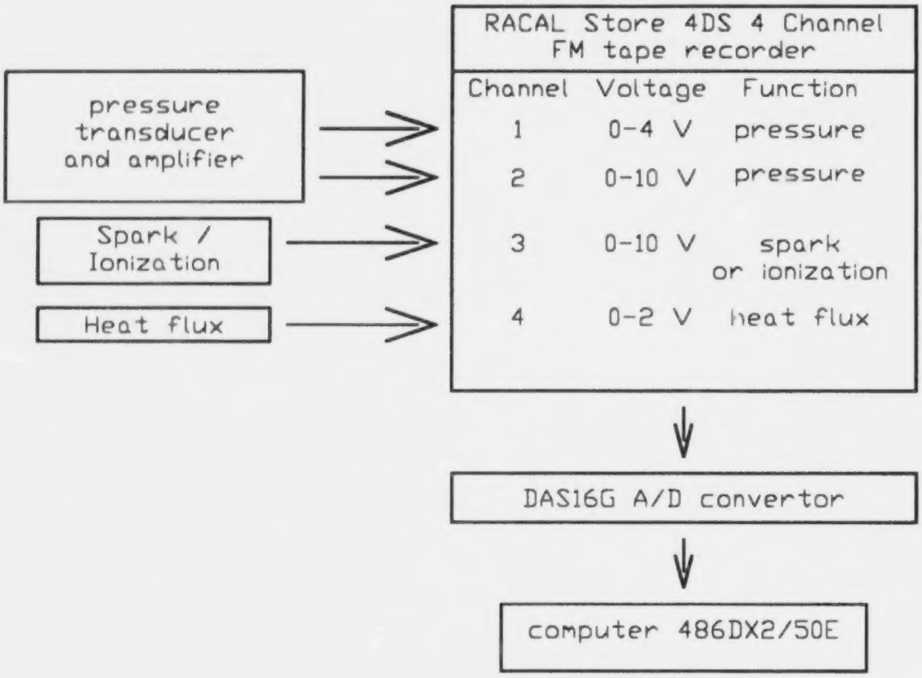
RACAL Store 4DS 4 Channel FM tape recorder
pressure transducer and amplifier
Spark / Ionization
Heat flux
DAS16G A/D convertor
computer 486DX2/50E

Channel	Voltage	Function
1	0-4 V	pressure
2	0-10 V	pressure
3	0-10 V	spark or ionization
4	0-2 V	heat flux

Figure G.1: Signal recording summary for the laminar case.

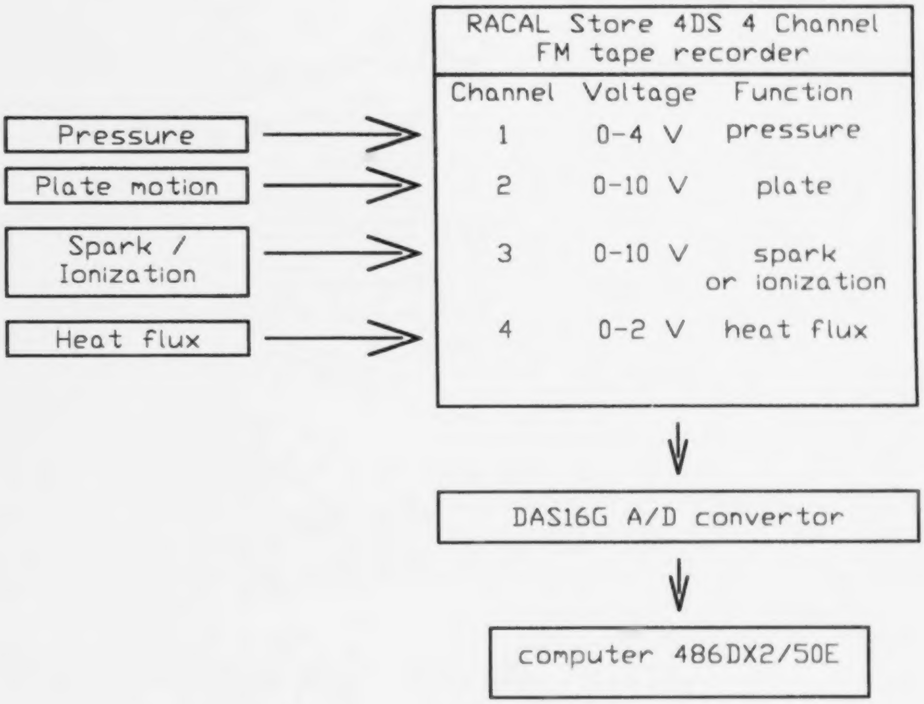
RACAL Store 4DS 4 Channel FM tape recorder
Channel
Voltage
Function
1
0-4 V
pressure
2
0-10 V
plate
3
0-10 V
spark or ionization
4
0-2 V
heat flux
Pressure
Plate motion
Spark / Ionization
Heat flux
DAS16G A/D convertor
computer 486DX2/50E

Figure G.2: Signal recording summary for the turbulent case.

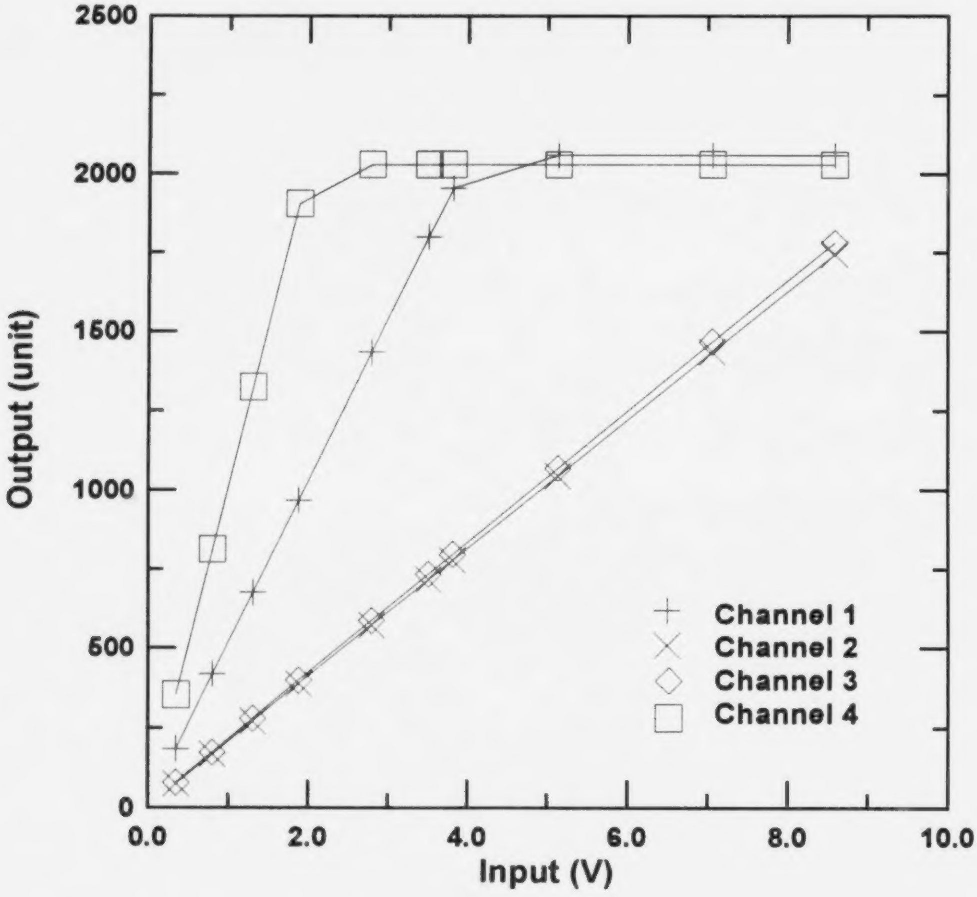

Figure G.3: The FM tape recorder calibration plots.

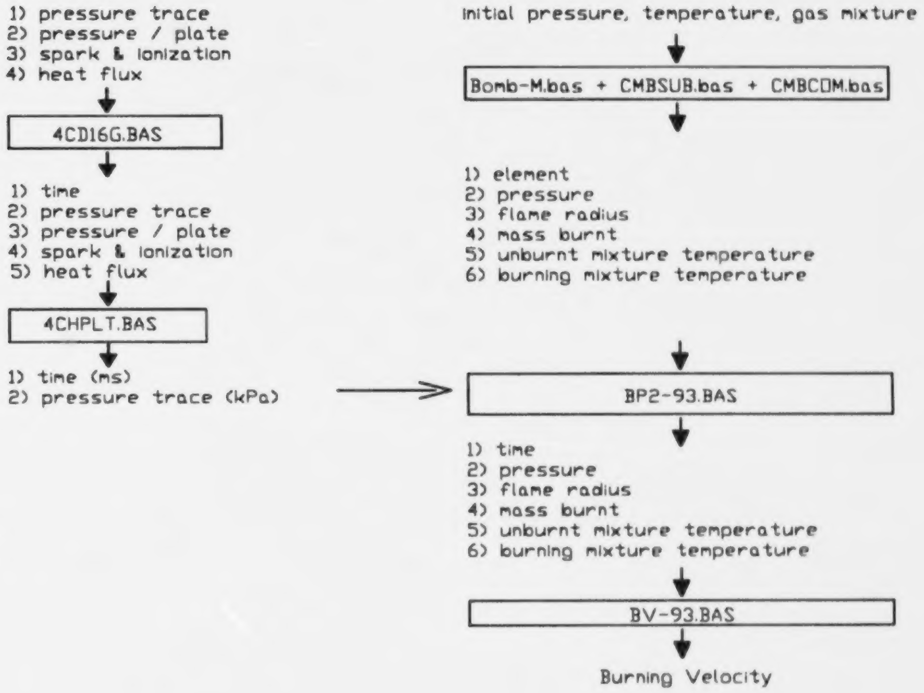
1) pressure trace
2) pressure / plate
3) spark & ionization
4) heat flux
4CD16G.BAS
1) time
2) pressure trace
3) pressure / plate
4) spark & ionization
5) heat flux
4CHPLT.BAS
1) time (ms)
2) pressure trace (kPa)
initial pressure, temperature, gas mixture
Bomb-M.bas + CMBSUB.bas + CMBCOM.bas
1) element
2) pressure
3) flame radius
4) mass burnt
5) unburnt mixture temperature
6) burning mixture temperature
BP2-93.BAS
1) time
2) pressure
3) flame radius
4) mass burnt
5) unburnt mixture temperature
6) burning mixture temperature
BV-93.BAS
Burning Velocity

Figure G.4: The path from pressure trace to burning velocity.

PROGRAM LISTING

PROGRAM 1: 4CD16G.BAS

```
DECLARE SUB dwrite (R%, c%, cm%, p%, f$, cm$(), dD!(), p!(), p$(), c1$(), c2$())
'
'    4CD16G.BAS
'    ***********
'
'    Sep-1992    DSK Ting
'
' This program uses four channels of DAS-16G board in the unipolar mode.
' It reads, de-interleaves, plots and saves data.
'

DECLARE SUB dasinit (lochan%, hichan%, gain%, freq!, flag%)
DECLARE SUB dasdma (freq!, gain%, np%)
DIM d%(40), x%(9001), dat%(9001)         ' declare data arrays
COMMON SHARED adr%, d%(), x%(), dat%()

  DIM gain(3)
' arrays for the de-interleaved data
  DIM dat1%(9001), dat2%(9001), dat3%(9001), dat4%(9001)
  gain(0) = 1: gain(1) = 10: gain(2) = 100: gain(3) = 500
' setting the # channels, gain, frequency
  lochan% = 0: hichan% = 3: gain% = 0: freq! = 4000!
  np% = 8000                         ' total # points
  n% = 1                             ' first point
  reduce = 16                        ' reduction factor

start:

' change the current setting ?
  SCREEN 9: COLOR 3, 1: CLS
  PRINT "gain = "; gain(gain%); ", freq = "; freq!; ", #points = "; np%
  INPUT "Enter=continue, 1=change gain, 2=change freq, 3=change #points >"; opt%
  IF opt% = 1 THEN
      INPUT "Gain (Enter 0=1, 1=10, 2=100, 3=500) ="; jk1
      IF jk1 = 1 OR 10 OR 100 OR 500 THEN gain% = jk1
  ELSEIF opt% = 2 THEN
      INPUT "Frequency ="; jk2
      IF 10 < jk2 < 10000 THEN freq! = jk2
  ELSEIF opt% = 3 THEN
      INPUT "total #points ="; jk3
      IF 10 < jk3 < 9001 THEN np% = jk3
  END IF

' trigger

  CLS : INPUT "Enter = trigger"; jk
  CALL dasinit(lochan%, hichan%, gain%, freq!, flag%)
  CALL dasdma(freq!, gain%, np%)

' Display the Y and X axis
  ymax = 3000
  range = np% / (hichan% + 1): CLS
  delta = range * 70 / 500: WINDOW (-delta, ymax)-(delta + range, -ymax)
  LINE (0, -ymax)-(0, ymax): LINE (0, 0)-(range, 0)
  LOCATE 1, 4: PRINT ymax: LOCATE 25, 4: PRINT -ymax;
  LOCATE 2, 10: PRINT np%; "points (total) @"; freq; " Hz, gain ="; gain(gain%)
  LOCATE 12, 6: PRINT offset: LOCATE 12, 71: PRINT offset + range
  LOCATE 14, 71: PRINT np% * 1000! / freq / reduce; "msec"
  FOR i = 1 TO 10
    LINE (i * range / 10, -ymax / 25)-(i * range / 10, ymax / 25)
  NEXT i
  COLOR 2, 1

' De-interleave, calculate and plot the four channels
  sum1 = 0: sum2 = 0: sum3 = 0: sum4 = 0
  count1 = 0: count2 = 0: count3 = 0: count4 = 0
  dt = 4 / freq! / reduce                    ' time step in sec
  FOR n = 1 TO np% - 7 STEP 4
     count1 = count1 + 1
     sum1 = sum1 + dat%(n)
     dat1%(count1) = dat%(n)
     IF n <= (hichan% + 1) THEN PSET (0, dat%(n)) ELSE LINE -(count1, dat%(n))
  NEXT n
  COLOR 3, 1
  FOR n = 2 TO np% - 6 STEP 4
     count2 = count2 + 1
     sum2 = sum2 + dat%(n)
     dat2%(count2) = dat%(n)
     IF n <= (hichan% + 1) THEN PSET (0, dat%(n)) ELSE LINE -(count2, dat%(n))
  NEXT n
  COLOR 2, 1
  FOR n = 3 TO np% - 5 STEP 4
     count3 = count3 + 1
     sum3 = sum3 + dat%(n)
     dat3%(count3) = dat%(n)
     IF n <= (hichan% + 1) THEN PSET (0, dat%(n)) ELSE LINE -(count3, dat%(n))
  NEXT n
  COLOR 3, 1
  FOR n = 4 TO np% - 4 STEP 4
     count4 = count4 + 1
     sum4 = sum4 + dat%(n)
     dat4%(count4) = dat%(n)
     IF n <= (hichan% + 1) THEN PSET (0, dat%(n)) ELSE LINE -(count4, dat%(n))
  NEXT n

' Statistics of the four channels
  mean1 = sum1 / count1
  mean2 = sum2 / count2
  mean3 = sum3 / count3
  mean4 = sum4 / count4
  sumsq1 = 0: sumsq2 = 0: sumsq3 = 0: sumsq4 = 0
  mEr1 = 0: mEr2 = 0: mEr3 = 0: mEr4 = 0
  imEr1 = 0: imEr2 = 0: imEr3 = 0: imEr4 = 0
  FOR n = 1 TO count1 - 1
     dev1 = dat1%(n) - mean1
     IF ABS(dev1) > mEr1 THEN
          mEr1 = ABS(dev1)
          imEr1 = n
     END IF
     sumsq1 = sumsq1 + dev1 * dev1

     dev2 = dat2%(n) - mean2
     IF ABS(dev2) > mEr2 THEN
          mEr2 = ABS(dev2)
          imEr2 = n
     END IF
     sumsq2 = sumsq2 + dev2 * dev2

     dev3 = dat3%(n) - mean3
    IF ABS(dev3) > mEr3 THEN
        mEr3 = ABS(dev3)
        imEr3 = n
    END IF
    sumsq3 = sumsq3 + dev3 * dev3

    dev4 = dat4%(n) - mean4
    IF ABS(dev4) > mEr4 THEN
        mEr4 = ABS(dev4)
        imEr4 = n
    END IF
    sumsq4 = sumsq4 + dev4 * dev4

  NEXT n

  rms1 = SQR(sumsq1 / count1)
  rms2 = SQR(sumsq2 / count2)
  rms3 = SQR(sumsq3 / count3)
  rms4 = SQR(sumsq4 / count4)
  LOCATE 15, 10
  PRINT "avg1 ="; mean1; " rms1 ="; rms1; " max error1 ="; mEr1; " @ point"; imEr1
  LINE (0, mean1)-(range, mean1), 11
  LOCATE 16, 10
  PRINT "avg2 ="; mean2; " rms2 ="; rms2; " max error2 ="; mEr2; " @ point"; imEr2
  LINE (0, mean2)-(range, mean2), 11
  LOCATE 17, 10
  PRINT "avg3 ="; mean3; " rms3 ="; rms3; " max error3 ="; mEr3; " @ point"; imEr3
  LINE (0, mean3)-(range, mean3), 11
  LOCATE 18, 10
  PRINT "avg4 ="; mean4; " rms4 ="; rms4; " max error4 ="; mEr4; " @ point"; imEr4
  LINE (0, mean4)-(range, mean4), 11

' Calculate the plate speed
  Vp = 0
  delay = 0
  nt% = 0
  dt = (hichan% + 1) / freq! / reduce
  FOR i = 5 TO count1 - 5
    IF dat4%(i - 1) < 600 AND dat4%(i) > 600 THEN
      IF dat4%(i - 2) < 600 AND dat4%(i + 2) > 600 THEN
        nt% = nt% + 1
        IF nt% = 1 THEN timeS = i * dt  ' passed 10 mm
        IF nt% = 6 THEN timeC = i * dt  ' passing the center
        IF nt% = 11 THEN
          timeE = i * dt                ' 10 mm left to go
          Vp = .1 / (timeE - timeS)     ' m/s
        END IF
      END IF
    END IF
    IF dat3%(i - 1) < 500 AND dat3%(i) > 500 THEN
        sparkt = i * dt                 ' spark time
        delay = (sparkt - timeC) * 1000 ' msec
    END IF
  NEXT i

  LOCATE 20, 10: PRINT "Plate speed = "; Vp; " m/s "
  LOCATE 21, 10: PRINT "Delay = "; delay; " ms "
  LOCATE 22, 10: PRINT "timeS = "; timeS; " s, timeE = "; timeE; " s "
  LOCATE 23, 10: PRINT "timeC = "; timeC; " s, sparkt = "; sparkt; " s "

' Option Keys
Options:
   LOCATE 24, 10: INPUT "Enter = Save file, 1 = Restart, 2 = Quit >"; opt%
   IF opt% > 1 THEN CLS : END
   IF opt% > 0 THEN GOTO start

' Save data
savef:
        run$ = "1"
        f$ = "C:\QB\DAS16\DATA\" + run$ + ".dat"
filename:
   CLS : PRINT "ABOUT TO WRITE TO "; f$
   INPUT "ENTER = Continue, ELSE ENTER A NEW FILE NAME. >"; fjk$
   IF fjk$ <> "" THEN
        run$ = fjk$
        f$ = "C:\QB\DAS16\DATA\" + run$ + ".dat"
        CLS
        GOTO filename
   END IF
   CLS
' Input parameters
   INPUT "Fuel = "; fuel$
   INPUT "Equivalence Ratio = "; eq
   INPUT "Turbulence intensity (m/s) = "; u
   INPUT "Plate diameter (mm)"; pD

   n% = count1 - 1
   REDIM com$(6), d!(n%, 5), par!(9), par$(9), col1$(5), col2$(5)
   com$(1) = "Recording of METRABYTE DAS-16G A/D converter board"
   com$(2) = "in GATEWAY 2000 at 50MHz"
   com$(3) = "DSK TING " + DATE$ + "   " + TIME$
   com$(4) = "data acquired by 4CD16G.BAS"
   com$(5) = "FILENAME = " + f$
   com$(6) = "Fuel = " + fuel$
   par!(1) = freq!: par$(1) = " FREQUENCY (Hz) "
   par!(2) = gain(gain%): par$(2) = " GAIN "
   par!(3) = reduce: par$(3) = " Reduction factor"
   par!(4) = (hichan% + 1) * 1000 / freq! / reduce: par$(4) = " dt (ms)"
   par!(5) = eq: par$(5) = " Equivalence ratio "
   par!(6) = pD: par$(6) = " Plate diameter (mm) "
   par!(7) = Vp: par$(7) = " Plate speed (m/s) "
   par!(8) = delay: par$(8) = " Spark delay (ms) "
   par!(9) = u: par$(9) = " Turbulence intensity (m/s) "
   col1$(1) = "  TIME": col2$(1) = " (msec) "
   col1$(2) = "CHANNEL1": col2$(2) = "integer"
   col1$(3) = "CHANNEL2": col2$(3) = "integer"
   col1$(4) = "CHANNEL3": col2$(4) = "integer"
   col1$(5) = "CHANNEL4": col2$(5) = "integer"
   FOR i = 1 TO n%
        d!(i, 1) = i * dt * 1000                ' time in msec
        d!(i, 2) = dat1%(i)
        d!(i, 3) = dat2%(i)
        d!(i, 4) = dat3%(i)
        d!(i, 5) = dat4%(i)
   NEXT i
   CALL dwrite(n%, 5, 6, 9, f$, com$(), d!(), par!(), par$(), col1$(), col2$())
   CLS : INPUT "Enter = Restart , 1 = End >"; ans%
   IF ans% = 0 THEN GOTO start

END

SUB dasdma (freq!, gain%, np%)
' COMMON SHARED adr%, d%(), x%(), dat%()
' mode 13 - write digital output OP0-3
  md% = 13
  flag% = 0
  d%(0) = 0                          ' first take it low
  CALL dasg(md%, BYVAL adr%, flag%)
  IF flag% THEN PRINT "ERROR MODE 13 (DIGITAL OUTPUT)": STOP
  PRINT "mode="; md%; " flag="; flag%

  d%(0) = 1                          ' then take it high
  CALL dasg(md%, BYVAL adr%, flag%)
  IF flag% THEN PRINT " Mode 13 (DIGITAL OUTPUT) Error #"; flag%: STOP
  PRINT "mode="; md%; " flag="; flag%

' mode 6 - do N A/D conversions and transfer to memory via DMA
  md% = 6
  memseg1% = &H7000             ' Memory segment to dump data
  d%(0) = np%                   ' Number of conversions required
  d%(1) = memseg1%                ' Number of A/D conversions
  d%(2) = 1                   ' 1 = internal trigger from timer
  d%(3) = 0                   ' 0 = One shot and finish (non-recycle)
                              ' 1 = Continuous D.M.A. (recycle) - try it!
  d%(4) = gain%
  CALL dasg(md%, BYVAL adr%, flag%)
  IF flag% <> 0 THEN PRINT " Mode 6 (DMA) Error #"; flag%: STOP
  PRINT "mode="; md%; " flag="; flag%

' mode 8 - read DMA/interrupt status

CHECSTAT: md% = 8
  CALL dasg(md%, BYVAL adr%, flag%)
  LOCATE 5, 1
  IF flag% <> 0 THEN PRINT " Mode 8 (DMA) Error #"; flag%: STOP
  PRINT "mode="; md%; " flag="; flag%
  PRINT "Word count     - "; d%(2)
  PRINT "memory segment - "; memseg1%
  IF d%(1) = 1 THEN GOTO CHECSTAT

' mode 9 - transfer data from memory to array
  md% = 9
  d%(0) = np%                   ' number of words to transfer
  d%(1) = memseg1%                ' memory segment to transfer from
  d%(2) = 0                     ' start transferring at conversion 0
  d%(3) = VARPTR(dat%(0))        ' location of DAT%(*) array
  d%(4) = 0                     ' 0 = don't recall channel information
  CALL dasg(md%, BYVAL adr%, flag%)
  IF flag% <> 0 THEN PRINT "Mode 9 (data transfer) Error"; flag%: STOP
  PRINT "mode="; md%; " flag="; flag%

END SUB

SUB dasinit (lochan%, hichan%, gain%, freq!, flag%)

' COMMON SHARED adr%, d%(), x%(), dat%()

' mode 0 - Initialization
  md% = 0
  d%(0) = &H300                       ' base I/O address
  d%(1) = 5                         ' interrupt level
  d%(2) = 1                         ' DMA level
  flag% = 0                         ' declare error variable
  adr% = VARPTR(d%(0))
  CALL dasg(md%, BYVAL adr%, flag%)     ' initialize
  IF flag% <> 0 THEN PRINT "Mode 0 (initialization) Error #"; flag%: STOP
  PRINT "mode="; md%; " flag="; flag%

' mode 17 - set programmable timer rate : SAMPLE RATE = 1000000/(d%(0)*d%(1))
  md% = 17
  d%(0) = 2
  d%(1) = 1000000! / d%(0) / freq!
  freq! = 1000000! / d%(0) / d%(1)
  CALL dasg(md%, BYVAL adr%, flag%)
  IF flag% <> 0 THEN PRINT "Mode 17 (timer) Error #"; flag%: STOP
  PRINT "mode="; md%; " flag="; flag%

' mode 1 - set multiplexer scan limits
  md% = 1
  d%(0) = lochan%                    ' lower limit
  d%(1) = hichan%                    ' upper limit
  CALL dasg(md%, BYVAL adr%, flag%)
  IF flag% <> 0 THEN PRINT "Mode 1 (scan limits) Error #"; flag%: STOP
  PRINT "mode="; md%; " flag="; flag%

END SUB

'
'  DWRITE     MD CHECKEL          7-Oct-1987
'
SUB dwrite (R%, c%, cm%, p%, f$, cm$(), dD!(), p!(), p$(), c1$(), c2$())
   '
   ' This routine writes data to standard 2-d storage
   ' files. The data includes variable #of rows, #of columns, #of comments,
   ' and #of numeric parameters as well as a string with each parameter and
   ' two strings with each column.
   '
   'The defined variables are: f$ - name of the file.
   '                    r%, c% - # of rows, # of columns
   '                    DD!(r%,c%) - numeric data array
   '                    cm% - # of comment strings in file
   '                    cm$(cm%) - comment strings in file
   '                    p% - # of numeric parameters in file
   '                    p!(p%) - numeric parameters
   '                    p$(p%) - numeric parameter strings
   '                    c1$(c%) - first column title string
   '                    c2$(c%) - second column title string
   '
32100 IF f$ = "" THEN
      PRINT SPACE$(79)
      LOCATE CSRLIN - 1, 1
      INPUT "Enter a unique OUTPUT file name >"; f$
      IF f$ = "" THEN EXIT SUB
      END IF
32110 OPEN f$ FOR APPEND AS 3
    IF LOF(3) > 0 THEN
          CLOSE #3
          PRINT SPACE$(79): PRINT SPACE$(79)
          LOCATE CSRLIN - 2, 1
          PRINT CHR$(7); " A FILE NAMED "; f$; " EXISTS NOW! "; CHR$(7)
          PRINT " Want to overwrite "; f$; "? [hit Y or N] > ";

32120       a$ = "": WHILE a$ = "": a$ = INKEY$: WEND
          IF a$ = "N" OR a$ = "n" THEN
                  f$ = "": GOTO 32100
              ELSEIF a$ <> "Y" AND a$ <> "y" THEN
                  GOTO 32120
```

```
                        END IF
                OPEN f$ FOR OUTPUT AS 3
                END IF
        'PRINT SPACE$(79)
      PRINT #3, f$
      PRINT #3, R%
      PRINT #3, c%
      PRINT #3, cm%
      PRINT #3, p%
      FOR dC% = 1 TO cm%: PRINT #3, cm$(dC%): NEXT
      FOR dC% = 1 TO p%: PRINT #3, p!(dC%): NEXT
      FOR dC% = 1 TO p%: PRINT #3, p$(dC%): NEXT
      FOR dC% = 1 TO c%: PRINT #3, c1$(dC%): NEXT
      FOR dC% = 1 TO c%: PRINT #3, c2$(dC%): NEXT
      FOR dR% = 1 TO R%
      FOR dC% = 1 TO c%: PRINT #3, dD!(dR%, dC%): NEXT: NEXT
      PRINT #3, f$
      CLOSE #3
      'LOCATE CSRLIN - 1, 1: PRINT SPACE$(79)
END SUB
```

PRPGRAM 2: 4CPLT93.BAS

```
DECLARE SUB Filter (i!(), f!(), n%, COV%)
'
'     4CPLT93.BAS
'     ************
'
'
'     September 25th 1993     DSK TING
'
' This program reads, plots and saves data from a data file generated
' by 4CD16G.BAS.
'
            REM $INCLUDE: 'C:\QB\LIB\PLOTCOM.BAS'
            REM $INCLUDE: 'C:\QB\LIB\COLORCHC.BAS'
            REM $DYNAMIC
' Dimension some arrays.
            REDIM dcom$(20), dpar$(20), dpar!(20), dd!(20, 20)
' Set up the graphics screen.
            SCRN% = 9
' Get the data file.
            DFN$ = "1"
GETFILE:
            DF$ = "C:\QB\DAS16\DATA\M-J93\" + DFN$ + ".dat"
            CLS : PRINT "Enter file name. (Enter= "; DF$; ")  >";
            INPUT DF1$
            IF DF1$ < > "" THEN
                        DFN$ = DF1$
                        GOTO GETFILE
            END IF
            GOSUB YESFILE
' Set # rows and # columns
            NROW% = DNR%
            NCOL% = DNC%
PLOTWHAT:
            CLS : INPUT "Enter column # for Y. (Enter=2) > "; coly
            IF coly = 0 THEN coly = 2
' Search the starting (SPARK) point
            FOR i = 2 TO DNR%
```

```
                IF dd!(i, 4) > 100 THEN
                        Ifirst = i + 2     'avoid the spark interference
                        GOTO Ionization
                END IF
        NEXT i
Ionization:
        ITime = 0
        FOR i% = Ifirst + 30 TO DNR%
                IF dd!(i%, 4) > 50 THEN
                        Ion% = i% - Ifirst
                        ITime = Ion% * (dd!(11, 1) - dd!(10, 1))
                        GOTO Startloop
                END IF
        NEXT i%
Startloop:
' Read Y and X data.
        n% = DNR% - Ifirst - 1
        REDIM X(n%), Y(n%)
        FOR i = 1 TO n%
                X(i) = dd!(i + Ifirst, 1) - dd!(Ifirst, 1)
                Y(i) = dd!(i + Ifirst, coly)
' Eliminate sparks caused by noise
                IF i > 3 THEN
                        IF Y(i) > 1.3 * Y(i - 1) OR Y(i) < .7 * Y(i - 1) THEN
                                Y(i) = Y(i - 1)
                        END IF
                END IF
        NEXT i
'
IF coly > 3 THEN GOTO Plotting
' Filter Y(i) to smooth it out.
'
        REDIM XYF(n%)
        NUMFILT = 0
        NCOV% = 4
FILTER1:
        IF NUMFILT < 2 THEN
                CALL Filter(Y(), XYF(), n%, NCOV%)
                FOR i = 4 TO n% - 4
                        Y(i) = XYF(i)
                NEXT i
                NUMFILT = NUMFILT + 1
                NCOV% = NCOV% - 1
                GOTO FILTER1
        END IF

' ********************Change to suit********************
' Convert pressure from digital unit to V and then to kPa
        IF coly = 2 THEN
                FOR i = 1 TO n%
                        Y(i) = .00195631# * Y(i) - .0122672#
                NEXT i
        ELSEIF coly = 3 THEN
                FOR i = 1 TO n%
                        Y(i) = .00493958# * Y(i) - .0280377
                NEXT i
        END IF
'
        PRINT "Initial pressure (V) = "; Y(5); " V"
        INPUT "Okay ? (Enter = Yes/Continue, 2 = No/Stop)"; ok%
        IF ok% <> 0 THEN STOP
' For P<200 kPa,
'  Y(kPa) = 1037.7 (X(V)) ^ 3 - 4186.21 (X(V)) ^ 2 + 5880.95 X(V) - 2605.77
'
' For P= >200 kPa,
'  Y(kPa) = 299.46 * X(V) + b1!

          PRINT "Initial pressure in kPa"
          INPUT "0=101.325 kPa, 1=151.988 kPa, 2=202.65 kPa, 3=50.66 kPa"; NPinit%
          IF NPinit% = 1 THEN
                    Pinit! = 151.988
                    Volt0 = 1.044
          ELSEIF NPinit% = 2 THEN
                    Pinit! = 202.65
          ELSEIF NPinit% = 3 THEN
                    Pinit! = 50.66
                    Volt0 = .898
          ELSE
                    Pinit! = 101.325
                    Volt0 = .963
          END IF
          ppt% = 4
          b0! = (Y(ppt%) + Y(ppt% + 1) + Y(ppt% + 2) + Y(ppt% + 3)) / 4
          PRINT "Initial pressure (V) = "; b0!

          Y(1) = Pinit!: flag% = 1
          FOR i = 2 TO n%
                    IF Y(i - 1) < 200 AND Pinit! < 200 THEN
                              Volt! = Y(i) - b0! + Volt0
                              Ytemp = 1037.7 * Volt! ^ 3 - 4186.21 * Volt! ^ 2
                              Y(i) = Ytemp + 5880.95 * Volt! - 2605.77
                    ELSE
                              IF flag% < 2 THEN b! = Y(i - 1) - 299.46 * (Y(i + 1) + Y(i + 2)) / 2
                              flag% = 3
                              Y(i) = 299.46 * Y(i) + b!
                    END IF
          NEXT i
' Filter Y(i) to smooth it out.
'
          REDIM XYF(n%)
          NUMFILT = 0
          NCOV% = 5
FILTER2:
          IF NUMFILT < 3 THEN
                    CALL Filter(Y(), XYF(), n%, NCOV%)
                    FOR i = 5 TO n% - 5
                              Y(i) = XYF(i)
                    NEXT i
                    NUMFILT = NUMFILT + 1
                    NCOV% = NCOV% - 1
                    GOTO FILTER2
          END IF
'
          Pjk = (Y(5) + Y(6)) / 2!
          PRINT "Initial pressure (kPa) = "; Pjk; " kPa"
          INPUT "Okay ? (Enter = Yes/Continue, 2 = No/Stop)"; ok2%
          IF ok2% < > 0 THEN STOP
' Maximum pressure rise (kPa)
          IF coly = 2 OR coly = 3 THEN
                    Pmax = 0
                    FOR i = 2 TO n% - 3
                              Yavg = (Y(i - 1) + Y(i) + Y(i + 1)) / 3!
                              IF Yavg > Pmax THEN
                                        Pmax = Yavg         ' Pmax (kPa)
```

```
                                tPmax = X(i)        ' Time at Pmax (ms)
                                iPmax% = i
                        END IF
                NEXT i
        END IF
Plotting:
'--------------------
' Data plotting section.
PLOTSECTION:
        XLB$ = "Time (msec)"
        YLB$ = "P (kPa)"
        SCREEN 0: WIDTH 80: COLOR 15, 1
        CLS : PRINT "Plotting"
        INDAX% = 0: XSUB% = 0: YSUB% = 0
        CALL AXES(X(), Y(), n%, XSUB%, YSUB%, Xmn, Xmx, Xdv, NXS%, Ymn, Ymx, Ydv, NYS%)
        Ymn = 0: Ydv = 200: Ymx = 1000
        Xmn = 0!: Xdv = 10: Xmx = 120
'
LINETYPE:
        LIN% = 1
        CHAR% = 0
        CALL PINI(SCRN%, 1): c% = ngc%
        CALL YAXIS(Ymn, Ymx, Ydv, YSUB%, NYSUBD%, YLB$, Y2$, Y3$, c%)
        CALL XAXIS(Xmn, Xmx, Xdv, XSUB%, NXSUBD%, XLB$, c%)
'
PLOTMORE:
        CALL LINPLT(X(), Y(), n%, CHAR%, 1, 6!, c%)
        LOCATE 3, 15: PRINT " File " + DF$
        LOCATE 5, 14: PRINT USING " Pmax =##### kPa"; Pmax
        LOCATE 5, 34: PRINT USING " at ### ms after spark"; tPmax
        LOCATE 6, 14: PRINT USING " Ionization at ### ms after spark"; ITime
'-----------------------
' Finished plots, now what?
'
OPTIONS:
         LOCATE 1, 1
         INPUT " 0=hard copy, 1=quit, 2=restart, 3=change Y, 4=save >"; opt
         IF opt = 4 THEN GOTO SAVE
         IF opt = 3 THEN GOTO PLOTWHAT
         IF opt = 2 THEN GOTO GETFILE
         IF opt = 1 THEN SCREEN 0: COLOR 15, 1: CLS : END
         IF opt = 0 THEN CALL PHCOPY(xyz$)
'
SAVE:
                SFN$ = DFN$
                SF$ = "C:\QB\DAS16\CDATA\M-J93\" + SFN$ + ".dat"
filename:
                CLS : PRINT "ABOUT TO WRITE TO "; SF$
                INPUT "ENTER = GO ON, ELSE ENTER A NEW FILE NAME.>"; SFN1$
                IF SFN1$ <> "" THEN
                                SFN$ = SFN1$
                                SF$ = "C:\QB\DAS16\CDATA\M-J93\" + SFN$ + ".dat"
                                GOTO filename
                END IF
'
                npt% = iPmax% - 1
                INPUT "Input # points (Enter = Auto)"; pt%
                IF pt% > 0 THEN npt% = pt%
                fuel$ = "Methane"
                INPUT "Fuel (Enter = Methane)"; fuel1$
                IF fuel1$ <> "" THEN fuel$ = fuel1$
                PRINT "Pmax = "; Pmax; " kPa, at tPmax = "; tPmax; " ms"
                INPUT "Maximum Pressure (Enter=Pmax)"; Pmaxjk
                IF Pmaxjk > 0 THEN Pmax = Pmaxjk
                INPUT "Time at Maximum Pressure (Enter=tPmax)"; tPmaxjk
                IF tPmaxjk > 0 THEN tPmax = tPmaxjk
                dt = X(11) - X(10)
                PRINT "t(n+1) - t(n) = "; dt; " msec "; " dt ="; dpar!(4); "msec"
                INPUT "Okay ? (Enter = Yes/Continue, 2 = No/Stop)"; ok3%
                IF ok3% <> 0 THEN STOP

                REDIM com$(6), d!(npt%, 2), par!(12), par$(12), col1$(2), col2$(2)
                FOR i = 1 TO npt%
                                d!(i, 1) = X(i)          'time in msec
                                d!(i, 2) = Y(i)          'P in kPa
                NEXT i
                com$(1) = "RECORDING THE EXPERIMENTAL PRESSURE TRACE"
                com$(2) = "DSK TING " + DATE$ + " AT " + TIME$
                com$(3) = "DATA ACQUIRED BY 4CPlt93.BAS"
                com$(4) = "FILENAME = " + SF$
                com$(5) = "Fuel = " + fuel$
                com$(6) = ""
                par!(1) = dpar!(1): par$(1) = " FREQUENCY (Hz) "
                par!(2) = dpar!(2): par$(2) = " Gain "
                par!(3) = dpar!(3): par$(3) = " Reduction Factor for Replay "
                par!(4) = dpar!(4): par$(4) = " dt (msec) "
                par!(5) = dpar!(5): par$(5) = " Equivalence Ratio "
                par!(6) = dpar!(6): par$(6) = " Plate Diameter (mm) "
                par!(7) = dpar!(7): par$(7) = " Plate Speed (m/s) "
                par!(8) = dpar!(8): par$(8) = " Spark Delay (ms) "
                par!(9) = dpar!(9): par$(9) = " Turbulence Intensity (# or m/s) "
                par!(10) = Pmax: par$(10) = " Maximum Pressure (kPa) "
                par!(11) = tPmax: par$(11) = " Time at Pmax (ms) "
                par!(12) = ITime: par$(12) = " Ionization Time (ms) "
                col1$(1) = "  TIME": col2$(1) = "(msec)"
                col1$(2) = " PRESS": col2$(2) = "   kPa"
                CALL dwrite(npt%, 2, 6, 12, SF$, com$(), d!(), par!(), par$(), col1$(), col2$())
                CLS : GOTO OPTIONS
'============================================================
================
' Subroutine YESFILE
'
' File reading subroutine.
'
YESFILE:
        CALL DDIM(DNR%, DNC%, DNCOM%, dnpar%, DF$, TITLE$)
        REDIM dcom$(DNCOM%), dpar$(dnpar%), dpar!(dnpar%), dd!(DNR%, DNC%)
        REDIM DCOL1$(DNC%), DCOL2$(DNC%)
        CALL DREAD(DNR%, DNC%, DNCOM%, dnpar%, DF$, dcom$(), dd!(), dpar!(), dpar$(), DCOL1$(), DCOL2$())
RETURN
'============================================================
================

REM $STATIC
SUB Filter (i(), f(), n%, COV%)
'
'

' THIS IS A SIMPLE AVERAGING LOW PASS FILTER.
' It makes each point of F equal to an average of all points within +/- cov%
' of the same point in the input array, I.
'
'

        IF COV% <= 0 THEN COV% = 4
        FOR i% = 1 TO n%
        SUM = i(i%)
                      FOR j% = 1 TO COV%
                                    m% = i% - j%
                                    IF m% > 0 THEN
                                            m = i(m%)
                                            ELSE
                                            m = i(1)
                                    END IF
                                    P% = i% + j%
                                    IF P% <= n% THEN
                                            P = i(P%)
                                            ELSE
                                            P = 2 * i!(n%) - i(n% + n% - P%)
                                    END IF
                                    SUM = SUM + m + P
                      NEXT j%
        f(i%) = SUM / (2 * COV% + 1)
        NEXT i%

END SUB
```

PROGRAM 3: BOMB-A.BAS

```
DECLARE SUB EQCONST ()
DECLARE SUB FLAME (IND!, Q!, W!, Pe!, FCA!, FHA!, FMW!, S!, Tr!, t!, MWR!, MWP!, FLAG%)
DECLARE SUB PROPCOEFF ()
DECLARE SUB REACTPROP (Equiv!, FCA!, FHA!, FMW!, MF!, MOXY#, MN2#, MWR!)
'
'     BOMB-A.BAS
'     **********
'
'     August 11th 1993      D.S-K. TING
'
' NOTE:  After any major alteration, update the above list.
'---------------------------------------------------------------------
' Based on BOMB.BAS by Alun Thomas.
'
'---------------------------------------------------------------------
' This program is used in conjunction with the program BP2-92.bas which uses
' measured pressure record and combines it with the calculated quantities
' from this program.  For most properties, a simple interpolation is used to
' match measured pressures with corresponding values from this program.  (See
' BP2-92.bas for more information.)
' By itself, this program calculates fates of elements of lean fuel-air
' mixtures at specified starting conditions, burning in a constant volume
' combustion cell.
' ******************************************************
' *elements are of equal initial unburnt radius square*
' *    i.e. dr(before ignition)^2 = constant           *
' ******************************************************
' The subroutines that are called in the CMBSUB.BAS subroutine file are
' fairly well tested and proven.
' Read CMBSUB.DOC for in understanding the program and subroutines.
'
' Thermodynamic properties and methods are used as described in:
'                 Rowland S. Benson,
'                 "Advanced Engineering Thermodynamics"
'                 Pergammon Press, 1977, 2nd Edition
'
'---------------------------------------------------------------------
' Include common statements and routines, then dimension some variables.
```

```
'
                REM $INCLUDE: 'C:\QB\COMB\CMBCOM.BAS'
                REM $INCLUDE: 'C:\QB\LIB\PLOTCOM.BAS'
                REM $INCLUDE: 'C:\QB\LIB\COLORCHC.BAS'
                REM $INCLUDE: 'C:\QB\COMB\CMBFN-RP.BAS'
                REM $DYNAMIC
'
                VERDAT$ = "August-93"
'
                REDIM IC(8, 7), I$(8), CC(6), CW(6), R(7), P(7), M#(6), W(8)
                REDIM Fuel$(2)
                DIM STORE(1400, 11)
'
' These are the INSCRN variables.
'
                x% = 5
                REDIM D$(x%), t%(x%), P$(x%), LG%(x%), L%(x%), c%(x%)
                REDIM IP$(x%), IP%(x%), IP!(x%), IP#(x%)
'-----------------------------------------------------------------
' Set up some constants.
'
                rmol = 8314.3           'ideal gas constant in J/kmol.K
'
' The subroutine PROPCOEFF fills an array with coefficients used in
' calculating enthalpy and Gibbs function for CO, CO2, H2, H2O, N2, O2,
' and fuel.  (See CMBSUB for details.)
' I$() is the alphanumeric name.
' W() is the molecular weight.
' IC() is the coefficient array.
'
                CALL PROPCOEFF
'
' The subroutine EQCONST calculates chemical equilibrium constants used
' for CO2 and CO2-H2O dissociation reactions.  The IC() array is used for
' this.  (See CMBSUB for details.)
'
                CALL EQCONST
'
'-----------------------------------------------------------------
' Get run type and set the cell volume and fuel type.
' Vtot is the bomb volume in m^3.
' FUEL% is an integer constant to indicate which fuel is present.
' FUEL$() contains the alphanumeric fuel names.
'
RUNTYPE:
                Vtot = .001882: Fuel% = 2
                Fuel$(1) = "C3H8"
                Fuel$(2) = " CH4"

'-----------------------------------------------------------------
' Enter initial conditions and number of volume elements to work on.
'
                Tinit = 293.15          ' pre-combustion temperature in K
                Pinit = 101325          ' pre-combustion pressure in Pa
                Equiv = .95             ' equivalence ratio
'
'-----------------------------------------------------------------
' Print a bit of a header and verify some parameters with user.
'
INPUTSECTION:
         COLOR 10, 1: PRINT
         PRINT "BOMB-R.bas "
```

```
        PRINT
        PRINT "Ting version of "; VERDAT$; ", run at "; TIME$; " on "; DATE$
'
        D$(1) = STR$(Vtot): t%(1) = 1: LG%(1) = 9: L%(1) = 12: c%(1) = 10
        P$(1) = "Enter volume of bomb in m3 (0=" + D$(1) + ") >"
        D$(2) = STR$(Tinit): t%(2) = 1: LG%(2) = 7: L%(2) = 14: c%(2) = 10
        P$(2) = "Enter initial temperature  (0=" + D$(2) + ") >"
        D$(3) = STR$(Pinit): t%(3) = 1: LG%(3) = 15: L%(3) = 16: c%(3) = 10
        P$(3) = "Enter initial pressure in Pa (0=" + D$(3) + ") >"
        D$(4) = STR$(Equiv): t%(4) = 1: LG%(4) = 7: L%(4) = 18: c%(4) = 10
        P$(4) = "Enter equivalence ratio (0<E<=1), (0=" + D$(4) + ") >"
        D$(5) = STR$(Fuel%): t%(5) = 0: LG%(5) = 3: L%(5) = 20: c%(5) = 10
        P$(5) = "Enter FUEL code (1=propane, 2=methane; default="
        P$(5) = P$(5) + D$(5) + ") >"
'
        CALL inscrn(5, 1, t%(), P$(), LG%(), D$(), L%(), c%(), IP$(), IP%(), IP!(), IP#(), FX$)
'
'--------------------------------------------------------------------
' Echo back some of the initial parameters for the user.
'
        CLS
        PRINT "INPUT VALUES:"
        PRINT
        IF IP!(1) > 0 THEN Vtot = IP!(1)
        PRINT "Bomb Volume is "; Vtot; " m^3"
        Rbomb = (.75 * Vtot / 3.141592654#) ^ (1! / 3!)
        IF IP!(2) > 0 THEN Tinit = IP!(2)
        PRINT "Initial Temperature is "; Tinit; " K"
        IF IP!(3) > 0 THEN Pinit = IP!(3)
        PRINT "Initial Pressure is "; Pinit; " Pa"
        IF IP!(4) > 0 AND IP!(4) <= 1 THEN Equiv = IP!(4)
        IF Fuel% = 1 THEN AFRSTOIC = 15.5797 ELSE AFRSTOIC = 17.12
        AFR = AFRSTOIC / Equiv
        PRINT USING "Equivalence ratio is #.###  (A/F=##.#)"; Equiv; AFR
'
GETN:
                Ntot% = 1500            '1500 elements
                Nb% = 500               '500 elements to burn
                PRINT "Total #elements (equally spaced in radius) = 1500"
                INPUT "Enter = go on, Else enter total #elements. >"; Njk
                IF Njk > 0 AND Njk < 1501 THEN Ntot% = Njk

                INPUT "#elements to burn (Default=500). >"; Nbjk
                IF Nbjk > 0 AND Nbjk < Ntot% THEN Nb% = Nbjk

'--------------------------------------------------------------------
' Get some of the fuel properties from the FUELSORT subroutine.
' This routine is attached to the bottom of this program.
' (Returns FCA, FHA, and FMW.)
'
                GOSUB FUELSORT
'
'$-----------------------------------------------------------------$
' MAIN LOOP:
'
' SELECT ELEMENT FOR PROCESSING - will burn Nb% elements
'
' REACTPROP determines the reactant properties (See CMBSUB).
' MPR = kmol of fuel / element
'
                CALL REACTPROP(Equiv, FCA, FHA, FMW, MF, MOXY#, MN2#, MWR)
                GMR = fngamR(Tinit)
```

```
                    Mass = MWR * Pinit * Vtot / rmol / Tinit
                    PRINT "Initial mass is: "; Mass; "  (MWR="; MWR; ")"
'
' Everything from here until the end of the loop is repeated Nb% times.
'
        FOR I% = 1 TO Nb%
'
                    dVRatio = (I% ^ (3 / 2) - (I% - 1) ^ (3 / 2)) / Ntot% ^ (3 / 2)
                    MPR = Mass * dVRatio / MWR / (MF + MOXY# + MN2#)
'
' Pressure before burning element I% is set to Pinit if I%=1 or to Pe,
' the pressure after burning the last element, if I% is greater than 1.
' Pi is the initial pressure of the element (not to be confused with Pinit).
'
                    IF I% = 1 THEN
                                                Pi = Pinit
                    ELSE
                                                Pi = Pe
                    END IF
'
' Estimate P after next element burns.
' Pe is the end pressure for the element which is just a guess now.
'
                    Pe = Pi + Equiv / Ntot% ^ (3 / 2) * Pinit
'
' Flag = 0 => P is only a guess.
'
                    IFLP = 0
'
' Treactants and GAMMAreactants are evaluated for this Pi.
'
                    Tr = Tinit * (Pi / Pinit) ^ ((GMR - 1) / GMR)
                    GMR = fngamR(Tr)
'
CALCVOLUMES:
'
' This section now calculates the volume of the remaining unburnts before and
' after combustion of this element. The work done to compress the unburnts is
' evaluated and then a loop adds the work done to compress each previously
' burned element.!If the correct pressure has been selected, the work done on
' all elements will equal the work done by the burning element during its
' combustion and expansion...ie it will match the difference between internal
' energy of that element before and after combustion. When this happens, the
' selected pressure will be the correct pressure after this element burns.
'
' If the correct pressure is guessed, the sum of the volumes will equal the
' total volume.
'
' Vub is the total volume of all the unburnt gases in m^3 BEFORE combustion
' of the I%th element (excludes the I%th element).
' Vua is the total volume of all the unburnt gases in m^3 AFTER combustion
' of the I%th element.
'
                    VuRatio = 1 - (I% / Ntot%) ^ (3 / 2)
                    Vub = Vtot * VuRatio * (Pinit / Pi) ^ (1 / GMR)
                    Vua = Vub * (Pi / Pe) ^ (1 / GMR)
'
' Calculate the work of compression  (Vub -> Vua) on unburnt elements in J.
' nagative => work done By the burning element
                    Wu = -(Pe * Vua - Pi * Vub) / (1 - GMR)
'
' Volume sum and work sum are set equal to the volume of unburned gas and
' work done to compress the unburned gas in m^3 and joules respectively.
'
                sumW = Wu
'
' If there are previously burned elements, calculate the volume of each before
' and after compression to new pressure, Pe. Then calculate the work done to
' compress each one and add it to the work sum done by the burning element.
'
' Vb is the volume of the Jth element before compression.
' Va is the volume of the Jth element after compression.
' Wb is the compression work of the Jth element in Joules.
' sumVba is the volume of the burnt gases after combustion of element I%.
'
' STORE(J,4) is the volume of the Jth element after combustion.
' STORE(J,1) is the pressure of the Jth element after combustion.
' STORE(J,10) is the specific heat ratio of products in element J. (fngamP(T))
'
                        IF I% > 1 THEN
                                       sumVba = 0!
                                       FOR J = 1 TO I% - 1
                                                Vb = STORE(J, 4) * (STORE(J, 1) / Pi) ^ (1 / STORE(J, 10))
                                                Va = STORE(J, 4) * (STORE(J, 1) / Pe) ^ (1 / STORE(J, 10))
                                                Wb = -(Pe * Va - Pi * Vb) / (1 - STORE(J, 10))
                                                'negative => work done By the burning element
                                                sumVba = sumVba + Va
                                                sumW = sumW + Wb
                                       NEXT J
                        END IF
                        sumV = Vua + sumVba
                        sumW2 = sumW
'
' Use subroutine FLAME to find the temperature of combustion of the burning
' element knowing its starting conditions and work output, sumW.
'
                        works = sumW / MPR             ' J/(kmol of fuel/element)
                        CALL FLAME(1, 0, works, Pe, FCA, FHA, FMW, Equiv, Tr, t, MWR, MWP, FLAG%)
'
' Calculate the volume this element would have if it burned to temperature T
' at pressure Pe. (molP is number of moles of products per mole of fuel, molR
' is moles of reactants per mole of fuel.  Hence Ve is in m^3 like V).
'
                        Ve = Vtot * dVRatio * Pinit / Pe * t / Tinit * molP / molR
'
' Compare this with volume left over from unburned gas and all previous burned
' elements at this pressure, Pe.
'
                        ErV = Ve - (Vtot - sumV)
'
' If the error is greater than .01%, then make a new estimate of pressure
' and go back to try again.
'
                        ErrLim = Ve * .0001
                        IF Pi < 1.1 * Pinit THEN ErrLim = Ve * .001
                        IF Pi > 2.5 * Pinit THEN ErrLim = Ve * .0002
                        IF ABS(ErV) > ErrLim THEN
'
' IFLP is a flag which determines whether a previous estimate has been made.
' If it has, extrapolate/interpolate to get a new estimate.
' Otherwise, simply make a small step in pressure.
'
                                       IF IFLP > 0 THEN
                                                Pe3 = (Pe * ErV1 - Pe1 * ErV) / (ErV1 - ErV)
```

```
                                                         Pe1 = Pe
                                                         Pe = Pe3
                                              ELSE
                                                         Pe1 = Pe
                                                         IFLP = 1
                                                         IF ErV > 0 THEN
                                                                          Pe = Pi + 1.2 * (Pe - Pi)
                                                         ELSE
                                                                          Pe = Pe + (Pe - Pi) / 1.2
                                                         END IF
                                              END IF
'
' Having established this estimate for pressure after combustion,
' record the current volume error and go back to re-calculate the
' volumes and compression work with the new pressure value.
'
                                              ErV1 = ErV
                                              GOTO CALCVOLUMES
                            END IF
'
' Calculation of volumes having converged, enter values for the I%th element
' into the storage array STORE.
'
         STORE(I%, 1) = Pe              'pressure after element I% burnt
         rR = ((Vtot - Vua) / Vtot) ^ (1 / 3)
         STORE(I%, 2) = rR              'relative flame radius after element I% burnt
         orR = (I% / Ntot%)             'relative radius before ignition
         STORE(I%, 3) = (I% / Ntot%) ^ (3 / 2)
                                                                                                      'mass fraction
burnt
         STORE(I%, 4) = Ve              'volume of element after combustion
         STORE(I%, 5) = Vub             'unburned volume before element has burned
         STORE(I%, 6) = Vua             'unburned volume after element has burned
         STORE(I%, 7) = Tr              'temperature of the reactants
         STORE(I%, 8) = t               'temperature of element after combustion
         STORE(I%, 9) = fngamR(Tr)      'specific heat ratio of reactants (element I%)
         STORE(I%, 10) = fngamP(t)      'specific heat ratio of products (element I%)
         STORE(I%, 11) = MWP            'molecular weight of products
'
'
' Print out a running listing to let the user know the progress of the
' calculations that are going on.
'
PRINT USING "###/####: P=######Pa, Tb=####k, r/R=#.### "; I%; Ntot%; Pe; t; rR
'
' The total work done is summed in order to compare this program with
' STANJAN.  (ie internal energy change = work done)
'
                            totW = totW + sumW2
                            PRINT "TOTAL WORK DONE IS "; totW
'
          NEXT I%
'
' This is the end of the main loop.
'$--------------------------------------------------------------$
' Make a warbling sound to notify user that the calculations are done.
'
                   FOR NSOUND = 1 TO 20
                                              FREQ = 100 + 10 * NSOUND ^ 2
                                              SOUND FREQ, 1
                   NEXT NSOUND
```

```
'--------------------------------------------------------------------
' Pause before going on.
'
                        INPUT "Pause. Enter = continue >"; jk

'--------------------------------------------------------------------
' Prepare all data for writing to data file.
'
            NR% = Nb%
            NC% = 6
            NCom% = 2
            NPar% = 6
            REDIM DD(NR%, NC%), COM$(NCom%), PAR(NPar%), PAR$(NPar%), C1$(NC%), C2$(NC%)
'
            COM$(1) = "BOMB-A output: Ting version of " + VERDAT$ + ", run on " + DATE$ + " at " + TIME$
            COM$(2) = "Burning " + STR$(Nb%) + " elements of " + STR$(Ntot%)

            Rbomb = (.75 * Vtot / 3.1415927#) ^ (1! / 3!)
            PAR(1) = Equiv: PAR$(1) = "Equivalence Ratio,"
            PAR(2) = Pinit / 1000!: PAR$(2) = "kPa Initial Pressure"
            PAR(3) = Tinit: PAR$(3) = "K Initial Temperature"
            PAR(4) = Rbomb: PAR$(4) = "m bomb radius"
            PAR(5) = Mass: PAR$(5) = "kg mixture mass"
            PAR(6) = Vtot: PAR$(6) = "m^3 volume of cell"
            C1$(1) = "Element": C2$(1) = " "
            C1$(2) = "Pressure": C2$(2) = "kPa"
            C1$(3) = "Fl Radius": C2$(3) = "Rb/R"
            C1$(4) = "Mass Brnt": C2$(4) = "Mb/M"
            C1$(5) = "Tu before": C2$(5) = "K"
            C1$(6) = "Tb after": C2$(6) = "K"
'
            DD(1, 1) = 0
            DD(1, 2) = Pinit / 1000!
            DD(1, 3) = 0
            DD(1, 4) = 0
            DD(1, 5) = Tinit
            DD(1, 6) = Tinit
'
            FOR I = 2 TO NR%
                        DD(I, 1) = I - 1
                        DD(I, 2) = STORE(I - 1, 1) / 1000!
                        DD(I, 3) = STORE(I - 1, 2)
                        DD(I, 4) = STORE(I - 1, 3)
                        DD(I, 5) = STORE(I - 1, 7)
                        DD(I, 6) = STORE(I - 1, 8)
            NEXT I
'
            Res$ = "1MA90"
            F$ = "C:\QB\PHD\BOMB\TheoR\" + Res$ + ".dat"
'
NAMEFILE:
            CLS
            PRINT "ABOUT TO WRITE TO "; F$
            INPUT "Hit enter to go on, else enter a new file name. >"; JUNK$
            IF JUNK$ < > "" THEN
                        F$ = "C:\QB\PHD\BOMB\TheoR\" + JUNK$ + ".dat"
                        GOTO NAMEFILE
            END IF
            CALL DWRITE(NR%, NC%, NCom%, NPar%, F$, COM$(), DD(), PAR(), PAR$(), C1$(), C2$())
            PRINT "Write to "; F$; " finished."
'--------------------------------------------------------------------
```

```
' End of the program.
'
END
'
'===============================================================
==============
'   FUELSORT
'   ********
'
' Fuelsort is a subroutine which switches the correct fuel into the
' property array and sets up correct fuel molecule variables.
'
FUELSORT:
    IF IP%(5) > 0 AND IP%(5) < 3 THEN FUEL% = IP%(5)
'
'__________________________________________________________________
' If fuel = propane.
'
    IF FUEL% = 1 THEN
        FCA = 3                 'fuel has FCA carbon atoms per atom
        FHA = 8                 'fuel has FHA hydrogens per atom
        FMW = 44.09               'fuel molar mass in kg/kgmol
'
'__________________________________________________________________
' If fuel = methane.
'
    ELSE
        FCA = 1
        FHA = 4
        FMW = 16.043
    END IF
'
'__________________________________________________________________
' If we don't have the current fuel in I$(7) then swap with I$(8).
'
    IF FUEL$(FUEL%) < > I$(7) THEN
        FOR I = 1 TO 7
            TEMP = IC(7, I)
            IC(7, I) = IC(8, I)
            IC(8, I) = TEMP
        NEXT I
        TEMP$ = I$(7)
        I$(7) = I$(8)
        I$(8) = TEMP$
    END IF
    PRINT "Fuel is " + I$(7) + " and coefficients are:"
    FOR I = 1 TO 7
        PRINT SPACE$(10); IC(7, I)
    NEXT I
RETURN
```

PROGRAM 4: CMBCOM.BAS

```
'   CMBCOM.BAS                          MD CHECKEL     17 NOV 1988
'
' Common block variables for the CMBSUB.BAS set of subroutines
'
' RMOL    = ideal gas constant, 8314.3 J/kgmol.k
' PN      = standard atmosphere, 101325 kPa
' IC(8,7) = coefficients for thermodynamic property functions
' CC()    = coefficients for CO2 dissociation reaction equilibrium constant
' CW()    = coefficients for water-gas dissociation equilibrium constant
' R()     = coefficients for the reactant mixture properties
' P()     = coefficients for the equilibrium product mixture properties
' M#()    = molar values of equilibrium products
' I$(8)   = names of the component gases
' MOLR    = # of moles of reactants per mole of fuel
' MOLP    = # of moles of products per mole of fuel
'
'

COMMON SHARED /CMBSUB1/ RMOL, PN, IC(), CC(), CW(), R(), P()
COMMON SHARED /CMBSUB2/ M#(), I$(), W(), MOLR, MOLP
```

PROGRAM 5: CMBSUB.BAS

```
DECLARE SUB EQCOMP (PE, FCA, FHA, T, MF, MOXY#, MN2#, MWP)
DECLARE SUB EQCONST ()
DECLARE SUB FLAME (IND!, Q!, W!, PE!, FCA!, FHA!, FMW!, S!, TR!, T!, MWR!, MWP!, FLAG%)
DECLARE SUB PROPCOEFF ()
DECLARE SUB PVARBL (Q, W, PI, FCA, FHA, FMW, S, TR, PE, T, MWR, MWP, VE)
DECLARE SUB REACTPROP (EQUIV, FCA, FHA, FMW, MF, MOXY#, MN2#, MWR)
'
'       CMBSUB.BAS
'       **********
'
'       17-NOV-88       M.D. CHECKEL
'       14-SEP-92       Cleaned up, checked and organized.
'                       -- D.S-K. Ting
'
' This package of subroutines is CMBSUB.BAS. It performs some common
' thermodynamic calculations using data from
'                       R.S. Benson,
'                       Advanced Engineering Thermodynamics
'                       2nd Ed, 1977. Appendix A
' Also see CMBSUB.DOC.
'
' <Use F2 to see the actual subroutines.>
'
'-----------------------------------------------------------------
' Set up common block variables.
'
          REM $INCLUDE: 'C:\QB\COMB\CMBCOM.BAS'
          REDIM SHARED IC(8, 7), I$(8), CC(6), CW(6), R(7), P(7), M#(6), W(8)
'
'-----------------------------------------------------------------
' Thermodynamic property coefficient data for the subroutine PROPCOEFF.
' (Data statements must be contained as part of a "main" program which
' is why they are not contained as part of the subroutine.)
'
' Data is taken from:   R.S. Benson,
'                       Advanced Engineering Thermodynamics
'                       2nd Ed, 1977. Appendix A
'
'
'
'       a1        a2        a3        a4     a5   a6      ho
'       P(1)      P(2)      P(3)      P(4)   P(5) P(6)    P(7)
'
DATA "  CO"   , 28.0134
DATA   3.317  ,3.7697e-4  , -3.2208e-8 ,-2.1945e-12 ,0, 4.63284, -1.13882e8
DATA " CO2"    , 44.00995
DATA    3.0959 ,2.73114e-3 , -7.88542e-7, 8.66002e-11,0, 6.58393, -3.93405e8
DATA "  H2"    ,  2.016
DATA   3.43328 ,-8.181e-6  ,  9.6699e-8 ,-1.44392e-11,0,-3.8447 ,0
DATA " H2O"    , 18.016
DATA   3.74292 , 5.65590e-4, 4.9524e-8 ,-1.81802e-11 ,0, 0.96514,-2.39082e8
DATA "  N2"    , 28.0155
DATA   3.34435 , 2.9426e-4 , 1.953e-9  ,-6.5747e-12  ,0, 3.75863,0
DATA "  O2"    , 31.9988
DATA  3.25304  , 6.5235e-4 ,-1.49524e-7, 1.53897e-11 ,0, 5.71243, 0
DATA "C3H8"    , 44.09
DATA  1.13711  , 1.45532e-2,-2.95876e-6, 0.0         ,0, 0.0    ,-0.90510e8
DATA " CH4"    , 16.04
DATA 1.93529,4.96462e-3,-1.24402e-6,1.62497e-10,-8.58611e-15,8.153,-6.69305e7
'
'------------------------------------------------------------------------

SUB EQCOMP (PE, FCA, FHA, T, MF, MOXY#, MN2#, MWP)
'=================================================================
==============
'
'     EQCOMP
'     ******
'
'     09-DEC-87      M.D. CHECKEL
'     14-SEP-92      Cleaned up, checked and organized.
'                    -- D.S-K, Ting
'
'
'
' This subroutine calculates the equilibrium composition of a hydro-carbon
' + air flame given a temperature, T. Additional information is the set of
' coefficients calculated in the main program for the CO2 dissociation and
' the water-gas reactions which are the only two reactions considered.
' The hydrocarbon is described by FCA=(# of carbons) and FHA=(# of hydrogens)
' Information is returned as M#(I) which are numbers of moles/mole of fuel.
' M#(1)=mCO, M#(2)=mCO2, M#(3)=mH2, M#(4)=mH2O, M#(5)=mN2, M#(6)=mO2
' The 6 constants (A1-A6 per Benson and Hfo) are also calculated for the
' equilibrium product mixture and returned as P(1) through P(7).
'
'
        M#(5) = MN2#
        IF MF <= 0 THEN
                M#(1) = 0
                M#(2) = 0
                M#(3) = 0
                M#(4) = 0
                M#(6) = MOXY#
                GOTO PROP
        END IF
'
' L% is a flag to sense failure to converge iterative solution starts by
' assuming no CO2 dissociates.
'
        L% = 0
        M#(2) = FCA
'
' IFLAG%=0 indicates this is first guess.
'
        IFLAG% = 0
        IF T < 500 THEN GOTO EFAIL
'
```

```
'----------------------------------------------------------------
' Calculate equilibrium constants at the current temperature, T.
'
          F = CC(1) * (1 - LOG(T)) - CC(2) * T - CC(3) * T ^ 2
          KCO2# = EXP(-(F - CC(4) * T ^ 3 - CC(5) + CC(6) / T / rmol))
          F = CW(1) * (1 - LOG(T)) - CW(2) * T - CW(3) * T ^ 2
          KWG# = EXP(-(F - CW(4) * T ^ 3 - CW(5) + CW(6) / T / rmol))
'
'----------------------------------------------------------------
' Calculate the kgmol of H2O,CO,H2,O2 and the total kgmol based on the
' assumed CO2.
'
INCL:
          L% = L% + 1
          M#(4) = FHA / 2! * M#(2) / ((FCA - M#(2)) / KWG# + M#(2))
          M#(1) = FCA - M#(2)
          M#(3) = FHA / 2! - M#(4)
'
'----------------------------------------------------------------
' Calculate CO2 "equilibrium constant" of this composition and see how it
' compares with that already calculated above.
'
          M#(6) = MOXY# - M#(2) - M#(1) / 2 - M#(4) / 2
          molP = M#(1) + M#(2) + M#(3) + M#(4) + M#(5) + M#(6)
          KPCO2# = M#(1) * SQR(M#(6) * PE / (molP * PN)) / M#(2)
          ER# = KCO2# - KPCO2#
'
' If error is small, go calculate property coefficients.
' Otherwise, make a new estimate of moles CO2.
'
          IF ABS(ER#) > KCO2# * .00001 THEN
'
' First iteration is to assume 1/2 of the CO2 dissociates.
'
                    IF IFLAG% = 0 THEN
                              EL# = ER#
                              ML# = M#(2)
                              M#(2) = .5 * FCA
                              IFLAG% = 1
'
' Subsequent iterations use geometric interpolation.
'
                    ELSE
                              M1# = (M#(2) * EL# - ML# * ER#) / (EL# - ER#)
                              IF M1# < 0 THEN M1# = .01       ' must have some CO2
                              IF M1# > FCA THEN M1# = FCA     ' but not more than FCA
                              ML# = M#(2)
                              EL# = ER#
                              M#(2) = M1#
                    END IF
'
' Failure printout message for subroutine.
'
                    IF L% < 501 THEN GOTO INCL
EFAIL:
                    PRINT CHR$(7); "EQCOMP failure: T="; T; ","; L%; " iterations"
                    M#(1) = 0
                    M#(2) = FCA
                    M#(3) = 0
                    M#(4) = FHA / 2!
                    M#(6) = MOXY# - FCA - FHA / 4!
                    T = -T
```

```
        END IF
'
'----------------------------------------------------------------
' Evaluate property coefficients for this equilibrium mixture.
'
PROP:
        FOR I = 1 TO 7
                P(I) = 0
                FOR J = 1 TO 6
                        P(I) = P(I) + M#(J) * IC(J, I)
                NEXT J
        NEXT I
'
'----------------------------------------------------------------
' Calculate the number of moles of product, MOLP, and the molecular weight
' of the product, MWP.
'
        molP = 0
        MWP = 0
        FOR J = 1 TO 6
                molP = molP + M#(J)
                MWP = MWP + M#(J) * W(J)
        NEXT J
        MWP = MWP / molP
'----------------------------------------------------------------
' End of subroutine.
'
        END SUB

SUB EQCONST
'==========================================================================
=============
'
'
'       EQCONST
'       *******
'
'       09-DEC-87       M.D. CHECKEL
'       14-SEP-92       Cleaned up, checked and organized.
'                       -- D.S-K. Ting
'
'
'
' This subroutine calculates a set of constants used for calculating
' chemical equilibrium coefficients for CO2 dissociation and the Water-Gas
' reaction. The basic idea is to minimize the gibbs free energy in the
' equilibrium mixture.
' ie ln(Kp) = -{ sum[nu*g(T)]p -sum[nu*g(T)]r } - deltaG298/(rmol*T)
' where nu is the stoichiometric coefficient for each reactant and product
' and deltaG298 is the difference in gibbs energy of formation at 298 k.
'
'----------------------------------------------------------------
' CO2 dissociation:        CO + (1/2) O2 <-> CO2
'                       Kco2 = MCO2/(MCO2(MCO*SQR(MO2*PIN/(mp*Pn))
'
'                CO      O2       CO2
       CC(1) = IC(1, 1) + IC(6, 1) / 2 - IC(2, 1)          ' 1st
       CC(2) = IC(1, 2) + IC(6, 2) / 2 - IC(2, 2)          ' 2nd
       CC(3) = (IC(1, 3) + IC(6, 3) / 2 - IC(2, 3)) / 2    ' 3rd
       CC(4) = (IC(1, 4) + IC(6, 4) / 2 - IC(2, 4)) / 3    ' 4th
       CC(5) = IC(1, 6) + IC(6, 6) / 2 - IC(2, 6)          ' 5th
       CC(6) = IC(1, 7) + 0 - IC(2, 7)                    ' hoR-hoP
```

```
'
'------------------------------------------------------------
' Water-Gas reaction:       CO + H2O <-> CO2 + H2
'                     Kwg = MCO2*MH2/(MCO*MH2O)
'
'            CO2    H2     CO     H2O
         CW(1) = -IC(2, 1) - IC(3, 1) + IC(1, 1) + IC(4, 1)         ' 1st
         CW(2) = -IC(2, 2) - IC(3, 2) + IC(1, 2) + IC(4, 2)         ' 2nd
         CW(3) = (-IC(2, 3) - IC(3, 3) + IC(1, 3) + IC(4, 3)) / 2   ' 3rd
         CW(4) = (-IC(2, 4) - IC(3, 4) + IC(1, 4) + IC(4, 4)) / 3   ' 4th
         CW(5) = -IC(2, 6) - IC(3, 6) + IC(1, 6) + IC(4, 6)         ' 5th
         CW(6) = -IC(2, 7) - 0 + IC(1, 7) + IC(4, 7)               ' hoR-hoP
'------------------------------------------------------------
' End of subroutine.
'
         END SUB

SUB FLAME (IND, Q, W, PE, FCA, FHA, FMW, S, TR, T, MWR, MWP, FLAG%)
'==============================================================
==============
'
'    FLAME
'    *****
'
'
'    10-DEC-87      M.D. CHECKEL
'    13-SEP-92      Cleaned up, checked and organized.
'                  -- D.S-K. Ting
'
'
' INPUTS:
'   IND = 0 for constant pressure, 1 for varying pressure
'   Q = heat transfer TO the element during combustion
'   W = work transfer FROM the gas during combustion (=0 if IND=0) (J/element)
'       - the units of Q and W are ( J/(1 kmol fuel + associated air) )
'   PE   = pressure at end of combustion (Pa)
'   FCA  = number of carbons per fuel atom (3 for propane, 1 for methane)
'   FHA  = number of hydrogen per fuel     (8 for propane, 4 for methane)
'   FMW  = fuel molar mass (kg/kmol)   (44.09 for propane)
'   S    = stoichiometric ratio (0<S<1) = (F/A)/(F/A)stoic
'   TR   = reactant mixture temperature (K)
'   MPR  = kmol of fuel / element
'
' OUTPUTS:
'   T    = flame temperature at equilibrium (K)
'   MWR  = molar mass of reactant mixture (kg/kmol)
'   MWP  = molar mass of products mixture (kg/kmol)
'
'------------------------------------------------------------
' Get the properties and property coefficients of the reactants.
'
         CALL REACTPROP(S, FCA, FHA, FMW, MF, MOXY#, MN2#, MWR)

'   calculate enthalpy of reactants in J/kmol at temperature TR
         x = R(2) * TR + R(3) * TR ^ 2 + R(4) * TR ^ 3 + R(5) * TR ^ 4
         enthr = rmol * TR * (R(1) + x) + R(7)
'
' Guess the initial temperature (based on equivalence ratio).
'
         T = TR + 2200 * S
'
FLSTRT:
```

```
          T1 = 0
          T3 = 0
          FLAG% = 0
'
'------------------------------------------------------------------
' Use subroutine EQCOMP to calculate equilibrium composition at temp T.
' Then calculate the work and energy quantities for first law analysis.
'
GETCOMP:
          CALL EQCOMP(PE, FCA, FHA, T, MF, MOXY#, MN2#, MWP)
          IF T <= 0 THEN T = 2000: GOTO FLSTRT
'    calculate enthalpy of reactants in kJ/kgmol at temperature T
          x = P(1) + P(2) * T + P(3) * T ^ 2 + P(4) * T ^ 3 + P(5) * T ^ 4
          enthp = rmol * T * (x) + P(7)
'

          IF IND = 0 THEN
                    eri# = enthr + Q - enthp          'mdc 910712: include HEAT
          ELSE
                    intr = enthr - molR * TR * rmol
                    intp = enthp - molP * T * rmol
                    eri# = intr + Q - W - intp
          END IF

'------------------------------------------------------------------
' Check the "balance" error in the first law of thermodynamics.
'
' If error is < 1000 J/(1 kmol.fuel + associated air), then T is OK, return.
'
          IF ABS(eri#) < 1000! THEN GOTO ENDFL
'
' Otherwise, try new combustion T.
' For the first iteration, just add or subtract 10 K.
'
          IF FLAG% = 0 THEN
                    T1 = T
                    FLAG% = 1
                    IF eri# < 0 THEN T = T - 10 ELSE T = T + 10
'
' For later estimates, use geometric interpolation.
'
          ELSE
                    T3 = (T * ET# - T1 * eri#) / (ET# - eri#)
                    T1 = T
                    T = T3
                    FLAG% = FLAG% + 1
          END IF
          ET# = eri#
          GOTO GETCOMP
'
'------------------------------------------------------------------
' End of subroutine.
'
ENDFL:
          END SUB

SUB PROPCOEFF
'=================================================================
=============
'
'     PROPCOEFF
'     *********
```

```
'
'     09-DEC-87       M.D. CHECKEL
'     14-SEP-92       Cleaned up, checked and organized.
'                       -- D.S-K Ting
'
'
'
' This subroutine simply fills an array with coefficients necessary to
' calculate enthalpy and gibbs function of reaction for 7 substances as
' listed below. The coefficients and methods of use are described in:
' Rowland S. Benson
' "Advanced Engineering Thermodynamics"
' Pergammon Press, 1977, 2nd Edition
' (eg pg 153, Appendix A)
' Propane is per Benson & Baduah, Int J Mech Eng Educ, Vol 4, No 1, p 93
'
'------------------------------------------------------------------
' Define some constants.
'
          rmol = 8314.3              'ideal gas constant in J/kgmol.k
          PN = 101325                'standard atmosphere (for Go and So)
'
'------------------------------------------------------------------
' Read in the data for the coefficients.  (Data is contained in the "main"
' program.
'
          FOR J = 1 TO 8
                    READ I$(J), W(J)
                    FOR L = 1 TO 7
                              READ IC(J, L)
                    NEXT
          NEXT
'
'------------------------------------------------------------------
' End of subroutine.
'
          END SUB

SUB PVARBL (Q, W, PI, FCA, FHA, FMW, S, TR, PE, T, MWR, MWP, VE)
'==============================================================
=============
'
'     PVARBL
'     ******
'
'
'     ??-???-??      M.D. CHECKEL
'     14-SEP-92      Cleaned up and organized.
'                      -- D.S-K. Ting
'
'
'
'
          IFLP = 0
          PE = PI + S * 9 * PI   'estimate PE=press after combustion
          x = 1
'
GTEMP:
          CALL FLAME(x, Q, W, PE, FCA, FHA, FMW, S, TR, T, MWR, MWP, FL%)
          VINIT# = rmol * TR / MWR / PI
          VE# = VINIT# * PI / PE * T / TR * molP / molR
          ERV# = VINIT# - VE#
```

```
'
' If the error is greater than .001% then make new estimate of pressure and
' go back to try again.  IFLP = flag to determine whether a previous estimate
' has been made. If it has, extrapolate/interpolate to get new estimate.
' Otherwise, simply make a small step in pressure.
'
        IF ABS(ERV#) > VINIT# / 10000 THEN
                IF IFLP > 0 THEN
                        PE3 = (PE * ERV1# - PE1 * ERV#) / (ERV1# - ERV#)
                        PE1 = PE
                        PE = PE3
                ELSE
                        PE1 = PE
                        IFLP = 1
                        IF ERV# > 0 THEN
                                PE = PI + 1.2 * (PE - PI)
                        ELSE
                                PE = PE + (PE - PI) / 1.2
                        END IF
                END IF
'
' Having established this estimate for pressure after combustion, record the
' current volume error and go back to re-calculate the volumes and
' compression work with the new pressure value.
'
                ERV1# = ERV#
                GOTO GTEMP
        END IF
'
ENDPV:
        VE = VE#
'-----------------------------------------------------------------------
' End of subroutine.
'
        END SUB

SUB REACTPROP (EQUIV, FCA, FHA, FMW, MF, MOXY#, MN2#, MWR)
'==============================================================
=============
'
'     REACTPROP
'     *********
'
'
'
'     09-DEC-87      M.D. CHECKEL
'     14-SEP-92      Cleaned up, checked and organized.
'                    -- D.S-K. Ting
'
'
'

' This routine calculates various properties and property coefficients for a
' hydrocarbon fuel + air mixture.

' The fuel is described as FCA=number of carbons per molecule (eg 3 for C3H8)
'                          FHA=number of hydrogens/molecule   (eg 8 for C3H8)
'                          FMW=fuel molar mass   kg/kmol  (eg 44.09 for C3H8)
' (If FMW is 16.043 then fuel must be methane.)
'
' The air is assumed to be 21% oxygen and 79% nitrogen (molar ratio 3.76190)
' The mixture strength is described as:
'                 EQUIV=(F/A)ratio / (F/A)stoich  ( <1=lean, >1=rich )
'
```

```
' The property coefficients of the mixture are calculated from the individual
' element coefficients stored in IC(7,6). IC(7,6) contains coefficients as
' described in PROPCOEFF.
'
' The outputs are MF  = 1 if fuel is present, 0 if it is not
'               MOXY#= moles of oxygen per mole of fuel
'               MN2# = moles of nitrogen per mole of fuel
'               MWR  = molar mass of reactants in kg/kmol
'               R(I) = mixture property coefficients to calculate mixture
'                    properties in J/kmol and J/kmol.k
'
'------------------------------------------------------------
' Determine the number of moles of OXYGEN and whether or not fuel is present.
'
        IF EQUIV > 0 THEN
                MOXY# = (FCA + FHA / 4!) / EQUIV
                MF = 1
        ELSE
                MOXY# = .21#
                MF = 0
        END IF
'
'------------------------------------------------------------
' Based on the number of moles of oxygen, determine the number of moles of
' reactant, number of moles of nitrogen, and molecular weight of reactants.
'
        molR = MF + MOXY# * (1# + .79# / .21#)
        MN2# = MOXY# * .79# / .21#
        MWR = (MOXY# * W(6) + MN2# * W(5) + MF * FMW) / molR
'
'------------------------------------------------------------
' Calculate the mixture property coeficients.
'
        FOR I = 1 TO 7
                R(I) = MF * IC(7, I) + MOXY# * IC(6, I) + MN2# * IC(5, I)
        NEXT I
'------------------------------------------------------------
' End of subroutine.
'
        END SUB
```

PROGRAM 6: BP2-93.BAS

```
'
'    BP2-93.BAS
'    **********
'
'    August 12th 1993     D.S-K. Ting
'
' BP2-93.bas is part 2 of Bomb-A.bas, Bomb-M.bas and/or Bomb-R.bas.
'
' This program calculates fates of elements of lean fuel-air mixtures
' at specified starting conditions, burning in a constant volume bomb,
' based on the recorded pressure trace from the bomb.  It reads results
' from Bomb-A, Bomb-M and/or Bomb-R and then interpolates them to match
' with the measured pressure results.
'
' Based on BOMB.BAS per Alun Thomas's BOMB.BAS with corrections re units, etc
' Thermodynamic properties and methods as described in:
'           Rowland S. Benson,
'           "Advanced Engineering Thermodynamics"
'           Pergammon Press, 1977, 2nd Edition
'
'----------------------------------------------------------------
' Include and dimension the files.
'
          REM $INCLUDE: 'C:\QB\LIB\PLOTCOM.BAS'
          REM $INCLUDE: 'C:\QB\LIB\COLORCHC.BAS'
          REM $DYNAMIC
'
          REDIM Time!(1501)
'
          NPAR% = 17: NCOM% = 5: NC% = 6
          REDIM Res(1501, NC%)
          REDIM com$(NCOM%), Par!(NPAR%), Par$(NPAR%), C1$(NC%), C2$(NC%)
'
          VERDAT$ = "August-1993"
'----------------------------------------------------------------
' Read the theoretical data file.
          DF$ = "1MA90"
GETF:
          DFP$ = "C:\QB\PHD\BOMB\TheoR\" + DF$ + ".DAT"
          CLS : PRINT "Enter the theoretical data file Enter="; DF$; ") >";
          INPUT ; DF2$
          IF DF2$ < > "" THEN
                    DF$ = DF2$
                    GOTO GETF
          END IF
'----------------------------------------------------------------
' File reading routine.
'
YESFILE:
          REDIM DD!(20, 20), DPar!(20), DPar$(20), DCOM$(20), DCOL1$(20), DCOL2$(20)
          CALL DDIM(DNR%, DNC%, DNCOM%, DNPAR%, DFP$, TITLE$)
          REDIM DCOM$(DNCOM%), DPar$(DNPAR%), DPar!(DNPAR%), DD(DNR%, DNC%)
          REDIM DCOL1$(DNC%), DCOL2$(DNC%)
'
          CALL DREAD(DNR%, DNC%, DNCOM%, DNPAR%, DFP$, DCOM$(), DD(), DPar!(), DPar$(), DCOL1$(),
DCOL2$())
'
'----------------------------------------------------------------
' Read the experimental data file.
          EF$ = DF$
GETRUN:
          EFP$ = "C:\QB\DAS16\CDATA\M-J93\" + EF$ + ".DAT"
          LOCATE 8, 1: CLS
          PRINT "Enter the experimental data file Enter="; EF$; ") >";
          INPUT ; EF2$
          IF EF2$ < > "" THEN
                    EF$ = EF2$
                    GOTO GETRUN
          END IF
'----------------------------------------------------------------
' File reading routine.
'
RFILE:
          REDIM ED!(20, 20), EPR!(20), EPR$(20), ECM$(20), ECL1$(20), ECL2$(20)
          CALL DDIM(NRR%, NCC%, NCM%, NPR%, EFP$, ETITLE$)
          REDIM ECM$(NCM%), EPR$(NPR%), EPR!(NPR%), ED(NRR%, NCC%)
          REDIM ECL1$(NCC%), ECL2$(NCC%)
```

```
'
        CALL DREAD(NRR%, NCC%, NCM%, NPR%, EFP$, ECM$(), ED(), EPR!(), EPR$(), ECL1$(), ECL2$())
'------------------------------------------------------------
' Set the maximum #points
        NP% = NRR%
        IF NP% > 1500 THEN NP% = 1500
'------------------------------------------------------------
' Set the maximum pressure to analyze
'
INPUTSECTION:
        COLOR 10, 1
        CLS
        PRINT "Ting version of "; VERDAT$; ", run at "; TIME$; " on "; DATE$
        MaxP = 5.5 * DPar!(2)
        PRINT "Maximum pressure to analyze ="; MaxP; "kPa"
        INPUT "Enter = go on, Else enter Maximum pressure in kPa >"; MaxP1
        IF MaxP1 <> 0 THEN MaxP = MaxP1
CLS
'------------------------------------------------------------
' Set up TIME array and determine the #points to analyze
'
        FOR I% = 1 TO NP%
                Time!(I%) = (ED(I%, 1) - ED(1, 1))    'start at time zero
                IF ED(I%, 2) > MaxP THEN
                        IMAXP% = I% - 1
                        GOTO TimeS
                END IF
        NEXT I%
TimeS:
'------------------------------------------------------------
' This is the start of the main loop where interpolation is done to
' determine various quantities from a data base file based on measured
' pressure.
'
        Res(1, 1) = Time!(1)      ' Time in ms.
        Res(1, 2) = DD(1, 2)      ' Pressure after combustion of element.
        Res(1, 3) = 0            ' relative radius of flame vs bomb radius
        Res(1, 4) = 0            ' mass fraction burned
        Res(1, 5) = DD(1, 5)      ' unburned gas temperature after combustion
        Res(1, 6) = DD(2, 6)      ' temperature of element after combustion

        FOR I% = 2 TO IMAXP%
                LOCATE 15, 1: PRINT "Calculation countdown . . . "; IMAXP% - I%; "   "
                Res(I%, 1) = Time!(I%)
                Res(I%, 2) = ED(I%, 2)
                FOR J% = 2 TO DNR%
                        IF DD(J%, 2) > ED(I%, 2) THEN
                                INTERP = (ED(I%, 2) - DD(J% - 1, 2)) / (DD(J%, 2) - DD(J% - 1, 2))
                                FOR K% = 3 TO 6
                                        Res(I%, K%) = DD(J% - 1, K%) + (DD(J%, K%) - DD(J% - 1, K%)) *
INTERP
                                NEXT K%
                                GOTO SKIPOUT
                        END IF
                NEXT J%
SKIPOUT:
        NEXT I%
'------------------------------------------------------------
' Make a warbling sound when the calculations are done.
'
        FOR NSOUND = 1 TO 10
                FREQ = 20 + 120 * NSOUND
                SOUND FREQ, 1
        NEXT NSOUND
'-------------------------------------------------------------
' Store the calculated quantities in an output file.
'
        Res$ = EF$
        F$ = "C:\QB\PHD\BOMB\RESULT\" + Res$ + ".Res"
'
NAMEFILE:
        PRINT "ABOUT TO WRITE TO "; F$
        INPUT "Enter = go on, else enter a new file. >"; JUNK$
        IF JUNK$ <> "" THEN
                F$ = "C:\QB\PHD\BOMB\RESULT\" + JUNK$ + ".Res"
                PRINT
                GOTO NAMEFILE
        END IF
'
        INPUT "Fuel ="; FL$
        com$(1) = "Output of bomb pressure trace analysis."
        com$(2) = "Ting version of " + VERDAT$ + ", run at " + TIME$
        com$(2) = com$(2) + " on " + DATE$
        com$(3) = "FILE = " + F$
        com$(4) = "FUEL = " + FL$
        com$(5) = ""
'
        Par!(1) = EPR!(1): Par$(1) = " FREQUENCY (Hz) "
        Par!(2) = EPR!(2): Par$(2) = " Gain "
        Par!(3) = EPR!(3): Par$(3) = " Reduction Factor for Replay "
        Par!(4) = EPR!(4): Par$(4) = " dt (msec) "
        Par!(5) = EPR!(5): Par$(5) = " Equivalence Ratio "
        Par!(6) = EPR!(6): Par$(6) = " Plate Diameter (mm) "
        Par!(7) = EPR!(7): Par$(7) = " Plate Speed (m/s) "
        Par!(8) = EPR!(8): Par$(8) = " Spark Delay (ms) "
        Par!(9) = EPR!(9): Par$(9) = " Turbulence Intensity (# or m/s) "
        Par!(10) = EPR!(10): Par$(10) = " Maximum Pressure (kPa) "
        Par!(11) = EPR!(11): Par$(11) = " Time at Pmax (ms) "
        Par!(12) = EPR!(12): Par$(12) = " Ionization Time (ms) "

        Par!(13) = DPar!(2): Par$(13) = " kPa Initial Pressure "
        Par!(14) = DPar!(3): Par$(14) = " K Initial Temperature "
        Par!(15) = DPar!(4): Par$(15) = " m bomb radius "
        Par!(16) = DPar!(5): Par$(16) = " kg mixture mass "
        Par!(17) = DPar!(6): Par$(17) = " m^3 cell volume "

'

        C1$(1) = " Time ": C2$(1) = "ms"
        C1$(2) = "Pressure": C2$(2) = "kPa"
        C1$(3) = " Radius ": C2$(3) = "rb/Rcell"
        C1$(4) = "Mass B": C2$(4) = "Mb/M"
        C1$(5) = "Tu bef": C2$(5) = "K"
        C1$(6) = "Tb after": C2$(6) = "K"

NR% = IMAXP%
CALL DWRITE(NR%, NC%, NCOM%, NPAR%, F$, com$(), Res(), Par!(), Par$(), C1$(), C2$())
'-------------------------------------------------------------
' Finish off program.
'
          PRINT : CLS
          INPUT "Enter = read another run, 1 = quit >"; IND%
          IF IND% = 0 THEN GOTO GETRUN
END
```

PROGRAM 7: BV-93.BAS

```
DECLARE SUB SLFILT (i!(), f!(), n%, COV%)
'
'    BV-93.BAS
'    *********
'
'    August 28th 1993     DSK TING
'
'
' This program calculates and plots burning velocities from output produced
' by BP2-93.BAS.
'
          REM $INCLUDE: 'C:\QB\LIB\PLOTCOM.BAS'
          REM $INCLUDE: 'C:\QB\LIB\COLORCHC.BAS'
          REM $DYNAMIC
'-------------------
' Dimension some arrays.
'
          DIM DCOL1$(20), DCOL2$(20)
          DIM dd!(20, 20), dpar!(20), dpar$(20), Dcom$(20)
'----------------
' Get the data file.
          DFN$ = "1"
GETFILE:
          DF$ = "C:\QB\PHD\BOMB\RESULT\" + DFN$ + ".Res"
          CLS : PRINT "Enter file name.  (Enter= "; DF$; ")  >";
          INPUT DF2$
          IF DF2$ < > "" THEN DFN$ = DF2$: GOTO GETFILE
          GOSUB YESFILE
'-------------------
' Set #rows and #columns.
          NROW% = DNR%
          NCOL% = DNC%
'--------------
' Set the X-axis.
PlotWhat:
          ColX = 3: CLS
          PRINT "If Column # < > 3, changes in plotting routine may be required."
          PRINT "Enter column# for X-axis. (Enter= "; ColX; ")  >";
          INPUT ColX2
          IF ColX2 > 0 THEN ColX = ColX2
'
STARTLOOP:
'----------------------------------------------------
' Calculate the burning velocity using geometric methods.
'
          Vtot = dpar!(17)
          Rcell = dpar!(15)
          Tinit = dpar!(14)
          dd(1, 5) = Tinit
          Pinit = dpar!(13)
          pii# = 3.141592654#
          n% = DNR% - 1
          REDIM X(10 + n%), XF(10 + n%), GRate(10 + n%), GRateF(10 + n%)
          REDIM Su(10 + n%), SuF(10 + n%)
          TimeL = dd(1, 1)
          Rlast = 0
          FOR i = 2 TO n%
                    Rb = dd(i, 3) * Rcell
                    dVjk = Pinit * dd(i - 1, 5) * Vtot / Tinit / dd(i - 1, 2)
                    dVub = dVjk * (dd(i, 4) - dd(i - 1, 4))
                    time = dd(i, 1)
```

```
                dt = (time - TimeL) * .001 'convert ms to s
                Rflame = SQR((Rlast ^ 2 + Rb ^ 2) / 2)
                IF (4 / 3 * pii# * Rflame ^ 3 + dVub) < 0 THEN
                        Ri = 0
                ELSE
                        Ri = (.75 / pii# * (4 / 3 * pii# * Rflame ^ 3 + dVub)) ^ (1 / 3)
                END IF
                dRi = Ri - Rflame
                Su(i) = (dRi / dt) * 100              'convert m/s to cm/s
' Flame Growth Rate.
                GRate(i) = ((Rb - Rlast) / dt) * 100   'convert m/s to cm/s
                X(i) = dd(i, ColX)
                IF ColX = 3 THEN X(i) = dd(i, ColX) * Rcell * 1000   'convert m to mm
                Rlast = Rb
                TimeL = time
        NEXT i
'---------------------------------------------
' Filter the flame growth rate and the burning velocity.
'
        NUMFILT = 0
        NCOV% = 4
FILTER1:
        IF NUMFILT < 3 THEN
                CALL SLFILT(GRate(), GRateF(), n%, NCOV%)
                FOR i = 2 TO n% - 2
                        GRate(i) = GRateF(i)
                NEXT i
                NUMFILT = NUMFILT + 1
                NCOV% = NCOV% - 1
                GOTO FILTER1
        END IF
'
        NUMFILT = 3
        NCOV% = 4
FILTER2:
        IF NUMFILT < 3 THEN
                CALL SLFILT(Su(), SuF(), n%, NCOV%)
                FOR i = 2 TO n% - 2
                        Su(i) = SuF(i)
                NEXT i
                NUMFILT = NUMFILT + 1
                NCOV% = NCOV% - 1
                GOTO FILTER2
        END IF

'--------------------
' Search For Keypoints.
'
        REDIM Timept(12), Ppt(12), Rpt(12), mbpt(12), Tupt(12)
        REDIM Rfirst(12), Rlast(12)

' Input the required r/Rcell
        Rreq1 = .4: Rreq2 = .45: Rreq3 = .5: Rreq4 = .55: Rreq5 = .6
        Rreq6 = .65: Rreq7 = .7: Rreq8 = .72: Rreq9 = .75: Rreq10 = .8
        Rreq11 = .85: Rreq12 = .9
'
        FOR i = 3 TO n%
                IF dd(i, 3) < Rreq1 AND dd(i - 2, 3) < Rreq1 THEN I1 = i
                IF dd(i, 3) < Rreq2 AND dd(i - 2, 3) < Rreq2 THEN I2 = i
                IF dd(i, 3) < Rreq3 AND dd(i - 2, 3) < Rreq3 THEN I3 = i
                IF dd(i, 3) < Rreq4 AND dd(i - 2, 3) < Rreq4 THEN I4 = i
                IF dd(i, 3) < Rreq5 AND dd(i - 2, 3) < Rreq5 THEN I5 = i
```

```
            IF dd(i, 3) < Rreq6 AND dd(i - 2, 3) < Rreq6 THEN I6 = i
            IF dd(i, 3) < Rreq7 AND dd(i - 2, 3) < Rreq7 THEN I7 = i
            IF dd(i, 3) < Rreq8 AND dd(i - 2, 3) < Rreq8 THEN I8 = i
            IF dd(i, 3) < Rreq9 AND dd(i - 2, 3) < Rreq9 THEN I9 = i
            IF dd(i, 3) < Rreq10 AND dd(i - 2, 3) < Rreq10 THEN I10 = i
            IF dd(i, 3) < Rreq11 AND dd(i - 2, 3) < Rreq11 THEN I11 = i
            IF dd(i, 3) < Rreq12 AND dd(i - 2, 3) < Rreq12 THEN I12 = i
      NEXT i
      Timept(1) = dd(I1, 1): Ppt(1) = dd(I1, 2)
      Rpt(1) = Rreq1 * Rcell * 1000     'convert m to mm
      mbpt(1) = dd(I1, 4): Tupt(1) = dd(I1, 5)
'
      Timept(2) = dd(I2, 1): Ppt(2) = dd(I2, 2)
      Rpt(2) = Rreq2 * Rcell * 1000     'convert m to mm
      mbpt(2) = dd(I2, 4): Tupt(2) = dd(I2, 5)
'
      Timept(3) = dd(I3, 1): Ppt(3) = dd(I3, 2)
      Rpt(3) = Rreq3 * Rcell * 1000     'convert m to mm
      mbpt(3) = dd(I3, 4): Tupt(3) = dd(I3, 5)
'
      Timept(4) = dd(I4, 1): Ppt(4) = dd(I4, 2)
      Rpt(4) = Rreq4 * Rcell * 1000     'convert m to mm
      mbpt(4) = dd(I4, 4): Tupt(4) = dd(I4, 5)
'
      Timept(5) = dd(I5, 1): Ppt(5) = dd(I5, 2)
      Rpt(5) = Rreq5 * Rcell * 1000     'convert m to mm
      mbpt(5) = dd(I5, 4): Tupt(5) = dd(I5, 5)
'
      Timept(6) = dd(I6, 1): Ppt(6) = dd(I6, 2)
      Rpt(6) = Rreq6 * Rcell * 1000     'convert m to mm
      mbpt(6) = dd(I6, 4): Tupt(6) = dd(I6, 5)
'
      Timept(7) = dd(I7, 1): Ppt(7) = dd(I7, 2)
      Rpt(7) = Rreq7 * Rcell * 1000     'convert m to mm
      mbpt(7) = dd(I7, 4): Tupt(7) = dd(I7, 5)
'
      Timept(8) = dd(I8, 1): Ppt(8) = dd(I8, 2)
      Rpt(8) = Rreq8 * Rcell * 1000     'convert m to mm
      mbpt(8) = dd(I8, 4): Tupt(8) = dd(I8, 5)
'
      Timept(9) = dd(I9, 1): Ppt(9) = dd(I9, 2)
      Rpt(9) = Rreq9 * Rcell * 1000     'convert m to mm
      mbpt(9) = dd(I9, 4): Tupt(9) = dd(I9, 5)
'
      Timept(10) = dd(I10, 1): Ppt(10) = dd(I10, 2)
      Rpt(10) = Rreq10 * Rcell * 1000     'convert m to mm
      mbpt(10) = dd(I10, 4): Tupt(10) = dd(I10, 5)
'
      Timept(11) = dd(I11, 1): Ppt(11) = dd(I11, 2)
      Rpt(11) = Rreq11 * Rcell * 1000     'convert m to mm
      mbpt(11) = dd(I11, 4): Tupt(11) = dd(I11, 5)
'
      Timept(12) = dd(I12, 1): Ppt(12) = dd(I12, 2)
      Rpt(12) = Rreq12 * Rcell * 1000     'convert m to mm
      mbpt(12) = dd(I12, 4): Tupt(12) = dd(I12, 5)

' Equation based on r/Rcell
      Rfirst(1) = .95 * Rreq1: Rlast(1) = 1.1 * Rreq1
      Rfirst(2) = .9 * Rreq2: Rlast(2) = 1.1 * Rreq2
      Rfirst(3) = .9 * Rreq3: Rlast(3) = 1.1 * Rreq3
      Rfirst(4) = .9 * Rreq4: Rlast(4) = 1.1 * Rreq4
      Rfirst(5) = .9 * Rreq5: Rlast(5) = 1.1 * Rreq5
```

```
        Rfirst(6) = .9 * Rreq6: Rlast(6) = 1.1 * Rreq6
        Rfirst(7) = .9 * Rreq7: Rlast(7) = 1.1 * Rreq7
        Rfirst(8) = .9 * Rreq8: Rlast(8) = 1.1 * Rreq8
        Rfirst(9) = .9 * Rreq9: Rlast(9) = 1.1 * Rreq9
        Rfirst(10) = .9 * Rreq10: Rlast(10) = 1.1 * Rreq10
        Rfirst(11) = .9 * Rreq11: Rlast(11) = 1.1 * Rreq11
        Rfirst(12) = .9 * Rreq12: Rlast(12) = 1.05 * Rreq12
'-----------------------
' Data plotting section.
'

PLOTSECTION:
        XLB$ = "Flame Radius (mm)"
        YLB$ = "Su (cm/s)"
        SCREEN 0: WIDTH 80: COLOR 15, 1
        CLS : PRINT "Data plotting section"
        INDAX% = 0: XSUB% = 0: YSUB% = 0
        CALL AXES(X(), GRate(), n%, XSUB%, YSUB%, Xmn, Xmx, Xdv, NXS%, Ymn, Ymx, Ydv, NYS%)
        Ymn = 0: Ydv = 20: Ymx = 300
        Xmn = 0: Xdv = 20: Xmx = 80
LINETYPE:
        LOCATE 1, 1: PRINT SPACE$(80): PRINT SPACE$(80): LOCATE 1, 1
        LIN% = 1
        CHAR% = 0
        CALL PINI(SCRN%, 1): c% = ngc%
        CALL YAXIS(Ymn, Ymx, Ydv, YSUB%, NYSUBD%, YLB$, y2$, Y3$, c%)
        CALL XAXIS(Xmn, Xmx, Xdv, XSUB%, NXSUBD%, XLB$, c%)
'
        CALL LINPLT(X(), Su(), n%, CHAR%, 1, 6!, c%)
        CALL LINPLT(X(), GRate(), n%, CHAR%, 1, 6!, c% + 1)
        LOCATE 28, 1: PRINT DF$
'

' Equation Of Line from Rfirst to Rlast.

FOR Nfit% = 1 TO 12

        Rffirst = Rfirst(Nfit%): Rflast = Rlast(Nfit%)
        Timefit = Timept(Nfit%): mbfit = mbpt(Nfit%)
        Rfit = Rpt(Nfit%): Pfit = Ppt(Nfit%): Tufit = Tupt(Nfit%)

        FOR i = 1 TO n%
                IF dd(i, 3) > Rffirst AND dd(i + 2, 3) > Rffirst THEN
                        f% = i - 1
                        Rstart = dd(f%, 3) * Rcell * 1000     'convert m to mm
                        GOTO fdl
                END IF
        NEXT i
fdl:
        FOR i = 1 TO n%
                IF dd(i, 3) > Rflast AND dd(i + 2, 3) > Rflast THEN
                        1% = i - 1
                        Rend = dd(1%, 3) * Rcell * 1000     'convert m to mm
                        GOTO fdf
                END IF
        NEXT i
fdf:
        nF% = 1% - f% - 1
        FOR i = 1 TO nF%
                GRateF(i) = GRate(i + f%)
                SuF(i) = Su(i + f%)
                XF(i) = X(i + f%)
        NEXT i
        REDIM lsc(2)
        CALL ls(nF%, 1, XF(), GRateF(), lsc(), r)
        ystart = lsc(1) + lsc(2) * Rstart
        y1F = lsc(1) + lsc(2) * Rfit
        yend = lsc(1) + lsc(2) * Rend
        CALL pplot(Rstart, ystart, 0, c%): CALL PPOINT(5, 6!, c% - 2)
        CALL pplot(Rend, yend, 1, 12): CALL PPOINT(5, 6!, c% + 1)

        REDIM lsc(2)
        CALL ls(nF%, 1, XF(), SuF(), lsc(), r)
        ystart = lsc(1) + lsc(2) * Rstart
        y2F = lsc(1) + lsc(2) * Rfit
        yend = lsc(1) + lsc(2) * Rend
        CALL pplot(Rstart, ystart, 0, c%): CALL PPOINT(4, 6!, c% - 2)
        CALL pplot(Rend, yend, 1, 12): CALL PPOINT(4, 6!, c% + 1)

        NFpt% = Nfit% + 2
        LOCATE NFpt%, 13: PRINT USING "r=##mm"; Rfit
        LOCATE NFpt%, 20: PRINT USING "Rate=####cm/s"; y1F
        LOCATE NFpt%, 35: PRINT USING "Su=####cm/s"; y2F
        LOCATE NFpt%, 46: PRINT USING " @####ms"; Timefit
        LOCATE NFpt%, 54: PRINT USING " P=####kPa"; Pfit
        LOCATE NFpt%, 64: PRINT USING " Tu=###K"; Tufit
        LOCATE NFpt%, 72: PRINT USING " mb=###%"; mbfit * 100
        LPRINT USING "   ####, ####cm/s, ####cm/s, ####ms, ####%, ####kPa, ####K"; Nfit%; y1F; y2F; Timefit; mbfit
* 100; Pfit; Tufit

        CALL pplot(Rfit, y1F, 0, c%): CALL PPOINT(6, 6!, c% - 1)
        CALL pplot(Rfit, y2F, 0, c%): CALL PPOINT(6, 6!, c% - 1)

NEXT Nfit%
LPRINT "    "; DF$: LPRINT : LPRINT

'----------------------------
' Finished plots, now what ?
'
OPTIONS:
        LOCATE 1, 1: PRINT SPACE$(80): PRINT SPACE$(80)
        LOCATE 1, 1: INPUT " 0=hard copy, 1=quit, 2=restart>"; opt%
        IF opt% = 2 THEN GOTO GETFILE
        IF opt% = 1 THEN SCREEN 0: COLOR 15, 1: CLS : END
        IF opt% = 0 THEN CALL phcopy(xyz$)
        GOTO OPTIONS
'================================================
================
'      YESFILE
' File reading subroutine.
'
YESFILE:
        CLS : CALL DDIM(DNR%, DNC%, DNCOM%, DNPAR%, DF$, TITLE$,
        REDIM Dcom$(DNCOM%), dpar$(DNPAR%), dpar!(DNPAR%), dd(DNR%, DNC%)
        REDIM DCOL1$(DNC%), DCOL2$(DNC%)
        CALL DREAD(DNR%, DNC%, DNCOM%, DNPAR%, DF$, Dcom$(), dd(), dpar!(), dpar$(), DCOL1$(), DCOL2$())
RETURN
'================================================
================

REM $STATIC
SUB SLFILT (i(), f(), n%, COV%)
'
' SUBROUTINE SLFILT IS A SIMPLE AVERAGING LOW PASS FILTER.
' It makes each point of F equal to an average of all points within +/- cov%
```

```
  ' of the same point in the input array, I.
  '
  '
      IF COV% <= 0 THEN COV% = 4
      FOR i% = 1 TO n%
      SUM = i(i%)
              FOR j% = 1 TO COV%
                      m% = i% - j%
                      IF m% > 0 THEN
                           m = i(m%)
                           ELSE
                           m = i(1)
                      END IF
                      P% = i% + j%
                      IF P% <= n% THEN
                           P = i(P%)
                           ELSE
                           P = 2 * i!(n%) - i(n% + n% - P%)
                      END IF
                      SUM = SUM + m + P
             NEXT j%
     f(i%) = SUM / (2 * COV% + 1)
     NEXT i%
END SUB
```

APPENDIX H: PREMIXED LAMINAR METHANE-AIR FLAME RESULTS

This appendix details the laminar methane-air flame experimental results. All major results are tabulated and plotted when necessary. Results given in Chapter 5 are not repeated here.

Both high speed schlieren video and pressure trace analyses are used to study the laminar methane-air flame growth in a 125 mm cubical combustion chamber. Mixture stoichiometry effects on flame growth and on overall combustion performance are studied. Premixed methane-air mixtures of 60% to 100% stoichiometric compositions are ignited at initial pressure, P_{init}, of 1 atm and initial temperature, T_{init}, of 300 K. For the 70% and the 90% stoichiometric mixtures, the effects of pressure on flame growth are studied by varying the initial pressure from 0.5 to 2 atm. Effects of ignition energy on laminar flame growth is studied by altering the ignition voltage supply from 100 to 500 V while keeping the capacitance at 2.5 μF.

A SP2000 Motion Analysis System high speed video camera manufactured by EASTMAN KODAK COMPANY of the Spin Physics Division is used to record flame growth at 2000 frames per second. The combustion chamber pressure rise is measured using a Norwood model 111 four-active-arm strain gauge pressure transducer with a gain of 500.

H.1: MIXTURE STOICHIOMETRY EFFECT ON COMBUSTION CHAMBER PRESSURE RISE

Table H.1 shows the effect of mixture stoichiometry on the maximum pressure rise, P_{max}, and the time taken to reach this maximum pressure, t_{Pmax}. From stoichiometric to 60% stoichiometric, the maximum pressure decreases while the time for maximum pressure rise increases significantly. As the mixture stoichiometry is reduced from 100% to 60% stoichiometric, the amount of energy release decreased and this lead to a decrease in the maximum pressure rise. Leaner mixtures also lead to slower reaction rate and hence, longer combustion times. As a consequence, the maximum pressure rise falls progressively short of the ideal adiabatic maximum pressure rise, as a leaner mixture is used. This trend is shown by the decreasing ratio of P_{max}/P_{amax}, where P_{amax} is the adiabatic maximum pressure rise.

H.2: FLAME GROWTH FROM SCHLIEREN IMAGES

Figure H.1 shows the flame growth under the effect of mixture stoichiometry. All mixtures are ignited at 1 atm and 300 K. Flame growth images from two runs are plotted for each mixture stoichiometry. The plots show that the experiments are highly repeatable. The flame grows slower as the mixture stoichiometry is decreased from stoichiometric to 60% stoichiometric.

Pressure has a negative effect on methane-air flame around atmospheric conditions. Figure H.2 shows the negative effect of pressure on 90% stoichiometric methane-air flame. The plots show that the flame grows slower with increasing pressure. The figure also shows a somewhat lower repeatability for the 2 atm case. The effects of pressure on 70% stoichiometric flame is illustrated in Figure H.3. As expected, increasing the pressure decreases the flame growth rate. The negative pressure effect appears to be more severe compared with the 90% stoichiometric case shown in Figure H.2.

H.3: LAMINAR FLAME GROWTH RATE AND LAMINAR BURNING VELOCITY

Flame growth rate is simply defined as the change in flame radius per unit time. From the schlieren images, the flame growth rate can be calculated as the increase in the flame radius between two consecutive images. Assuming isotropic flame enabled the deduction of flame radius from the cross-sectional area in the plane direction. Whenever possible, flame growth rates are calculated at relative flame radius, r/R_{cell}, of 0.2, 0.25, 0.3, 0.35, 0.4, 0.45 and 0.5. These relative flame radii correspond to 15.32, 19.15, 22.98, 26.81, 30.64, 34.47 and 38.30 mm radius flames. Linear fits between ±10% of the required relative flame radii are used to calculate the flame growth rates. For the r/R_{cell} of 0.2 case, the flame growth rate is calculated from linear fit from 95% to 110% of the required relative flame radius. The flame growth rate at r/R_{cell} of 0.5 is calculated from linear fit from 90% to 105% of 0.5.

From the pressure trace analysis, the multi-zone thermodynamic model allowed the interpolation of the experimental pressure trace with the theoretical pressure trace. This resulted in pressure, mass burnt, flame radius, unburnt and burnt temperatures as functions of time. The flame growth rate is simply calculated as the rate of change of the flame radius. Flame growth rate is calculated at 0.4, 0.45, 0.5, 0.55, 0.6, 0.65, 0.7, 0.72, 0.75, 0.8, 0.85 and 0.9 relative radius flames whenever possible. Linear fits of ±10% of the selected relative flame radii are used for the flame growth rate calculation. Flame growth rate at 0.4 relative flame radius is calculated based on linear fit from 95% to 110% of 0.4. Linear fit from 90% to 105% is used to deduce the flame growth rate calculation at 0.9 relative flame radius. Laminar flame growth rate results are summarized in Table H.2 along with the laminar burning velocity results.

Burning velocity is calculated using a GEOMETRIC METHOD as described in Appendix G. The schlieren images gave the flame radius as a function of time. The flame growth is correlated with pressure rise, mass burnt, unburnt and burnt temperatures after interpolation with the theoretical results generated from the multi-zone thermodynamic model. Burning velocities from both schlieren and pressure trace analyses are calculated at the same flame sizes as the flame growth calculation. These laminar burning velocity results are tabulated in Table H.2 along with the flame growth rate results. Due to relatively large noise to signal ratio in the early pressure trace, the laminar burning velocity results for a flame of radius less than 38 mm obtained from pressure trace analysis fluctuated significantly. At r/R_{cell} of 0.40, only burning velocities within ±30% of the mean value (justified by the high speed schlieren analysis) are accepted. Burning velocities outside ±20% the mean value are rejected for 0.45 relative radius flame. As the flame grows, the noise to signal level becomes progressively smaller. For flames of relative flame radius, r/R_{cell}, larger than 0.45 any burning velocity outside the ±10% of the mean value is rejected.

H.4: CORRELATIONS BETWEEN MASS FRACTION BURNT, PRESSURE, UNBURNT MIXTURE TEMPERATURE, FLAME SIZE AND MIXTURE STOICHIOMETRY

Table H.3a summarizes the mass fraction burnt and pressure rise as function of flame size and mixture stoichiometry. All mixtures are ignited at 1 atm and 300 K. The relative flame radii listed correspond to the flame growth rate and burning velocity calculation points. The table shows that even up to 55 mm radius flame (r/R_{cell} of 0.72) the mass fraction burnt is less than 15% and the pressure rise is less than doubled.

Table H.3b illustrates the corresponding unburnt temperatures as function of flame size and mixture stoichiometry. The table shows that up to 55 mm radius flame the unburnt temperature rises about 50 K due to compression. Tables H.3a and H.3b show that in the region before a perfectly spherical flame front (with its centre point at the centre of the spark gap) is in contact with the walls, the mass fraction burnt, pressure rise and unburnt temperature rise are relatively small.

H.5: PRESSURE EFFECT ON THE COMBUSTION PROCESS

Pressure effects on maximum pressure rise and on the time to reach maximum pressure rise for 90% stoichiometric methane-air flames are summarized in Table H.4a. The results for 70% stoichiometric methane-air flames are summarized in Table H.4b.

For hydrocarbon-air flame at atmospheric conditions, pressure usually suppresses the flame growth. Table H.5a tabulates the effect of pressure on the burning velocity of 90% stoichiometric methane-air flames. The pressure range considered is from 0.5 to 2.0 atm.

The pressure is found to have a larger effect on the burning velocities of leaner mixtures. The pressure suppression on 70% stoichiometric methane-air flames is summarized in Table H.5b.

H.5: IGNITION ENERGY EFFECT ON THE COMBUSTION PROCESS

Ignition energy supply by the high voltage capacitance unit is varied to study the effect on flame growth. The ignition voltage supply is from 100 to 500 V while keeping the capacitance at 2.5 μF. In other words, the ignition energy supply is altered from 12.5 to 312.5 mJ.

Table H.6 shows the effect of ignition voltage supply on the overall combustion process. Only the 70% and 90% stoichiometric methane-air flames are considered. Taking the experimental scatter into account, the change of ignition energy supply from 12.5 to 312.5 mJ has a negligible effect on the maximum pressure rise and the total combustion duration.

Figure H.4 shows the voltage supply effect on 90% stoichiometric methane-air flame growth based on schlieren flame images. Only mixtures ignited at 1 atm and 300 K are considered. The change of supply voltage from 500 to 200 V does not seem to affect the early flame growth significantly. For flames larger than 30 mm, it appears that the higher ignition voltage supply leads to a slower flame growth. As the changes are relatively small, further discussion awaits closer examination.

The voltage supply effect on 70% stoichiometric methane-air flame growth based on schlieren images is shown in Figure H.5. For the conditions considered, the change in the supply voltage by a factor of 2.5 has a negligible effect on the early flame growth rate. The larger voltage supply cases seem to lead to slower flame growth for flames larger than 30 mm. This trend is consistence with that of 90% stoichiometric case but the magnitude is much smaller. The intention behind using a relative high voltage supply compared to the automotive ignition system is solely to ensure ignition of very lean and/or high turbulence mixtures. The obvious conclusion is that over the range of conditions considered, the relatively higher ignition voltage supply does not alter the combustion process significantly.

Table H.1: The effects of mixture stoichiometry on maximum pressure rise. $P_{init}=1$ atm, $T_{init}=300$ K.

Date	Video run#	Pressure run#	Ø	P_{max} (kPa)	P_{max} /P_{amax}	t_{Pmax} (ms)
25/5/93		1Ea	1	814	0.88	60
		1Eb	1	808	0.87	59
		1Ec	1	794	0.86	58
		1Ed	1	803	0.87	59
	1000	1Ee	1	778	0.84	62
	1010	1Ef	1	786	0.85	58
average				797	0.86	59
26/5/93	1020	9Ea	0.9	743	0.84	78
	1030	9Eb	0.9	745	0.84	75
average				744	0.84	76
	1040	8Ea	0.8	682	0.82	108
	1050	8Eb	0.8	685	0.83	112
average				683	0.83	110
	1060	7Ea	0.7	602	0.79	206
	1070	7Eb	0.7	598	0.79	206
average				600	0.79	206
	1080	6Ea	0.6	271	0.39	≈600
	1090	6Eb	0.6	259	0.38	≈600
average				265	0.38	≈600

Table H.2: The effects of mixture stoichiometry on laminar flame growth rate and laminar burning velocity. $P_{init}=1$ atm, $T_{init}=300$ K.

	average flame growth rate (cm/s)					average burning velocity (cm/s)				
r/R_{cell}	Ø =1.0	0.9	0.8	0.7	0.6	1.0	0.9	0.8	0.7	0.6
[v] 0.20	242	181	126	69	27	32	25	19	11	5
[v] 0.25	243	189	124	69	25	33	25	19	12	5
[v] 0.30	242	184	128	70	24	34	27	20	12	4
[v] 0.35	237	182	124	68	22	33	27	19	12	4
[v] 0.40	240	178	123	66		35	27	20	12	
[v] 0.45	231	168	117	63		34	26	20	11	
[v] 0.50	221	164	110	60		34	27	19	12	
0.40	246	174		78	27	36	26	19	14	5
0.45	186	158	84	75	18	27	25	14	14	4
0.50	202	149	95	72	20	32	25	17	14	5
0.55	212	134	97	58	21	36	24	18	12	5
0.60	181	141	87	56	19	32	27	18	12	5
0.65	179	140	85	52	17	35	29	18	12	4
0.70	168	135	84	51	15	36	31	20	14	4
0.72	158	124	78	48	14	36	29	20	13	4
0.75	147	116	73	44	11	36	29	20	13	3
0.80	123	97	66	36		35	29	21	12	
0.85	99	76	52	27		36	29	20	11	
0.90	81	61	41	20		37	29	20	10	

[v] from schlieren video images.

Table H.3a: The effects of mixture stoichiometry on mass fraction burnt and pressure rise. $P_{init}=1$ atm, $T_{init}=300$ K.

	average mass fraction burnt (%)					average pressure (kPa)				
r/R_{cell}	Ø=1	0.9	0.8	0.7	0.6	1.0	0.9	0.8	0.7	0.6
[v] 0.20	0.1	0.1	0.1	0.1	0.1	102	102	102	102	102
[v] 0.25	0.2	0.2	0.2	0.2	0.3	103	103	103	103	103
[v] 0.30	0.3	0.4	0.4	0.4	0.5	104	104	104	104	104
[v] 0.35	0.5	0.6	0.6	0.7	0.8	106	106	106	107	106
[v] 0.40	0.8	0.9	1.0	1.1		109	109	109	109	
[v] 0.45	1.3	1.3	1.5	1.6		113	113	113	113	
[v] 0.50	1.8	1.9	2.1	2.2		118	118	118	117	
0.40	1	1	1	1	1	109	109	109	109	109
0.45	1	1	1	2	2	113	113	113	113	113
0.50	2	2	2	2	3	119	118	118	118	118
0.55	3	3	3	3	4	125	125	125	124	124
0.60	4	4	4	4	5	134	134	134	133	132
0.65	5	5	6	6	7	146	146	145	144	143
0.70	7	7	8	8	9	163	162	161	160	158
0.72	8	8	9	9	10	171	170	170	168	166
0.75	10	10	11	11	13	186	185	184	182	
0.80	14	14	15	16		220	219	216	213	
0.85	20	21	22	23		273	270	266	260	
0.90	30	31	33	35		362	356	348	337	

[v] from schlieren video images.

Table H.3b: The effects of mixture stoichiometry on unburnt temperature. $P_{init}=1$ atm, $T_{init}=300$ K.

	average unburnt gas temperature (K)				
r/R_{cell}	Ø=1.0	0.9	0.8	0.7	0.6
[v] 0.20	301	301	301	301	301
[v] 0.25	301	301	301	301	301
[v] 0.30	302	302	302	302	302
[v] 0.35	304	304	304	304	304
[v] 0.40	306	306	306	306	
[v] 0.45	309	309	309	309	
[v] 0.50	312	312	312	312	
0.40	306	306	306	306	306
0.45	309	309	309	309	309
0.50	313	313	313	313	312
0.55	318	318	318	317	317
0.60	324	324	323	323	323
0.65	331	331	331	330	330
0.70	341	341	340	340	339
0.72	346	345	345	344	343
0.75	353	353	352	352	350
0.80	369	369	368	367	
0.85	390	390	389	387	
0.90	420	418	416	413	

[v] from schlieren video images.

Table H.4a: The effects of pressure on maximum pressure rise of 90% stoichiometric methane-air flame. $T_{init}=300$ K.

Date	Video run#	Pressure run#	P_{init} (atm)	P_{max} (kPa)	P_{max}/P_{init}	T_{Pmax} (ms)
26/5/93	1100	9P5a	0.5	≈350	≈6.9	61
	1110	9P5b	0.5	≈350	≈6.9	62
	1020	9Ea	1	743	7.3	78
	1030	9Eb	1	745	7.4	75
	1180	9P15a	1.5	1177	7.7	85
	1190	9P15b	1.5	1173	7.7	82
		9P2a	2	1630	8.0	99
	1220	9P2b	2	1655	8.2	92
	1230	9P2c	2	1611	7.9	93

Table H.4b: The effects of pressure on maximum pressure rise of 70% stoichiometric methane-air flame. $T_{init}=300$ K.

Date	Video run#	Pressure run#	P_{init} (atm)	P_{max} (kPa)	P_{max}/P_{init}	T_{Pmax} (ms)
26/5/93	1120	7P5a	0.5	≈275	≈5.4	140
	1130	7P5b	0.5	≈275	≈5.4	143
	1060	7Ea	1	602	5.9	206
	1070	7Eb	1	598	5.9	206
	1160	7P15a	1.5	933	6.1	267
	1170	7P15b	1.5	929	6.1	266
	1240	7P2a	2	1232	6.1	335
	1250	7P2b	2	1205	5.9	347

Table H.5a: The effects of pressure on laminar flame growth rate and laminar burning velocity of 90% stoichiometric methane-air flame.
P_{init}=1 atm, T_{init}=300 K.

	average flame growth rate (cm/s)				average burning velocity (cm/s)			
r/R_{cell}	P_{init} =0.5	1.0	1.5	2.0	0.5	1.0	1.5	0.6
^{v}0.20	207	181	169	151	29	25	24	21
^{v}0.25	215	189	171	148	31	25	24	21
^{v}0.30	218	184	169	150	31	27	24	22
^{v}0.35	219	182	168	148	33	27	25	22
^{v}0.40	218	178	164	146	33	27	25	22
^{v}0.45	211	168	158	137	33	26	25	22
^{v}0.50		164	150	131		27	24	22
0.40		174	164	139		26	24	21
0.45		158	175	117		25	27	18
0.50		149	153	116		25	25	19
0.55		134	110	105		24	20	19
0.60		141	105	108		27	20	20
0.65		140	103	104		29	21	22
0.70		135	96	98		31	23	22
0.72		124	96	94		29	23	22
0.75		116	88	89		29	25	23
0.80		97	76	80		29	27	25
0.85		76	60	70		29	28	26
0.90		61		57		29	28	27

^{v} from schlieren video images.

Table H.5b: The effects of pressure on laminar flame growth rate and laminar burning velocity of 70% stoichiometric methane-air flame.
$P_{init}=1$ atm, $T_{init}=300$ K.

	average flame growth rate (cm/s)				average burning velocity (cm/s)			
r/R_{cell}	P_{init} =0.5	1.0	1.5	2.0	0.5	1.0	1.5	2.0
[v] 0.20	89	69	56	52	14	11	9	9
[v] 0.25	89	69	56	50	15	12	10	8
[v] 0.30	91	70	56	49	16	12	9	9
[v] 0.35	87	68	54	47	15	12	9	8
[v] 0.40	88	66	53	46	16	12	9	8
[v] 0.45	84	63	51	44	16	11	9	8
[v] 0.50	81	60	47	42	16	12	9	8
0.40		78		45		14		8
0.45		75		39		14		8
0.50		72	50	36		14	10	7
0.55		58	44	37		12	9	8
0.60		56	36	36		12	8	8
0.65		52	32	34		12	8	8
0.70		51	32	32		14	8	8
0.72		48	32	31		13	9	8
0.75		44	31	29		13	9	8
0.80		36	28	24		12	10	8
0.85		27	22	19		11	9	8
0.90		20	15	12		10	8	6

[v] from schlieren video images.

Table H.6: The effects of ignition energy on laminar methane-air flame. $P_{init}=1$ atm, $T_{init}=300$ K.

Date	Video run#	Pressure run#	Ø	Voltage Supply (V)	P_{max} (kPa)	T_{Pmax} (ms)
26/5/93	1020	9Ea	0.9	500	743	78
	1030	9Eb	0.9	500	745	75
	1260	9I400a	0.9	400	754	72
	1270	9I400b	0.9	400	752	71
	1280	9I300a	0.9	300	741	72
	1290	9I300b	0.9	300	748	71
	1300	9I200a	0.9	200	753	82
	1310	9I200b	0.9	200	746	71
	1060	7Ea	0.7	500	602	206
	1070	7Eb	0.7	500	598	206
	1340	7I400a	0.7	400	611	187
	1350	7I300a	0.7	300	607	190
	1360	7I200a	0.7	200	611	194
	1370	7I200b	0.7	200	610	190

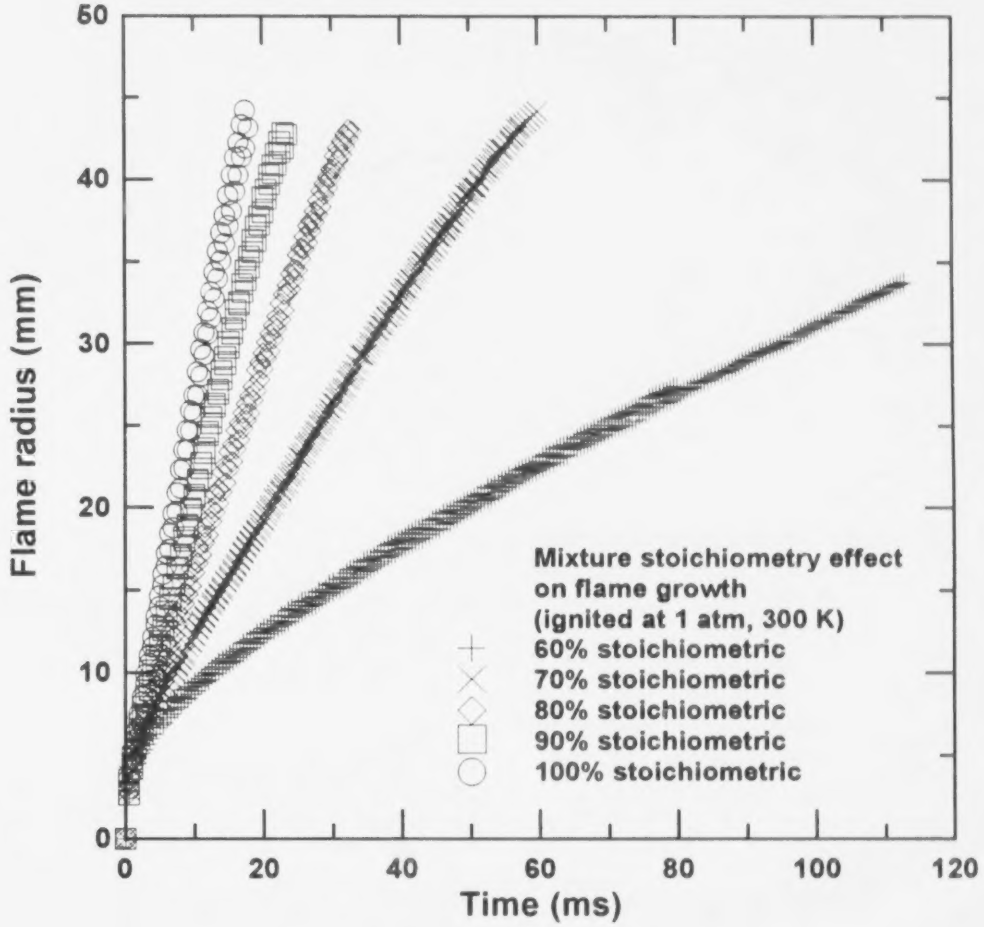

Figure H.1: The effects of mixture stoichiometry on laminar flame growth. $P_{init}=1$ atm; $T_{init}=300$ K.

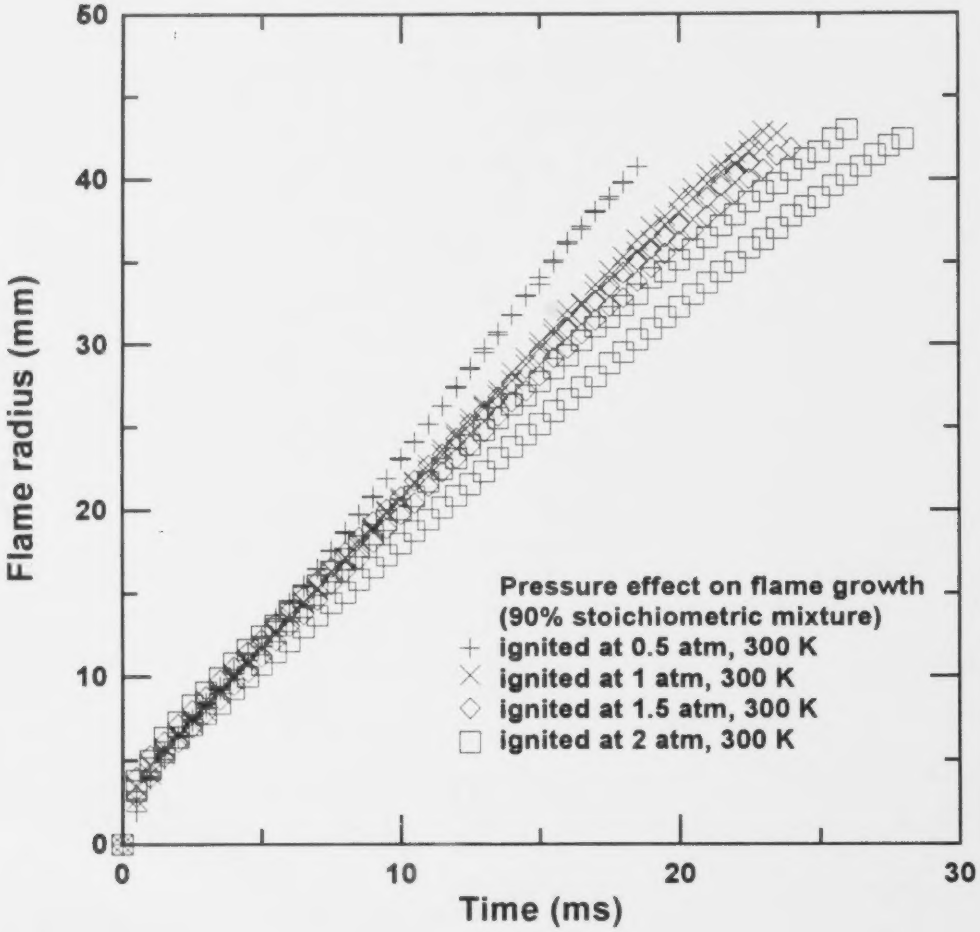

Figure H.2: The effects of pressure on 90% stoichiometric methane-air flame. P_{init}=0.5, 1.0, 1.5, 2.0 atm; T_{init}=300 K.

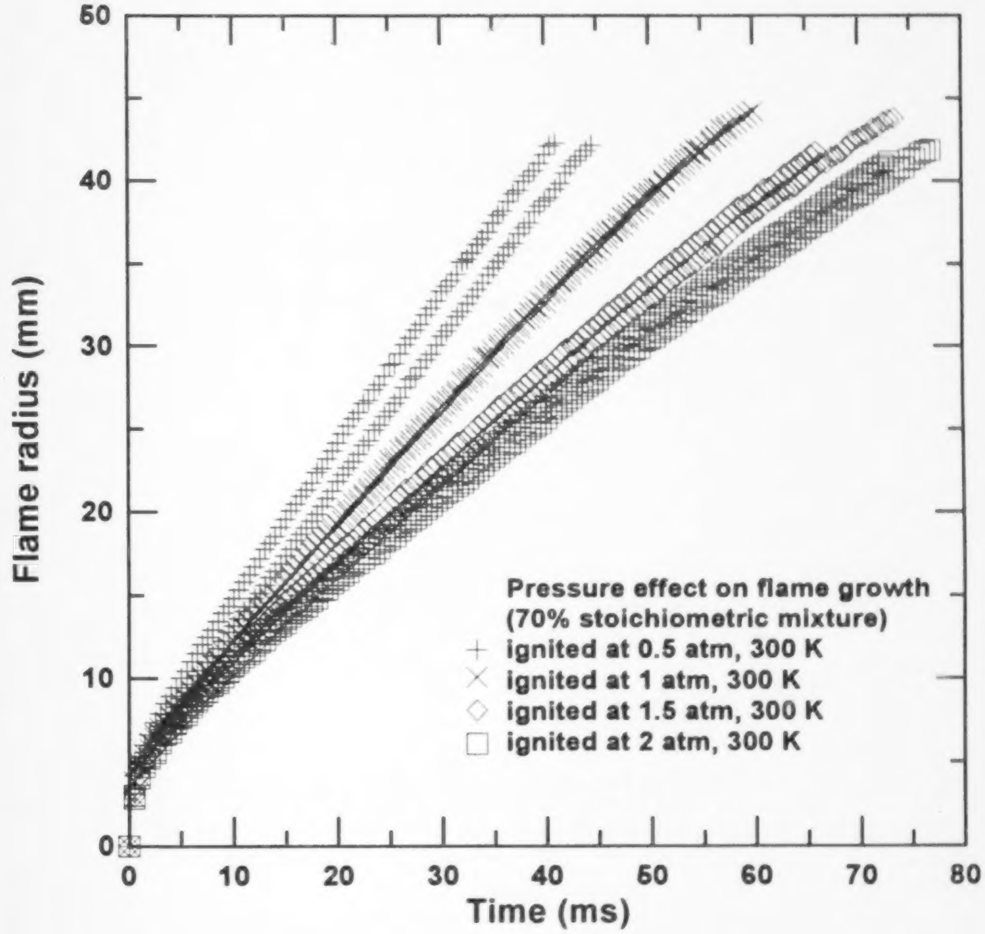

Figure H.3: The effects of pressure on 70% stoichiometric methane-air flame. P_{init}=0.5, 1.0, 1.5, 2.0 atm; T_{init}=300 K.

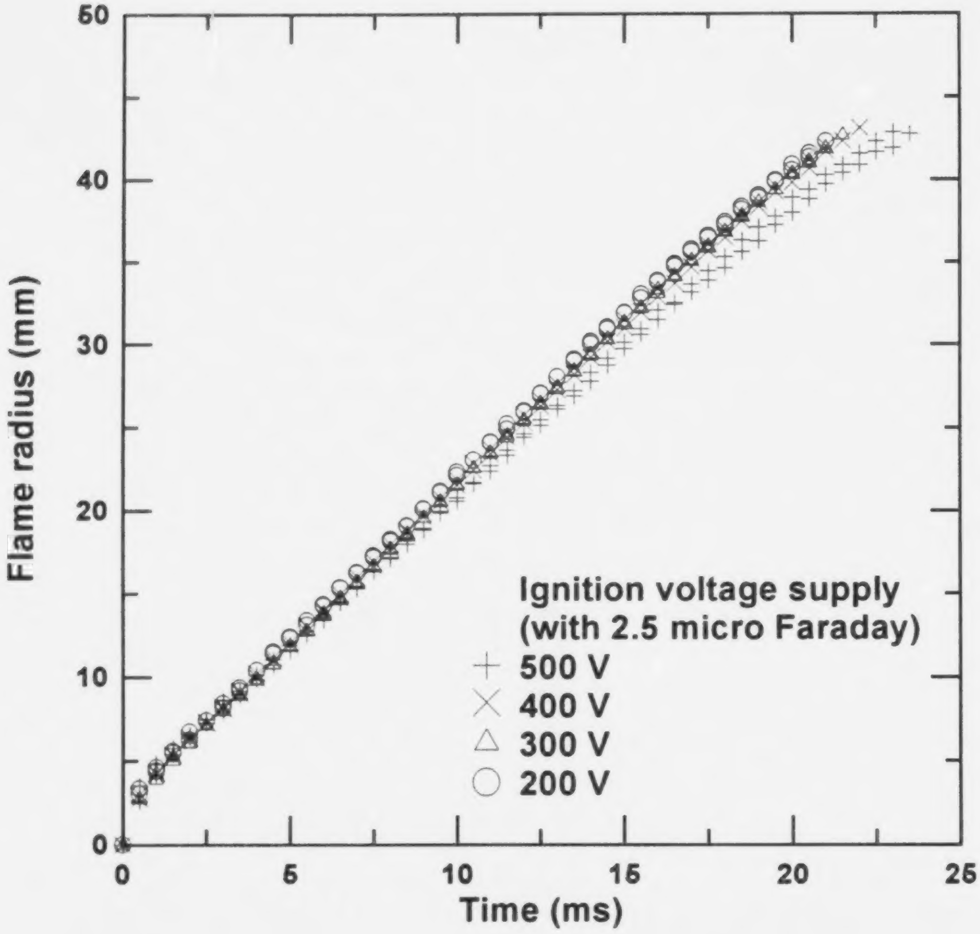

Figure H.4: The effects of ignition voltage supply on 90% stoichiometric methane-air flame.

P_{init}=1 atm; T_{init}=300 K; voltage supply=500, 400, 300, 200 V, capacitance=2.5 μF.

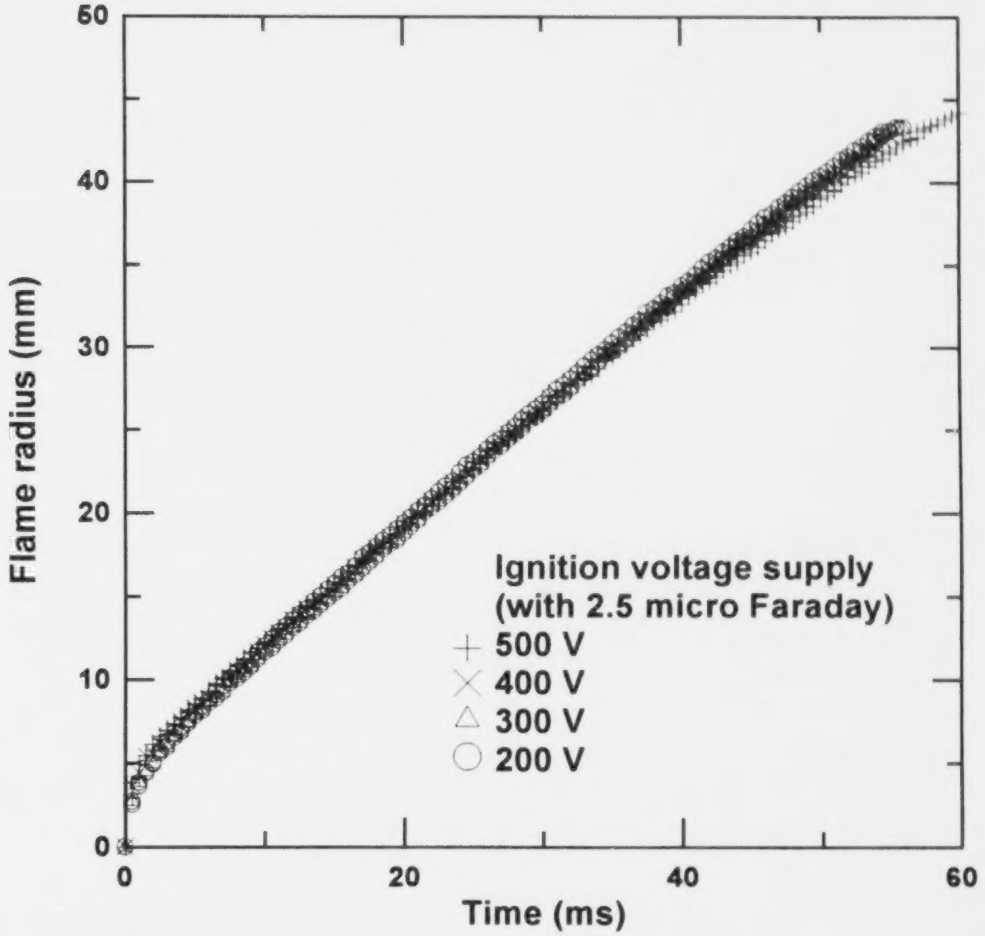

Figure H.5: The effects of ignition voltage supply on 70% stoichiometric methane-air flame.

$P_{init}=1$ atm; $T_{init}=300$ K; voltage supply=500, 400, 300, 200 V, capacitance=2.5 μF.

APPENDIX I: PREMIXED TURBULENT METHANE-AIR FLAME RESULTS

This appendix documents the turbulent methane-air flame growth results which are not given in Chapter 6. It also describes the "thread and glue" method used in estimating the two-dimensional schlieren flame perimeter.

I.1: TURBULENT BURNING VELOCITY-TURBULENCE INTENSITY RELATION

Figures I.1a, I.1b, I.1c and I.1d show typical 55 mm radius, 0.9 equivalence ratio turbulent burning velocity-turbulence intensity relations. The normalized turbulent burning velocity, S_{to}/S_{lo}-1, is plotted against the normalized turbulence intensity, u'/S_{lo}, for perforated plate hole diameter of 2.5, 5, 10 and 20 mm cases as shown in Figures I.1a, I.1b, I.1c and I.1d respectively. The turbulent and laminar burning velocities are estimated from the pressure trace analysis. The reference laminar burning velocity, S_{lo}, is estimated from

$$S_l = S_{lo} \left(\frac{P}{P_o}\right)^{Pexp} \left(\frac{T}{T_o}\right)^{Texp} \qquad \text{I.1}$$

where S_l is the instantaneous laminar burning velocity, P is the pressure, T is the unburnt mixture temperature, P_o is 1 atm, T_o is 300 K, the values for Pexp are -0.43 and -0.26 for 0.7 and 0.9 equivalence ratio flames respectively, and Texp is 2. It is assumed that the same expression applies for the turbulent case. In other words,

$$S_t = S_{to} \left(\frac{P}{P_o}\right)^{Pexp} \left(\frac{T}{T_o}\right)^{Texp} \qquad \text{I.2}$$

where S_t is the instantaneous turbulent burning velocity and S_{to} is the reference turbulent burning velocity at 1 atm and 300 K.

Similarly typical 55 mm radius, 0.7 equivalence ratio turbulent burning velocity-turbulence intensity relations are illustrated in Figures I.2a, I.2b, I.2c and I.2d. The normalized turbulent burning velocity, S_{to}/S_{lo}-1, is plotted as a function of the normalized turbulence intensity, u'/S_{lo}, for plate hole diameter of 2.5, 5, 10 and 20 mm cases as shown in Figures I.2a, I.2b, I.2c and I.2d respectively.

I.2: THE 0.6 EQUIVALENCE RATIO TURBULENT FLAME GROWTH

Typical 0.6 equivalence ratio turbulent flame growth from schlieren images are compared with the pressure trace analysis. Typical flame growth results obtained from using the perforated plates with 20, 5 and 2.5 mm diameter holes are plotted in Figures I.3a, I.3b and I.3c respectively.

I.3: THREAD AND GLUE METHOD

The schlieren images are zoomed into eight inch by ten inch black and white photographs. A sheet of transparency is sprayed with dry glue and placed on top of the photograph. A thread is then used to trace the edge of the flame to estimate the flame perimeter. The accuracy of this estimation becomes worst with increasing turbulence intensity. For a 30 mm radius laminar flame image, the standard deviation in the two-dimensional flame perimeter estimation is about 2 mm and the standard deviation in the two-dimensional flame cross-sectional area estimation using the program called FLASH is about 17 mm^2. For a roughly 35 mm radius turbulent flame (turbulence intensity of about 2 m/s and integral scale of about 8 mm), the standard deviations are approximately 14 mm and 27 mm^2 for perimeter and area estimations respectively.

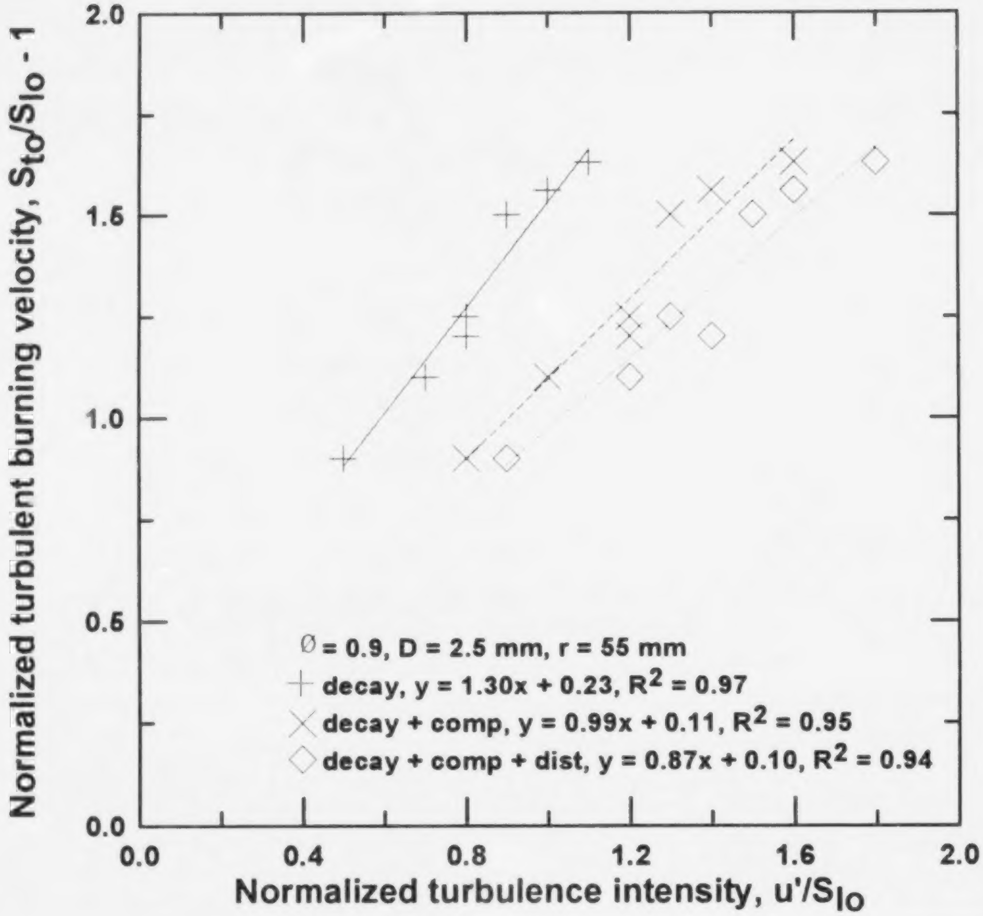

Figure I.1a: Plots of S_{to}/S_{lo} - 1 against u'/S_{lo} for fine scale, 55 mm radius, 0.9 equivalence ratio turbulent flame.
D=2.5 mm; $\Lambda \approx 1.5$ mm; T_{init}=300 K; P_{init}=1 atm.

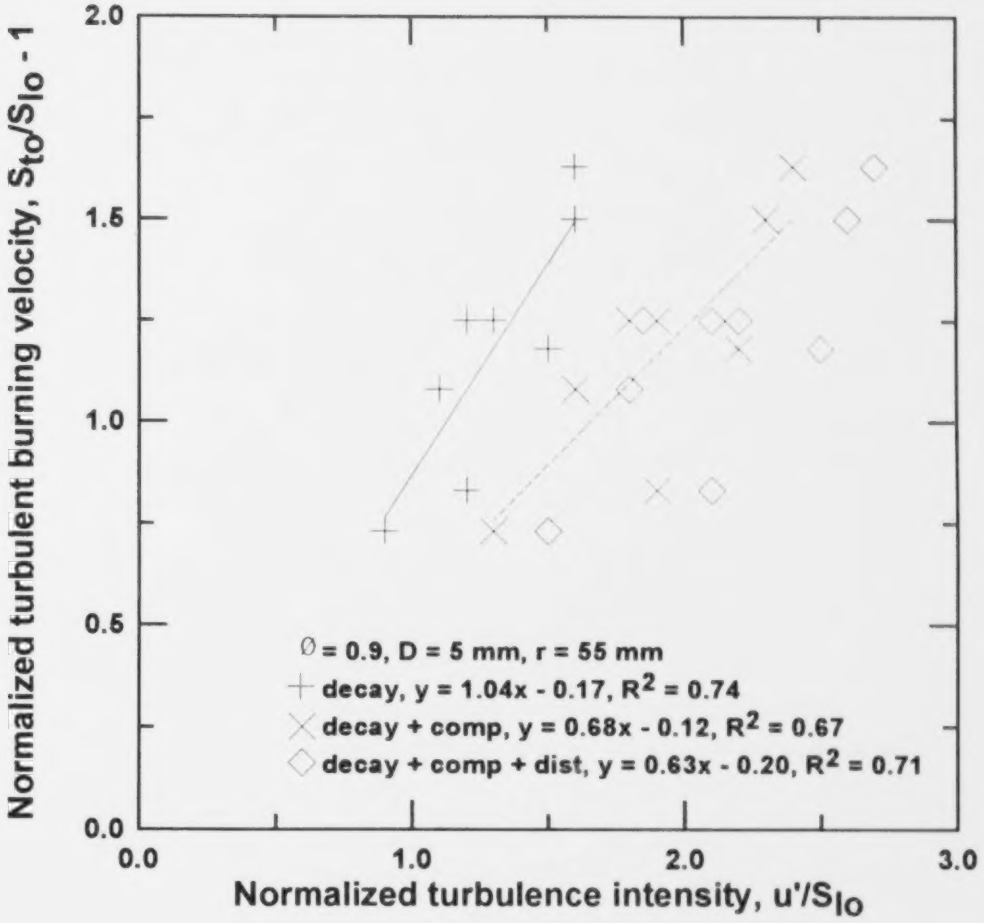

Figure I.1b: Plots of S_{to}/S_{lo} - 1 against u'/S_{lo} for small scale, 55 mm radius, 0.9 equivalence ratio turbulent flame.
D=5 mm; $\Lambda \approx 2$ mm; T_{init}=300 K; P_{init}=1 atm.

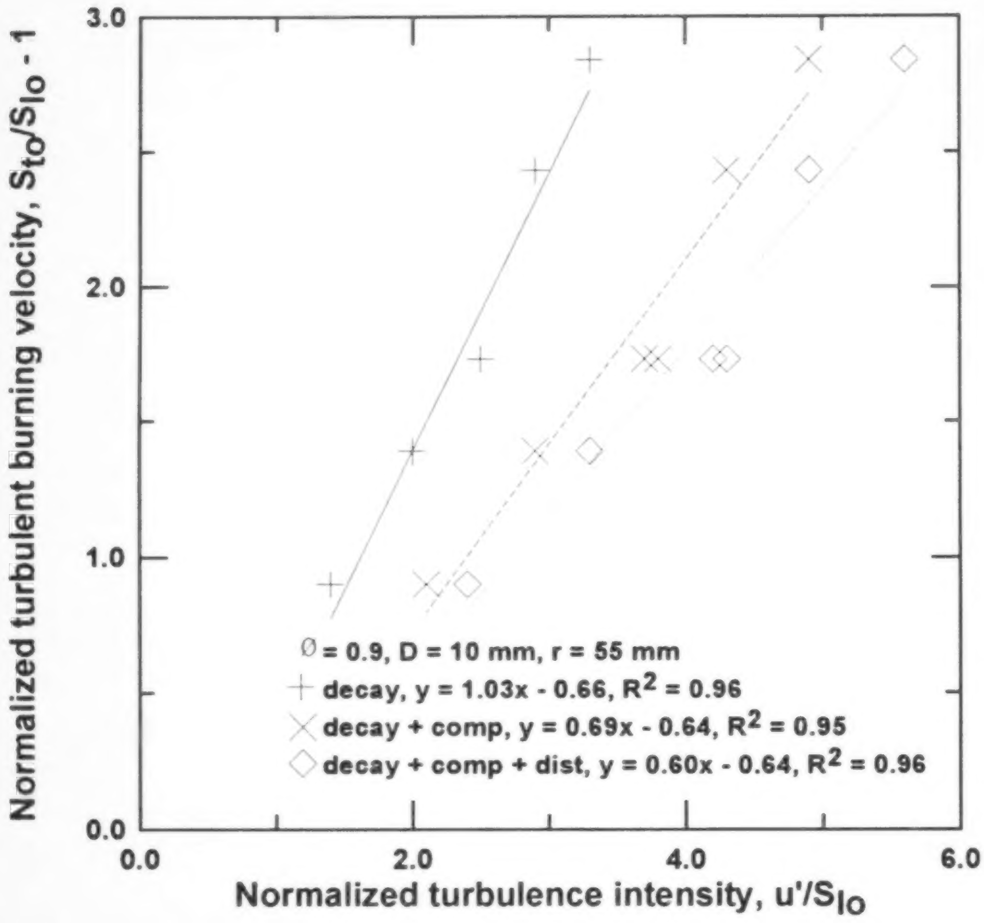

Figure I.1c: Plots of S_{to}/S_{lo} - 1 against u'/S_{lo} for medium scale, 55 mm radius, 0.9 equivalence ratio turbulent flame.
D=10 mm; Λ≈4 mm; T_{init}=300 K; P_{init}=1 atm.

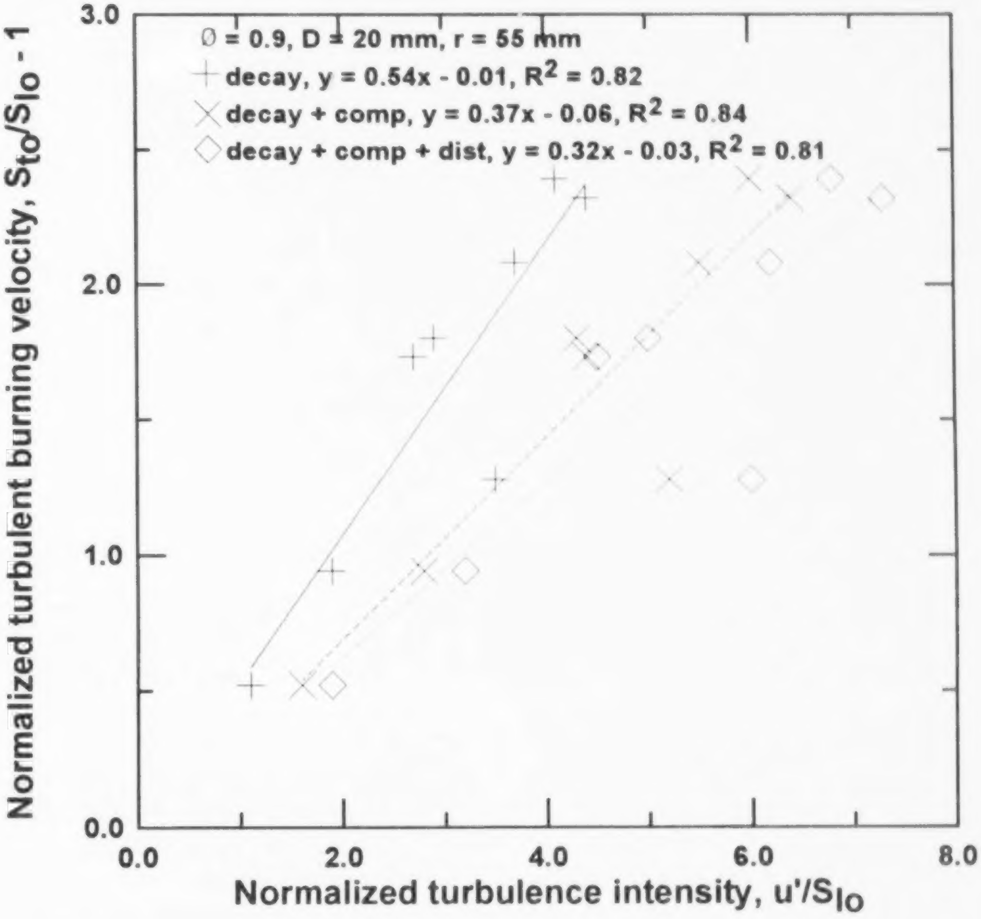

Figure I.1d: Plots of S_{to}/S_{lo} - 1 against u'/S_{lo} for large scale, 55 mm radius, 0.9 equivalence ratio turbulent flame.
D=20 mm; Λ≈8 mm; T_{init}=300 K; P_{init}=1 atm.

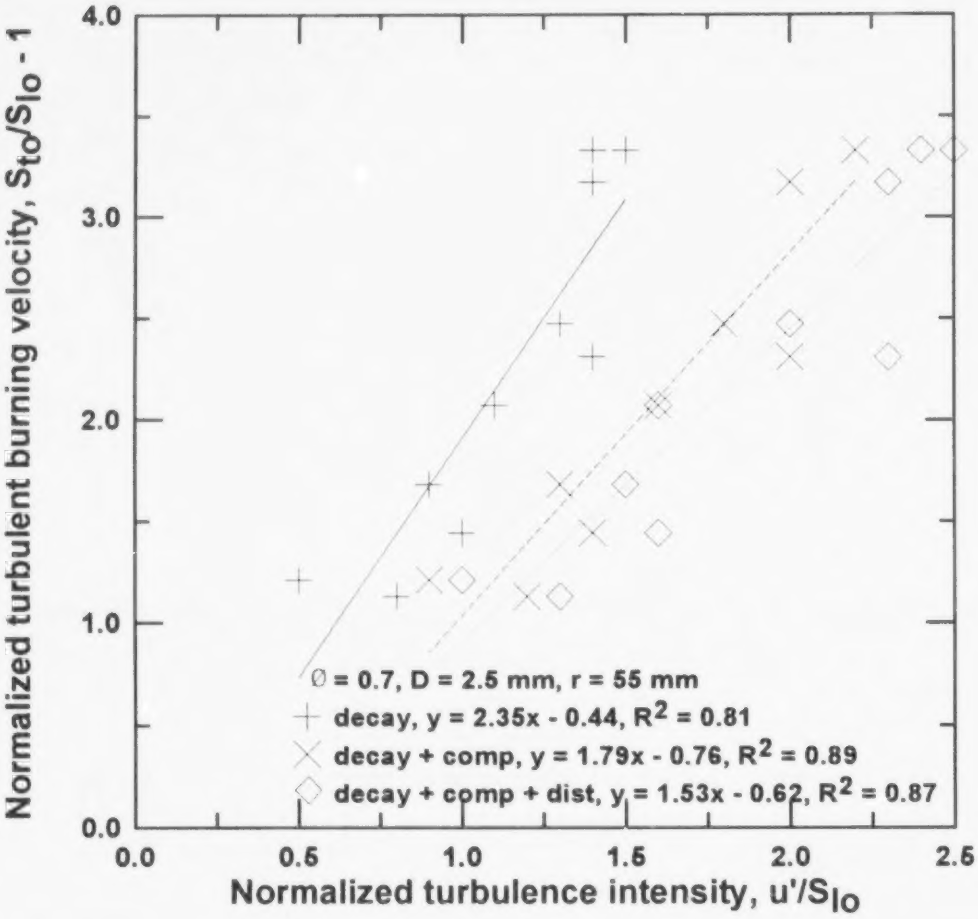

Figure I.2a: Plots of S_{to}/S_{lo} - 1 against u'/S_{lo} for fine scale, 55 mm radius, 0.7 equivalence ratio turbulent flame.
D=2.5 mm; Λ≈1.5 mm; T_{init}=300 K; P_{init}=1 atm.

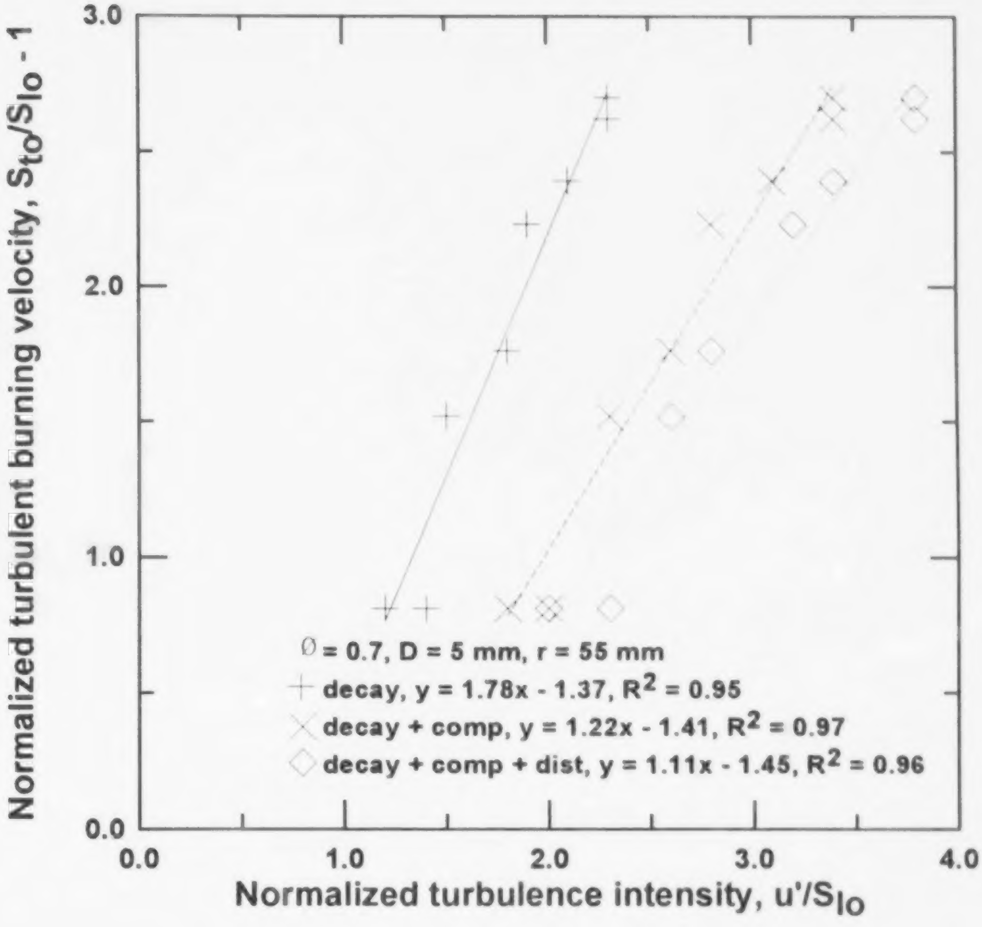

Figure I.2b: Plots of S_{to}/S_{lo} - 1 against u'/S_{lo} for small scale, 55 mm radius, 0.7 equivalence ratio turbulent flame.
$D=5$ mm; $\Lambda\approx2$ mm; $T_{init}=300$ K; $P_{init}=1$ atm.

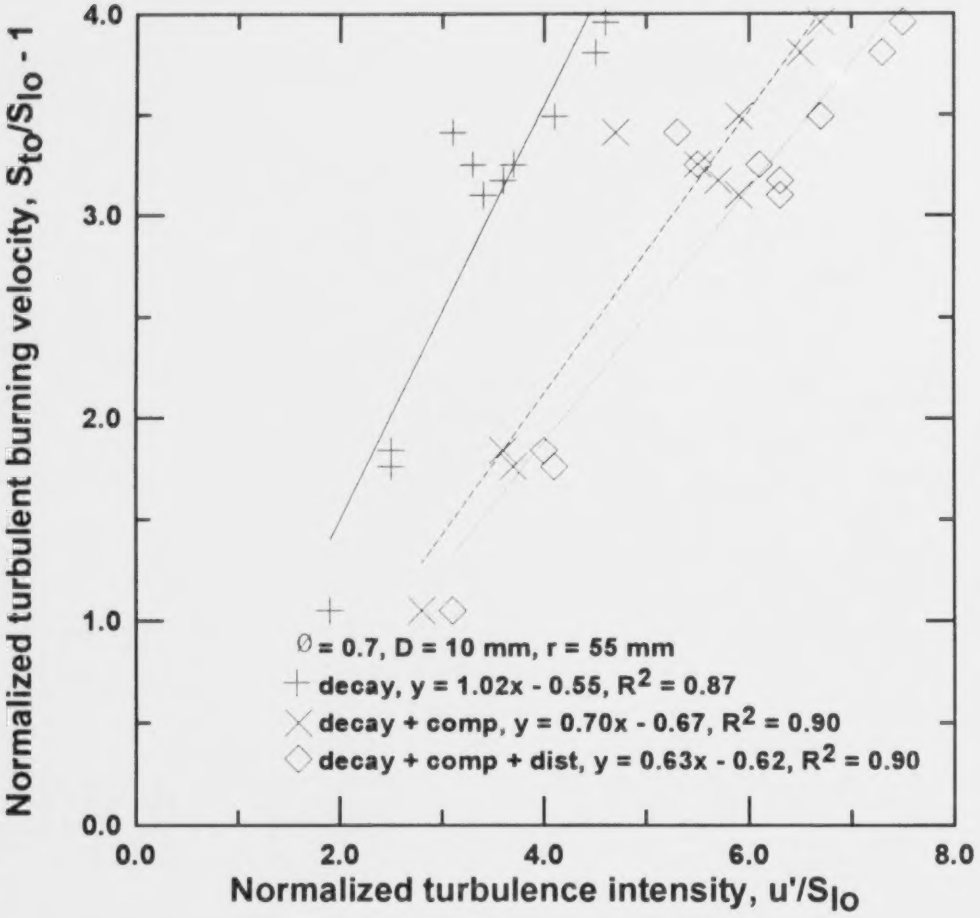

Figure I.2c: Plots of S_{to}/S_{lo} - 1 against u'/S_{lo} for medium scale, 55 mm radius, 0.7 equivalence ratio turbulent flame.
D=10 mm; $\Lambda \approx 4$ mm; T_{init}=300 K; P_{init}=1 atm.

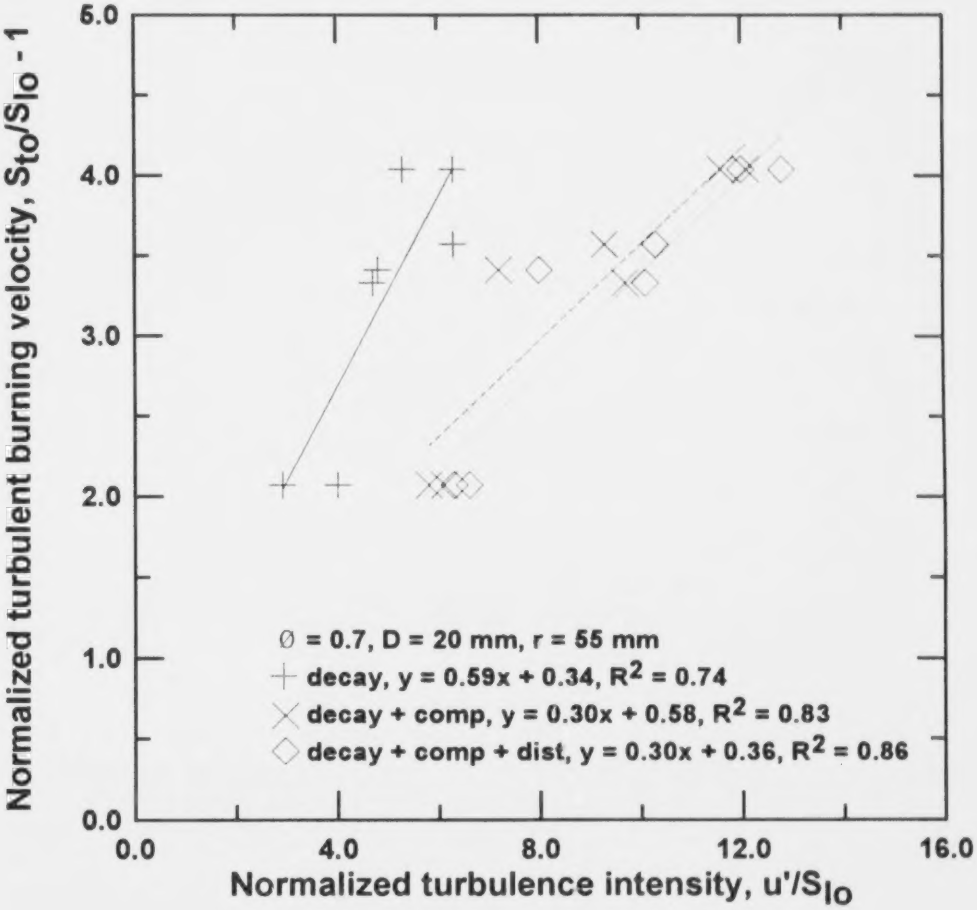

Figure I.2d: Plots of S_{to}/S_{lo} - 1 against u'/S_{lo} for large scale, 55 mm radius, 0.7 equivalence ratio turbulent flame.
$D=20$ mm; $\Lambda\approx8$ mm; $T_{init}=300$ K; $P_{init}=1$ atm.

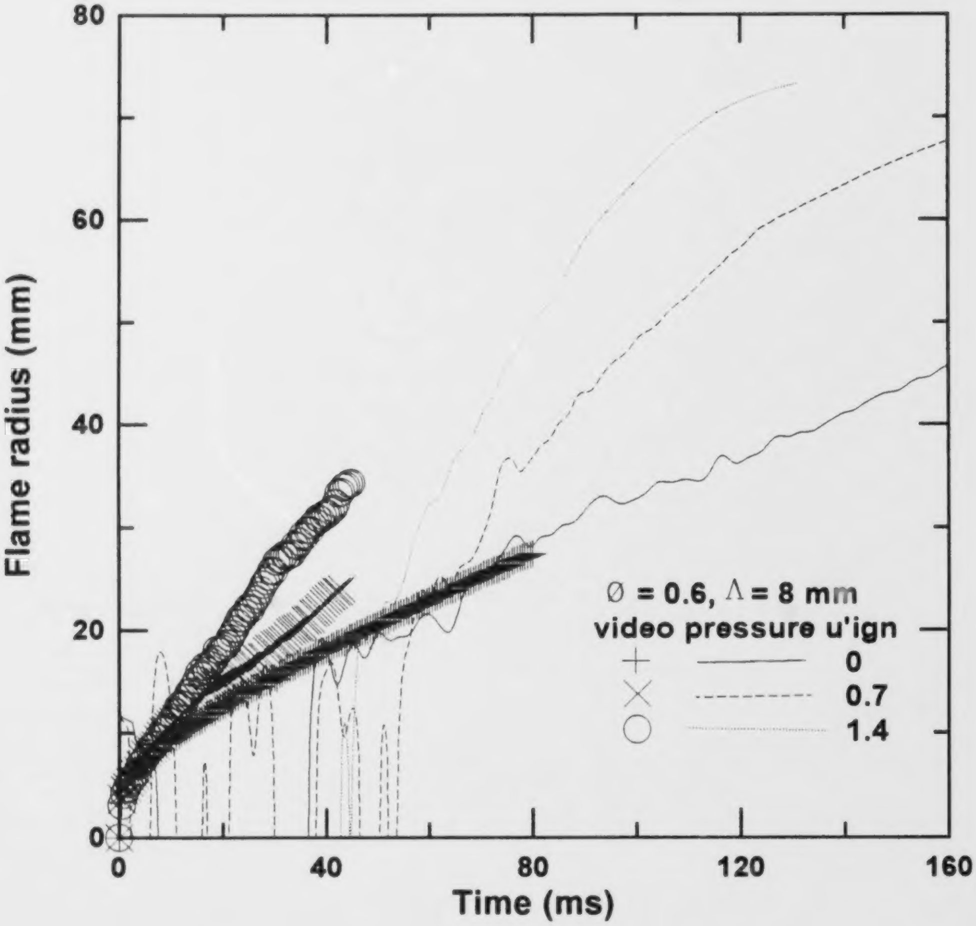

Figure I.3a: Typical 0.6 equivalence ratio turbulent flame growth from schlieren images compared with pressure trace analysis.
$\Lambda \approx 8$ mm; $P_{init}=1$ atm; $T_{init}=300$ K.

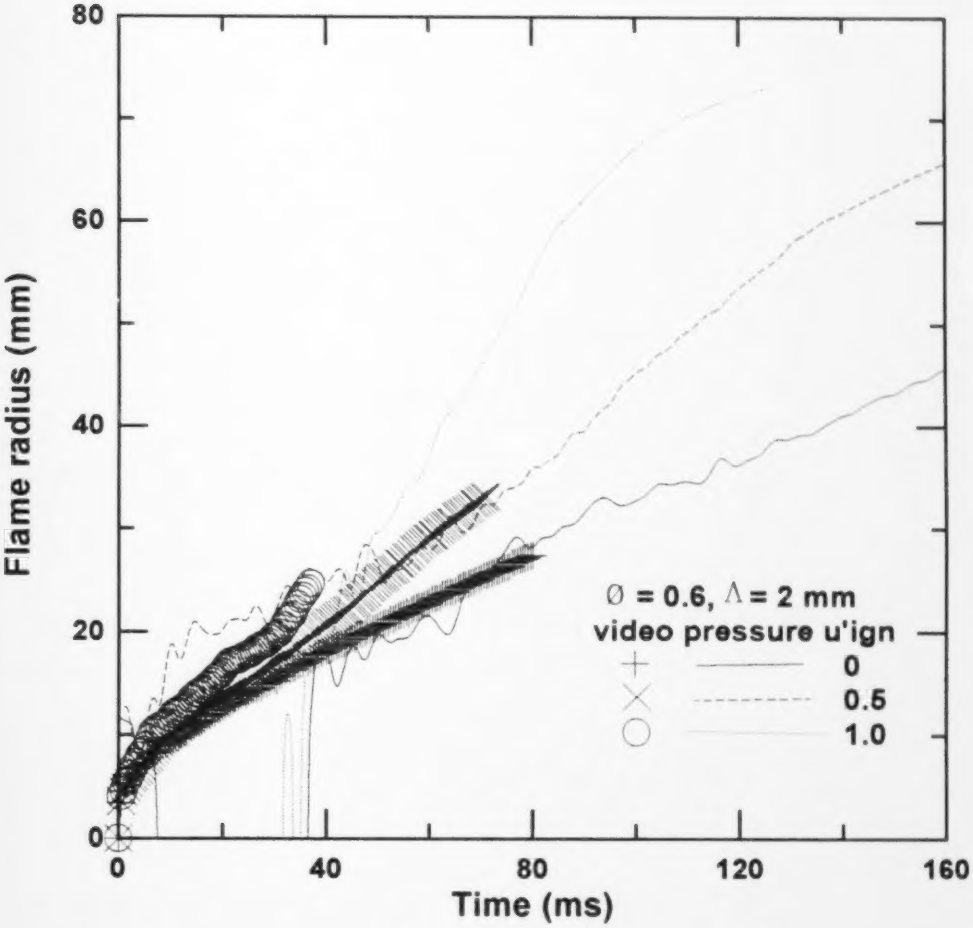

Figure I.3b: Typical 0.6 equivalence ratio turbulent flame growth from schlieren images compared with pressure trace analysis.
Λ≈2 mm; P_{init}=1 atm; T_{init}=300 K.

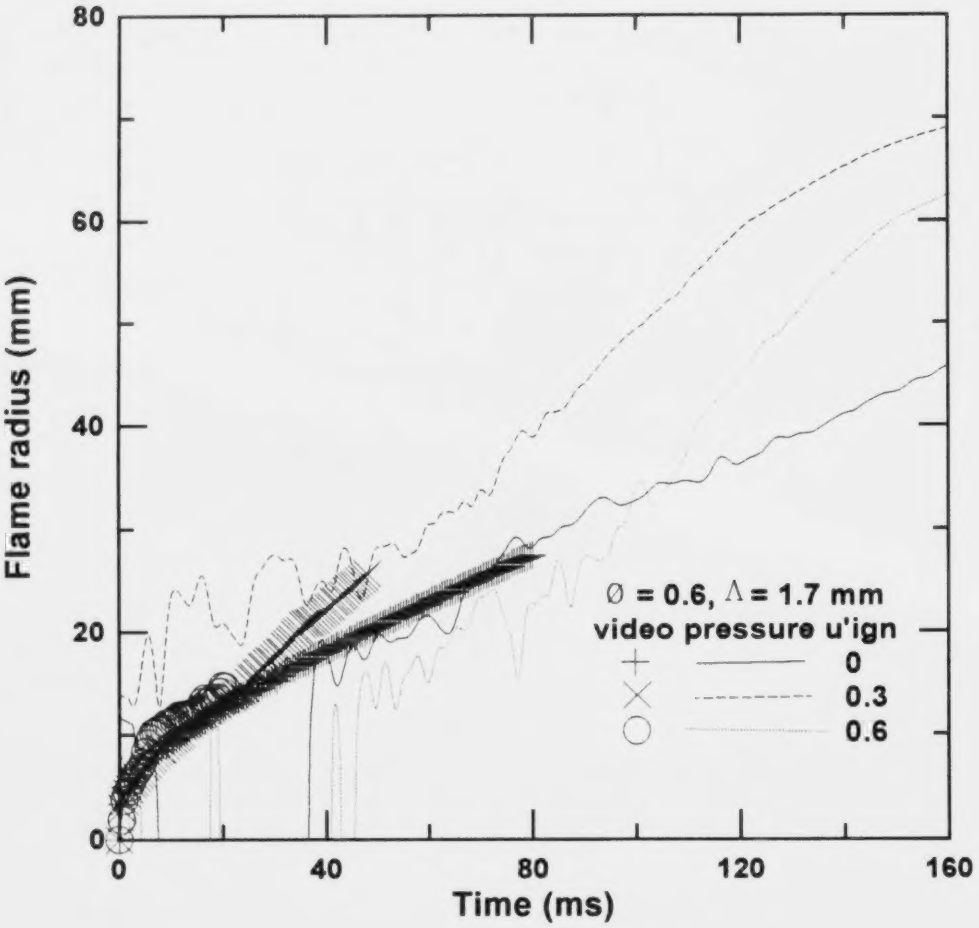

Figure I.3c: Typical 0.6 equivalence ratio turbulent flame growth from schlieren images compared with pressure trace analysis.
$\Lambda \approx 1.8$ mm; $P_{init} = 1$ atm; $T_{init} = 300$ K.